U-Pb-Hf isotopic data from detrital zircons in late Carboniferous and Mid-Late Triassic sandstones, and also Carboniferous granites from the Tauride and Anatolide continental units in S Turkey: implications for Tethyan palaeogeography

U-Pb-Hf isotopic data from detrital zircons in Late Carboniferous and Mid-Late Triassic sandstones, and also Carboniferous granites from the Tauride and Anatolide continental units in S Turkey: implications for Tethyan paleogeography

Journal:	*International Geology Review*
Manuscript ID	TIGR-2019-0106.R2
Manuscript Type:	Data Article
Date Submitted by the Author:	n/a
Complete List of Authors:	Ustaomer, Timur; Istanbul University, Department of Geology Ustaömer, Petek Ayda; Yildiz Technical University, Natural Sciences Research Center Robertson, Alastair; University of Edinburgh, School of GeoSciences Gerdes, Alex; University of Frankfurt, Petrology and geochemistry
Keywords:	provenance, sandstone, detrital zircon, U-Pb & Lu-Hf isotopes, Taurides, Anatolides, Gondwana, Tethys

U-Pb-Hf isotopic data from detrital zircons in Late Carboniferous and Mid-Late Triassic sandstones, and also Carboniferous granites from the Tauride and Anatolide continental units in S Turkey: implications for Tethyan paleogeography

Timur Ustaömer[1], Petek Ayda Ustaömer[2], Alastair H.F. Robertson[3], Axel Gerdes[4]

[1]Department of Geology, Faculty of Engineering, İstanbul University-Cerrahpaşa, 34320 Avcılar, Istanbul, Turkey; timur@istanbul.edu.tr

[2]Natural Sciences Research Centre, Yıldız Technical University, Davutpaşa-Esenler, İstanbul, Turkey

[3]School of GeoSciences, University of Edinburgh, James Hutton Road, Edinburgh EH9 3FE, UK

[4]Department of Geosciences, Goethe University-Frankfurt, Frankfurt, Germany

Abstract

Zircons from Carboniferous sandstones (three samples) and Mid-Late Triassic sandstones (four samples) from the Tauride and Anatolide continental units were analysed for U-Pb-Hf isotopes. For comparison, zircons were also analysed from Carboniferous granites of the Afyon Zone, Anatolides (three samples). A NE African/Arabian source is inferred for both the Carboniferous sandstones of the Taurides (Aladağ) and the Anatolides (Konya Complex). In contrast, the Carboniferous Karaburun Melange is characterised by a NW African provenance. A prominent Devonian population occurs in the Carboniferous Karaburun Melange, characterised by mainly positive $\varepsilon_{Hf(t)}$ values that differ significantly from those of the Devonian granites of the Sakarya continental crustal unit (Pontides). Middle-Late Triassic Tauride sandstones include minor Paleozoic and Early Mesozoic zircons. In contrast, Devonian and Carboniferous zircons are relatively abundant in Late Triassic sandstones of the Karaburun Peninsula. The Hf isotopic compositions of 25 Carboniferous-aged zircons from three samples of Mid-Late Triassic sandstone and one of Late Carboniferous age (one sample) overlap with the $\varepsilon_{Hf(t)}$ values of Carboniferous arc-type granites in the Anatolides. Taking account of the available U-Pb and Lu-Hf isotopic data from comparative crustal units, the Devonian zircon populations from the melanges in the Karaburun Peninsula and the Konya Complex are inferred to have a westerly source (e.g. granitic rocks of Aegean region or central European). A tectonic model is proposed in which Paleozoic Tethys sutured during the late Carboniferous in the west (Aegean region westwards), leaving an eastward-widening oceanic gulf in which sandstone turbidites accumulated, including Devonian zircons.

Key Words: *provenance, sandstone, detrital zircon, U-Pb & Lu-Hf isotopes, Taurides, Anatolides, Gondwana, late Carboniferous, Late Triassic; Tethys*

1. Introduction

Detrital zircon geochronology is a well-established technique for the study of sandstone provenance (Davis *et al.* 2003; Fedo *et al.* 2003). The potential is significantly enhanced when Lu-Hf isotopic analysis is included, as this helps to distinguish crustal types (Hawkesworth and Kemp 2006a, b; Kemp *et al.* 2006). Interpretation is most effective when zircon U-Pb and Lu-Hf data are combined and compared with continental source units that have well-dated and isotopically characterised zircon populations (e.g. Linnemann *et al.* 2014, Henderson et al. 2016). However, clear-cut compositional source differences may not exist within different parts of all orogenic belts. For example, Anatolia is made up of continental and oceanic units that were progressively assembled from Late Precambrian to Neogene time (e.g. Şengör and Yılmaz 1981; Robertson and Dixon 1984; Moix *et al.* 2008; Robertson *et al.* 2012). Several continental fragments detached from Gondwana, drifted across Tethys and accreted to Eurasia during Paleozoic-Eocene time (Stampfli 2000; Stampfli *et al.* 2001; Robertson *et al.* 2004; Okay *et al.* 2006). As a result, the sedimentary provenance, as represented by detrital zircon age and Lu-Hf data is likely to be complex, variable and may not simply fingerprint opposing continents.

By the late Carboniferous to Late Triassic, the main time interval considered here, Gondwana-derived continental crust existed both to the south and to the north of Tethyan oceanic crust (P.A. Ustaömer *et al.* 2011, 2012a; Ustaömer *et al.* 2013, 2016a). Identification of Gondwanan vs. Eurasian provenance cannot therefore rely solely on the recognition of distinctive Precambrian Gondwana-derived detrital zircon populations but must account of all of the geological evidence from the region. Anatolia experienced significant episodes of continental margin and/or or oceanic arc volcanism, especially during Late Palaeozoic-Triassic time, which provided distinctive age populations and crustal signatures. However, potential source arcs are exotic terranes of debatable position with regard to Gondwana or

Eurasia. Additional clues to provenance are nevertheless provided by minor Late Paleozoic-early Mesozoic zircon populations and related Lu-Hf data, as presented here, which fingerprint specific tectonic-magmatic events.

With the above challenges in mind, we have selected two key time periods that are critical to the regional tectonic reconstruction of Gondwana and Eurasia, and that include sandstones with zircons suitable for isotopic analysis. The area sampled extends over c. 800 km E-W (Fig. 1). The first of these time periods is the late Carboniferous when subduction of Paleotethys took place (Şengör *et al.* 1984; Robertson and Dixon, l984; Ustaömer and Robertson l993; Pickett and Robertson, 1996; Göncüoğlu *et al.* 2000). The second time period, the Mid-Late Triassic, was characterised by rifting of Neotethys along the north margin of Gondwana and further subduction of Paleotethys (Göncüoğlu *et al.* 2003; Robertson *et al.* 2004**)**.

Here, building on initially reported results (Ustaömer *et al.* 2012, 2016b, 2018), we have the following specific objectives:

1. To provide a reference for zircon populations of the largest existing crustal unit in the region, namely the Tauride continental unit (Tauride microcontinent), which extends over > 1300 km E-W, by combining new and existing data;

2. To test whether the Tauride continental unit shows a close compositional affinity with Gondwana to the south, and if so, which part.

3. To compare the zircon geochronology of the Tauride continental unit with the adjacent Anatolide continental unit, which itself comprises both the Afyon Zone and the Tavşanlı Zone, that together make up the Anatolide continental unit (Fig. 1).

4. To infer the crustal composition and age of Carboniferous arc-related granitic rocks in the region, using a combination of new and existing data.

5. To use new Lu-Hf isotopic data to help test whether crustal units of similar age are actually likely to be of similar provenance, and to help indicate where suitable source units may be located.

6. To synthesise the new and existing U-Pb and Lu-Hf isotopic data and thereby test several alternative regional tectonic models. Different published models imply northward subduction, southward subduction or dual subduction of Paleotethys, and also models in which Paleotethys was either closed in the west by latest Carboniferous or remained open throughout the Mediterranean region until Late Triassic time. In addition, many models consider the Taurides and the Anatolides (including both the Afyon Zone and the Tavşanlı Zone) to represent different parts of a single Gondwana-related continent (Anatolide-Tauride Block) (Şengör and Yılmaz 1981; Okay and Tüysüz 1999; Robertson et al. 2005). However, other tectonic models infer that the Anatolide continental unit was located along the southern margin of Eurasia during the Late Paleozoic until it rifted, drifted southwards and collided with the Taurides during the Late Triassic (Stampfli 2000; Stampfli *et al.* 2001; Eren et al. 2004).

2. Methods and data reduction

Three Late Carboniferous and four Late Triassic sandstones, together with three Carboniferous metagranites, were sampled from geologically well-constrained units (Figs. 1, 2; see Supplementary Table 1 for GPS coordinates of the samples). Geological maps of the sample locations are included in the Supplementary material.

Zircon grains were extracted at the Department of Geology, İstanbul University-Cerrahpaşa. The samples were first cut into slices and altered edges were removed. The slices were then crushed twice and further reduced in a roller mill. This was followed by washing and drying in an oven at 70 °C for c. 10 hours. The dry samples were then sieved using mesh sizes of 63 µm, 125 µm, 250 µm, 500 µm, 1 mm and 2 mm. The sieves were shaken mechanically for 30 minutes for each sample. Individual size fractions were stored in plastic bags. Samples with size fractions of <500 µm were further processed using a Frantz magnetic separator and heavy liquid (sodium polytungstate) separation. The zircons were then handpicked, mounted in epoxy tablets and polished, followed by cathodoluminescence (CL) imaging and isotopic analyses. The CL images were obtained using a SEM Jeol JSM-6490, equipped with Gatan MiniCL at Goethe University Frankfurt (GUF). Selected cathodoluminescence images of the detrital zircons are included in the supplementary material.

Uranium, thorium and lead isotope analyzes were carried out by laser ablation-inductively coupled plasma-mass spectrometry (LA-ICP-MS) at GUF, using a slight modification of the method previously reported in Gerdes & Zeh (2006, 2009) and Zeh & Gerdes (2012). A ThermoScientific Element 2 sector field ICP-MS was coupled to a Resolution S-155 (Resonetics) 193 nm ArF Excimer laser (CompexPro 102, Coherent), equipped with a two-volume ablation cell (Laurin Technic, Australia). The laser was fired with 5.5 Hz at a fluence of about 3 J cm^{-2}. The above configuration, using a spot size of 26µm and a depth penetration of 0.6µm s^{-1}, yielded a sensitivity of 9000-13000 cps/µg g^{-1} for ^{238}U. Raw data were corrected offline for background signal, common Pb, laser-induced elemental fractionation, instrumental mass discrimination, and time-dependent elemental fractionation of Pb/U using an in-house MS Excel© spreadsheet program (Gerdes & Zeh 2006, 2009). Laser-induced elemental fractionation and instrumental mass discrimination

were corrected by normalization to a reference zircon GJ-1 (0.0982 ± 0.0003; ID-TIMS GUF value). Repeated analyses of the reference zircon Plesovice, Felix and 91500 (Slama *et al.* 2008; Millonig *et al*. 2012; Wiedenbeck *et al.* 1995) during the same analytical session yielded an accuracy of 1% and a reproducibility of <2% (2 SD). All uncertainties are reported at 2σ level. The data are summarised in Supplementary Tables 2 and 3 (see Supplementary Table 4 for the whole data set).

Hafnium isotope measurements were performed using a Thermo-Finnigan NEPTUNE multi collector ICP-MS at GUF, coupled to the Resolution M50 193nm ArF Excimer (Resonetics) laser system following the method described by Gerdes and Zeh (2006, 2009). Spots of 40 µm in diameter were drilled with a repetition rate of 5.5 Hz and an energy density of 6 J/cm^2 during 50s of data acquisition. The instrumental mass bias for Hf isotopes was corrected using the exponential law and a $^{179}Hf/^{177}Hf$ value of 0.7325. For Yb isotopes, the mass bias was corrected using the Hf mass bias of the individual integration step multiplied by a daily βHf/βYb offset factor (Gerdes and Zeh 2009). All data were adjusted relative to the JMC475 of $^{176}Hf/^{177}Hf$ ratio = 0.282160. The quoted uncertainties are quadratic additions of the within-run precision of each analysis combined with the reproducibility of the JMC475 (2SD = 0.0028%, n = 8). The accuracy and the daily reproducibility of the method were verified by repeated analysis of the reference zircon GJ-1, Plesovice, and Temora (see Supplementary Table 5), which yielded $^{176}Hf/^{177}Hf$ of 0.282007 ±0.000025 (2 SD, n=55), 0.282475 ±0.000016 (n=33), and 0.282682 ±0.000028 (n=22), respectively. This is in very good agreement with previously published results (e.g., Gerdes and Zeh, 2006; Slama *et al*. 2008) and with the LA-MC-ICPMS long-term average of GJ-1 (0.282010 ±0.000025; n > 800), Plesovice (0.282483 ±0.000025, n > 300), and Temora (0.282483 ±0.000023, n > 250) reference zircons at GUF.

The initial $^{176}Hf/^{177}Hf$ values are expressed as εHf(t), which is calculated using a decay constant value of 1.867×10−11 year^{-1}, CHUR after Bouvier *et al.* (2008) $^{176}Hf/^{177}Hf_{CHUR,today}$ = 0.282785 and $^{176}Lu/^{177}Hf_{CHUR,today}$ = 0.0336) and the apparent U-Pb ages obtained for the respective domains (see Supplementary Table 5). For the calculation of Hf two-stage model ages (T_{DM}) in billion years, the measured $^{176}Lu/^{177}Hf$ of each spot (first stage = age of zircon), a value of 0.0113 for the average continental crust, and a depleted mantle $^{176}Lu/^{177}Lu_{DM}$ = 0.0384 and $^{176}Hf/^{177}Hf_{DM}$ = 0.28315 (average MORB; Chauvel *et al.* 2008) were all used. The data are summarised in Supplementary Tables 2 and 3 (see Supplementary Table 5 for the whole data set).

The degree of concordance was calculated using the $^{206}Pb/^{238}U$ and the $^{207}Pb/^{206}Pb$ ages. The calculated ages are considered to be valid when they are 90-110% concordant. $^{206}Pb/^{238}U$ ages are used for <1 Ga, whereas $^{207}Pb/^{206}Pb$ ages are used for >1 Ga (see Supplementary material). The age data obtained during this study are illustrated as concordia plots and as density and kernel density estimate plots which highlight the different zircon populations.

The $(^{176}Hf/^{177}Hf)_i$ ratio was calculated from a series of measured isotopes of Yb, Lu and Hf (Supplementary Table 5), as described by Gerdes and Zeh (2006, 2009). $\varepsilon_{Hf(t)}$ represents the deviation of $^{176}Hf/^{177}Hf$ from the chondritic (CHUR) values for the calculated U-Pb ages of the samples studied. Positive values indicate mantle-derived melts with or without crustal influence, whereas negative values are indicative of recycled, old crust-derived melts. The data obtained are displayed on U-Pb age (Ma) versus $\varepsilon_{Hf(t)}$ plots and are compared with the evolution of different geochemical reservoirs including CHUR, depleted mantle and continental crust of various ages. The CHUR line (zero) separates positive and negative $\varepsilon_{Hf(t)}$ values. The depleted mantle array is also marked (DM). The line of the mantle array represents new crust, for example, juvenile crust forms close to the mantle array (see

Dhuime *et al.* 2011 for an explanation of the method). With time, the isotopic ratio evolves parallel to the average crustal evolution trend. In principle, different age populations can have different crustal origins and therefore the Lu-Hf isotopic data are reported below for each of the age populations that were identified in the different geological units.

The new data are displayed in full in Supplementary Tables 2 and 3 in the following categories: number of spots analysed; number of concordant results; age ranges (oldest to youngest); maximum age of deposition; major populations, peak ages (for main populations) and $\varepsilon_{Hf(t)}$ values (for each prominent population); percentage of zircons with $\varepsilon_{Hf(t)}$. Small data clusters are also highlighted. Lu-Hf data are available for the majority of the radiometrically dated sandstones.

The geochronological plots were produced using the spreadsheets ISOPLOT (Ludwig 2003) and Density Plotter (Vermeesch 2012).

The International Stratigraphic Chart of the International Commission on Stratigraphy is used here for the timescale (Cohen *et al.* 2013; updated).

3. Results

Our new data are reported moving generally from the east to the west, which takes account of the increased geological complexity of the Aegean region (Fig. 1).

3.1 Tauride sandstones

3.1.1 Eastern Taurides

Although the Tauride crust is widely accepted as a coherent paleo-tectonic unit prior to late Mesozoic time, it nowadays includes both relatively autochthonous and relatively allochthonous units as a result of late Mesozoic-early Cenozoic collision-related deformation

(e.g. Şengör and Yılmaz 1981; Okay and Tüysüz 1999; Robertson *et al.* 2005). Sandstones were studied from the Aladağ Nappe in the Yahyalı area (Figs. 1 and 2 log a). The Aladağ Nappe is interpreted as an eastward extension of the relatively autochthonous eastern Tauride carbonate platform although it is now a relatively allochthonous unit (Tekeli 1980; Tekeli *et al.* 1984). A sample of quartzarenite (orthoquartzite) (see Supplementary Fig. 1) was analysed from near the top of the Köşkdere Formation. A Late Carboniferous age has been assigned to this formation based on the paleontologically determined age of interbedded limestones and the presence of the Early Permian Girvanella zone c. 40 m above the sample locality (Tekeli *et al.* 1984; Ayhan and Lengeranlı 1986). The quartzarenite is made up of silica-cemented, rounded to subrounded quartz grains (>90%), with rare muscovite and opaque minerals. Zircon and tourmaline are accessory phases.

Detrital zircons from one sample of thick-bedded, medium-grained, varicoloured (white, pink, to orange) quartzarenite (S3) were analysed for U-Pb isotopes (Ustaömer *et al.* 2012). The zircons are dominantly well-rounded, which is consistent with prolonged transport from a relatively distal source area and/or several stages of reworking from clastic sedimentary rocks (Fedo *et al.* 2003). A few of the zircons are euhedral or subhedral suggesting nearby derivation. CL images of the zircons (Fig. 3a; see also Supplementary Fig. 2) show that 86% of the crystals are internally homogeneous, whereas the remainder have xenocrystic cores, enveloped by younger zircon. The homogeneous zircons generally show oscillatory zoning, sector zoning and, or complex growth zoning, consistent with an igneous origin (Corfu et al. 2003). Th/U ratios range from 0.01-1.3 (Fig. 4). Xenocrystic cores have rounded margins and commonly exhibit pale or dark grey luminescence without visible zoning, or show weak zoning, consistent with a metamorphic origin (Corfu *et al.* 2003). The Th/U ratios of the individual zircons and where present, the internal zircon

domains (n=22) are <0.1 (Fig. 4). Rare zircon grains show fir tree-type zoning, typical of metamorphic zircons (Corfu *et al.* 2003).

The numerical U-Pb age data are shown as a concordia diagram and as histograms and kernel density plots in Figure 5 a,b. The ages of the metamorphic zircon domains, where present, range from 2487-555 Ma, with Neoproterozoic ages predominating. Zircon percentage abundances are shown in Figure 6. The dominant age population is Tonian-Stenian (40.5%), followed by Ediacaran-Cryogenian (37.8%) and then by Paleoproterozoic (11.7%). There is a small Archean age cluster (9.9%) (see also Supplementary Table 2).

3.1.2 Central Taurides

The Central Taurides are dominated by the Tauride Autochthon (Geyikdağ), as well exposed in the Anamas-Akseki area (Fig. 1). As a composite succession, Precambrian metamorphic rocks are overlain by Cambro-Ordovician quartzitic sandstones, neritic carbonates and shales. There is then a regional unconformity, followed by Carboniferous terrigenous sediments and neritic carbonates. Unconformably above there are then varied Triassic terrigenous clastic sedimentary rocks, and finally the regional-scale Jurassic-Cretaceous Tauride carbonate platform succession (Dumont and Monod 1976; Dumont 1978; Dumont and Kerey 1975; Gutnic *et al*. l979; Özgül *et al.* 1997) (Fig. 2 log b).

Two contrasting siliciclastic successions are exposed in the Anamas-Akseki area (Geyikdağ). The older Kasımlar Formation in the southeast, of Mid-Late Triassic age, comprises deep-marine, normal-graded sandstone-shale turbidites, with occasional interbedded debris-flow deposits (Fig. 2 log b). The younger Üzümdere Formation (c. 60 km to the northwest), of Late Triassic-earliest Jurassic age, is made up of shallow-marine, deltaic to terrestrial limestone, sandstone and conglomerate (Fig. 2 log c). No underlying succession

is exposed in this area; however, the sandstones are overlain by the regional Jurassic-Cretaceous Tauride carbonate platform succession (Monod 1977; Şenel 1996).

3.1.2.1 Kasımlar Formation

Two samples of respectively, fine and coarse-grained sandstone (K.12.75 & K.12.78) were collected from near Kasımlar town (Fig. 1; see Supplementary Fig. 3). They comprise monocrystalline and polycrystalline quartz, muscovite, biotite and phyllite lithoclasts. Zircon crystals occur within muscovite-quartz-bearing detrital grains and also as isolated grains within the matrix.

The first sample (K.12.75) contains both euhedral and variably rounded to well-rounded zircons, all of which show oscillatory zoning but only rarely core and mantle structure. (Fig. 3b, see Supplementary Fig. 4). Th/U ratios range from 0.05-1.95, of which 90% have ratios of 0.2-1 (Fig. 4). Two unzoned zircon rims with pale grey luminescence have ratios of 0.05 and 0.08, typical of metamorphic crystallisation. The zircons in the second sample (K.12.78) are variably rounded, together with a few euhedral crystals (see Supplementary Fig. 5). Most have oscillatory zoning and homogeneous internal structure, although a few have core and mantle structure (e.g. Fig. 3b, spots 294 and 346). Some of the zircons have sector zoning and other recrystallization textures (e.g. Fig. 3b, spots 327 and 338). The Th/U ratios of 111 spots analysed range from 0.1-3.86, with 98% being >0.3, indicating a magmatic origin (Fig. 4).

The age data are displayed as zircon percentage abundances (Fig. 6), and the U-Pb data as a whole as concordia (Fig. 7a, b), histograms and a kernel density estimate plot (Fig. 8 a, b). The dominant age population is Tonian-Stenian (33%), followed by Ediacaran-Cryogenian (29%) and Paleoproterozoic (11%). There are also small clusters of Archean and Paleozoic ages. All of the geological systems from Cambrian to Permian are well-represented

in the two samples (21 and 11 concordant ages, respectively). One of the samples (K.12.78) includes two Triassic (Anisian-Ladinian) zircons. Lu-Hf analyses of the two sandstone samples are plotted on an age (Ma) vs. $\varepsilon_{Hf(t)}$ diagram in Figure 9 a-b. The major populations exhibit highly evolved to strongly juvenile $\varepsilon_{Hf(t)}$ values (see Supplementary Table 3).

3.1.2.2 Üzümdere Formation

The sample from the Üzümdere Formation (K.13.77) was collected from typical thick-bedded, reddish-brown, medium-grained sandstone (see Fig. 1 and also Supplementary Fig. 6 for sample location). Angular to sub-rounded grains of felsic volcanic rocks, quartz mica schists, chert and quartzite occur in decreasing order of abundance. Zircons are variably rounded and show oscillatory growth zoning; sector zoning is locally present (e.g. Fig. 3c; see Supplementary Fig. 7). In some cases, zoning is poorly defined or complex (see also Supplementary material). Th/U ratios range from 0.05-3.78, consistent with an igneous origin; however, a single grain has a ratio of 0.05, indicative of a metamorphic origin (Fig. 4).

The zircon percentage abundances are shown in Figure 6, and the U-Pb concordia diagram in Fig. 7c; histograms and also kernel density estimates for the U-Pb data are in Figure 8c. The dominant age population is Ediacaran-Cryogenian (30%), followed by Tonian-Stenian (22.6) and Cambrian (18.3%). Paleoproterozoic (12.9%) and Ordovician zircons form small clusters. Plotted on an age (Ma) vs. $\varepsilon_{Hf(t)}$ diagram (Fig. 9c), the Lu-Hf data for the major populations exhibit highly evolved to strongly juvenile $\varepsilon_{Hf(t)}$ values (see also Supplementary Table 3).

3.1.3 Anatolides

The Afyon Zone, the more southerly of the two crustal units making up the Anatolide continental unit includes a structurally complex, composite unit which outcrops northwest of

the major city of Konya (Fig. 1). The Afyon Zone was metamorphosed to high-P/low-T conditions during Paleocene time (Candan *et al.* 2005; Pourteau *et al*. 2010, 2013; Özdamar *et al.* 2013).

3.1.3.1 Konya Complex

The Konya Complex encompasses an intact Late Silurian-early Carboniferous carbonate platform succession, which is depositionally overlain by a Carboniferous melange (Fig. 2 log d). The melange includes blocks of black ribbon chert and recrystallized neritic to pelagic limestone of Silurian, Devonian and Carboniferous ages, together with volumetrically minor basic igneous rocks (e.g., basalt, gabbro). The melange is unconformably overlain by non-marine to shallow-marine mixed terrigenous-carbonate sediments of Triassic age, with the addition of basic to felsic alkaline volcanic rocks in some areas (Özcan *et al. 1990*; Eren *et al.* 2004; Göncüoğlu *et al.* 2000, 2007; Candan *et al*. 2009; Robertson and Ustaömer 2009a, 2011; Akal *et al.* 2012; Güven *et al.* 2012; Özdamar *et al.* 2013; see also Supplementary Fig. 8).

One sample (K13.75) of medium-bedded, medium-grained sandstone was analysed from the Carboniferous melange matrix (Fig. 1 and Supplementary Fig. 8). This is dominated by polycrystalline and monocrystalline quartz, plagioclase, quartzite and granite, together with minor zircon and tourmaline. Most zircons are rounded, together with a small number of euhedral grains. Most grains show oscillatory zoning, consistent with a magmatic origin (Fig. 3d; see Supplementary Fig. 9). Some CL images have sector zoning, post-crystallisation alteration, or recrystallisation textures, although some crystals lack internal zoning. Core and mantle structure is occasionally present but without zoning in the mantle rims. Th/U ratios of <0.1 in the rims indicate a metamorphic origin (Fig. 4). The Th/U ratios of analysed spots range from 0.04-2.58 and, together with oscillatory zoning, indicate an igneous origin.

Concordant ages from the metamorphic rims of the zircons range from 635-555 Ma (Ediacaran). U-Pb concordia plots, histograms and kernel density estimates are shown in Figure 5c-d, and zircon percentage abundances in Figure 6 (see also Supplementary Table 2). The dominant population is Tonian-Stenian-aged (43%), followed by Ediacaran-Cryogenian (34%) then Paleoproterozoic (12.2%). Small clusters of Archean and Cambro-Ordovician age also occur. When plotted on an age (Ma) vs. $\varepsilon_{Hf(t)}$ diagram, the major populations indicated by the Lu-Hf analyses exhibit highly evolved to strongly juvenile $\varepsilon_{Hf(t)}$ values (Fig. 10a; see also Supplementary Table 2).

3.1.4 Karaburun Peninsula

The Karaburun Peninsula of westernmost (Aegean) Turkey (Fig. 1; Supplementary Fig. 10) is dominated by a Paleozoic melange with a Mesozoic cover succession of rift-related and platform carbonates (Erdoğan 1990; Erdoğan *et al.* 1990; Robertson and Pickett 2000; Robertson and Ustaömer 2009b; Okay *et al.* 2012). The melange is cut by a small (<1 km in diameter) Early Triassic granite (Akal *et al.* 2011; Ustaömer *et al.* 2016).

Although unmetamorphosed, the Paleozoic-Mesozoic of the Karaburun Peninsula is treated below as a separate tectonic unit from the Taurides because there is no unbroken outcrop continuity between the two areas. However, the two crustal bodies can be broadly correlated based mainly on the presence of similar Mesozoic carbonate platform successions (Erdoğan 1990; Erdoğan *et al.* 1990; Robertson and Pickett 2000; Okay *et al.* 2012).

3.1.4.1 Karaburun Melange

The melange, which has no exposed base (Fig. 2 log e), is dominated by Silurian, Devonian and Carboniferous blocks of neritic to pelagic limestone, black ribbon chert and rare basic to intermediate-composition extrusive igneous rocks (Kozur 1997, 1998; Robertson and Ustaömer 2009b). Blocks of Silurian-Devonian pelagic carbonates are rich in

cephalopods, similar to coeval counterparts in the Taurides (Göncüoğlu *et al.* 2007). The melange matrix is unfossiliferous. However, recent detrital zircon age dating suggests a Permian-Carboniferous age (Löwen *et al.* 2017; see below). The matrix is dominated by lithoclastic sandstone turbidites together with some debris-flow deposits. The melange is unconformably overlain by an Early Triassic succession, mostly conglomerate and neritic to pelagic limestone, radiolarian chert and alkaline volcanic-rocks (Erdoğan *et al.* 1990; Robertson and Pickett, 2000; Robertson and Ustaömer 2009 a, b, 2011).

A sample (K.13.102) of medium to thick-bedded pebbly sandstone was collected from the melange matrix in the northern part of the Karaburun Peninsula (Fig. 2 log e). The sandstone is poorly sorted with angular grains set in a fine-grained matrix. The main components are polycrystalline quartz, chert, granite and quartz-chlorite-muscovite schist fragments. The granitic grains are dominated by quartz, plagioclase and orthoclase. Less common volcanic rocks fragments include quartz phenocrysts, set in a recrystallized felsic matrix. Monocrystalline quartz grains exhibit undulose extinction and deformation lamellae. Zircons occur within some quartz grains in the form of thin, elongate euhedral inclusions. In contrast, zircons in the matrix are commonly rounded.

Although some zircons lack internal zoning, most show oscillatory zoning or, rarely, convolute zoning**,** complex growth zoning, or sector zoning (Fig. 3e; see Supplementary Fig. 11). In some cases, grain margins are recrystallized (although the grain size was too small to analyse). A few zircons have xenocrystic core and mantle structure, with either one or two growth envelopes of metamorphic origin. Th/U ratios range from 0.01-1.51 (Fig. 4). Two values (0.05 and 0.01) are indicative of a metamorphic origin, for which the U-Pb ages are 572 Ma (Ediacaran) and 2600 Ma (Palaeo-Proterozoic).

U-Pb Concordia, histogram and kernel density estimate diagrams of the detrital zircons are shown in Figure 5e, f and their percentage abundances in Figure 6. The dominant population is Devonian (30.9%), followed by Paleoproterozoic (26.8%) and then Ediacaran-Cryogenian (20.6%). Small clusters of Archean age also occur in this sample. For the Lu-Hf analyses, on the age (Ma) vs. $\varepsilon_{Hf(t)}$ diagram (Fig. 10b), 60% of the Devonian population exhibits superchondritic $\varepsilon_{Hf(t)}$ values, whereas the other major populations have highly evolved to strongly juvenile $\varepsilon_{Hf(t)}$ values (see also Supplementary Table 2).

3.1.4.2 *Güvercinlik Formation*

The cover succession in the Karaburun Peninsula includes an intact succession of Late Triassic sandstones, named the Güvercinlik Formation, which allows close comparison with the sandstones of similar age in the adjacent Taurides (see above). The Güvercinlik Formation includes fluvio-deltaic to shallow-marine mudrocks, sandstones and minor coarser-grained clastic sedimentary rocks. The formation can be correlated with the regionally distributed Çayır Formation which is of latest Triassic-Early Liassic age throughout the Tauride autochthon (Geyikdağ), and also within parts of the associated (relatively allochthonous) Bolkar and Hadim Nappes (Monod and Akay 1984; Erdoğan 1990; Robertson and Pickett 2000; Çakmakoğlu and Bilgin 2006; Mackintosh and Robertson, 2009).

One sample of red, poorly sorted, fine to medium-grained non-marine sandstone (K.13.104) was collected from the Late Triassic Güvercinlik Formation (Fig. 2 log e; see Supplementary Fig. 10). The sandstone contains monocrystalline and polycrystalline quartz, together with rare lithoclasts of phyllite and felsic volcanic rocks. Zircons, ranging from rounded to subhedral, were observed in the matrix (Fig. 3f; see Supplementary Fig. 12). Oscillatory zoning predominates indicative of a magmatic origin. Most grains have a

homogeneous internal fabric but a few have core and mantle structure. Th/U ratios range from 0.05-2.26, of which four values are <0.1, consistent with a metamorphic origin (Fig. 4). The zircon percentage abundances (Fig. 6), U-Pb concordia (Fig. 7d) and both the histogram and kernel density estimates (Fig. 8d) indicate that three populations of equal size (20.9%) dominate the sample; i.e. Carboniferous, Ediacaran-Cryogenian and Paleoproterozoic. There is also a subordinate Tonian-Stenian population (16.3%) and small clusters of Archean, Devonian (30.9%) and Cambro-Ordovician ages (Fig. 6). In the age (Ma) versus $\varepsilon_{Hf(t)}$ diagram (Fig. 9d), the major Carboniferous population exhibits evolved $\varepsilon_{Hf(t)}$ values, whereas the other major populations have highly evolved to strongly juvenile $\varepsilon_{Hf(t)}$ values (Fig. 9d). Only 23% of the zircons exhibit positive $\varepsilon_{Hf(t)}$ values (see Supplementary Table 3). The main juvenile zircon formation events occurred at 2.1 Ga (Palaeoproterozoic), 0.8-0.5 Ga (Neoproterozoic) and 354 Ma (earliest Carboniferous).

3.2 Carboniferous granitic rock data

To supplement the age data for potential source rocks in the region, we analysed zircons from Late Paleozoic granites of the Afyon Zone (Anatolide continental unit), in which the host rocks are quartzite, phyllite and meta-carbonates (Fig. 1). Candan *et al.* (2016) have recently reported several small (km-sized) isolated plutons of Carboniferous porphyritic and granoblastic metagranite from the Simav-Alaçam area, near the northwestern margin of the Afyon Zone (Fig. 1; Supplementary Fig. 13). Seven different bodies were recently dated by the zircon U-Pb method (Candan *et al.* 2016), yielding 330-315 Ma for porphyritic metagranites (three samples) and ~320 Ma for granoblastic metagranites (two samples).

To test and extend the available age data, we sampled one each of the previously dated porphyritic (TM.17.33) and granoblastic (TM.17.35) metagranites and also collected a sample from an undated nearby porphyritic metagranite (TM.17.34; see Supplementary Fig.

13 for sample locations). Our new Lu-Hf isotopic data from these granitic rocks shed light on the possible provenance of the Carboniferous and Triassic sandstones studied and other crustal units in the region.

Our new U-Pb ages (see Supplementary material for the whole data set) for the metagranites yielded Carboniferous crystallisation ages, consistent with the previous results (Candan *et al.* 2016). Two porphyritic metagranite samples, one of which was dated at 314.9±2.4 Ma by Candan *et al.* (2016), gave TuffZirc ages of 313.24 +1.43 -0.68 Ma (TM.17.33) and 316.00 +0.81 -0.88 Ma (TM.17.34), respectively. Zircons from the porphyritic metagranites are homogenous, except for TM.17.33 that contains one inherited zircon of Devonian age (400±3 Ma; 92% concordant). Zircons from a granoblastic metagranite intrusion (TM.17.35) that was previously dated at 321.9±2.6 Ma (Candan *et al.* 2016) are dominated by core and mantle-type zircons, indicating the role of crustal melting. Some homogenous zircons and the rims of the core and mantle-type zircons yielded Carboniferous ages ranging from 343 to 313 Ma. Th/U ratios of some of the rims are <0.1, suggesting a metamorphic origin. The ages of the metamorphic rims are variable but some are dated at <319 Ma. The density probability curve for the Carboniferous igneous zircon domains (see Supplementary material) produced two peaks, at 332.9±1.9 Ma and 323.4±1.9 Ma. The younger age is interpreted as the crystallisation age of the pluton and the older age an earlier magmatic event. The ages of the inherited cores range from 3095 Ma (Mesoarchean) to 361 Ma (Upper Devonian). Five of the zircon cores are Devonian (391 to 371 Ma), two Ordovician (~456 Ma), 10 Ediacaran (628 to 550 Ma), and five others have older ages. Of the few Carboniferous ages in this sample some have very low Th/U contents (<0.1) suggesting that the metagranite was affected by late Carboniferous metamorphism.

On the age (Ma) vs. $\varepsilon_{Hf(t)}$ diagram (Fig. 11), the U-Pb-Hf isotopic measurements indicate that all of the metagranite samples have subchondritic $\varepsilon_{Hf(t)}$ values, ranging from -

12.6 to -5.3 in sample TM.17.35, from -17.6 to -4.9 in sample TM.17.33 and from -9.4 to -3.2 in sample TM.17.34, indicating a crustal origin for the Carboniferous felsic magmatism. Hf model ages range from 2.11 to 1.33 Ga.

4. Previous U-Pb and Lu-Hf zircon data

We now summarise previous data from the Tauride and Anatolide continental units and the Karaburun Melange to enable synthesis and regional comparison of the different tectonic units.

4.1 Tauride units

U-Pb-Hf analyses are available for eight samples of the Neoproterozoic metamorphic basement of the Tauride autochthon (Dipoyraz Dağ), and for four samples of sandstone from its Paleozoic-Early Mesozoic sedimentary cover (Abbo *et al.* 2015) (Fig. 1). One of these samples is from the Kasımlar Formation in the Karacahisar area, c. 25 km northeast of the two samples studied by us. This sample is dominated by Neoproterozoic-aged zircons, together with a single concordant Permian zircon.

Sandstones of Cambro-Ordovician age were collected from the northern part of the Tauride autochthon during this study (i.e. Seydişehir Formation) but unfortunately did not yield usable zircons. However, some U-Pb detrital zircon data do exist for Late Ordovician glacial sediments (diamictites and lonestones) that are exposed in the Central and Eastern Taurides (four samples) and also in the Arabian Platform of SE Turkey (one sample) (Gürsu *et al.* 2017). The major zircon populations in these samples are Neoproterozoic with minor clusters of Paleoproterozoic and Archean age.

4.2 Menderes Massif

The Menderes Massif is a regional-scale metamorphic assemblage in western Anatolia (Fig. 1) that is dominated by Paleozoic schist and Mesozoic meta-carbonate rocks, with a Precambrian high-grade metamorphic basement (Okay 2001; Özer *et al.* 2001; Candan 2011).

U-Pb-Hf zircon data are available for both the Neoproterozoic basement schists and paragneisses (six samples), and the overlying Early Paleozoic meta-siliciclastic succession (three samples) (Zlatkin *et al.* 2013). The overall age range of the main zircon populations resembles that from the Tauride basement in the Karacahisar area (Abbo *et al.* 2015; see above) although individual age populations vary. The maximum depositional age of the basement schists is constrained as Late Ediacaran (570- 550 Ma), as indicated by the age of the youngest detrital zircons in the schists (570 Ma) and the age of cross-cutting felsic intrusions (550 Ma). In contrast to the Karacahisar area, the basement schists in the Menderes Massif appear to have received little input from 1.0 (Tonian) and 2.5 Ga (Paleoproterozoic) crustal units. The detrital zircon age spectra of the overlying Early Paleozoic meta-siliciclastic sediments resemble those of Ordovician sandstones in Jordan (Morag et al. 2011).

4.3 Karaburun Peninsula

U-Pb detrital zircon ages have been reported from siliciclastic sandstones of the Karaburun Melange and related formations of Late Paleozoic and Early Mesozoic ages (15 samples) (Löwen *et al.* 2017). U-Pb ages range from Archean to Triassic in these sandstones. Permo-Carboniferous, Devonian, Silurian, Ordovician and Late Neoproterozoic zircon populations were used to infer source areas. The authors assumed that the north-Gondwana margin was magmatically inactive since the Cambrian, and that it remained isolated from lithologies affected by the Variscan orogeny. The provenance was therefore considered to be

from the north, from the Sakarya, Pelagonian and/or Rhodope zones of western Turkey, Greece and, or Bulgaria. Two samples from the Karaburun Melange (Dikendağı Formation of Löwen *et al.* 2017) have very similar populations to those in the Palaeozoic and Mesozoic siliciclastic sediments of the Taurides and the Afyon Zone (Konya Complex melange), as reported here.

4.4 Konya Complex

U-Pb detrital zircon ages from meta-sandstones of the clastic upper part of the Konya Complex (six samples) and the overlying early Mesozoic sedimentary cover (two samples) were recently reported by Löwen et al. (2019). These authors subdivided the clastic upper part of the complex into two parts: a lower melange unit and an overlying 'flysch' unit. In summarising their data below we use the same criteria for concordance as we do with our data. On this basis, the ages of detrital zircon populations of the three samples from the melange unit is identical to the one sample (K.13.75) reported in this study (i.e. Silurian, Ordovician, Cambrian and Precambrian), although the number of zircons in individual populations vary from sample to sample. The overlying 'flysch' unit, on the other hand, differs from the melange unit with a variable input (53%-T.14.36, 22%-T.14.39 and 2%-T.14.22) from a Devonian igneous provenance. Two of their samples with Devonian zircons also contain Tonian-Stenian (0.8-1.1 Ga) zircons, whereas the remaining one lacks a Tonian-Stenian population, similar to our Karaburun melange sample. The maximum age of deposition based on the youngest concordant detrital zircon is Silurian (423 Ma) for the melange unit and Carboniferous (308 Ma) for the 'flysch' unit. As for the Karaburun melange, Löwen et al. (2019) envisage the Devonian granites of the Sakarya Zones (Eurasia) as the source of the Devonian detrital zircons in their 'flysch' unit, whereas the melange matrix was sourced from the N-Gondwana margin.

The two Triassic sandstone samples (T.14.29 and T.14.30) of Löwen *et al.* (2019) yielded abundant Permian (275 Ma) to Triassic (206 Ma) zircons (90% of the whole data) but no Devonian zircons and only six grains of Precambrian zircons. The Permo-Triassic zircon population is characterised by a high-U content in one of the samples. The authors suggest that the source of the Triassic zircons was the S-Eurasian margin. However, there are alternatives. For example, volcanic rocks (meta-trachyandesite, meta-rhyolites) alternate with red, continental clastics in the Kadınhanı-Konya area. Available geochronological data indicates that the volcanism in this area took place during Permian (~259 Ma) to Triassic (~220 Ma) (Akal *et al.* 2012, Güven *et al*. 2012; Ustaömer *et al.* 2016; Özdamar *et al.* 2013), similar to the age range of the Permo-Triassic detrital zircons. However, a detailed comparison of the Permian-Triassic detrital zircons and lavas is not yet possible because Hf data are available only for a few of the lavas (Ustaömer *et al.* 2016a).

5. Discussion

Below, we consider the implications of the combined new and published U-Pb and Lu-Hf data for the provenance, paleogeography and tectonic setting of the Carboniferous and Triassic units studied, and the regional development of Tethys. In the discussion, we assume that there has been, at most, only modest (several hundred kms) E-W lateral (strike-slip) displacement of the Gondwana versus Eurasian crustal units, which is compatible with Pangea-A-type reconstructions (e.g. Garfunkel, 2004; Smith, 2006). However, we exclude consideration of Pangea-A type reconstructions which infer thousands of kms of relative displacement because of absence of definite supporting geological evidence (e.g. Muttoni *et al.* 2003).

5.1 N Gondwana provenance

The Precambrian age populations (i.e. Edicaran and Tonian) from the Tauride units as a whole are effectively identical to those of the NE African-Arabian shield (Ustaömer *et al.* 2012, 2016, 2018; Zlatkin *et al.* 2013; Abbo *et al.* 2015; Gürsu *et al.* 2017). Most of the new and pre-existing Lu-Hf isotopic data for Neoproterozoic zircons are also consistent with derivation from NE Africa-Arabia.

Our U-Pb data for the Carboniferous sandstones of the matrix of the melange in the Konya Complex (part of the Afyon Zone) show close similarities with the sandstones from the eastern Tauride continental unit (Aladağ Nappe) (Figs. 12, 13). The Aladağ Nappe (Fig. 2 log a) is restored as part of the northern margin of the Tauride microcontinent in view of its stratigraphic similarities with the Tauride continental unit as a whole (Tekeli 1980; Özgül 1976). Detrital zircons from a cobble in the basal conglomerate of the Carboniferous succession in the south-central Taurides (Karacahisar Dome) (Fig. 1**)** have yielded a similar zircon age-distribution population (Abbo *et al.* 2015). In addition, a Devonian zircon population has very recently been reported from the Konya Complex (Löwen *et al.* 2018, 2019).

The source rocks of both the Tauride and the Anatolide Carboniferous sandstones were predominantly Neoproterozoic, with sparse Palaeoproterozoic and Archean zircons (Fig. 13). For the Anatolide continental unit, our Lu-Hf data indicate derivation from a combination of juvenile and evolved sources. Some of the Neoproterozoic zircon populations in the Konya Melange sandstones have juvenile hafnium isotopic signatures, consistent with derivation from a juvenile source like the Arabian-Nubian shield (Robinson *et al.* 2014). The presence of strongly evolved Neoproterozoic zircons is suggestive of derivation from igneous sources formed by mixing of juvenile melts with older continental crust. Overall, the Neoproterozoic zircons are likely to have been derived from diverse sources within the NE Africa-Arabia. The Precambrian zircon populations of the Carboniferous Konya Complex

and the Tauride Kasımlar and Üzümdere formations are effectively identical (Figs. 12, 13), suggesting that the southerly provenance persisted for a very long time period.

The poorly dated Early Paleozoic (i.e., post-Precambrian/pre-Carboniferous) sedimentary cover of the Menderes Massif (Fig. 1) has U-Pb age populations and hafnium isotopic compositions (Zlatkin *et al.* 2013) that are similar to the Tauride and Anatolide continental units. The Menderes Massif has been correlated with the Anatolides (Ketin l964; Şengör and Yılmaz l981) implying that it represents a single crustal block, despite lacking the characteristic Anatolide high-pressure/low-temperature metamorphism (Candan *et al.* 2010; Pourteau *et al.* 2013). Alternatively, it has been suggested that the Menderes Massif was separated from the Anatolide continental unit (to the north) by a sedimentary basin during the Mesozoic (Pourteau *et al.* 2016). In addition, the Menderes Massif is generally accepted to have been separated from the Tauride carbonate platform to the southwest (Bey Dağları) (Fig. 1) by an intra-continental basin (Tavas basin) (Poisson 1977, 1984; Şenel *et al.* 1991; Collins and Robertson, 1998; Robertson *et al.* 2013). In our view, the Menderes Massif is best interpreted as being closely related, compositionally and paleogeographically, to the Tauride continental unit (Özer *et al.* 2001; Robertson *et al.* 2012, 2103; Barrier *et al.* 2018).

Several factors support a dominantly Gondwana-related source for all of the Late Paleozoic-early Mesozoic sandstones mentioned above, other than those of the Karaburun Melange and its cover succession (see below): 1. The Carboniferous and Late Triassic sandstones are all dominated by Late Precambrian zircons; 2. The relative abundance of Cambrian zircons in the Late Triassic Tauride cover succession (Üzümdere Formation) is suggestive of erosion of Cambrian volcanic rocks, as represented by the nearby Sandıklı Porphyroids, near Sandıklı (Fig. 1) (Kröner and Şengör 1990; Gürsu and Göncüoğlu 2006, 2008). Surface uplift related to Triassic rifting of Neotethys liberated the granitic and schistose detritus that now resides within the Triassic sandstones; 3. Granitic intrusions

within the Tauride-related units, for example the Carboniferous meta-granitic rocks of the Afyon Zone (Candan *et al.* 2016; this study) represent a nearby source of Carboniferous grains within the Triassic sandstones; 4. Localised Early Triassic meta-granites in the Menderes Massif (Koralay *et al.* 2001; Ustaömer *et al*. 2016) are possible nearby sources for rare Early Triassic zircons, consistent with their slightly positive $\varepsilon_{Hf(t)}$ signatures as reported by Ustaömer *et al.* 2016 (their fig. 13); 5. The small granite in the Karaburun Peninsula (Akal *et al.* 2011; Ustaömer *et al.* 2016a) could also be considered as a source for the rare Early Triassic zircons, although this seems unlikely because the $\varepsilon_{(Hf)t}$ composition of the Karaburun granite is highly negative in contrast to the Menderes Triassic granite and the two Triassic detrital zircons.

The compositional homogeneity and commonly well-rounded texture of the Precambrian zircon grain populations in both the Tauride and Anatolide sandstones (Fig. 3; see also supplementary material) suggest that the erosional products of the source schistose basement were widely dispersed and well mixed in the shelf seas that prevailed along the north margin of Gondwana. These Gondwana-derived sandstones are well represented by the shallow-marine sandstones of mainly Ordovician-Carboniferous age within the Tauride continental unit (e.g. Geyikdağ) and related allochthonous units (e.g. Bolkar and Hadim Nappes) (Özgül, 1976; Mackintosh and Robertson, 2012; Wehrmann *et al.* 2010). Some of these sandstones are likely to have been derived directly from local basement highs within the Tauride crust (e.g. Sandıklı Massif) (Mackintosh and Robertson, 2012). The distal continental margin (northerly) crust of pre-Jurassic age is largely concealed by the Late Cretaceous-Early Cenozoic southward emplacement of allochthonous continental margin units (e.g., Bozkır, Bolkar and Hadim nappes) and ophiolite-related units. Also, the distal (southward) edge of the Tauride crust is largely concealed by the northward emplacement of the Antalya Complex (Antalya Nappes) in SW Turkey, including both continental margin

and ophiolite-related units. One possibility is that the Cambrian and Ordovician zircons could be explained by pulsed extension of the northern margin of Gondwana, prior to final break-up during the Triassic. On the other hand, the Carboniferous zircons may relate to subsequent subduction-related magmatism, as locally documented in the Afyon Zone (Candan *et al.* 2016).

The Tauride Paleozoic shelf successions were uplifted and locally eroded to produce large volumes of sand during the Triassic rifting of Neotethys. From the Late Permian onwards, the Tauride microcontinent became progressively isolated from Gondwana. Rifting during the late Permian produced shallow, localised marine basins and highs, whereas deep basins formed by Early-Middle Triassic time, followed by regional continental break-up during the Late Triassic-Early Jurassic to form the S Neotethys (Gutnic *et al.* 1979; Robertson and Dixon l984; Garfunkel 2004; Robertson *et al.* 2012, 2013; Barrier *et al.* 2018). The zircons in the Middle-Late Triassic sandstones were, therefore, derived from the Precambrian basement of the Tauride continental unit directly or, more probably, from its Paleozoic cover rather than directly from Gondwana.

5.2 Provenance of Carboniferous zircons

Cambrian, Ordovician, Devonian (minor) and Carboniferous ages are recorded in the Late Triassic Kasımlar and Üzümdere Formations (Figs. 6, 7). As noted above, potential source rocks, for example, felsic igneous rocks are exposed in locally the Anatolide continental unit, including the Cambrian felsic Sandıklı Porphyroids (Gürsu and Göncüoğlu 2005, 2006) and both Ordovician granites (Okay *et al.* 2008; Özbey *et al.* 2013a,b) and Carboniferous granites (Candan *et al.* 2016; this study).

The provenance of the Karaburun Melange and Konya Complex sandstones differs from that of the Tauride Carboniferous units. Devonian zircon populations are reported from

some samples in the Karaburun Melange (Löwen *et al.* 2017) and also from the Konya Complex (Löwen *et al.* 2018, 2019). Devonian-aged zircon cores are also recorded in the one sample of Carboniferous Anatolide granites analysed by us (sample TM.17.35) (Fig. 11). The Triassic cover sandstones in the Karaburun Peninsula also contain a prominent Devonian-Carboniferous zircon population (Löwen *et al.* 2017)(Figs. 8d, 12). In contrast, Devonian zircons are absent from the Eastern Tauride Carboniferous sandstones; conversely, Tonian and Stenian zircons are not recorded in the Karaburun Melange. Paleoproterozoic zircons (c. 2 Ga) are more abundant in the Karaburun Melange sandstones compared to both the Konya Complex and the Eastern Tauride (Aladağ Nappe) sandstones. A clastic source other than NE Africa alone, therefore, seems to be needed for both the Anatolide and Karaburun Melange Carboniferous sandstones.

The Carboniferous and Triassic sandstones have marked similarities suggesting some degree of common provenance, especially the prominent Ediacaran population (Fig. 6). Cryogenian and Tonian-Stenian populations occur in all samples, except for the Karaburun melange sandstone that lacks the 1.1-0.9 Ga zircon population (Fig. 12). 1.1-0.9 Ga zircons exist in the overlying Late Triassic Güvercinlik Formation. However, Neoproterozoic zircon populations are subordinate in the Güvercinlik Formation compared to the Tauride Triassic sandstones (Figs. 6, 12). Also, the Paleoproterozoic population (ca. 2 Ga) in the Karaburun Melange Triassic cover succession is enriched compared to that in the Tauride Triassic sandstones (Figs. 12, 13). The Carboniferous zircon population is similarly enriched in the Late Triassic Karaburun Melange cover sandstones compared to the corresponding Late Triassic Tauride sandstones in which only a few grains of this age range occur. All of the above evidence points to a specific, probably localised, provenance for the Karaburun Melange that is not completely shared by any of the other units discussed above. Similarly, a

local provenance seems possible for the Permian-Triassic zircons in the Konya Complex (e.g. Kadınhanı volcanics).

Below, we evaluate the wider region for suitable source units:

In northern Turkey, the Pontide crustal unit broadly represents the evolving southerly active continental margin of Eurasia, at least during Late Paleozoic to mid-Cenozoic time (Fig. 1). Here, we highlight several lithology and age distributions that may shed light on the provenance of the crustal units farther south.

Within the Pontide crustal unit, the Sakarya Zone (Fig. 1) includes meta-clastic rocks that are dominated by Precambrian zircons of NE Gondwana-Arabia affinities, similar to the Carboniferous sandstones of both the Anatolide and Tauride crustal units (P.A. Ustaömer *et al.* 2012a; Ustaömer *et al.* 2013). Carboniferous zircons in sandstones from the Aegean islands of Chios, Inousses and Psara, adjacent to the Karaburun Peninsula, have been interpreted to represent derivation from the Sakarya Zone, assuming that it then formed part of the S-Eurasian active continental margin (Meinhold *et al.* 2008, Meinhold and Frei 2008). Similarly, Löwen *et al.* (2017) infer the presence of a large amount of arc-derived sand, which they interpret as having been derived from a continental margin arc within the Sakarya Zone. The Late Paleozoic zircons in the Karaburun melange sandstones were, therefore, sourced from the Eurasian active continental margin, effectively to the north in this interpretation. However, potential source Carboniferous crustal units are also widely exposed in the Balkan region and in both central and western Europe, for example the Austro-Alpine and Armorican crustal units (Meinhold *et al.* 2010a, b).

Despite the published correlations with S-Eurasia (Meinhold *et al.* 2010a, b; Löwen *et al.* 2017), a northerly (Eurasian) arc-related source should not necessarily be assumed because, as noted above Carboniferous granitic magmatism also affected the Anatolide

continental unit in the Afyon Zone (Candan *et al*. 2016; this study) and could also exist elsewhere. Minor Carboniferous volcanism is also known from the northern part of the Central Tauride crustal unit (MTA 2002, Göncüoğlu *et al.* 2007; Mackintosh and Robertson 2009) and also in the Tauride-related Çataloturan nappe (Aladağ Nappes) in the Eastern Taurides (Göncüoğlu *et al.* 2007). One possible explanation for the Carboniferous magmatism in the Afyon Zone is that the host crustal unit was part of the S-Eurasian margin, until it rifted and drifted southwards to amalgamate with the Tauride continental unit during late Triassic time (Stampfli, 2000; Stampfli *et al.* 2001; Eren *et al.* 2004). This model has been tested extensively by recent fieldwork; however, this has not confirmed the existence of an oceanic suture (Paleotethyan) between the Anatolide and Tauride continental units (Mackintosh and Robertson, 2012).

An alternative approach is to determine whether the isotopic data from the Carboniferous granites of the Afyon Zone are similar to the isotopic data from the Carboniferous granites of the Sakarya Zone. The available zircon Hf isotopic data for the two Carboniferous granite assemblages are compared in Figure 14. The Lu-Hf isotopic compositions of the Carboniferous zircons of the Anatolide and Tauride sandstones are also plotted. The green dashed line in the figure, corresponding to ca. -5 $\varepsilon_{Hf(t),}$ separates Sakarya crustal unit granites above from the Afyon Zone granites below. The Carboniferous detrital zircons plot in the Afyon Zone granite field, consistent with this as a source for sandstones. Another potential source would be now-eroded volcanic equivalents.

In summary, it is possible that the voluminous Carboniferous arc-derived detritus within the Tauride and Karaburun Triassic sandstones could have a relatively southerly, Gondwana-related provenance. This would remove the requirement to infer sources from both Gondwana and Eurasia within the Carboniferous clastic sediments, right down to the level of individual turbidite beds.

5.3. Provenance of Devonian zircons

Devonian zircons form the most prominent population in the Karaburun Melange sandstones and are also present in the overlying Güvercinlik Formation (Löwen *et al.* 2017; this study) (Fig. 12). A small cluster of Devonian zircons (n=5) also exists in the Kasımlar Formation. Carboniferous sandstones of the Konya Complex (Anatolides) also contain Devonian zircons (Löwen *et al.* 2017) unlike the Tauride Carboniferous sandstones (as so far reported). Also, Devonian inherited zircons are common in the Carboniferous meta-granites of the Afyon Zone (Candan *et al.* 2016; this study) (Fig. 11). Assuming a local source for the Devonian zircons, Devonian zircon-bearing granitic plutons are likely to exist within the unexposed (or simply unexplored) deep-level crust of the Afyon Zone. Such crust could also be buried beneath the Tauride or Anatolide thrust sheets or be eroded. However, the Devonian zircons in the Karaburun Melange are so abundant as to suggest a provenance in the vicinity (i.e. Aegean Turkey) or possibly from farther north, northwest or west.

The Sakarya crustal unit in the NW Turkey locally includes Devonian granites (Okay *et al.* 1996; Aysal *et al.* 2012; Sunal *et al.* 2012), as in the Biga Peninsula (Fig. 1), which can therefore be considered as a possible source of the Devonian zircons in the Karaburun Melange. However, the late Carboniferous sandstones of the Karaburun Peninsula have different $\varepsilon_{Hf(t)}$ values (Fig. 15). The zircons in the Devonian granites define a tight cluster with $\varepsilon_{Hf(t)}$ values ranging from −8.5 to −7.1, other than for one with an $\varepsilon_{Hf(t)}$ value of −4.5. In contrast, the Devonian detrital zircons in the late Carboniferous sandstones of the Karaburun Peninsula exhibit $\varepsilon_{Hf(t)}$ values ranging from −2.1 to +5.4. 61% of the data are superchondritic (Fig. 15). Also, the metasedimentary country rocks of the Sakarya Zone granites have zircon populations indicative of a NE African provenance (P.A. Ustaömer *et al.* 2012a; Ustaömer *et al.* 2016a), unlike the Karaburun Melange that has a provenance similar to NW Africa. Where exposed, the dated zircon populations in southern Turkey are all of NE African type

(Menderes Massif; Zlatkin *et al.* 2013); Karacahisar Massif (Abbo *et al.* 2015), Bitlis Massif-E Taurides (P.A. Ustaömer *et al*. 2012b). In contrast, the provenance of the Karaburun Melange Carboniferous sandstones is characterised by Ediacaran-Cryogenian and Palaeoproterozoic (ca. 2 Ga) zircons, with an absence of Tonian-Stenian zircons that are typical of a NW African source (Henderson *et al.* 2016). Direct supply of zircons from the Devonian granites of the Sakarya Zone to the Karaburun Melange (together with the adjacent Greek islands) and the Konya Complex is , therefore, unlikely.

Looking farther northwest and west, Devonian orthogneisses and dykes occur within the Vertiskos Terrane of the Serbo-Macedonian Massif (Greece), representing a late, but volumetrically minor, phase of magmatism after the emplacement of widespread Silurian arc-type magmatic rocks (Himmerkus *et al.* 2009). Hf isotopic data are not available for these Devonian intrusions but derivation of Devonian zircons from the Vertiscos terrane is unlikely because Silurian zircons are not recorded in the Karaburun Melange sandstones. Devonian zircon populations are also present in sandstones of the Aegean region (Keay and Lister, 2002, Meinhold *et al.* 2010a, b; Zlatkin *et al.* 2018**)** although no source granitic rocks of this age have yet been reported, which is not surprising as it is largely submarine. Another possible source region for the Devonian zircons is the Variscan granitic massifs of central Europe. Similar Devonian ages are reported from granitic intrusions in Central Europe including the Saxo-Thuringian (ca. 375 Ma), Teplá-Barrandian and Moldanubian units (Bohemian Massif) (Linnemann *et al.* 2004, 2007, 2014; Drost *et al.* 2011; Kosler *et al.* 2014; Eckelmann *et al.* 2014; Dörr et al. 2017). However, more age and Hf isotopic data are needed to test these alternative sediment sources.

Assuming the Devonian zircons were sourced from a continental margin arc broadly to the west, within the Aegean region or central Europe, rather than from the Sakarya continental unit farther north in Turkey, how could they have reached the Karaburun

Peninsula and the Konya Complex (Afyon Zone) during the late Carboniferous? A possible explanation is that Palaeotethys sutured in the west during the late Carboniferous, extending as far east as the Aegean region but remained open farther east within what is now Anatolia (Zanchi *et al.* 2003; Okay *et al*. 2006; Robertson and Ustaömer (2009a, b; 2011) (Fig. 16). In this interpretation, sediments were eroded from Devonian and, or Carboniferous crust in the west and were then transported into a surviving deep-marine Tethyan embayment to the east where they were mainly deposited by turbidity currents. Sands are known to be transported by turbidity currents up to ca. 2000 km in modern trench settings, for example in the Aleutian (Piper *et al.* 1973) and Peru-Chile trenches (Schweller *et al.* 1981). It is, therefore, plausible that deep-marine sands flowed generally eastwards from the by-then sutured Paleotethys in the Aegean region or farther west, at least as far as the Konya Complex outcrop, c. 500 km east of the Karaburun Peninsula. The presence of 0.8-1.1 Ga zircons characterises the NE Africa/Arabian-Sahara provenance, whereas the absence of this age assemblage indicates a NW Africa provenance. Sands could have travelled eastwards along the northern margin of Gondwana from a region of NW African provenance (e.g. central Europe). The sands then passed over the submerged Anatolide continental unit (Afyon Zone), where they mixed with more locally derived sands of NE Africa/Arabian-Sahara provenance, as exposed in the Konya Complex.

6. Conclusions

1. Late Carboniferous sandstones of the eastern Taurides (Aladağ Nappe) and the Anatolides (Konya Complex) have very similar Precambrian zircon populations that are interpreted to have been derived from NE Gondwana (NE Africa/Arabia).

2. Carboniferous zircon populations, characteristic of the more northerly-located Sakarya crustal unit of the Pontides (N Turkey) are absent from the Carboniferous

Eastern Tauride and Anatolide (Konya Complex) sandstones. A northerly, Variscan orogenic source is, therefore, unlikely.

3. The Precambrian zircon populations of the Mid-Late Triassic Tauride sandstones were also derived from NE Gondwana. Small zircon populations of Cambrian, Ordovician and Carboniferous age in these sandstones, including Tauride and Anatolide crustal units, indicates the existence of previously poorly known magmatic events along the northern margin of Gondwana.

4. The Carboniferous zircon populations of the Karaburun Melange (westernmost Aegean Turkey), and to a lesser extent those of the overlying Late Triassic sandstones include Carboniferous and Devonian zircon populations that are absent from the Carboniferous and Triassic Taurides sandstones. This evidence points to a regionally distinct source for these sandstones.

5. Provenance interpretation is significantly aided by combining U-Pb and $\varepsilon_{Hf(t)}$ data for detrital zircons. For example, $\varepsilon_{Hf(t)}$ values of the Devonian zircon populations in the late Carboniferous sandstones of the Karaburun Melange are mainly positive. This contrasts with the negative $\varepsilon_{Hf(t)}$ values of the Devonian granites that form a small part of the Sakarya continental margin arc in NW Turkey. These Devonian granites are, therefore, unlikely to represent the source of the Devonian zircons in the Karaburun Peninsula and the Konya Complex melange.

6. The Precambrian zircon populations of the Carboniferous and Triassic sandstones of the Karaburun Peninsula are indicative of an ultimate NW African, Gondwanan source that differs from the Precambrian zircon populations of the Tauride and Anatolide continental units (i.e. Konya melange).

7. The abundance of Devonian zircons in the sandstone turbidites of the Carboniferous Karaburun Melange hints at a still unidentified source, probably within the submarine Aegean region. The nearest confirmed source of Devonian granitic rocks with the appropriate detrital zircon populations is the Variscan orogen of central European. Eastward long-distance sedimentary transport by turbidity currents is plausible.

8. The Devonian zircons reported from the upper 'flysch' unit of the Konya Melange could have a relatively local origin with no requirement for mixing of material, down to the scale of single turbidites, from opposing Gondwanan and Eurasian sources.

9. In our proposed tectonic model, Paleotethys sutured from the Atlantic to the Aegean region to form the Variscan orogenic belt during the Carboniferous, whereas Paleotethyan oceanic crust remained in an eastward-widening embayment farther east. During the late Carboniferous, sand of mainly Precambrian, Carboniferous and locally Devonian age was transported both northwards and eastwards generally by turbidity currents. Westerly and more easterly derived zircons variably mixed to produce the composite age assemblages, as recorded in the Konya Melange.

10. Interpretation of terranes created by microplate amalgamation is likely to be complex and cannot rely on the existence of simple end member age distributions to infer provenance.

Acknowledgements

This study was supported by TUBİTAK research Grants No. 111R015 and 115Y213. Partial support was provided by the Istanbul University Research Fund (Projects No. 4087, BEK-

20839 and YÖP-45681). We thank Linda Marko (Frankfurt) for assistance with the laboratory processing of zircons at Frankfurt. TU and PAU thank Gernold and Janet Zulauf for their continuing help and logistical support during their five visits to Frankfurt to carry out the isotopic analysis. Esen Arpat and Necdet Özgül are thanked for their help and support during the field work in the Aladağ region. Necdet Özgül made valuable suggestions concerning the Late Triassic units sampled in the Tauride Autochthon. Constructive comments that were provided by Aral Okay and two anonymous reviewers were greatly appreciated. We also thank Robert Stern for his comments and editorial handling of the manuscript.

References

Abbo, A., Avigad, D., Gerdes, A., and Güngör, T., 2015, Cadomian basement and Paleozoic to Triassic siliciclastics of the Taurides (Karacahisar dome, south-central Turkey): Paleogeographic constraints from U–Pb–Hf in zircons: Lithos, v. 227, p. 122–139. doi: 10.1016/j.lithos.2015.03.023

Akal, C., Koralay, O.E., Candan, O., Oberhänsli, R., and Chen, F., 2011, Geodynamic significance of the early Triassic Karaburun granitoid (Western Turkey) for the opening history of Neotethys: Turkish Journal of Earth Sciences, v. 20, p. 255–271. doi: 10.3906/yer-1008-1

Akal, C., Candan, O., Koralay, O.E., Oberhansli, R., Chen, F.K., and Prelevic, D., 2012, Early Triassic potassic volcanism in the Afyon Zone of the Anatolides/Turkey: implications for the rifting of Neo-Tethys: International Journal of Earth Sciences, v, 101, p. 177-194. doi:10.1007/s00531-011-0654-2

Ayhan, A., and Lengeranlı, Y., 1986, Yahyalı-Demirkazık (Aladağlar Yöresi) Arasının Tektonostratigrafik Özellikleri: Jeoloji Mühendisliği Dergisi, v. 27, p. 31-45 [in Turkish]. (Tectonostratigraphical Features of Aladağ Region Between Yahyalı and Demirkazık).

Aysal, N., Ustaömer, T., Öngen, S., Keskin, M., Köksal, F., Peytcheva, I., and Fanning, M., 2012, Origin of the Lower–Middle Devonian magmatism in the Sakarya Zone, NW Turkey: geochronology, geochemistry and isotope systematics: Journal of Asian Earth Sciences, v. 45, p. 201–222. doi:10.1016/j.jseaes.2011.10.011

Barrier, E., Vrielynck, B., Brouillet, J.F., and Brunet, M.F., 2018, Paleotectonic Reconstruction of the Central Tethyan Realm. Tectonono-Sedimentary-Palinspastic Maps from Late Permian to Pliocene. CCGM/CGMW, Paris, Atlas of 20 maps (scale: 1/15000000).

Bouvier, A., Vervoort, J., and Patchett, P., 2008, The Lu–Hf and Sm–Nd isotopic composition of CHUR: constraints from unequilibrated chondrites and implications for the bulk composition of terrestrial planets: Earth Planet Sci Letters, v. 273, p. 48–57. doi:10.1016/j.epsl.2008.06.010

Candan, O., Oberhansli, R., Akal, C., Koralay, O.E., Pourteau, A., and Cetinkaplan, M., 2009, Stratigraphy and Alpine metamorphism of the Afyon Zone: 62nd Geological Kurultai of Turkey, 13–17th April 2009, MTA-Ankara, Turkey, Abstract 32–33.

Candan, O., Koralay, O.E., Akal, C., Kaya, O., Oberhansli, R., Dora, O.O., Konak, N., and Chen, F., 2011, Supra-Pan-African unconformity between core and cover series of the Menderes Massif/Turkey and its geological implications: Precambrian Research, v. 184, p. 1–23.

Candan, O., Akal, C., Koralay, O.E., Okay, A.I., Oberhänsli, R., Prelević, D., and Mertz-Kraus, R., 2016, Carboniferous granites on the northern margin of Gondwana, Anatolide-Tauride Block, Turkey – Evidence for southward subduction of Paleotethys: Tectonophysics, v. 683, p. 349–366. doi:10.1016/j.tecto.2016.06.030

Çakmakoğlu, A., and Bilgin, Z.R., 2006, Pre-Neogene stratigraphy of the Karaburun Peninsula (W of İzmir, Turkey): Bulletin of Mineral Research and Exploration, v. 132, p. 1–32.

Chauvel, C., Lewin, E., Carpentier, M., Arndt, N.T, and Marini, J., 2008, Role of recycled oceanic basalt and sediment in generating the Hf– Nd mantle array: Nature Geoscience, v. 1(1), p. 64–67.

Cohen, K.M., Finney, S.C., Gibbard, P.L., and Fan, J.X., 2013, The ICS international chronostratigraphic chart: Episodes, v. 36, p. 199–204.

Collins, A., and Robertson, A.H.F., 1998, Processes of Late Cretaceous to Late Miocene episodic thrust-sheet translation in the Lycian Taurides, southwestern Turkey: Journal of the Geological Society, London, v. 155, p. 759–772.

Corfu, F., Hanchar, J.M., Hoskin, P.W.O., and Kinny, P., 2003, Atlas of zircon textures. In Hanchar J.M. and Hoskin, P.W.O., eds., Zircon. Mineralogical Society of America: Reviews in Mineralogy and Geochemistry, v. 53, p. 469–500.

Davis , D., W., Williams, I.,S., and Krogh, T.E., 2003, Historical development of zircon geochronology: Reviews in Mineralogy and Geochemistry, v. 53, p. 145–181.

Dörr, W., Zulauf, G., Gerdes, and Löeckle, F., 2017, Provenance of Upper Devonian clastic (meta)sediments of the Böllstein Odenwald (Mid-German-Crystalline-Zone, Variscides): International Journal of Earth Sciences, v. 106, p. 2927-2943. doi:10.1007/s00531-017-1473-x)

Drost, K., Gerdes, A., Jeffries, T., Linnemann, U., and Storey, C., 2011, Provenance of Neoproterozoic and early Paleozoic siliciclastic rocks of the Teplá-Barrandian unit (Bohemian Massif): Evidence from U–Pb detrital zircon ages: Gondwana Research, v. 19, p. 213-231. doi:10.1016/j.gr.2010.05.003

Dumont, J.P., 1978, Karacahisar kubbesi içinde (Isparta Bölgesi, Türkiye) yüzeyleyen iki tip Paleozoyik taban ve bunların Orta Triyastan once meydana gelen eski tip tektonik hat tarafından ayrılmaları: Maden Tetkik ve Arama Dergisi, V. 90, p. 74–78 (in Turkish). (The Two Types of Paleozoic base in the Karacahisar Dome (Isparta Region, Turkey) and Their Separation by a Pre-Triassic Tectonic Lineament).

Dumont, J.P., and Kerey, E., 1975, Eğridir gölü güneyinin temel jeolojik etüdü: Türkiye Jeoloji Kurumu Bülteni v. 18, p. 169–174 (in Turkish). (Basic Geological Study of Southern Part of Lake Eğirdir).

Dumont, J.P., and Monod, O., 1976, Dipoyraz Dağ masifinin Triyasik karbonatlı serisi (Batı Toroslar, Türkiye): Maden Tetkik ve Arama Dergisi, v. 87, p. 26-38 (in Turkish). (Triassic Carbonate Series of Dipoyraz Dağ Massif (Western Taurides, Turkey)).

Eckelmann, K., Nesbor, H-D, Königshof, P., Linnemann, U., Hofmann, M., Lange, J-M., and Sagawe, A., 2014, Plate interactions of Laurussia and Gondwana during the formation of Pangaea — Constraints from U–Pb LA–SF–ICP–MS detrital zircon ages of Devonian and Early Carboniferous siliciclastics of the Rhenohercynian zone, Central European Variscides: Gondwana Research v. 25, p. 1484-1500. doi:10.1016/j.gr.2013.05.018

Erdoğan, B., 1990, Tectonic Relations Between İzmir-Ankara Zone and Karaburun Belt: Bulletin of the Mineral Research and Exploration, v. 110, p. 1-15.

Erdoğan, B., Altıner, D., Güngör, T., and Özer, S., 1990, The stratigraphy of the Karaburun Peninsula. Bulletin of the Mineral Research and Exploration, v. 111, p. 1–23.

Eren, Y., Kurt, H., Rosselet, F., and Stampfli, G., 2004, Palaeozoic deformation and magmatism in the northern area of the Anatolide block (Konya), witness of the Palaeotethys active margin: Eclogae Geologicae Helvetiae, v. 97, p. 293–306. doi:10.1007/s00015-003-1131-8

Fedo, C., M., Sircombe, K., N., and Rainbird, R., H., 2003, Detrital zircon analyses of the sedimentary record. in Hanchar, J., M., Hoskin, P., W., O., eds., Zircon. Reviews in Mineralogy and Geochemistry, v. 53, p. 277–303.doi:10.2113/0530277

Garfunkel, Z., 2004, Origin of the Eastern Mediterranean basin: A re-evaluation: Tectonophysics, v. 391, p. 11–34. doi:10.1016/j.tecto.2004.07.006

Gerdes, A., and Zeh, A., 2006, Combined U–Pb and Hf isotope LA-(MC-) ICP-MS analyses of detrital zircons: comparison with SHRIMP and new constraints for the provenance and age of an Armorican metasediment in Central Germany: Earth Planet Science Letters, v. 249, p. 47–62.doi:10.1016/j.epsl.2006.06.039

Gerdes, A., and Zeh, A., 2009, Zircon formation versus zircon alteration-new insights from combined U–Pb and Lu–Hf in situ LA-ICP-MS analyses of Archean zircons from the Limpopo Belt: Chemical Geology, v. 261(3–4), p. 230–243. doi: 10.1016/j.chemgeo.2008.03.005

Göncüoğlu, M.C., Kozur, H., Turhan, N., and Göncüoğlu, Y., 2000, Stratigraphy of the Silurian-Lower Carboniferous rock units in Konya area. I Congresso Iberico de Palaeontologia/XVI Jornades le la Sociedad Española de Palaeontologia. VII International Meeting: International Geological Correlation Programme, v. 421, p. 227–228.

Göncüoğlu, M.C., Turhan, N., and Tekin, U.K., 2003, Evidence of Triassic rifting and opening of the Neotethyan İzmir–Ankara Ocean and discussion on the presence of Cimmerian events at the northern edge of the Tauride– Anatolide Platform, Turkey. Bolletino della Societa Geologica Italiana, Special volume, v. 2, p. 203–212.

Göncüoğlu, M.C., Çapkınoğlu, Ş., Gürsu, S., Noble, P., Turhan, N., Tekin, U.K., Okuyucu, C., and Göncüoğlu, Y., 2007, The Mississippian in the Central and Eastern

Taurides (Turkey): constraints on the tectonic setting of the Tauride–Anatolide platform: Geologica Carpathica, v. 58, p. 427–442.

Gutnic, M., Monod, O., Poisson, A., and Dumont, J.-F., 1979, Géologie des Taurides Occidentales (Turquie): Mémoires de la Société Géologique de France, No. 137, 112 pp.

Gürsu, S., and Göncüoğlu, M.C. 2005, Early Cambrian back-arc volcanism in the western Taurides, Turkey: implications for rifting along the northern Gondwanan margin: Geological Magazine, v. 142, p. 617-631.

Gürsu, S., and Göncüoğlu, M.C., 2006, Petrogenesis and tectonic setting of Cadomian felsic igneous rocks, Sandıklı area of the western Taurides, Turkey: International Journal of Earth Sciences, v. 95, p. 741-757. doi:10.1007/s00531-005-0064-4

Gürsu, S., and Göncüoğlu, M.C., 2008, Petrogenesis and geodynamic evolution of the Late Neoproterozoic post-collisional felsic magmatism in NE Afyon area, western central Turkey. in Ennih, N., and Lie Geois, J.-P., eds., The Boundaries of the West African Craton. Geological Society, London, Special Publications, v. 297, p. 409–431.

Gürsu, S., Möller, A., Usta, D., Köksal, S., Ateş, Ş., Sunkari, E. D., and Göncüoğlu, M.C., 2017, Laser Ablation Inductively Coupled Plasma Mass Spectrometry U-Pb Dating of Detrital and Magmatic Zircons of Glacial Diamictites and Pebbles in Late Ordovician Sediments of the Taurides and Southeast Anatolian Autochthon Belt, Turkey: Indications for Their Arabian-Nubian Provenance: The Journal of Geology, v. 125-2, p. 165-202.doi: 10.1086/690199

Güven, A., Ustaömer, T., and Peytcheva, I., 2012, Late Triassic crustal extension in NW Konya (Afyon Zone): new finding from LAICP-MS U–Pb zircon dating of the Ladik dyke swarm and the Kadınhanı meta-volcanics, in 5th Geochemistry Symposium, 23–25 May 2012, Denizli, Abstracts, p. 122–123.

Hawkesworth, C., J., and Kemp, A.I.S., 2006a, Using hafnium and oxygen isotopes in zircon to unravel the record of crustal evolution: Chemical Geology, v. 226, p.144–162.doi: 10.1016/j.chemgeo.2005.09.018

Hawkesworth, C.J., and Kemp, A.I.S., 2006b. Evolution of the continental crust: Nature, v. 443, p. 811–817. doi:10.1038/nature05191

Henderson, B.J., Collins, W.J., Murphy, J.B., Gutierrez-Alonso, G., and Hand, M., 2016, Gondwanan basement terranes of the Variscan–Appalachian orogen: Baltican, Saharan and West African hafnium isotopic fingerprints in Avalonia, Iberia and the Armorican Terranes: Tectonophysics, v. 681, p. 278-304. doi: 10.1016/j.tecto.2015.11.020

Himmerkus, F., Reischmann, T., and Kostopoulos, D., 2009, Serbo-Macedonian revisited: a Silurian basement terrane from northern Gondwana in the Internal Hellenides, Greece: Tectonophysics, v. 473, p. 20–35.

Karslı, O., Dokuz, A., and Kandemir, R., 2016, Subduction-related Late Carboniferous to Early Permian Magmatism in the Eastern Pontides, the Camlik and Casurluk plutons: Insights from geochemistry, whole-rock Sr–Nd and in situ zircon Lu–Hf isotopes, and U–Pb geochronology: Lithos, v. 266-267, p. 98-114. doi: 10.1016/j.lithos.2016.10.007

Keay, S., and Lister, G., 2002, African provenance for the metasediments and metaigneous rocks of the Cyclades, Aegean Sea, Greece: Geology, v. 30(3), p. 235-238.

Kemp, A.I.S., Hawkesworth, C.J., Paterson, B.A., and Kinny, B.D, 2006,Episodic growth of the Gondwana supercontinent from hafnium and oxygen isotopes in zircon: Nature, v. 439, p. 580–583. doi:10.1038/nature04505

Ketin, İ., 1966, Tectonic units of Anatolia (Asia Minor): Bulletin of the Mineral Research and Exploration, v. 66, p. 23–34.

Koralay, O.E., Satır, M., Dora, and O.Ö., 2001, Geochemical and geochronological evidence for Early Triassic calc-alkaline magmatism in the Menderes Massif, western Turkey: International Journal of Earth Sciences, v. 89, p. 822–835

Košler, J., Konopasek, J., Slama, J., and Vrana, S., 2014, U–Pb zircon provenance of Moldanubian metasediments in the Bohemian Masif: Journal of the Geological Society, London, v. 171, p. 83–95. doi:10.1144/jgs2013-059

Kozur, H.W., 1997, First discovery of Muellerisphaerida (inc. sedis) and Eoalbaillella (Radiolaria) in Turkey and the age of the siliciclastic sequence (clastic series) in Karaburun peninsula: Freiberger Forschungshefte, v. 466, p. 33–59.

Kozur, H.W., 1998, The age of the siliciclastic series ("Karareis formation") of the western Karaburun peninsula, western Turkey: Paleontologica Polonica, v. 58, p. 172–187.

Kröner, A., and Şengör, A.M.C., 1990, Archean and Proterozoic ancestry in late Precambrian to early Paleozoic crustal elements of southern Turkey revealed by single-zircon dating: Geology, v. **18,** p. 1186-1190.

Linnemann, U., McNaughton, N.J., Romer, R.L., Gehmlich, M., Drost, K., and Tonk, C., 2004. West African provenance for Saxo-Thuringia (Bohemian Massif): Did Armorica ever leave pre-Pangean Gondwana? – U/Pb-SHRIMP zircon evidence and the Nd-isotopic record: International Journal of Earth Sciences, v. 93, p. 683-705. doi:10.1007/s00531-004-0413-8

Linnemann, U., Gerdes, A., Drost, K., and Bushmann, B., 2007, The continuum between Cadomian orogenesis and opening of the Rheic Ocean: Constraints from LA-ICP-MS U-Pb zircon dating and analysis of plate-tectonic setting (Saxo-Thuringian zone, northeastern Bohemian Massif, Germany), in Linnemann, U., Nance, R.D., Kraft, P., and Zulauf, G., eds., The evolution of the Rheic Ocean: From Avalonian-Cadomian active margin to Alleghenian-Variscan collision: Geological Society of America Special Paper, v. 423, p. 61–96.

Linnemann, U., Gerdes, A., Hofmann, M., and Marko, L., 2014, The Cadomian Orogen: Neoproterozoic to Early Cambrian crustalgrowth and orogenic zoning along the periphery of the West African Craton—Constraints from U–Pb zircon ages and Hf isotopes (Schwarzburg Antiform, Germany): Precambrian Research, v. 244, p. 236-278. doi: 10.1016/j.precamres.2013.08.007

Löwen, K, Meinhold, G., Güngör, T., and Berndt, J., 2017, Palaeotethys-related sediments of the Karaburun Peninsula, western Turkey: constraints on provenance and stratigraphy from detrital zircon geochronology: International Journal of Earth Sciences, v. 106 (8), p. 2771-2796. doi:10.1007/s00531-017-1458-9

Löwen, K, Meinhold, G., Arslan, A., Güngör, T., and Berndt, J., 2018, Evolution of the Palaeotethys in the Eastern Mediterranean: Age, provenance and tectonic setting of the Upper Palaeozoic Konya Complex and its Mesozoic cover sequence (south-central Turkey): GeoBonn 2018, 2-6 September 2018, Bonn, Germany, Abstracts, pp. 61.

Löwen, K, Meinhold, G., Arslan, A., Güngör, T., and Berndt, J., 2019, Evolution of the Paleotethys in the Eastern Mediterranean: a multi-method approach to unravel the age, provenance and tectonic setting of the Upper Paleozoic Konya Complex and its Mesozoic cover sequence (south-central Turkey): International Geology Review, doi: 10.1080/00206814.2019.1616619

Ludwig, K.R., 2003, Isoplot 3.00—a geochronological toolkit for Microsoft Excel: Berkeley Geochronological Center Special Publication 4.

Mackintosh, P.W., and Robertson, A.H.F., 2009, Structural and sedimentary evidence from the northern margin of the Tauride platform in south central Turkey used to test alternative models of Tethys during Early Mesozoic time: Tectonophysics, v. 473, p. 149–172. doi:10.1016/j.tecto.2008.10.031

Mackintosh, P.W., and Robertson, A.H.F., 2012, Late Devonian–Late Triassic sedimentary development of the central Taurides, S Turkey: Implications for the northern margin of Gondwana: Gondwana Research, v. 21, p. 1089-1114. doi:10.1016/j.gr.2011.07.016

Meinhold, G., and Frei, D., 2008, Detrital zircon ages from the islands of Inousses and Psara, Aegean Sea, Greece: constraints on depositional age and provenance: Geological Magazine, v. 145, p. 886-891. doi:10.1017/S0016756808005505

Meinhold, G., Reischmann, T., Kostopoulos, D., Lehnert, O., Matukov, D., and Sergeev, S., 2008, Provenance of sediments during subduction of Palaeotethys: Detrital zircon ages and olistolith analysis in Palaeozoic sediments from Chios Island, Greece: Palaeogeography, Palaeoclimatology, Palaeoecology, v. 263, p. 71–91. doi:10.1016/j.palaeo.2008.02.013

Meinhold, G., Reischmann, T., Kostopoulos, D., Frei, D., and Larionov, A.N., 2010a, Mineral chemical and geochronological constraints on the age and provenance of the eastern

Circum-Rhodope Belt low-grade metasedimentary rocks, NE Greece: Sedimentary Geology, v. 229, p. 207–223.doi:10.1016/j.sedgeo.2010.06.007

Meinhold, G., Kostopoulos, D., Frei, D., Himmerkus, F., and Reischmann, T., 2010b, U–Pb LA-SF-ICP-MS zircon geochronology of the Serbo-Macedonian Massif, Greece: palaeotectonic constraints for Gondwana-derived terranes in the Eastern Mediterranean: International Journal of Earth Sciences, v. 99, p. 813–832. doi:10.1007/s00531-009-0425-5

Millonig, L.J., Gerdes, A., and Groat, L.A., 2012, U–Th–Pb geochronology of metacarbonatites and meta-alkaline rocks in the southern Canadian Cordillera: a geodynamic perspective: Lithos, v. 152, p. 202–217.doi:10.1016/j.lithos.2012.06.016

Moix, P., Beccaletto, L., Kozur, H.W., Hochard, V., Rosselet, F., and Stampfli, G.M., 2008, A new classification of the Turkish terranes and sutures and its implication for the paleotectonic history of the region: Tectonophysics, v. 451, p. 7–39. doi: 10.1016/j.tecto.2007.11.044

Monod, O., 1977. Réchérches géologique dans le Taurus occidental au sud de Beyşehir (Turquie). PhD thesis, Université Paris-Sud Orsay, 442 pp.

Monod, O., and Akay, E., 1984, Evidence for a Late Triassic–Early Jurassic orogenic event in the Taurides, in Robertson, A.H.F., Dixon, J.E., eds., The Geological Evolution of the Eastern Mediterranean: Geological Society, London, Special Publication, v. 17, p. 113–122.

Morag, N., Avigad, D., Gerdes, A., Belousovac, E., and Harlavand, Y., 2011, Crustal evolution and recycling in the northern Arabian-Nubian Shield: New perspectives from zircon Lu–Hf and U–Pb systematics: Precambrian Research, v. 186, p. 101-116. doi: 10.1016/j.precamres.2011.01.004

MTA, 2002. 1:500,000 Geological Map of Turkey. Maden Tektik ve Arama Enstitüsü (MTA), Ankara.

Muttoni, G., Kent, D.V., Garzanti, E., Brack, P., Nielss, A., and Gaetani, M., 2003, Early Permian 'B' to Late Permian 'A': Earth and Planetary Science Letters, v. 215, p. 379-394

Okay, A.I., Satır, M., Maluski, H., Siyako, M., Monie, P., Metzger, R., and Akyüz, S., 1996, Paleo- and Neo-Tethyan events in northwestern Turkey: geologic and geochronologic constraints: In: Yin, A., Harrison, T.M., Eds., The Tectonic Evolution of Asia., Cambridge University Press, p. 420–441.

Okay, A. I., and Tüysüz, O., 1999, Tethyan sutures of northern Turkey. In: Mascle, A., and Jolivet, L., eds., The Mediterranean Basin: Tertiary Extension within the Alpine Orogen. Geological Society, London, Special Publications, v. 156, p. 475–515.

Okay, A.I., Satır, M., and Siebel, W., 2006, Pre-Alpide Palaeozoic and Mesozoic orogenic events in the Eastern Mediterranean region, in Gee, D., G., and Stephenson, R.A., eds., European Litosphere Dynamics. Geological Society, London, Memoirs, v. 32, p. 389-405.

Okay, A.İ., Satır, M. and Shang, C.K., 2008, Ordovician metagranite from the Anatolide–Tauride block, northwest Turkey—geodynamic implications: Terra Nova, v. 20, p. 280–288. doi:10.1111/j.1365-3121.2008.00818.x

Okay, A.İ., İşintek, İ., Altıner, D., Özkan-Altıner, S., and Okay, N., 2012. An olistostrome–mélange belt formed along a suture: Bornova Flysch zone, western Turkey. Tectonophysics 568-569, 282-295. doi:10.1016/j.tecto.2012.01.007

Özbey, Z., Ustaömer, T., Robertson, A.H.F., and Ustaömer, P.A., 2013a, Tectonic significance of Late Ordovician granitic magmatism and clastic sedimentation on the northern margin of Gondwana (Tavşanlı Zone, NW Turkey): Journal of Geological Society, London, v. 170, p. 159–173. doi:10.1144/jgs2011-091

Özbey, Z., Ustaömer, T., and Robertson, A.H.F., 2013b, Mesozoic magmatic and sedimentary development of the Tavşanlı Zone (NW Turkey): implications for rifting, passive magrin development and ocean crust emplacement, in Robertson, A.,H.,F., Parlak, O., Ünlügenç, U.,C., eds., Geological Development of Anatolia and the Easternmost Mediterranean Region: Geological Society, London, Special Publications, v. 372, p. 141-165.

Özcan, A., Göncüoğlu, M., C., Turhan, N., Şentürk, K.C., and Uysal, Ş., 1990, Konya-Kadınhanı-Ilgın Dolayının Temel Jeolojisi: Maden Tetkik ve Arama Genel Müdürlüğü Rapor

no: 9535, 132 s, Ankara. (Basic Geology of the Konya-Kadınhanı-Ilgın Region: MTA Report No: 9535, pp.132, Ankara, (unpublished)).

Özdamar, Ş., Billor, M.Z., Sunal, G., Esenli, F., and Roden, M.F., 2013, First U–Pb SHRIMP zircon and $^{40}Ar/^{39}Ar$ ages of metarhyolites from the Afyon–Bolkardag Zone, SW Turkey: Implications for the rifting and closure of the Neo-Tethys: Gondwana Research, v. 24, p. 377–391. doi:10.1016/j.gr.2012.10.006

Özer, S., Sözbilir, H., Özkar, İ., and Sarı, B., 2001, Stratigraphy of Upper Cretaceous–Palaeogene sequences in the southern and eastern Menderes Massif (western Turkey): International Journal of Earth Sciences, v. 89 (4), p. 852-866. doi: 10.1007/s005310000142

Özgül, N., 1976, Some geological aspects of the Taurus orogenic belt (Turkey): Bulletin of the Geological Society of Turkey, v. 19, p. 65–78.

Özgül, N., 1997, Stratigraphy of the tectono-stratigraphic units around Hadim-Bozkır-Taşkent region (northern part of the Central Taurides, Turkey): Bulletin of the Geological Society of Turkey, v. 119, p. 113–174.

Pickett E.A., and Robertson, A.H.F., 1996, Formation of the Late Palaeozoic-Early Mesozoic Karakaya Complex and related ophiolites in NW Turkey by Paleotethyan subduction-accretion: Journal of the Geological Society, London, v. 153, p. 995-1009.

Piper, D.J.W., von Huene, R., and Duncan, J., R., 1973, Late Quaternary sedimentation in the active eastern Aleutian trench: Geology, v. 1 (1), 19-22. doi: 10.1130/0091-7613

Poisson, A., 1977, Récherches Géologiques dans les Taurides Occidentales, Turquie. PhD thesis, University of Paris-Sud, Orsay, France.

Poisson, A., 1984, The extension of the Ionian trough into southwestern Turkey, in, Dixon, J., E., and Robertson, A., H.,F., eds., The geological evolution of the eastern Mediterranean: Geological Society of London Special Publication, v. 17, p. 241-249.

Pourteau, A., Candan, O., and Oberhansli, R., 2010, High-pressure metasediments in central Turkey: Constraints on the Neotethyan closure history: Tectonics, v. 29, TC5004. doi:10.1029/2009TC002650

Pourteau, A., Sudo, M., Candan, O., Lanari; P., Vidal, O., and Oberhansli, R., 2013,, Neotethys closure history of Anatolia: insights from ^{40}Ar–^{39}Ar geochronology and *P*–*T* estimation in high - pressure metasedimentary rocks: Journal of Metamorphic Geology, v. 31, p. 585-606. doi:10.1111/jmg.12034

Porteau A., Oberhansli, R., Candan, O., and Barrier, E., 2016, Neotethyan closure history of western Anatolia: a geodynamic discussion: International Journal of Earth Science, v. 105, p. 203-224. doi:10.1007/s00531-015-1226-7

Robertson, A.H.F., and Dixon, J., E., 1984, Introduction: Aspects of the geological evolution of the Eastern Mediterranean, in: J., E., Dixon and A., H., F., Robertson, eds., The Geological Evolution of the Eastern Mediterranean, Geological Society, London, Special Publication: v. 17, p. 1-74.

Robertson, A.H.F., and Pickett, E.A., 2000, Palaeozoic-Early Tertiary Tethyan evolution of mélanges, rift and passive margin units in the Karaburun Peninsula (western Turkey) and Chios island (Greece), in Bozkurt, E., Winchester, J., A., Piper, J., D., A., eds., Tectonics and Magmatism in Turkey and the Surrounding Area: The Geological Society, London, Special Publication, v. 173, p. 43–82.

Robertson, A.H.F., Ustaömer, T., Pickett, E.A., Collins, A.S., Andrew, T., and Dixon, J.E. 2004, Testing models of Late Palaeozoic–Early Mesozoic orogeny in Western Turkey. Support for an evolving open-Tethyan model: Journal of the Geological Society, London, v. 161, p. 501–511. doi: 10.1144/0016-764903-080

Robertson, A.,H.F., and Ustaömer, T., 2009a, Formation of the upper Palaeozoic Konya Complex and comparable units in southern Turkey subduction–accretion processes: implications for the tectonic development of Tethys in the Eastern Mediterranean region: Tectonophysics, v. 473, p. 113–148. doi: 10.1016/j.tecto.2008.10.027

Robertson, A.H.F., and Ustaömer, T., 2009b, Upper Palaeozoic subduction/accretion processes in the closure of Palaeotethys: evidence from the Chios Melange (E Greece), the Karaburun Melange (W Turkey) and the Teke Dere Unit (SW Turkey): Sedimentary Geology, v. 220, p. 29–59.doi:10.1016/j.sedgeo.2009.06.005

Robertson, A.H.F., and Ustaömer, T., 2011, Role of tectonic-sedimentary melange and Permian–Triassic cover units, central southern Turkey in Tethyan continental margin evolution: Journal of Asian Earth Sciences, v. 40, p. 98–120. doi: 10.1016/j.jseaes.2010.09.001

Robertson, A. H. F., Parlak, O., and Ustaömer, T., 2012, Overview of the Palaeozoic-Neogene evolution of Neotethys in the Eastern Mediterranean region (southern Turkey, Cyprus, Syria): Petroleum Geoscience, v. 18, p. 381–404. doi: 10.1144/petgeo2011-091

Robertson, A.H.F., Parlak, O., and Ustaömer, T., 2013, Late Palaeozoic-Early Cenozoic tectonic development of Southern Turkey and the easternmost Mediterranean region: evidence from the inter-relations of continental and oceanic units. In: Robertson, A.H.F., Ustaömer, T., and Parlak, O., eds.,Geological Evolution of the Anatolia and the Eastern Mediterranean Region: Geological Society, London, Special Publication, v. 372, p. 9-48.

Robinson, F.A., Foden, J.D., Collins, A.S., and Payne, J.L., 2014, Arabian Shield magmatic cycles and their relationship with Gondwana assembly: Insights from zircon U–Pb and Hf isotopes: Earth and Planetary Science Letters, v. 408, p. 207-225. doi: 10.1016/j.epsl.2014.10.010

Schweller, W.J., Kulm, L.D., and Prince, R.A. 1981, Tectonics structure, and sedimentary framework of the Peru-Chile Trench, in: Kulm, L.D., Dymond, J., Dasch, E.J., Hussong, D.M., eds., Submarine fans and related turbidite systems. Springer-Verlag, New York, p. 23–28.

Slama, J., Košler, J., Condon, D.J., Crowley, J.L., Gerdes, A., Hanchar, J.M., Horstwood, M.S.A., Morris, G.A., Nasdala, L., Norberg, N., Schaltegger, U., Schoene, B., Tubrett, M.N., and Whitehouse, M.J., 2008, Plešovice zircon—a new natural reference material for U–Pb and Hf isotopic microanalysis: Chemical Geology, v. 249, p. 1–35**.** doi: 10.1016/j.chemgeo.2007.11.005

Smith, A.G., 2006, Tethyan ophiolite emplacement, Africa to Eurasia motions, andAtlantic spreading. In: Robertson, A.H.F., Mountrakis, D. (Eds.), Tectonic Develop-ment of the Eastern Mediterranean Region. Geological Society of London SpecialPublication, vol. 260, pp. 11–35.

Stampfli, G.M., 2000, Tethyan Oceans, in Bozkurt, E., Winchester, J.A., Piper, J.D.A., eds., Tectonics and Magmatism in Turkey and the Surrounding Area. The Geological Society, London, Special Publication, v. 173, p. 1-23.

Stampfli, G.M., Mosar, J., Favre, P., Pellevuit, A., and Vannay, J.-C., 2001, Permo-Mesozoic evolution of the western Tethys realm: the Neo-Tethys East Mediterranean Basin connection in Ziegler, P., Cavazza, W., Robertson, A.H.F., and Crasquin-Soleau, A., eds., Peri-Tethyan Rift/Wrench Basins and Passive Margins: Peri-Tethys Memoire, v. 5, p. 51–108.

Sunal, G., 2012, Devonian magmatism in the western Sakarya Zone, Karacabey region, NW Turkey: Geodinamica Acta, v. 25 (3-4), p. 183-201.

Şenel, M., 1991, Palaeocene-Eocene sediments interbedded with volcanics within the Lycian Nappes: Faralya Formation: Bulletin of Mineral Research and Exploration (Turkey), v. 113, p. 1–14.

Şenel, M., Gedik, İ., Dalkılıç, H., Serdaroğlu, M., Bilgin, A.Z., Uğuz, M.F., Bölükbaşı, A.S., Korucu, M., and Özgül, N., 1996, Stratigraphy of the Autochthonous and Allochthonous Units at the Eastern Part of the Isparta Angle, Western Taurides-Turkey: MTA Bulletin, v. 118, p. 111-160.

Şengör, A.M.C., and Yılmaz, Y., 1981, Tethyan evolution of Turkey: a plate tectonic approach: Tectonophysics, v. 75, p. 181–241. doi:10.1016/0040-1951(81)90275-4

Şengör, A.M.C., 1984, The Cimmeride Orogenic System and the Tectonics of Eurasia, in Sengör, A.M. C., ed., The Cimmeride Orogenic System and the Tectonics of Eurasia. Geological Society of America, 1–82. doi:10.1130/SPE195-p1

Tekeli, O., 1980, Toroslarda Aladağların yapısal evrimi. Türkiye Jeoloji Kurumu Bülteni; v. 23, p. 11-14 (in Turkish). (Structural Evolution of Aladağ Mountains in Taurus Belt).

Tekeli, O., Aksay, A., Ürgün, B.M., and Işık, A., 1984, Geology of the Aladağ Mountains, in Tekeli, O., Göncüoğlu, M.C., eds., Geology of the Taurus Belt: Proceedings of International Tauride Symposium. Mineral Research and Exploration Institute (MTA) of Turkey, Publications, p. 143-158.

Toker, V., Sonel, N., Ayyıldız, T., and Albayrak, M., 1993, Akseki kuzeyi-Üzümdere (Antalya) civarının Stratigrafisi: Türkiye Jeoloji Bülteni, v. 36, p. 56-71 (in Turkish) (Stratigraphy of the Northern Portion of Akseki-Üzümdere (Antalya) Vicinity).

Ustaömer, P.A., Mundil, R., and Renne, P.R., 2005, U/Pb and Pb/Pb zircon ages for arc related intrusions of the Bolu Massif (W Pontides, NW Turkey): Evidence for Late Precambrian (Cadomian) age: Terra Nova, v. 17, p. 215-223. doi:10.1111/j.1365-3121.2005.00594.x

Ustaömer, P.A., Ustaömer, T., Gerdes, A., and Zulauf, G., 2011, Detrital zircon ages from a Lower Ordovician quartzite of the İstanbul exotic terrane (NW Turkey): evidence for Amazonian affinity: International Journal of Earth Sciences, v. 100, p. 23-41. doi:10.1007/s00531-009-0498-1

Ustaömer, P.A., Ustaömer, T., and Robertson, A.H.F., 2012a, Ion Probe U–Pb dating of the Central Sakarya basement: a peri-Gondwana terrane cut by late Lower Carboniferous subduction/collision-related granitic magmatism: Turkish Journal of Earth Sciences, v. 21, p. 905-932. doi:10.3906/yer-1103-1

Ustaömer, P.A., Ustaömer, T., Gerdes A., Robertson A.H.F., and Collins, A.S., 2012b, Evidence of Precambrian sedimentation/magmatism and Cambrian metamorphism in the Bitlis Massif, SE Turkey utilising whole-rock geochemistry and U-Pb LA-ICP-MS zircon dating: Gondwana Research, v. 21, p. 1001-1018. doi:10.1016/j.gr.2011.07.012

Ustaömer, T., Robertson, A.H.F., 1993, A Late Palaeozoic-Early Mesozoic marginal basin along the active southern continental margin of Eurasia: evidence from the Central Pontides (Turkey) and adjacent regions: Geological Journal, v. 28, p. 219-238.

Ustaömer, T., and Robertson, A.H.F., 1997, Tectonic-sedimentary evolution of the eastern Mediterranean, in Robinson, A.G., ed., Regional and Petroleum Geology of the Black Sea and Surrounding Region. American Association of Petroleum Geologists Memoir, Tulsa, Oklahama, p, 68, p. 255-290.

Ustaömer, T., Gerdes, A., Ustaömer P.A., and Robertson, A.H.F., 2012, U-Pb LA-SF-ICP-MS dating of detrital zircons from an Upper Carboniferous quartzite in the Siyah Aladağ Nappe, Yahyalı-Kayseri, E Taurides: source area characteristics, in Yalçın, M.N., Çorbacıoğlu, H., Aksu, Ö., and Bozdoğan, N., eds., Palaeozoic of Northern Gondwana and its Petroleum Potential, a Field Workshop, 9-14 September 2012, Kayseri-Turkey, Extended Abstracts, p. 108-110.

Ustaömer, T., Robertson, A.H.F., Ustaömer, P.A., Gerdes, A., and Peytcheva, I., 2013, Constraints on Variscan and Cimmerian magmatism and metamorphism in the Pontides (Yusufeli–Artvin area), NE Turkey from U–Pb dating and granite geochemistry: In Robertson, A. H. F., Parlak, O. & Ünlügenç, U. C. (eds) Geological Development of Anatolia and the Easternmost Mediterranean Region. Geological Society, London, Special Publications, v. 372, p. 49–74.

Ustaömer, T., Ustaömer, P.A., Robertson, A.H.F., and Gerdes, A., 2016a, Implications of U–Pb and Lu–Hf isotopic analysis of detrital zircons for the depositional age, provenance and tectonic setting of the Permian–Triassic Palaeotethyan Karakaya Complex, NW Turkey: International Journal of Earth Sciences, v. 105, p. 7-38. doi:10.1007/s00531-015-1225-8

Ustaömer, T., Ustaömer, P.A., Robertson, A.H.F., and Gerdes, A., 2016b, Testing alternative tectonic models of Palaeotethys in the E Mediterranean region: new U-Pb and Lu-Hf isotopic analyses of detrital zircons from Late Carboniferous and Late Triassic sandstones associated with the Anatolide and Tauride blocks (S Turkey): Geophysical Research Abstracts, Vol. 18, EGU2016-15469-1.

Ustaömer, T., Ustaömer, P.A., Robertson, A.H.F., and Gerdes, A., 2018, U-Pb and Lu-Hf isotopic data from detrital zircons in Late Carboniferous and Late Triassic sandstones used to determine provenance and test alternative tectonic models of the tectonic setting of the

Anatolide and Taurides, S Turkey: GeoBonn 2018, 2-6 September 2018, Bonn, Germany, Abstracts, pp. 65.

Vermeesch, P., 2012, On the visualisation of detrital age distributions: Chemical Geology, v.312-313, 190-194.doi:10.1016/j.chemgeo.2012.04.021

Wehrmann, A., Yılmaz, I., Yalçın, M.N., Wilde, V., Schindler, E., Weddige, K., Saydam Demirtas, G., Özkan, R., Nazik, A., Nalcıoğlu, G., Kozlu, H., Karslıoğlu, Ö., Jansen, U., Ertuğ, K., Brocke, R., and Bozdoğan, N., 2010, Devonian shallow-water sequences from the North Gondwana coastal margin (Central and Eastern Taurides, Turkey): sedimentology, facies and global events: Gondwana Research, v. 17, p. 546–560. doi:10.1016/j.gr.2009.09.011

Wiedenbeck, M., Allé, P., Corfu, F., Griffin, W.Lç, Meier, M., Oberli, F., von Quadt, A., Roddick, J.C., and Spiegel, W., 1995, Three natural zircon standards for U–Th–Pb, Lu–Hf, trace element and REE analyses: Geostandarts Newsletter, v. 19, p. 1–23. doi: 10.1111/j.1751-908X.1995.tb00147.x

Xiang, W., Griffin, W.L., Chen, J., Huang, P., and Ziang, L., 2011, U and Th contents and Th/U ratios of zircon in felsic and mafic magmatic rocks: improved zircon-melt distribution coefficients: Acta Geologica Sinica, v. 85, p. 164-174. doi:10.1111/j.1755-6724.2011.00387.x

Zanchi, A., Garzanti, E., Larghi, C., and Angiolini,L., 2003, The Variscan orogeny in Chios (Greece): Carboniferous accretion along a Palaeotethyan active margin: Terra Nova, v.15, no. 3, p. 213-223. doi:10.1046/j.1365-3121.2003.00483.x

Zlatkin, O., Avigad, D., and Gerdes, A., 2013, Evolution and provenance of Neoproterozoic basement and Lower Paleozoic siliciclastic cover of the Menderes Massif (western Taurides): Coupled U–Pb–Hf zircon isotope geochemistry: Gondwana Research, v. 23, p. 682-700. doi:10.1016/j.gr.2012.05.006

Zlatkin, O., Avigad, D., and Gerdes, A., 2018, New Detrital Zircon Geochronology From the Cycladic Basement (Greece): Implications for the Paleozoic Accretion of Peri-Gondwanan Terranes to Laurussia: Tectonics, v. 37 (12), p. 4679-4699. doi: 10.1029/2018TC005046

Figure captions

Figure 1: Simplified tectonic map of southern Turkey showing the locations of the samples studied and the logs in Fig. 2 (MTA, 2002). The tectonic subdivisions of the metamorphic Anatolide continental unit to the north and the non-metamorphic Tauride crustal units to the south are indicated. The Anatolide continental unit including the Tavşanlı and Afyon zones experienced HP/LT metamorphism during Late Cretaceous and Palaeocene times, respectively. The Menderes Massif to the west records orogenic events during the Ediacaran-Cambrian and Eocene-Recent periods. The Tauride continental unit includes autochthonous successions, including Bey Dağları, Geyik Dağ, Akseki-Anamas and Belemedik (as shown in blue), and also from overlying thrust sheets, including the Lycian Nappes in the west, the Beyşehir-Hoyran-Hadim Nappes in the centre, the Aladağ Nappes in the east and the Antalya and Alanya tectonic units in the south of the region. Abbreviations: SP Sandıklı Porphyroid; BHHN Beyşehir-Hoyran-Hadim Nappes; Y Yahyalı; BG Beyşehir Lake; EG Eğirdir Lake. Inset: the wider distribution of suture zones throughout Turkey extending into Iran, Armenia, Georgia and the Russian Federation. IPS Intra-Pontide Suture, IAES Izmir-Ankara-Erzincan Suture, BZS Bitlis-Zagros Suture

Figure 2: Stratigraphic logs of the successions sampled in the Tauride continental unit and the overlying allochthonous units. The sample locations and their stratigraphic position are indicated by red arrows. Sources of information: Aladağ Nappe: Tekeli *et al*. (1984), Özgül (1976), Ayhan and Lengeranlı (1986); Afyon Zone (Konya Region): Robertson and Ustaömer (2011); Karaburun Peninsula: Robertson and Ustaömer (2009a,b), Çapkınoğlu and Bilgin (2006), Erdoğan *et al.* (1990); Bey Dağları (Tauride autochthon): Poisson (1984), Şenel 1996; Akseki (Tauride autochthon): Monod (1977).

Figure 3: Selected cathodoluminescence images of detrital zircons from metasandstones of the Konya Complex (Afyon Zone), Central Taurides. The circles marked on the zircons show the locations of the spots analysed; the numbers within the circles indicate the individual spots. Scale bars=20 μm in panel a. $^{206}Pb/^{238}U$ ages are used for <1Ga and $^{206}Pb/^{207}Pb$ ages are used for >1 Ga. Errors are at 1σ level.

Figure 4: Age versus Th/U diagram for detrital zircons from all of the sandstones discussed in the paper. Th/U=3.7 indicates the average Th/U ratios of zircons from mafic igneous source rocks; Th/U=0.93 indicates the average Th/U ratios of zircons from intermediate-composition igneous source rocks; Th/U=0.59 indicates the average Th/U ratios of zircons from felsic igneous rocks (Xiang *et al.* 2011).

Figure 5: Concordia (left) and density-kernel density estimates plot (right) for the sandstones analysed during this work. a, b Köşkdere Formation; c, d Konya Complex; e, f Karaburun Melange. The numbers indicate the peak ages in Ma.

Figure 6: Pie charts showing different age spectra of the detrital zircons in the Carboniferous (left) and Triassic (right) sandstones analysed during this work.

Figure 7: Concordia plots for Triassic sandstones analysed during this work. a, b Kasımlar Formation; c Üzümdere Formation, d Güvercinlik Formation.

Figure 8: Histogram and kernel density estimate plots for Triassic sandstones analysed during this work. a, b Kasımlar Formation; c Üzümdere Formation, d Güvercinlik Formation. The numbers indicate peak ages in Ma.

Figure 9: Age versus $\varepsilon_{Hf(t)}$ plots of Triassic sandstones analysed during this work from: a-b Kasımlar Formation; c Üzümdere Formation and d Güvercinlik Formation. Curves are kernel density estimates for each of the samples. Arrow shows the crustal evolution path. DM

Depleted Mantle, CHUR Chondritic Uniform Reservoir, ANS Arabian-Nubian Shield (Robinson *et al.* 2014).

Figure 10: Age versus $\varepsilon_{Hf(t)}$ plots of Carboniferous sandstones analysed during this work from, a Konya Complex and, b Karaburun Melange. Arrow shows the crustal evolution path. See the caption of Figure 9 for the abbreviations.

Figure 11: Age versus $\varepsilon_{Hf(t)}$ plots of Carboniferous meta-granites of the Afyon Zone analysed during this work. The red dashed lines represent crustal evolution paths of TDM =1.3 and 2.1 Ga with $^{176}Lu/^{177}Hf$=0.0013. See the caption to Figure 9 for abbreviations.

Figure 12: Normalised probability plot for all of the samples analysed during this study, ranging in age from 0-1200 Ma. See text for explanation.

Figure 13: Cumulative probability plot of all the samples analysed in this study. The diagram shows that the sandstones from the Karaburun Peninsula (K.13.102 and K.13.104) differ in the ages of prominent zircon populations in the samples from all of the other areas and units considered in this paper (both new and published data). Common to all of the samples is the rarity or absence of Early to Mid-Mesoproterozoic zircons (horizontal lines between 1.1 to 1.6 Ga) and the abundance of Neoproterozoic zircons. The samples from the Anatolide and Tauride continental units (excluding the two samples from the Karaburun Peninsula) indicate a similar provenance as for the Precambrian zircons, irrespective of depositional age. Late Palaeozoic zircons in these sandstones appear in the Late Triassic sandstones and reach a maximum of 15% of the whole data set.

Figure 14: U-Pb age versus $\varepsilon_{Hf(t)}$ of Carboniferous granites from the Sakarya continental margin arc and the Afyon Zone. All of the Carboniferous detrital zircons in the Carboniferous and Triassic sandstones from the Anatolide and Tauride continental units are

plotted for comparison. Data from the Sakarya Zone are from Ustaömer *et al.* 2016 (KK.09.04) and our unpublished data (K.12.111); Karslı *et al.* 2016 (CM21, CS10). See text for explanation.

Figure 15: U-Pb age versus $\varepsilon_{Hf(t)}$ of: 1) Devonian metagranite from the Sakarya continental margin arc and 2) Devonian detrital zircons in the Late Carboniferous sandstone of the Karaburun Melange. The Devonian metagranite exhibits a tight cluster of $\varepsilon_{Hf(t)}$ values from -8.5 to -7.1, with corresponding Hf model ages of 1.5-1.4 Ga (Ustaömer *et al.* 2016). In contrast, the Devonian detrital zircons in the Karaburun Melange sandstones differ significantly, with $\varepsilon_{Hf(t)}$ values straddling the CHUR line and Hf model ages of <1.1 Ga. Several other Devonian metagranites of the Sakarya continental margin arc (Pontides) exhibit $\varepsilon_{Nd(401-389)}$ values of -9 to -8, with corresponding Nd model ages of 1.9-1.8 Ga (Aysal *et al.* 2012).

Figure 16: Palaeogeographic sketch map showing the inferred tectonic setting of the Aegean region and central and northern Turkey during the late Carboniferous (c. 310 Ma). Siliciclastic sediments were shed from the Anatolide and Tauride Anatolide continental units in the south and east, whereas, in the west, Devonian zircon-rich sand are inferred to have been come from the adjacent Aegean region or from, the Variscan terranes in central Europe. The solid arrow indicates the inferred sedimentary transport direction.

Electronic supplement

Supplementary Table 1: GPS coordinates of the samples analysed.

Supplementary Table 2: Summary of U-Pb and Lu-Hf data for Carboniferous sandstones.

Supplementary Table 3: Summary of U-Pb and Lu-Hf data for Triassic sandstones.

Supplementary Table 4: Uranium-lead analytical data.

Supplementary Table 5: Lutetium-hafnium analytical data.

Supplementary figure captions

Supplementary Figure 1: Geological map of the Aladağ region, Eastern Tauride continental unit, showing the location of the upper Carboniferous quartzite sample (S3) analysed for zircon U-Pb analysis. This is a small part of a larger map that was produced during the first author's joint fieldwork with Esen Arpat and Necdet Özgül in 2008. Satellite images of the area were used during the mapping.

Supplementary Figure 2: Selected cathodoluminescence images of detrital zircons from the upper Carboniferous quartzite of the Köşkdere Formation, Siyah Aladağ Nappe, Eastern Tauride continental unit. The open circles on the zircons show the locations of the spots analysed; the numbers within the circles indicate the individual spots; the red numbers above the zircons refer to the name of the zircon crystals. The ages obtained from the metamorphic zircon growths are indicated by the blue numbers and those from the igneous zircons by the black numbers. $^{206}Pb/^{238}U$ ages are used for <1Ga and $^{206}Pb/^{207}Pb$ ages are used for >1 Ga. Errors are at 1σ. The scale bars are 20 μm.

Supplementary Figure 3: Simplified geological map of the Karacahisar-Seydişehir area, central Tauride continental unit, showing the sample locations. None of the samples collected

from the Cambro-Ordovician Seydişehir Formation yielded usable zircons. Zircons from the samples 75 and 78 from the Kasımlar Formation were analysed for U-Pb-Hf isotopic analysis. Map modified after (Şenel 1997).

Supplementary Figure 4: Selected cathodoluminescence images of detrital zircons from sandstone sample K.12.75 of the Late Triassic Kasımlar Formation, Tauride continental unit. The open circles on the zircons show the locations of the spots analysed; the numbers within the circles indicate the individual spots. $^{206}Pb/^{238}U$ ages are used for <1Ga and $^{206}Pb/^{207}Pb$ ages are used for >1 Ga. Errors are at 1σ level.

Supplementary Figure 5: Selected cathodoluminescence images of detrital zircons from sandstone sample K.12.78 of the Late Triassic Kasımlar Formation, Tauride continental unit. The open circles on the zircons show the locations of the spots analysed; the numbers within the circles indicate the individual spots. $^{206}Pb/^{238}U$ ages are used for <1Ga and $^{206}Pb/^{207}Pb$ ages are used for >1 Ga. Errors are at 1σ level.

Supplementary Figure 6: Simplified geological map of the Üzümdere area, Tauride continental unit, showing the location of the sandstone sample (K.13.77) analysed. Map re-drawn after Monod (1977) and Toker *et al.* (1993).

Supplementary Figure 7: Selected cathodoluminescence images of detrital zircons from sandstone of the Late Triassic Üzümdere Formation, Tauride continental unit. The open circles on the zircons show the locations of the spots analysed; the numbers within the circles indicate the individual spots. $^{206}Pb/^{238}U$ ages are used for <1Ga and $^{206}Pb/^{207}Pb$ ages are used for >1 Ga. Errors are at 1σ level.

Supplementary Figure 8: Geological map of the Sızma-Ladik area of Konya, showing the location of the meta-sandstone sample (K.13.75) analysed from the Konya Complex. See Robertson and Ustaömer (2009a) for data sources.

Supplementary Figure 9: Selected cathodoluminescence images of detrital zircons from metasandstone of the Konya Complex, Afyon Zone, central Anatolide continental unit. The open circles on the zircons show the locations of the spots analysed; the numbers within the circles indicate the individual spots. $^{206}Pb/^{238}U$ ages are used for <1Ga and $^{206}Pb/^{207}Pb$ ages are used for >1 Ga. Errors are at 1σ level.

Supplementary Figure 10: Simplified geological map of the Karaburun Peninsula showing the locations of the samples (K.13.102 and K.13.104) analysed during this study. See Robertson and Ustaömer (2009b) for data sources.

Supplementary Figure 11: Selected cathodoluminescence images of detrital zircons of sandstone from the Karaburun Melange. The open circles on the zircons show the locations of the spots analysed; the numbers within the circles indicate the individual spots. $^{206}Pb/^{238}U$ ages are used for <1Ga and $^{206}Pb/^{207}Pb$ ages are used for >1 Ga. Errors are at 1σ level.

Supplementary Figure 12: Selected cathodoluminescence images of detrital zircons of sandstone sample from the Late Triassic Güvercinlik Formation (Tauride continental unit). The open circles on the zircons show the locations of the spots analysed; the numbers within the circles indicate the individual spots. $^{206}Pb/^{238}U$ ages are used for <1Ga and $^{206}Pb/^{207}Pb$ ages are used for >1 Ga. Errors are at 1σ level.

Supplementary Figure 13: Simplified geological map of the Simav-Alaçam area (after Candan *et al.* 2016), showing the locations of the metagranite samples from the Afyon Zone, Anatolide continental unit (TM.17.33, TM.17.34 and TM.17.35) analysed in this study.

U-Pb~~- and Lu-~~Hf isotopic data from detrital zircons in Late Carboniferous and Mid-Late Triassic sandstones, and ~~from~~ also Carboniferous granites from~~used to help determine the provenance and tectonic setting of~~ the Tauride and Anatolide continental units in S Turkey: implications for Tethyan paleogeography~~continental crust in S Turkey~~

Timur Ustaömer[1], Petek Ayda Ustaömer[2], Alastair H.F. Robertson[3], Axel Gerdes[4]

[1]Department of Geology, Faculty of Engineering, İstanbul University-Cerrahpaşa, 34320 Avcılar, Istanbul, Turkey; timur@istanbul.edu.tr

[2]Natural Sciences Research Centre, Yıldız Technical University, Davutpaşa-Esenler, İstanbul, Turkey

[3]School of GeoSciences, University of Edinburgh, James Hutton Road, Edinburgh EH9 3FE, UK

[4]Department of Geosciences, Goethe University-Frankfurt, Frankfurt, Germany

Abstract

Zircons from Carboniferous sandstones (three samples) and~~, or~~ Mid-Late Triassic sandstones (four samples) ~~were analysed~~ from the Taurides and Anatolide continental units were analysed for U-Pb-Hf isotopes.~~(i.e., Konya Complex melange). Zircons were also analysed from Late Triassic sandstones from the Karaburun Peninsula (far west).~~ For comparison, zircons were also analysed from Carboniferous granites of the Afyon Zone, Anatolides (three samples~~Afyon Zone~~). A NE African/Arabian source is inferred for both the Carboniferous sandstones of the Taurides (Aladağ) and the Anatolides (Konya Complex). In contrast, the Carboniferous Karaburun Melange is characterised by a NW African provenance. A prominent Devonian population occurs in the Carboniferous Karaburun Melange, characterised by mainly positive $\varepsilon_{Hf(t)}$ values that differ significantly from those of the Devonian granites~~ic rocks~~ of the Sakarya continental crustal unit ~~unit~~ (Pontides). ~~-~~Middle-Late Triassic Tauride sandstones include minor Paleozoic and Early Mesozoic zircons. In contrast, Devonian and Carboniferous zircons are ~~more~~ relatively abundant in Late Triassic sandstones of the Karaburun Peninsula. The Hf isotopic composition 25 Carboniferous-aged zircons from three samples of Mid-Late Triassic sandstone and one of Late Carboniferous age overlap with the $\varepsilon_{Hf(t)}$ values of Carboniferous arc-type granites in the Anatolides. Taking account of the available U-Pb and Lu-Hf isotopic data from comparative~~regional~~ crustal units, the Devonian zircon populations from the melanges in the Karaburun Peninsula and the Konya Complex ~~melange zircon populations~~ are inferred to have a westerly source (e.g.

granitic rocks of Aegean or ~~similar to those of~~ central European ~~granitic rocks)~~. A tectonic model is proposed in which Paleozoic Tethys sutured during the late Carboniferous in the west~~W~~ (Aegean region westwards), leaving an eastward-widening oceanic gulf in which ~~Devonian zircons accumulated in~~ sandstone turbidites accumulated, including Devonian zircons~~, together with abundant Carboniferous arc detritus~~.

Key Words: *provenance, sandstone, detrital zircon, U-Pb & Lu-Hf isotopes, Taurides, Anatolides, Gondwana, late Carboniferous, Late Triassic; Tethys*

1. Introduction

Detrital zircon geochronology is a well-established technique for the study of sandstone provenance (Davis *et al.* 2003; Fedo *et al.* 2003). The potential is significantly enhanced when Lu-Hf isotopic analysis is included ~~that~~ as this helps to distinguish crustal types (Hawkesworth and Kemp 2006a, b; Kemp *et al.* 2006). Interpretation is most effective when ~~combined~~ zircon U-Pb and Lu-Hf data are combined and compared with continental source units ~~with~~ that have well-dated and isotopically characterised zircon populations (e.g. Linnemann *et al.* 2014, Henderson et al. 2016). However, clear-cut compositional source differences may not exist within different parts of all~~in some~~ orogenic belts. ~~Specifically~~For example, Anatolia is made up of continental and oceanic units that were progressively assembled from Late Precambrian to Neogene time (e.g. Şengör and Yılmaz 1981; Robertson and Dixon 1984; Moix *et al.* 2008; Robertson *et al.* 2012). Several continental fragments detached from Gondwana, drifted across Tethys and accreted to Eurasia ~~continental margin~~ during Paleozoic-Eocene time (Stampfli 2000; Stampfli *et al.* 2001; Robertson *et al.* 2004~~5~~; Okay *et al.* 2006). As a result, the

sedimentary provenance, as represented by detrital zircon age and Lu-Hf data ~~age data~~ is likely to be complex, ~~and~~ variable and may not simply fingerprint opposing continents.

By the late Carboniferous to ~~-~~Late Triassic, the main time interval considered here, Gondwana-derived continental crust existed both to the south and to the north of Tethyan oceanic crust (P.A. Ustaömer *et al.* 2011, 2012a; Ustaömer *et al.* 2013, 2016a). Identification of Gondwanan vs. Eurasian provenance cannot~~,~~ therefore~~,~~ rely solely on the recognition of distinctive Precambrian Gondwana-derived detrital zircon populations but must ~~take full~~ account of all of the geological evidence from ~~of~~ the region. ~~and alternative tectonic reconstructions.~~ Anatolia experienced significant important episodes of continental margin and/or or oceanic arc volcanism, especially during Late Palaeozoic-Triassic time, which provided ~~additional~~ distinctive age populations and crustal signatures. However, the potential source arcs are exotic terranes of debatable position with regard to Gondwana or Eurasia. Additional clues to provenance are nevertheless provided especially by minor Late Paleozoic-early Mesozoic zircon populations and related Lu-Hf data, as presented here, which fingerprint specific tectonic-magmatic events.

With the above challenges in mind, we have ~~our approach here is to~~ selected two key time periods that are critical to the regional tectonic reconstruction of Gondwana and Eurasia~~interpretation~~, and that include sandstones with zircons suitable for isotopic analysis. The area sampled extends over c. 800 km E-W (Fig. 1). The first of these time periods is the late Carboniferous when~~period that involved~~ subduction of Paleotethys took place~~between Gondwana and Eurasia~~ (Şengör *et al.* 1984; Robertson and Dixon, l984; Ustaömer and Robertson l993~~5~~; Pickett and Robertson, 1996; Göncüoğlu *et al.* 2000). —The second time period, the Mid-Late Triassic, was characterised

by~~encompassed~~ rifting of Neotethys along the north margin of Gondwana and further subduction of Paleotethys (Göncüoğlu *et al.* 2003; Robertson *et al.* 2004).

~~Consideration of two time periods helps to widen the aerial coverage and identification of any changes in zircon provenance. The area that we sampled extends over c. 800 km E-W (Fig. 1), with~~ Here, building on initially reported results (Ustaömer *et al.* 2012, 2016b, 2018), we have the following ~~main~~ specific objectives:

1. To ~~help~~ provide a reference for zircon populations of the largest existing crustal unit in the region, namely the Tauride continental unit (Tauride microcontinent), which extends over > 1300 km E-W, by combining new and existing data;

2. To test whether the Tauride continental unit ~~microcontinent~~ shows a close compositional affinity with Gondwana to the south, and if so, which part.

3. To compare the zircon geochronology of the Tauride continental unit ~~microcontinent~~ with the adjacent Anatolide continental unit which itself comprises both the Afyon Zone and the Tavşanlı Zone, that together make up the Anatolide continental unit (Fig. 1). ~~In different interpretations, the Anatolide continental unit has been related to either Gondwana or Eurasia during Late Palaeozoic-Early Mesozoic time.~~

4. To infer the crustal composition and age of Carboniferous arc-related granitic rocks in the region, using a combination of new and existing data.

5. To use new Lu-Hf isotopic data to help test whether crustal units of potentially similar age are actually likely to be of similar provenance, and to help indicate~~determine~~ where suitable source units ~~are~~ may be located.

6. To synthesise the ~~integrate~~ new and existing U-Pb and Lu-Hf isotopic data and thereby ~~to~~ test several ~~different~~ alternative regional tectonic models. ~~These include~~Different published models that imply ~~involving~~ northward subduction, ~~or~~ southward subduction ~~(~~or dual~~)~~ subduction of Paleotethys, and also models in which Paleotethys was either closed in the west by latest Carboniferous or remained open throughout the Mediterranean region until Late Triassic ~~Early Mesozoic~~ time. In addition, many models consider the Taurides and the Anatolides (including both the Afyon Zone and the Tavşanlı Zone) to represent different parts of a single Gondwana-related continent (Anatolide-Tauride Block) (Şengör and Yılmaz 1981; Okay and Tüysüz 1999; Robertson et al. 2005). However, other tectonic models infer that the Anatolide continental unit was located along the southern margin of Eurasia during the Late Paleozoic until it rifted, drifted southwards and collided with the Taurides during the Late Triassic (Stampfli 2000; Stampfli *et al.* 2001; Eren et al. 2004).

2. Methods and data reduction

Three Late Carboniferous and four Late Triassic sandstones, together with three Carboniferous metagranites were sampled from geologically well-constrained units (Figs. 1, 2, see Supplementary Table 1 for GPS coordinates of the samples). Geological maps of the sample locations are included in the Supplementary material.

Zircon grains were extracted at the Department of Geology, İstanbul University-Cerrahpaşa. The samples were first cut into slices and altered edges were removed. The slices were then crushed twice and further reduced in a roller mill. This was followed by washing and drying in an oven at 70 °C for c. 10 hours. The dry samples were then sieved using mesh sizes of 63 µm, 125 µm, 250 µm, 500 µm, 1 mm and 2 mm. The sieves were shaken mechanically for 30 minutes for each sample. Individual size

fractions were stored in plastic bags. Samples with size fractions of <500 µm were further processed using a Frantz magnetic separator and heavy liquid (sodium polytungstate) separation. The zircons were then handpicked, mounted in epoxy tablets and polished, followed by cathodoluminescence (CL) imaging and isotopic analyses. The CL images were obtained using a SEM Jeol JSM- 6490, equipped with Gatan MiniCL at Goethe University Frankfurt (GUF). Selected cathodoluminescence images of the detrital zircons are included in the supplementary material.

Uranium, thorium and lead isotope analyzes were carried out by laser ablation-inductively coupled plasma-mass spectrometry (LA-ICP-MS) at GUF, using a slightly modification of the method previously reported in Gerdes & Zeh (2006, 2009) and Zeh & Gerdes (2012). A ThermoScientific Element 2 sector field ICP-MS was coupled to a Resolution S-155 (Resonetics) 193 nm ArF Excimer laser (CompexPro 102, Coherent), equipped with a two-volume ablation cell (Laurin Technic, Australia). The laser was fired with 5.5 Hz at a fluence of about 3 J cm^{-2}. With tThe above configuration, usingwith a spot size of 26µm and a depth penetration of 0.6µm s^{-1}, this yielded a sensitivity of 9000-13000 cps/µg g^{-1} for ^{238}U. Raw data were corrected offline for background signal, common Pb, laser-induced elemental fractionation, instrumental mass discrimination, and time-dependent elemental fractionation of Pb/U using an in-house MS Excel© spreadsheet program (Gerdes & Zeh 2006, 2009). Laser-induced elemental fractionation and instrumental mass discrimination were corrected by normalization to a reference zircon GJ-1 (0.0982 ± 0.0003; ID-TIMS GUF value). Repeated analyses of the reference zircon Plesovice, Felix and 91500 (Slama *et al.* 2008; Millonig *et al*. 2012; Wiedenbeck *et al.* 1995) during the same analytical session yielded an accuracy of better 1% and a reproducibility of <2% (2 SD). All uncertainties are

reported at ~~the~~ 2σ level. The data are summarised in Supplemantary Tables 2 and 3 (see Supplementary Table~~s~~ 4 for the whole data set).

Hafnium isotope measurements were performed using a Thermo-Finnigan NEPTUNE multi collector ICP-MS at GUF, coupled to the Resolution M50 193nm ArF Excimer (Resonetics) laser system following the method described by Gerdes and Zeh (2006, 2009). Spots of 40 µm in diameter were drilled with a repetition rate of 5.5 Hz and an energy density of 6 J/cm^2 during 50s of data acquisition. The instrumental mass bias for Hf isotopes was corrected using the exponential law and a $^{179}Hf/^{177}Hf$ value of 0.7325. For Yb isotopes, the mass bias was corrected using the Hf mass bias of the individual integration step multiplied by a daily βHf/βYb offset factor (Gerdes and Zeh 2009). All data were adjusted relative to the JMC475 of $^{176}Hf/^{177}Hf$ ratio = 0.282160. The ~~and~~ quoted uncertainties are quadratic additions of the within-run precision of each analysis combined with ~~and~~ the reproducibility of the JMC475 (2SD = 0.0028%, n = 8). The ~~A~~accuracy and the daily reproducibility of the method were verified by repeated analysi~~e~~s of the reference zircon GJ-1, Plesovice, and Temora (see Supplementary Table 5), which yielded ~~a~~ $^{176}Hf/^{177}Hf$ of 0.282007 ±0.000025 (2 SD, n=55), 0.282475 ±0.000016 (n=33), and 0.282682 ±0.000028 (n=22), respectively. This is in very good agreement with previously published results (e.g., Gerdes and Zeh, 2006; Slama *et al*. 2008) and with the LA-MC-ICPMS long-term average of GJ-1 (0.282010 ±0.000025; n > 800), Plesovice (0.282483 ±0.000025, n > 300), and Temora (0.282483 ±0.000023, n > 250) reference zircon~~s~~ at GUF.

The initial $^{176}Hf/^{177}Hf$ values are expressed as εHf(t), which is calculated using a decay constant value of 1.867×10−11 year^{-1}, CHUR after Bouvier *et al.* (2008) $^{176}Hf/^{177}Hf_{CHUR,today}$ = 0.282785 and $^{176}Lu/^{177}Hf_{CHUR,today}$ = 0.0336) and the apparent U-Pb ages obtained for the respective domains (see Supplementary Table 5). For the

calculation of Hf two-stage model ages (T_{DM}) in billion years, the measured $^{176}Lu/^{177}Hf$ of each spot (first stage = age of zircon), a value of 0.0113 for the average continental crust, and a depleted mantle $^{176}Lu/^{177}Lu_{DM}$ = 0.0384 and $^{176}Hf/^{177}Hf_{DM}$ = 0.28315 (average MORB; Chauvel *et al.* 2008) were all used. The data are summarised in Supplementary Tables 2 and 3 (see Supplementary Table 5 for the whole data set).

The degree of concordance was calculated using the $^{206}Pb/^{238}U$ and the $^{207}Pb/^{206}Pb$ ages. The calculated ages are considered to be valid when they are 90-110% concordant. $^{206}Pb/^{238}U$ ages are used for <1Ga, whereas $^{207}Pb/^{206}Pb$ ages are used for >1 Ga (see Supplementary material). The age data obtained during this study are illustrated as concordia plots and as density and kernel density estimate plots which highlight the different zircon populations.

The $(^{176}Hf/^{177}Hf)_i$ ratio was calculated from a series of measured isotopes of Yb, Lu and Hf (Supplementary Table 5), as described by Gerdes and Zeh (2006, 2009). $\varepsilon_{Hf(t)}$ represents the deviation of $-^{176}Hf/^{177}Hf$ from the chondritic (CHUR) values for the calculated U-Pb ages of the samples studied. Positive values indicate mantle-derived melts with or without crustal influence, whereas negative values are indicative of recycled, old crust-derived melts. The data obtained are displayed on U-Pb age (Ma) versus $\varepsilon_{Hf(t)}$ plots and are compared with the evolution of different geochemical reservoirs, including CHUR, depleted mantle and continental crust of various ages. The CHUR line (zero) separates positive and negative $\varepsilon_{Hf(t)}$ values. The depleted mantle array is also marked (DM). The line of the mantle array represents new crust, ~~(see Dhuime *et al.* 2011 for an explanation of the method). F~~ for example, juvenile crust forms close to the mantle array (see Dhuime *et al.* 2011 for an explanation of the method). With time, the isotopic ratio evolves parallel to the average crustal evolution trend. In principle, different age populations can have different crustal origins and therefore the Lu-Hf

isotopic data are reported below for each of the age populations that were identified in the different geological units.

To facilitate description and interpretation the new data are displayed in full summarised in Supplementary Tables 2 and 3 in the following categories: number of spots analysed; number of concordant results; the age ranges (oldest to youngest); maximum age of deposition; major populations, peak ages (foref main populations) and $\varepsilon_{Hf(t)}$ values (from for each prominent population); percentage of zircons with $\varepsilon_{Hf(t)}$. Small data clusters are also highlighted. Lu-Hf data are available for the majority of the radiometrically datedgiven for sandstones. for which U-Pb age data are available.

The geochronological plots were produced using the spreadsheets ISOPLOT (Ludwig 2003) and Density Plotter (Vermeesch 2012).

The International Stratigraphic Chart of the International Commission on Stratigraphy is used here for the timescale (Cohen *et al.* 2013; updated).

3. Results

Our new data are reported Below, we summarise new U-Pb radiometric age dating combined with Lu-Hf isotopic analysis of detrital zircons that were extracted from sandstones of Carboniferous and Triassic age, related to the Tauride and, or Anatolide continental units, moving generally from the east to the west, which takes account of the increased geological complexity of the Aegean region (Fig. 1). Preliminary results were summarised by Ustaömer *et al.* 2012, 2016, 2018. Additional supporting documentation is given in the Supplementary material which comprises geological maps of sample locations and selected cathodoluminescence images of detrital zircons.

3.1 Tauride sandstones

3.1.1 Eastern Taurides

Although the Tauride crust is widely accepted as a coherent paleo-tectonic unit prior to late Mesozoic time, it nowadays includes both relatively autochthonous and relatively allochthonous units as a result of late Mesozoic-early Cenozoic collision-related deformation (e.g. Şengör and Yılmaz 1981; Okay and Tüysüz 1999; Robertson et al. 2005). Sandstones were~~as~~ studied from the Aladağ Nappe in the Yahyalı area (Figs. 1 and 2 log a). The Aladağ Nappe is interpreted as an eastward extension of the relatively autochthonous eastern Tauride carbonate platform although it is now a relatively allochthonous unit (Tekeli 1980; Tekeli *et al.* 1984). A sample of quartzarenite (orthoquartzite) (see Supplementary Fig. 1) was analysed from near the top of the Köşkdere Formation. A Late Carboniferous age ~~is~~ has been assigned to this formation based on the paleontologically determined age of interbedded limestones and the presence of the Early Permian Girvanella zone c~~a~~. 40 m above the sample locality (Tekeli *et al.* 1984; Ayhan and Lengeranlı 1986). The quartzarenite is made up of silica-cemented, rounded to subrounded quartz grains (>90%), with rare ~~mica~~ muscovite and opaque minerals. Zircon and tourmaline are accessory phases.

Detrital zircons from one sample of thick-bedded, medium-grained, varicoloured (white, pink, to orange) quartzarenite (S3) were analysed for U-Pb isotopes (Ustaömer *et al.* 2012). The zircons are dominantly well-rounded, which is consistent with prolonged transport from a relatively distal source area and/or several stages of reworking from ~~a pre-existing~~ clastic sedimentary ~~unit~~ rocks (Fedo et al. 2003). A few of the zircons are euhedral or subhedral suggesting nearby derivation ~~from a nearby source area~~. CL images of the zircons (Fig. 3a; see also Supplementary Fig. 2) show that 86% of the

crystals are internally homogeneous, whereas the remainder have xenocrystic cores, enveloped by younger zircon. The homogeneous zircons ~~grains~~ generally show oscillatory zoning, sector zoning and, or complex growth zoning, consistent with an igneous origin (Corfu et al. 2003). Th/U ratios range from 0.01-13.37 (Fig. 4). Xenocrystic cores have rounded margins and commonly exhibit pale or dark grey luminescence without visible zoning, or show weak zoning, consistent with a metamorphic origin (Corfu *et al.* 2003). The Th/U ratios of the individual zircons and where present, the internal zircon domains (n=221) are <0.1 (Fig. 4). Rare zircon grains show fir tree-type zoning, typical of metamorphic zircons (Corfu *et al.* 2003).

The numerical U-Pb age data are shown as a concordia diagram and as histogram and kernel density plots in Figure 5 a,b. The ages of the metamorphic zircon domains, where present, range from 2487-555 Ma, with Neoproterozoic ages predominating. Zircon percentage abundances are shown in Figure 6. The dominant age population is Tonian-Stenian– (40.5%), followed by Ediacaran-Cryogenian (37.8%) and then by Paleoproterozoic (11.7%). There is a small Archean age cluster (9.9%) (see also Supplementary Table 2).

3.1.2 Central Taurides

The ~~outcrops in the~~ Central Taurides are dominated by the Tauride Autochthon (Geyikdağ), as well exposed in the ~~(~~Anamas-Akseki area~~)~~ (Fig. 1). As a composite succession, ~~In general,~~ Precambrian metamorphic rocks are overlain ~~locally~~ by Cambro-Ordovician quartzitic sandstones, neritic carbonates and shales. There is then~~,~~ ~~terminating in~~ a regional unconformity, followed by~~. There are then~~ Carboniferous terrigenous sediments and neritic carbonates. Unconformably above there are then ~~this come~~ varied Triassic terrigenous clastic sedimentary rocks, and finally the regional-scale

~~regional~~ Jurassic-Cretaceous Tauride carbonate platform succession (Dumont and Monod 1976; Dumont 1978; Dumont and Kerey 1975; Gutnic *et al*. 1979; Özgül *et al.* 1997) (Fig. 2 log b).

Two contrasting siliciclastic successions are exposed in the Anamas-Akseki ~~different~~ areas (Geyikdağ). The older Kasımlar Formation~~of these~~ in the southeast, ~~termed the Kasımlar Formation,~~ of Mid-Late Triassic age, comprises deep-marine, normal-graded sandstone-shale turbidites, with occasional interbedded~~of~~ debris-flow deposits ~~interbeds~~ (Fig. 2 log b). The younger Üzümdere Formation ~~of the two successions~~ (c. 60 km to the northwest), ~~the Üzümdere Formation,~~ of Late Triassic-earliest Jurassic age, is made up og shallow-marine, deltaic to terrestrial limestone, sandstone and conglomerate (Fig. 2 log c). No underlying succession is exposed in this area, however, ~~but~~ the sandstones are overlain by the regional Jurassic-Cretaceous Tauride carbonate platform succession (Monod 1977; Şenel 1996).

3.1.2.1 Kasımlar Formation

Two samples of respectively, fine and coarse-grained sandstone (K.12.75 & K.12.78) were collected from near Kasımlar town (Fig. 1; see Supplementary Fig. 3). They~~se~~ comprise monocrystalline and polycrystalline quartz, muscovite, biotite and phyllite lithoclasts. Zircon crystals occur within ~~detrital grains of both~~ muscovite~~- and~~ quartz-bearing detrital grains and also as isolated grains within the matrix.

The first sample (K.12.75) contains both euhedral and variably rounded to well-rounded zircons, all of which show oscillatory zoning but only rarely core and mantle structure. (Fig. 3b, see Supplementary Fig. 4). Th/U ratios range from 0.05-1.95, of which 90% have ratios of 0.2-1 (Fig. 4). Two unzoned zircon rims with pale grey luminescence have ratios of 0.05 and 0.08, typical of metamorphic crystallisation. The

zircons in the second sample (K.12.78) are variably rounded, together with a few euhedral crystals (see Supplementary Fig. 5). Most have oscillatory zoning and homogeneous internal structure, although a few have core and mantle structure (e.g. Fig. 3b, –spots 294 and 346). Some of the zircons have sector zoning and other recrystallization textures (e.g. Fig. 3b, -spots 327 and 338). The Th/U ratios of 111 spots analysed range from 0.1-3.86, with 98% being >0.3, and so indicating a magmatic origin (Fig. 4).

The age data are displayed as Zzircon percentage abundances are shown in (Figure 6), and the U-Pb data as a whole are summarised as concordia (Fig. 7a, b) and also as histograms and a kernel density estimate plot (in Fig.ure 8 a, b). The dominant age population is Tonian-Stenian (33%), followed by Ediacaran-Cryogenian (29%) and Paleoproterozoic (11%). There are also small clusters of Archean and Paleozoic ages. All of the geological systems from Cambrian to Permian are well-represented in the two samples (21 and 11 concordant ages, respectively). One of the samples (K.12.78) includes two Triassic (Anisian-Ladinian) zircons. Lu-Hf analyses of the two sandstone samples are plotted on an age (Ma) vs. $\varepsilon_{Hf(t)}$ diagram in Figure 9 a-b. The major populations of exhibit highly evolved to strongly juvenile $\varepsilon_{Hf(t)}$ values (see also Supplementary Table 3).

3.1.2.2 Üzümdere Formation

The sample from the Üzümdere Formation (K.13.77) was collected from typical thick-bedded, reddish-brown, medium-grained sandstone (see Fig. 1 and also Supplementary Fig. 6 for sample location). AIt is composed of angular to sub-rounded grains of felsic volcanic rocks, quartz mica schists, chert and quartzitemetamorphic, igneous and sedimentary rocks, occur in decreasing order of abundance. Zircons are

variably rounded and show oscillatory growth zoning; sector zoning is locally present (e.g. Fig. 3c; see Supplementary Fig. 7). In some cases, zoning is poorly defined or complex (see also Supplementary material). Th/U ratios range from 0.05-3.78, consistent with an igneous origin; however, a single grain has a ratio of 0.05, indicative of a metamorphic origin (Fig. 4).

Zircon percentage abundances are shown in Figure 6; the U-Pb concordia diagram in Fig. 7c; histograms and also kernel density estimates for the U-Pb data are in Figure 8c. The dominant age population is Ediacaran-Cryogenian (30%), followed by Tonian-Stenian (22.6) and Cambrian (18.3%). Paleoproterozoic (12.9%) and Ordovician zircons form small clusters. Plotted on an age (Ma) vs. $\varepsilon_{Hf(t)}$ diagram (Fig. 9c), the Lu-Hf data for the major populations exhibit highly evolved to strongly juvenile $\varepsilon_{Hf(t)}$ values (see also Supplementary Table 3).

3.1.3 Anatolides

The Afyon Zone, the more southerly of the two crustal units making up the Anatolide continental unit includes a structurally complex, composite unit which outcrops northwest of the major city of Konya (Fig. 1). The Afyon Zone was metamorphosed to high-P/low-T conditions during Paleocene time (Candan *et al.* 2005; Pourteou *et al.* 2010, 2013; Özdamar *et al.* 2013).

3.1.3.1 Konya Complex

The highly deformed Konya Complex encompasses an intact Late Silurian-early Carboniferous carbonate platform succession, which is depositionally overlain by a Carboniferous melange unit (Fig. 2, log d). The melange includes blocks of black ribbon chert and recrystallized neritic to pelagic limestone of Silurian, Devonian and Carboniferous ages, together with volumetrically minor basic igneous rocks (e.g., basalt,

gabbro). The melange is unconformably overlain by non-marine to shallow-marine mixed terrigenous-carbonate sediments of Triassic age, with the addition of basic to felsic alkaline volcanic rocks in some areas (Özcan *et al. 1990*; Eren *et al.* 2004; Göncüoğlu *et al.* 2000, 2007; Candan *et al*. 2009; Robertson and Ustaömer 2009a, 2011; Akal *et al.* 2012; Güven *et al.* 2012; Özdamar *et al.* 2013; see also Supplementary Fig. 8).

One sample (K13.75) of medium-bedded, medium-grained sandstone was analysed from the Carboniferous melange matrix (Fig. 1 and Supplementary Fig. 8). This ~~sandstone~~ is dominated by polycrystalline and monocrystalline quartz, plagioclase, quartzite and granite, together with minor zircon and tourmaline. Most zircons are rounded, together with a small number of euhedral grains. Most grains show oscillatory zoning, consistent with a magmatic origin (Fig. 3d; see Supplementary Fig. 9). Some CL images have ~~show~~ sector zoning, post-crystallisation alteration, or recrystallisation textures, although some crystals lack internal zoning. Core and mantle structure is occasionally present but without zoning in the mantle rims. Th/U ratios of <0.1 in the rims indicate a metamorphic origin (Fig. 4). The Th/U ratios of analysed spots ~~analysed~~ range from 0.04-2.58 ~~that~~and, together with ~~the presence of~~ oscillatory zoning, indicate an igneous origin. Concordant ages from the metamorphic rims of the zircons range from 635-555 Ma (Ediacaran). U-Pb concordia plots, histograms and kernel density estimates are shown in Figure 5c-d, and zircon percentage abundances in Figure 6 (see also Supplementary Table 2). The dominant population is Tonian-Stenian-aged (43%), followed by Ediacaran-Cryogenian (34%) then ~~and~~ Paleoproterozoic (12.2%). Small clusters of Archean and Cambro-Ordovician age also occur. When plotted on an age (Ma) vs. $\varepsilon_{Hf(t)}$ diagram, the major populations indicated by the Lu-Hf analyses exhibit

highly evolved to strongly juvenile $\varepsilon_{Hf(t)}$ values (Fig. 10a; see also Supplementary Table 2).

3.1.4 Karaburun Peninsula

The Karaburun Peninsula of westernmost (Aegean) Turkey (Fig. 1; Supplementary Fig. 10) is dominated by a Paleozoic melange with a Mesozoic cover succession of rift-related and platform carbonates (Erdoğan 1990; Erdoğan *et al.* 1990; Robertson and Pickett 2000; Robertson and Ustaömer 2009b; Okay *et al.* 2012). The melange is cut by a small (<1 km in diameter) Early Triassic granite (Akal et al. 2011; Ustaömer et al. 2016).

Although unmetamorphosed, the Paleozoic-Mesozoic of the Karaburun Peninsula is treated below as a separate tectonic unit from the Taurides because there is no unbroken outcrop continuity between the two areas. However, the two crustal bodies can be broadly correlated based mainly on the presence of similar Mesozoic carbonate platform successions (Erdoğan 1990; Erdoğan *et al.* 1990; Robertson and Pickett 2000; Okay *et al.* 2012).

3.1.4.1 Karaburun Melange

~~This melange is also exposed in the Karaburun Peninsula of westernmost (Aegean) Turkey (Fig. 1; Supplementary Fig. 10). Although there is no continuous outcrop between the overlying Mesozoic succession in the Karaburun Peninsula and the Taurides to the southeast, the two can units be correlated mainly based on the presence of similar Mesozoic carbonate platform succession (Erdoğan 1990; Erdoğan *et al.* 1990; Robertson and Pickett 2000; Okay *et al.* 2012).~~

The melange, which has no exposed base (Fig. 2 log e), is dominated by Silurian, Devonian and~~to~~ Carboniferous blocks of neritic to pelagic limestone, black ribbon chert and rare basic to intermediate-composition extrusive igneous rocks (Kozur 1997, 1998; Robertson and Ustaömer, 2009b). Blocks of Silurian-Devonian pelagic carbonates are rich in cephalopods, similar to coeval counterparts in the Taurides (Göncüoğlu *et al.* 2007~~; Robertson and Ustaömer, 2000b~~). The melange matrix is unfossiliferous. However, recent detrital zircon age dating suggests a Permian-Carboniferous age (Löwen *et al.* 2017~~8~~; see below). The matrix is dominated by lithoclastic sandstone turbidites together with some debris-flow deposits. The melange is unconformably overlain by an Early Triassic succession, mostly conglomerate and neritic to pelagic limestone, radiolarian chert and alkaline volcanic-rocks (Erdoğan *et al.* 1990; Robertson and Pickett, 2000; Robertson and Ustaömer 2009 a, b, 2011).

A sample (K.13.102) ~~was collected from~~of medium to thick-bedded pebbly sandstone was collected from ~~of~~ the melange matrix in the northern part of the Karaburun Peninsula (Fig. 2 log e). The sandstone is poorly sorted~~,~~ with angular grains set in a fine-grained matrix. The main components are polycrystalline quartz, chert, granite and quartz-chlorite-muscovite schist fragments. The granitic grains are dominated by quartz, plagioclase and orthoclase. Less common volcanic rocks fragments include quartz phenocrysts set in a recrystallized felsic matrix. Monocrystalline quartz grains exhibit undulose extinction and deformation lamellae. Zircons occur within some quartz grains in the form of thin, elongate euhedral inclusions. In contrast, zircons in the matrix are commonly rounded.

Although some zircons lack internal zoning, most show oscillatory zoning or, rarely, convolute zoning**,** complex growth zoning or sector zoning (Fig. 3e; see Supplementary Fig. 11). In some cases, grain margins are recrystallized (although the

grain size was too small to analyse). A few zircons have xenocrystic core and mantle structure, with either one or two growth envelopes of metamorphic origin. Th/U ratios range from 0.01-1.51 (Fig. 4). Two values (0.05 and 0.01) are indicative of a metamorphic origin, for which the U-Pb ages are 572 Ma (Ediacaran) and 2600 Ma (Palaeo-Proterozoic).

U-Pb Concordia, histogram and kernel density estimate diagrams of the detrital zircons are ~~given~~ shown in Figure~~.~~ 5e, f and their percentage abundances in Figure 6. The dominant population is Devonian (30.9%), followed by Paleoproterozoic (26.8%) and then by Ediacaran-Cryogenian (20.6%). Small clusters of Archean age also occur in thi~~s~~se sample. For the Lu-Hf analyses, o~~O~~n the age (Ma) vs. $\varepsilon_{Hf(t)}$ diagram ~~for the Lu-Hf analyses~~ (Fig. 10b), 60% of the Devonian population exhibits superchondritic $\varepsilon_{Hf(t)}$ values, whereas the other major populations have highly evolved to strongly juvenile $\varepsilon_{Hf(t)}$ values (see also Supplementary Table 2).

3.1.4.2 *Güvercinlik Formation*

The cover succession in the Karaburun Peninsula includes a intact succession of Late Triassic sandstones, named the Güvercinlik Formation, which allows close comparison with the sandstones of similar age in the adjacent Taurides (see above). ~~Also from the Karaburun Peninsula, one sample of sandstone (K.13.104) was collected from the Late Triassic~~The Güvercinlik Formation ~~(Fig. 2 log e; Supplementary Fig. 10). This formation~~ includes fluvio-deltaic to shallow-marine mudrocks, sandstones and minor coarser-grained clastic sedimentary rocks. The ~~Güvercinlik F~~formation can be~~is~~ correlated with the regionally distributed Çayır Formation which is of latest Triassic-Early Liassic age throughout the Tauride autochthon (Geyikdağ) ~~s~~ and also within parts of the associated (relatively allochthonous) ~~adjacent~~ Bolkar and Hadim Nappes (Monod

and Akay 1984; Erdoğan 1990; Robertson and Pickett 2000; Çakmakoğlu and Bilgin 2006; Mackintosh and Robertson, 2009).

~~The formation is regionally overlain by Jurassic-Cretaceous shallow-water platform carbonates, similar to the Taurides.~~

~~A~~One sample of red, poorly sorted, fine to medium-grained non-marine sandstone (K.13.104) was collected from the Late Triassic Güvercinlik Formation (Fig. 2 log e; see Supplementary Fig. 10). ~~(see Supplementary material for location)~~ The sandstone contains monocrystalline and polycrystalline quartz, together with rare lithoclasts of phyllite and felsic volcanic rocks. Zircons, ranging from rounded to subhedral, were observed in the matrix (Fig. 3~~fe~~; see Supplementary Fig. 12). Oscillatory zoning predominates indicative of a magmatic origin. Most grains have a homogeneous internal fabric but a few have core and mantle structure. Th/U ratios range from 0.05-2.26, of which four values are <0.1, consistent with a metamorphic origin (Fig. 4). The zircon percentage abundances (Fig. 6), U-Pb concordia (Fig. 7d) and both the histogram and kernel density estimates (Fig. 8d) indicate that three ~~the dominant~~ populations of equal size (20.9%) dominate the sample; i.e. Carboniferous, Ediacaran-Cryogenian and Paleoproterozoic. There is also a subordinate Tonian-Stenian population (16.3%) and small clusters of Archean, ~~is~~ Devonian (30.9%) and Cambro-Ordovician ages (Fig. 6). ~~, followed by Paleoproterozoic (26.8%) and Ediacaran-Cryogenian (20.6%). There is also a small cluster of Archean ages (Fig. 6).~~ In the age (Ma) versus $\varepsilon_{Hf(t)}$ diagram (Fig. 9d), the major Carboniferous population exhibits evolved $\varepsilon_{Hf(t)}$ values, whereas the other major populations ~~show~~ have highly evolved to strongly juvenile $\varepsilon_{Hf(t)}$ values (Fig. 9d). Only 23% of the zircons exhibit~~s~~ positive $\varepsilon_{Hf(t)}$ values (see Supplementary Table 3). The main juvenile zircon formation events occurred at 2.1 Ga (Palaeoproterozoic), 0.8-0.5 Ga (Neoproterozoic) and 354 Ma (earliest Carboniferous).

3.2 Carboniferous granitic rock data

To supplement the age data for potential source rocks in the region, we have also analysed zircons from Late Paleozoic granites of the Afyon Zone (Anatolides continental unit), in which the host rocks are quartzite, phyllite and meta-carbonates (Fig. 1). Candan *et al.* (2016) have recently reported several small (km-sized) isolated plutons of Carboniferous porphyritic and granoblastic metagranite from the Simav-Alaçam area, near the northwestern margin of the Afyon Zone (Fig. 1; Supplementary Fig. 13). Seven different bodies were recently dated by the zircon U-Pb method (Candan *et al.* 2016), yielding 330-315 Ma for porphyritic metagranites (three samples) and ~320 Ma for granoblastic metagranites (two samples).

To test and extend the available age data, we sampled one each of the previously dated porphyritic (TM.17.33) and granoblastic (TM.17.35) metagranites and also collected a sample from an undated nearby porphyritic metagranite (TM.17.34; see Supplementary Fig. 13 for sample locations). Our new Lu-Hf isotopic data from these granitic rocks help shed light on the possible provenance of the Carboniferous and Triassic sandstones studied and other crustal units in the region. ~~Their Lu-Hf isotopic compositions aid comparisons with Carboniferous and Triassic sandstones elsewhere (see below).~~

~~The~~ Our new U-Pb ages (see Suplementary material for the whole data set) ~~of~~ for the metagranites yielded Carboniferous crystallisation ages, consistent with the ~~earlier~~ previous results (Candan *et al.* 2016). Two porphyritic metagranite samples, one of which was dated at 314.9±2.4 Ma by Candan *et al.* (2016), gave TuffZirc ages of 313.24 +1.43 -0.68 Ma (TM.17.33) and 316.00 +0.81 -0.88 Ma (TM.17.34), respectively. Zircons from the porphyritic metagranites are homogenous, except for TM.17.33 that

contains one inherited zircon of Devonian age (400±3 Ma; 92% concordant). Zircons from a granoblastic metagranite intrusion (TM.17.35) that was previously dated at 321.9±2.6 Ma (Candan *et al.* 2016) are dominated by core and mantle-type zircons, indicating the role of crustal melting. Some homogenous zircons and the rims of the core and mantle-type zircons yielded Carboniferous ages~~,~~ ranging from 343 to 313 Ma. Th/U ratios of some of the rims are <0.1, suggesting a metamorphic origin. The ages of the metamorphic rims are variable but some are dated at <319 Ma.

The density probability curve for the Carboniferous igneous zircon domains (see Supplementary material) produced two peaks, at 332.9±1.9 Ma and 323.4±1.9 Ma. The younger age is interpreted as the crystallisation age of the pluton and the older age an earlier magmatic event. The ages of the inherited cores range from 3095 Ma (Mesoarchean) to 361 Ma (Upper Devonian). Five of the zircon cores are Devonian (391 to 371 Ma), two Ordovician (~456 Ma), 10 Ediacaran (628 to 550 Ma) and five others have older ages. Of the few Carboniferous ages ~~are few~~ in this sample ~~and~~ some ~~of these~~ have very low Th/U contents (<0.1) suggesting that the metagranite was affected by late Carboniferous metamorphism.

On the age (Ma) vs. $\varepsilon_{Hf(t)}$ diagram (Fig. 11), the U-Pb-Hf isotopic measurements indicate that all of the the metagranite samples have subchondritic $\varepsilon_{Hf(t)}$ values, ranging from -12.6 to -5.3 in sample TM.17.35, from -17.6 to -4.9 in sample TM.17.33 and from -9.4 to -3.2 in sample TM.17.34, indicating a crustal origin for the Carboniferous felsic magmatism. Hf model ages range from 2.11 to 1.33 Ga.

4. Previous U-Pb and Lu-Hf zircon data

We now summarise previous data from the Tauride and Anatolide continental units and the Karaburun Melange to enable synthesis and regional comparison of the different tectonic units.

4.1 Tauride units

U-Pb-Hf analyses are available for eight samples of the Neoproterozoic metamorphic basement of the Tauride ~~A~~autochthon (Dipoyraz Dağ), and for four samples of sandstone ~~samples~~ from its Paleozoic-Early Mesozoic sedimentary cover (Abbo *et al.* 2015) (Fig. 1). One of these samples is from the Kasımlar Formation in the ~~(~~Karacahisar area~~)~~, c~~a~~. 25 km northeast of the two samples studied by us. This sample is dominated by Neoproterozoic-aged zircons, together with a single concordant Permian zircon.

Sandstones of Cambro-Ordovician age ~~that~~ were collected from the northern part of the Tauride autochthon during this study (i.e. Seydişehir Formation) but unfortunately did not yield usable zircons. However, some U-Pb detrital zircon data do exist for ~~a~~ Late Ordovician glacial ~~unit~~ sediments (diamictites and lonestones) that are exposed in the Central and Eastern Taurides (four samples) and also in the Arabian Platform of SE Turkey (one sample) (Gürsu *et al.* 2017). The major zircon populations in these samples are Neoproterozoic with minor clusters ~~at~~ of Paleoproterozoic and Archean age.

4.2 Menderes Massif

The Menderes Massif is a regional-scale metamorphic assemblage in western Anatolia (Fig. 1) that is dominated by Paleozoic schist and Mesozoic meta-carbonate rocks with a Precambrian high-grade metamorphic basement (Okay 2001; Özer *et al.* 2001; Candan 2011).

U-Pb-Hf zircon data are available for both the Neoproterozoic basement schists and paragneisses (six samples) and the overlying Early Paleozoic meta-siliciclastic succession (three samples) (Zlatkin *et al.* 2013).~~Zlatkin *et al.* (2013) provided U-Pb zircon data for the Neoproterozoic basement and Early Paleozoic siliciclastic cover of the Menderes Massif (Fig. 1).~~ The overall age range of the main zircon populations resembles that~~ose~~ from the Tauride basement in the Karacahisar area (Abbo *et al.* 2015; see above) ~~but~~ although individual age populations vary. The maximum depositional age ~~of deposition~~ of the basement schists is constrained as Late Ediacaran (570- 550 Ma), as indicated ~~-~~by the age of the youngest detrital zircons in the schists (570 Ma) and the age of cross-cutting felsic intrusions (550 Ma). In contrast to the ~~basement schists in the~~ Karacahisar area, the basement schists in th~~os~~e ~~of the~~ Menderes Massif appear to have received little input from 1.0 (Tonian) and 2.5 Ga (Paleoproterozoic) crustal units. The detrital zircon age spectra of the overlying Early Paleozoic meta-siliciclastic sediments resemble those of Ordovician sandstones in Jordan (Morag et al. 2011).

4.3 Karaburun Peninsula

~~Löwen *et al.* (2018) reported~~ U-Pb detrital zircon ages have been reported from siliciclastic sandstones of the Karaburun Melange and related formations of Late Paleozoic and Early Mesozoic ages (15 samples) (Löwen et al. 2017). ~~The~~ U-Pb ages range from Archean to Triassic in these sandstones. Permo-Carboniferous, Devonian, Silurian, Ordovician and Late Neoproterozoic zircon populations were used to infer source areas. The authors assumed that the north~~-~~-Gondwana margin was magmatically inactive since the Cambrian, and that it remained isolated from lithologies affected by the Variscan ~~source~~orogeny. The ~~-~~provenance was therefore considered to be from the north, from the Sakarya, Pelagonian and/or Rhodope zones of western~~W~~ Turkey, Greece and, or Bulgaria. Two samples from the Karaburun Melange (Dikendağı Formation of

Löwen *et al.* 20178) have very similar populations to those in the Palaeozoic and Mesozoic siliciclastic sediments of the Taurides and the Afyon Zone (Konya Complex melange), as reported here.

4.4 Konya Complex

U-Pb detrital zircon ages from meta-sandstones of the clastic upper part of the Konya Complex (six samples) and the overlying early Mesozoic sedimentary cover (two samples) were recently reported by Löwen et al. (2019). These authors subdivided the clastic upper part of the complex into two parts: a lower melange unit and an overlying 'flysch unit'. In summarising their data below we use the same criteria for concordance as we do with our data. On this basis, the ages of detrital zircon populations of the three samples from the melange unit is identical to the one sample (K.13.75) reported in this study (i.e. Silurian, Ordovician, Cambrian and Precambrian), although the number of zircons in individual populations vary from sample to sample. The overlying 'flysch' unit, on the other hand, differs from the melange unit with a variable input (53%-T.14.36, 22%-T.14.39 and 2%-T.14.22) from a Devonian igneous provenance. Two of their samples with Devonian zircons aslo contain Tonian-Stenian (0.8-1.1 Ga) zircons, whereas the remaining one lacks a Tonian-Stenian population, similar to our Karaburun melange sample. The maximum age of deposition based on the youngest concordant detrital zircon is Silurian (423 Ma) for the melange unit and Carboniferous (308 Ma) for the 'flysch' unit. As for the Karaburun melange, Löwen et al. (2019) envisage the Devonian granites of the Sakarya Zones (Eurasia) as the source of the Devonian detrital zircons in their 'flysch' unit, whereas the melange matrix was sourced from the N-Gondwana margin.

The two Triassic sandstone samples (T.14.29 and T.14.30) of Löwen et al. (2019) yielded abundant Permian (275 Ma) to Triassic (206 Ma) zircons (90% of the whole data) but no Devonian zircons and only six grains of Precambrian zircons. The Permo-Triassic zircon population is characterised by a high-U content in one of the samples. The authors suggest that the source of the Triassic zircons was the S-Eurasian margin. However, there are alternatives. For example, volcanic rocks (meta-trachyandesite, meta-rhyolites) alternate with red, continental clastics in the Kadınhanı-Konya area. Available geochronological data indicates that the volcanism in this area took place during Permian (259 Ma) to Triassic l (220 Ma) (Akal et al. 2012, Güven et al. 2012; Ustaömer et al. 2016; Özdamar et al. 2013), similar to the age range of the Permo-Triassic detrital zircons. However, a detailed comparison of the Permian-Triassic detrital zircons and lavas is not yet possible because Hf data are available only for a few of the lavas (Ustaömer et al. 2016a).

5. Discussion

Below, we consider the implications of the combined new and ~~existing~~ published U-Pb and Lu-Hf data for the provenance, paleogeography and tectonic setting of the Carboniferous and Triassic units studied, and the regional development of Tethys. In the discussion, we assume that there has been, at most, only modest (several hundred kms) E-W lateral (strike-slip) displacement of the Gondwana versus Eurasian crustal units, which is compatible with Pangea-A-type reconstructions (e.g. Garfunkel, 2004; Smith, 2006). However, we exclude consideration of Pangea-A type reconstructions which infer thousands of kms of relative displacement because of absence of definite supporting geological evidence (e.g. Muttoni *et al.* 2003).

5.1 N Gondwana provenance

The Precambrian age populations (i.e. Edicaran and Tonian) from the Tauride units as a whole are effectively identical to those of the NE African-Arabian shield (Ustaömer *et al.* 2012, 2016, 2018; Zlatkin *et al.* 2013~~4~~; Abbo *et al.* 2015; Gürsu *et al.* 2017). Most of the new and pre-existing Lu-Hf isotopic data for Neoproterozoic zircons are also consistent with derivation from NE Africa~~n~~-Arabia.~~,~~

Our U-Pb data for the Carboniferous sandstones of the matrix of the melange in the Konya Complex ~~melange matrix~~ (part of the Afyon Zone) show close similarities with the sandstones from the eastern Tauride continental units~~s~~ (Aladağ Nappe) (Figs. 12, 13). The Aladağ Nappe ~~succession~~ (Fig. 2 log a) is restored as part of the northern margin of the Tauride microcontinent in view of its stratigraphic similarities with the Tauride continental units~~s~~ as a whole (Tekeli 1980; Özgül 1976). Detrital zircons from a cobble in the basal conglomerate of the Carboniferous succession in the south-central Taurides (Karacahisar Dome) (Fig. 1**)** have yielded a similar zircon age-distribution population (Abbo *et al.* 2015). In addition, ~~Löwen *et al.* (2018b) report~~ a Devonian zircon population has very recently been reported from the Konya Complex (Löwen *et al.* 2018, 2019).

The source rocks of both the Tauride and the Anatolide Carboniferous sandstones were predominantly Neoproterozoic, with sparse Palaeoproterozoic and Archean~~-aged~~ zircons (Fig. 13). For the Anatolide continental unit, o~~O~~ur Lu-Hf data indicate derivation from a combination of juvenile and evolved sources~~ for the Anatolides~~. Some of the Neoproterozoic zircon populations in the Konya Melange sandstones have juvenile hafnium isotopic signatures, consistent with derivation from a juvenile source like the Arabian-Nubian shield (Robinson *et al.* 2016). The presence of strongly evolved Neoproterozoic zircons is suggestive of derivation from igneous sources formed by mixing of juvenile melts with older continental crust. ~~the Pan-African orogenic belt in~~

~~NE Africa.~~ Overall, the Neoproterozoic zircons are likely to have been derived from diverse sources within the NE Africa-Arabia. The Precambrian zircon populations of the Carboniferous Konya Complex and the Tauride Kasımlar and Üzümdere formations are effectively identical (Figs. 12, 13) ~~indicating~~ suggesting that the southerly provenance persisted for a very long time period.

The poorly dated Early Paleozoic (i.e., post-Precambrian/pre-Carboniferous) sedimentary cover of the Menderes Massif (Fig. 1) has U-Pb age populations and hafnium isotopic compositions (Zlatkin *et al.* 2013) that are similar to the Taurides and Anatolide continental units. The Menderes Massif has been correlated with the Anatolides (Ketin l964; Şengör and Yılmaz l981) implying that it represents a single crustal block, despite ~~although it~~ lackings the characteristic Anatolide high-pressure/low-temperature metamorphism (Candan *et al.* 2010; Pourteou *et al.* 2013). Alternatively, it has been suggested that the Menderes Massif was separated from the Anatolide continental units (to the north) by a sedimentary basin during the Mesozoic (Porteau *et al.* 2016). In addition, the Menderes Massif is generally accepted to have been separated from the Tauride carbonate platform to the southwest (Bey Dağları) (Fig. 1) by an intra-continental basin (Tavas basin) (Poisson 1977, 1984; Şenel *et al.* 1991; Collins and Robertson, 1998; Robertson *et al.* 2013). In our view, t~~T~~he Menderes Massif is best interpreted as being closely related, compositionally and paleogeographically, to the Tauride ~~microcontinent~~ continental unit (Özer *et al.* 2001; Robertson *et al.* 2012, 2103; Barrier *et al.* 2018).

Several factors support ~~(or are consistent with)~~ a dominantly Gondwana-related source for all of the Late Paleozoic-early Mesozoic sandstones ~~discussed~~ mentioned above, other than those of the Karaburun Melange and its cover succession (see below):

1. The Carboniferous and Late Triassic sandstones are all dominated by Late

Precambrian zircons; 2. The relative abundance of Cambrian zircons in the Late Triassic Tauride cover succession (Üzümdere Formation) is suggestive of erosion of Cambrian volcanic rocks, as represented by the nearby ~~(~~Sandıklı Porphyroids~~,), as exposed~~ near Sandıklı (Fig. 1) (Kröner and Şengör 1990; Gürsu and Göncüoğlu 2006, 2008). Surface uplift related to Triassic rifting of Neotethys liberated the granitic and schistose detritus that now resides ~~occurs~~ within the Triassic sandstones; 3. Granitic intrusions within the Tauride-related units, for example the Carboniferous meta-granitic rocks of the Afyon Zone (Candan *et al.* 2016; this study) represent a nearby source of Carboniferous grains within the Triassic sandstones; 4. Localised Early Triassic meta-granites in the Menderes Massif (Koralay *et al.* 2001;~~Akal *et al.* 2011;~~ Ustaömer *et al*. 2016) are possible nearby sources for rare Early Triassic zircons, as ~~which is also~~ consistent with their slighly positive $\varepsilon_{Hf(t)}$ ~~hafnium~~ signatures as reported by Ustaömer *et al.* 2016 (their fig. 13); 5. The small granite in the Karaburun Peninsula (Akal *et al.* 2011; Ustaömer *et al.* 2016a) could also be considered as a source for the rare Early Triassic zircons although this seems unlikely because the $\varepsilon_{(Hf)t}$ composition of the Karaburun granite is highly negative in contrast to the Menderes Triassic granite and the two Triassic detrital zircons. ~~.~~

The compositional homogeneity and commonly well-rounded texture of the Precambrian zircon grain populations in both the Tauride and Anatolide sandstones (Fig. 3; see also supplementary material) ~~—~~suggest that the erosional products of the source schistose basement were widely dispersed and well mixed in the shelf seas that prevailed along the ~~bordering the~~ north margin of Gondwana. These Gondwana-derived sandstones are well ~~accumulated widely along the north Gondwana margin, now~~ represented by the shallow-marine sandstones of mainly Ordovician-Carboniferous age within the Taurides continental unit (e.g. Geyikd ~~D~~ağ) and related allochthonous units (e.g. Bolkar and Hadim Nappes) (Özgül, 1976; Mackintosh and Robertson, 2012;

Wehrmann et al. 2010). Some of these sandstones are likely to ~~could~~ have been derived directly from local basement highs within ~~in~~ the Tauride crust (e.g. Sandıklı Massif) (~~Özgül, 1976;~~ Mackintosh and Robertson, 2012). The distal continental margin (northerly) crust of pre-Jurassic age is largely concealed by the Late Cretaceous-Early Cenozoic southward emplacement of allochthonous continental margin units (e.g., Bozkır, Bolkar and Hadim nappes) and ophiolite-related units. Also, the distal (southward) edge of the Tauride crust is largely concealed by the northward emplacement of the Antalya Complex (Antalya Nappes) in SW Turkey, including both continental margin and ophiolite-related units. One possibility is that

~~Small zircon populations of Cambrian, Ordovician, Permian age and also isolated instances of Devonian, Carboniferous and Triassic zircons in the Tauride Triassic sandstones indicate magmatic events of these ages somewhere along the north margin of Gondwana, although potential source igneous rocks are poorly known (MTA 2002).~~ ~~T~~the Cambrian and Ordovician zircons could~~an~~ be explained by pulsed extension of the northern margin of Gondwana, prior to final break-up during the Triassic. On the other hand, ~~T~~the Carboniferous zircons may relate to subsequent subduction-related magmatism, as locally documented in the Afyon Zone (Candan et al. 2016). ~~(Konya Complex) and the Taurides (e.g. Sultan Dağ) (Göncüoğlu *et al.* 2007; Mackintosh and Robertson 2009; Robertson and Ustaömer, 2011).~~

The Tauride Paleozoic shelf successions were uplifted and locally eroded to produce large volumes of sand~~stones~~ during the Triassic rifting of Neotethys. From the Late Permian onwards, the Tauride microcontinent became progressively isolated from Gondwana. Rifting during the late Permian produced shallow, localised marine basins and highs, whereas deep basins formed by Early-Middle Triassic time, followed by regional continental break-up during the Late Triassic-Early Jurassic to form the S

Neotethys (Gutnic *et al.* 1979; Robertson and Dixon 1984; Garfunkel 2004; Robertson *et al.* 2012, 2013; Barrier *et al.* 2018). The zircons in the Middle-Late Triassic sandstones were, therefore, derived from the Precambrian basement of the Tauride continental unit directly or, more probably, from ~~the~~ its Paleozoic cover ~~of the rifted Tauride crustal unit~~ rather than directly from Gondwana.

5.2 Provenance of Carboniferous zircons

Cambrian, Ordovician, Devonian (minor) and Carboniferous ages are recorded in the Late Triassic Kasımlar and Üzümdere Formations (Figs. 6, 7). As noted above, p~~P~~otential source rocks, for example, felsic igneous rocks are ~~locally~~ exposed in locally the Anatolide continental units, including the Cambrian felsic Sandıklı Porphyroids (Gürsu and Göncüoğlu 2005, 2006) and both Ordovician granites (Okay *et al.* 2008; Özbey *et al.* 2013a,b) and Carboniferous granites (Candan *et al.* 2016; this study).

The provenance of the Karaburun Melange and Konya Complex sandstones differs from that of the Tauride Carboniferous units. Devonian zircon populations are reported from ~~occur in~~ some samples in the Karaburun Melange (Löwen *et al.* 2017~~8 a~~) and also ~~in~~ from the Konya Complex (Löwen *et al.* 2018, 2019 ~~b~~). Devonian-aged zircon cores are also recorded in one sample of Carboniferous Anatolide granites analysed by us (sample TM.17.35) (Fig. 11). The Triassic cover sandstones in the Karaburun Peninsula also contain a prominent Devonian-Carboniferous zircon population (Löwen *et al.* 2017~~8 a~~)(Figs. 8d, 12). In contrast, Devonian zircons are absent from the E~~e~~astern Tauride Carboniferous sandstones~~,~~; ~~whereas~~ conversely, Tonian and Stenian zircons are not recorded in the Karaburun Melange. ~~Also,~~ Paleoproterozoic zircons (c. 2 Ga) are more abundant in the Karaburun Melange sandstones compared to both the Konya Complex and the ~~eastern~~ Eastern Tauride (Aladağ Nappe) sandstones. A clastic source

other than NE Africa alone, therefore, seems to be needed for both the Anatolide and Karaburun Melange Carboniferous sandstones.

The Carboniferous and Triassic sandstones have marked similarities suggesting some degree of common provenance, especially the prominent Ediacaran population (Fig. 6). Cryogenian and Tonian-Stenian populations occur in all samples, except for the Karaburun melange sandstone that lacks the 1.1-0.9 Ga zircon population (Fig. 12). 1.1-0.9 Ga zircons do exist in the overlying Late Triassic Güvercinlik Formation. However, Neoproterozoic zircon populations are subordinate in the Güvercinlik Formation compared to the Tauride Triassic sandstones (Figs. 6, 12). ~~-~~Also, the Paleoproterozoic population (ca. 2 Ga) in the Karaburun Melange Triassic cover succession is enriched~~hanced~~ compared to that in the Tauride Triassic sandstones (Figs. 12, 13). The Carboniferous zircon population is similarly ~~enhanced~~ enriched in the Late Triassic Karaburun Melange cover sandstones compared to the corresponding Late Triassic Tauride sandstones ~~Tauride~~ in which only a few grains of this age range occur. ~~This~~ All of the above evidence points to~~suggests that~~ a specific, probably localised, provenance is required for the Karaburun Melange that is not completely shared by any of the other units discussed above. Similarly, a local provenance seems possible for the Permian-Triassic zircons in the Konya Complex (e.g. Kadınhanı volcanics). Below, we evaluate the wider region for suitable source units.

Below, we evaluate the wider region for suitable source units:

In northern Turkey, the Pontide crustal unit broadly represents the evolving southerly active continental margin of Eurasia, at least during Late Paleozoic to mid-Cenozoic time (Fig. 1). Here, we highlight several lithology and age distributions that may shed light on the provenance of the crustal units farther south.

Within the Pontides crustal unit, the Sakarya Zone (Fig. 1) includes meta-clastic rocks that are dominated by Precambrian zircons of NE Gondwana-Arabia affinities, similar to the Carboniferous sandstones of both the Anatolides and Taurides crustal units (P.A. Ustaömer *et al.* 2012a; Ustaömer *et al.* 2010, 2013). Carboniferous zircons in sandstones from the Aegean islands of Chios, Inousses and Psara, adjacent to the Karaburun Peninsula, have been interpreted to represent derivation from the Sakarya Zone, assuming that it then formed part of the S-Eurasian active continental margin (Meinhold *et al.* 2008, Meinhold and Frei 2008). Similarly, Löwen *et al.* (2017) envisioned infer the presence of a large amount of arc-derived sand, which they see as having been derived from a continental margin arc within the Sakarya Zone. The Late Paleozoic Sakarya continental arc as the source of the Late Paleozoic zircons in the Karaburun melange sandstones were, therefore, sourced from the Eurasian active continental margin, effectively to the north in this interpretation. However, Ppotential source Carboniferous crustal units are also widely exposed in the Balkan region and in both central and western Europe, for example the Austro-Alpine and Armorican crustal units (Meinhold *et al.* 2010a, b).

On the other hand, Despite the published correlations with the S-Eurasia (Meinhold *et al.* 2010a, b; Lowen *et al.* 2017), a northerly (Eurasian) arc-related source should not necessarily be assumed uncritically because, as noted above Carboniferous granitic plutonism also affected the Anatolide crustal continental unit in the Afyon zZone (Candan *et al.* 2016; this study) and could also exist elsewhere. Minor Carboniferous volcanism is also known from the northern part of the Central Tauride Autochthon crustal unit (MTA 2002, Göncüoğlu *et al.* 2007; Mackintosh and Robertson 2009) and also in the Tauride-related Çataloturan nappe (Aladağ Nappes) in the Eastern

Taurides (Göncüoğlu et al. 2007) although the tectonic affinities of these units remain debatable. One possible explanation for the Carboniferous magmatism in the Afyon Zone is that the host crustal unit was part of the S-Eurasian margin until it rifted and drifted southwards to amalgamate with the Tauride continental unit during late Triassic time (Stampfli, 2000; Stampfli *et al.* 2001; Eren *et al.* 2004). This model has been tested extensively by recent fieldwork, however, this has not confirmed the existence of an oceanic suture (Paleotethyan) between the Anatolide and Tauride continental units (Mackintosh and Robertson, 2012).

An alternative approach is to determine whether the isotopic data from the Carboniferous granites of the Afyon Zone are similar to the isotopic data fron the Carboniferous granites of the Sakarya Zone.

The available zircon Hf isotopic data for the two Carboniferous granite assemblages ~~of the Sakarya Zone~~ are compared ~~with those from the Carboniferous granites of the Afyon Zone~~ in Figure 14. The Lu-Hf isotopic compositions of the Carboniferous zircons ~~in~~ of the Anatolide and Tauride sandstones are also plotted. The green dashed line in the figure, corresponding to ca. -5 $\varepsilon_{Hf(t),}$ separates Sakarya crustal unit granites above from the Afyon Zone granites below. The Carboniferous detrital zircons plot in the Afyon Zone granite field, consistent with this as a source for sandstones. ~~—~~Another potential source would be now-eroded ~~surface —~~volcanic equivalents.

In summary, it is possible that the voluminous Carboniferous arc-derived detritus within the Tauride and Karaburun Triassic sandstones could have a relatively southerly, Gondwana-related provenance. This would remove the requirement to infer sources from both Gondwana and Eurasia within the Carboniferous clastic sediments, right down to

the level of , ~~which could explain the intimate mixing of Carboniferous and Gondwana-derived zircons within~~ individual turbidite beds.

5.3. Provenance of Devonian zircons

Devonian zircons form the most prominent population in the Karaburun Melange sandstones and are also present in the overlying Güvercinlik Formation (Löwen *et al.* 2017~~8a~~; this study) (Fig. 12). A ~~-~~small cluster of Devonian zircons (n=5) also exists in the Kasımlar Formation. Carboniferous sandstones of the Konya Complex (Anatolides) also contain Devonian zircons (Löwen *et al.* 2017~~8a~~) unlike the Tauride Carboniferous sandstones (as so far reported). Also, Devonian inherited zircons are common in the Carboniferous meta-granites of the Afyon Zone (Candan *et al.* 2016; this study) (Fig. 11). Assuming a local source for the Devonian zircons,~~By implication, undiscovered~~ Devonian zircon-bearing granitic plutons are likely to exist within~~ed~~ the unexposed (or simply unexplored) deep-level crust of the Afyon Zone. ~~-~~Such crust could also be buried beneath the Tauride or Anatolide thrust sheets or be eroded. However, the ~~abundance of~~ Devonian zircons in the Karaburun Melange are so abundant as to suggest a provenance in the vicinity (i.e. Aegean Turkey) or possibly from farther north, northwest or west~~points to a major westerly source~~.

The Sakarya crustal unit in the NW Turkey ~~west~~ locally includes Devonian granites (Okay et al. 1996; Aysal et al. 2012; Sunal et al. 2012), as in the Biga Peninsula (Fig. 1), which ~~was~~ can therefore be considered as a possible source of the Devonian zircons in the Karaburun Melange. However, the late Carboniferous sandstones of the Karaburun Peninsula have ~~dissimilar~~ different $\varepsilon_{Hf(t)}$ values (Fig. 15). The zircons in the Devonian granites define a tight cluster ~~of~~ with $\varepsilon_{Hf(t)}$ values ranging from −8.5 to −7.1, other than for one with an $\varepsilon_{Hf(t)}$ value of −4.5. In contrast, the Devonian detrital zircons in

the late Carboniferous sandstones of the Karaburun Peninsula exhibit $\varepsilon_{Hf(t)}$ values ranging from −2.1 to +5.4. 61% of the data are superchondritic (Fig. 15). Also, the metasedimentary country rocks of the Sakarya Zone granites have zircon populations indicative of a NE African provenance (P.A. Ustaömer *et al.* 2012a; Ustaömer *et al.* 2016a), unlike the Karaburun Melange that has a provenance similar to NW Africa. Where exposed, the dated zircon populations in southern Turkey are all of NE African type (Menderes Massif; Zlatkin *et al.* 2013); Karacahisar Massif (Abbo et al. 2015), Bitlis Massif-E Taurides (P.A. Ustaomer *et al*. 2012b). In contrast, the provenance of the Karaburun Melange Carboniferous sandstones is characterised by Ediacaran-Cryogenian and Palaeoproterozoic (ca. 2 Ga) zircons, with an absence of Tonian-Stenian zircons, that are typical of a NW African source (Henderson *et al.* 2016~~5~~). Direct supply of zircons from the Devonian granites of the Sakarya Zone to the Karaburun Melange (~~including~~ together with the adjacent Greek islands) and the Konya Complex is, therefore, ~~seems~~ unlikely.

~~Rare~~ Looking farther northwest and west, Devonian orthogneisses and dykes occur within the Vertiskos T~~t~~errane of the Serbo-Macedonian Massif (Greece), representing a late, but volumetrically minor, phase of magmatism after the emplacement of widespread, Silurian arc-type magmatic rocks~~sm~~ (Himmerkus *et al.* 2009), although these appear to be volumetrically minor. Hf isotopic data are not available for these Devonian intrusions but derivation of Devonian zircons from the Vertiscos terrane is unlikely because Silurian zircon are not recorded in the Karaburun Melange sandstone. Devonian zircon populations are also present in sandstones of the Aegean region (Keay and Lister, 2002, Meinhold et al. 2010a, b; Zlatkin *et al.* 2018**)** although no source granitic rocks of this age have yet been reported, which is not surprising as it is largely submarine. Another possible source region for the Devonian

zircons is the Variscan granitic massifs of central Europe~~thereabouts~~. Similar Devonian ages are reported from granitic intrusions in central Europe ~~The combined sedimentary and igneous age evidence instead points to a more westerly provenance for the Devonian zircons. The nearest known crustal units with similar Devonian zircon populations are~~ including the Saxo-Thuringian (ca. 375 Ma), Teplá-Barrandian and Moldanubian units (Bohemian Massif) (Linnemann *et al.* 2004, 2007, 2014; Drost *et al.* 2011; Kosler *et al.* 2014; Eckelmann *et al.* 2014; Dörr et al. 2017). However, more age and Hf isotopic data are needed to test these alternative sediment sources.

Assuming the Devonian zircons were sourced from a continental margin arc broadly to the west, within the Aegean region or central Europe, rather than from~~to the west of~~ the Sakarya continental unit farther north in Turkey, how could ~~(e.g. Aegean and, or central Europe) how did~~ they have reached the Karaburun Peninsula and the Konya Complex ~~Afyon Zone~~ (Afyon Zone~~Konya Complex~~) during the late Carboniferous? A possible explanation is that Palaeotethys sutured in the west during the late Carboniferous, extending as far east as the Aegean region but remained~~, during the late Carboniferous, while remaining~~ open farther east within what is now Anatolia (Zanchi *et al.* 2003; Okay *et al*. 2006; Robertson and Ustaömer (2009a, b; 2011) (Fig. 16). In this interpretation, sediments were eroded from Devonian and, or Carboniferous crust in the west and were then ~~flowed~~ transported into ~~the~~ a surviving deep-marine Tethyan embayment to the east where they were mainly deposited by turbidity currents. Sands are known to be transported by turbidity currents up to ca. 2000 km in modern trench settings, for example in the Aleutians (Piper *et al.* 1973) and Peru-Chile trenches (Schweller *et al.* 1981). It is therefore plausible that deep-marine sands flowed generally eastwards from the by-then sutured Paleotethys in the Aegean region or father west, at least as far as the Konya Complex outcrop~~,~~ (c~~a~~. 500 km east of the Karaburun

Peninsula). The presence of 0.8-1.1 Ga zircons characterises the NE Africa/Arabian-Sahara provenance, whereas the absence of this age assemblage indicates a NW Africa provenance. Sands could have travelled eastwards along the northern margin of Gondwana from a region of NW African provenance (e.g. central Europe). The sands then passed over the submerged Anatolide continental unit (Afyon Zone), where they mixed with more locally derived sands of NE Africa/Arabian-Sahara provenance, as exposed in the Konya Complex.

~~In summary, the sandstone turbidites of the Karaburun and Konya melange matrices are dominated by a mixture of NE Gondwana, Carboniferous and Devonian continental arc-derived detritus, with no requirement for clastic material to cross the remnant Paleotethys from the Sakarya continental arc to the north (Fig. 16).~~

6. Conclusions

~~1. New U-Pb and Lu-Hf isotopic data for detrital zircons from southern Turkey exemplify challenges related to zircon provenance analysis within a complex orogenic belt made up of dispersed crustal units. Taking account of new and existing isotopic data and the regional tectonic setting lead to the following conclusions:~~

~~2.~~1. ~~-~~Late Carboniferous sandstones of the eastern Taurides (Aladağ Nappe) and the Anatolides (Konya Complex) have very similar Precambrian zircon populations that are~~,~~ interpreted to have been derived from NE Gondwana (NE Africa/Arabia).

3.2. Carboniferous zircon populations, characteristic of the more northerly-located Sakarya crustal unit of the Pontides (N Turkey), are absent from the Carboniferous Eastern Tauride and Anatolide (Konya Complex) sandstones. A, opposing the northerly, Variscan orogenic belt as a possible source is therefore unlikely for these units.

4.3. The Precambrian zircon populations of the Mid-Late Triassic Tauride sandstones were also derived from NE Gondwana. Small zircon populations of Cambrian, Ordovician and Carboniferous age in these sandstones, including Tauride and Anatolide crustal units, indicates the existence of previously poorly known magmatic events along the northern margin of represent pulsed rifting of the north Gondwana margin.

5.4. The Carboniferous zircon populations of the Karaburun Melange (westernmost Aegean Turkey), and to a lesser extent those of the overlying Late Triassic sandstones include Carboniferous and Devonian aged zircon populations that are absent from the Carboniferous and Triassic Taurides sandstones. This evidence points to a regionally distinct source for these sandstones.

6.5. Provenance interpretation is significantly aided by combining U-Pb and $\varepsilon_{Hf(t)}$ data for detrital zircons. For example, $\varepsilon_{Hf(t)}$ values of the Devonian zircon populations in the late Carboniferous sandstones of the Karaburun Melange are mainly positive. This contrasts with the subchondritic negative $\varepsilon_{Hf(t)}$ values of the Devonian granites which form a small part of the Sakarya continental crust margin arc in NW Turkey. These Devonian granites are

therefore unlikely to represent the source of the Devonian zircons in the Karaburun Peninsula and the Konya Complex melange.

~~7.~~6. The Precambrian-aged zircon populations of the Carboniferous and Triassic sandstones of the Karaburun Peninsula are indicative of an ultimate NW African, Gondwanan source that differs from the Precambrian zircon populations of the Tauride and Anatolide continental units (i.e. Konya melange).

~~8.~~7. The abundance of Devonian zircons in the sandstone turbidites of the Carboniferous Karaburun Melange hints at a still unidentified source, probably within the submarine Aegean region. The nearest ~~known~~ confirmed source of Devonian granitic rocks with the appropriate detrital zircon populations ~~and Lu-Hf isotopic signatures~~ is the Variscan orogen~~located in the Variscan orogen~~ of central European. Eastward long-distance orogen-parallel sedimentary transport by turbidity currents is plausible. ~~However, the presence of Devonian zircons within Aegean region sandstones hints at a more local Devonian granitic source.~~

8. The Devonian zircons reported from the upper 'flysch' unit of the Konya Melange could also have a relatively local origin with no requirement for mixing of material, down to the scale of single turbidites, from opposing Gondwanan and Eurasian sources.

9. In ~~the~~ our proposed tectonic model, Paleotethys sutured from the Atlantic to the Aegean region to form the Variscan orogenic belt during the Carboniferous, whereas some Paleotethyan oceanic crust remained in an eastward-widening embayment farther east. ~~As a result, d~~During the late

Carboniferous detritus sand of mainly Precambrian, Carboniferous and locally Devonian age was transported both northwards and eastwards, generally within by turbidity currentses. Westerly and more easterly derived zircons variably mixed to produce the composite age assemblages, as recorded in the Konya Melange.

10. Interpretation of terranes created by microplate amalgamation is likely to be complex and cannot rely on the existence of simple end member age distributions to infer provenance.

Acknowledgements

This study was supported by TUBİTAK research Grants No. 111R015 and 115Y213. Partial support was provided by the Istanbul University Research Fund (Projects No. 4087, BEK-20839 and YÖP-45681). We thank Linda Marko (Frankfurt) for assistance with the laboratory processing of zircons at Frankfurt. TU and PAU thank Gernold and Janet Zulauf for their continuing help and logistical support during their five visits to Frankfurt to carry out the isotopic analysis. Esen Arpat and Necdet Özgül are thanked for their help and support during the field work in the Aladağ region. Necdet Özgül made valuable suggestions concerning the Late Triassic units sampled in the Tauride Autochthon. Constructive comments that were provided by Aral Okay and two anonymous reviewers were greatly appreciated. We also thank Robert Stern for his comments and editorial handling of the manuscript.

References

Abbo, A., Avigad, D., Gerdes, A., and Güngör, T., 2015, Cadomian basement and Paleozoic to Triassic siliciclastics of the Taurides (Karacahisar dome, south-central Turkey): Paleogeographic constraints from U–Pb–Hf in zircons: Lithos, v. 227, p. 122–139. doi: 10.1016/j.lithos.2015.03.023

Akal, C., Koralay, O.E., Candan, O., Oberhänsli, R., and Chen, F., 2011, Geodynamic significance of the early Triassic Karaburun granitoid (Western Turkey) for the opening history of Neotethys: Turkish Journal of Earth Sciences, v. 20, p. 255–271. doi: 10.3906/yer-1008-1

Akal, C., Candan, O., Koralay, O.E., Oberhansli, R., Chen, F.K., and Prelevic, D., 2012, Early Triassic potassic volcanism in the Afyon Zone of the Anatolides/Turkey: implications for the rifting of Neo-Tethys: International Journal of Earth Sciences, v, 101, p. 177-194. doi:10.1007/s00531-011-0654-2

Ayhan, A., and Lengeranlı, Y., 1986, Yahyalı-Demirkazık (Aladağlar Yöresi) Arasının Tektonostratigrafik Özellikleri: Jeoloji Mühendisliği Dergisi, v. 27, p. 31-45 [in Turkish]. (Tectonostratigraphical Features of Aladağ Region Between Yahyalı and Demirkazık).

Aysal, N., Ustaömer, T., Öngen, S., Keskin, M., Köksal, F., Peytcheva, I. and, Fanning, M., 2012, Origin of the Lower–Middle Devonian magmatism in the Sakarya Zone, NW Turkey: geochronology, geochemistry and isotope systematics: Journal of Asian Earth Sciences, v. 45, p. 201–222. doi:10.1016/j.jseaes.2011.10.011

~~**Augussson, C., Willner, A.P., Rüsing, T., Niemeyer, H., Gerdes, A., Adams, C.J. and Miller, H., 2016**, The crustal evolution of South America from a zircon Hf perspective: Terra Nova, v. 28, p. 128-137. doi:10.1111/ter.12200~~

Barrier, E., Vrielynck, B., Brouillet, J.F., and Brunet, M.F., 2018, Paleotectonic Reconstruction of the Central Tethyan Realm. Tectonono-Sedimentary-Palinspastic Maps from Late Permian to Pliocene. CCGM/CGMW, Paris, Atlas of 20 maps (scale: 1/15000000).

Bouvier, A., Vervoort, J., and Patchett, P., 2008, The Lu–Hf and Sm–Nd isotopic composition of CHUR: constraints from unequilibrated chondrites and implications for the bulk composition of terrestrial planets: Earth Planet Sci Letters, v. 273, p. 48–57. doi:10.1016/j.epsl.2008.06.010

Candan, O., Oberhansli, R., Akal, C., Koralay, O.E., Pourteau, A., and Cetinkaplan, M., 2009, Stratigraphy and Alpine metamorphism of the Afyon Zone: 62nd Geological Kurultai of Turkey, 13–17th April 2009, MTA-Ankara, Turkey, Abstract 32–33.

Candan, O., Koralay, O.E., Akal, C., Kaya, O., Oberhansli, R., Dora, O.O., Konak, N., and Chen, F., 2011, Supra-Pan-African unconformity between core and cover series of the Menderes Massif/Turkey and its geological implications: Precambrian Research, v. 184, p. 1–23.

Candan, O., Akal, C., Koralay, O.E., Okay, A.I., Oberhänsli, R., Prelević, D., and Mertz-Kraus, R., 2016, Carboniferous granites on the northern margin of Gondwana, Anatolide-Tauride Block, Turkey – Evidence for southward subduction of Paleotethys: Tectonophysics, v. 683, p. 349–366. doi:10.1016/j.tecto.2016.06.030

Çakmakoğlu, A., and Bilgin, Z.R., 2006, Pre-Neogene stratigraphy of the Karaburun Peninsula (W of İzmir, Turkey): Bulletin of Mineral Research and Exploration, v. 132, p. 1–32.

Chauvel, C., Lewin, E., Carpentier, M., Arndt, N.T, and Marini, J., 2008, Role of recycled oceanic basalt and sediment in generating the Hf– Nd mantle array.:Nature Geoscience, v. 1(1), p. 64–67

Cohen, K.M., Finney, S.C., Gibbard, P.L., and Fan, J.X., 2013, The ICS international chronostratigraphic chart: Episodes, v. 36, p. 199–204.

Collins, A., and Robertson, A.H.F., 1998, Processes of Late Cretaceous to Late Miocene episodic thrust-sheet translation in the Lycian Taurides, southwestern Turkey: Journal of the Geological Society, London, v. 155, p. 759–772.

Corfu, F., Hanchar, J.M., Hoskin, P.W.O., and Kinny, P., 2003, Atlas of zircon textures. In Hanchar J.M. and Hoskin, P.W.O., eds., Zircon. Mineralogical Society of America: Reviews in Mineralogy and Geochemistry, v. 53, p. 469–500.

Davis , D., W., Williams, I.,S., and Krogh, T.E., 2003, Historical development of zircon geochronology: Reviews in Mineralogy and Geochemistry, v. 53, p. 145–181.

~~**Dhuime, B., Hawkesworth, C., and Cawood, C., 2011,** When continents formed: Science, v. 331, p. 154–155.~~

~~**Dörr, W., Zulauf, G., Gerdes, A., Lahaye, Y., and Kowalczyk, G., 2015**, A hidden Tonian basement in the eastern Mediterranean: age constraints from U–Pb data of magmatic and detrital zircons of the External Hellenides (Crete and Peloponnesus): Precambrian Research, v. 258, p. 83–108.doi:10.1016/j.precamres.2014.12.015~~

Dörr, W., Zulauf, G., Gerdes, and Löeckle, F., 2017, Provenance of Upper Devonian clastic (meta)sediments of the Böllstein Odenwald (Mid-German-Crystalline-Zone, Variscides): International Journal of Earth Sciences, v. 106, p. 2927-2943. doi:10.1007/s00531-017-1473-x)

Drost, K., Gerdes, A., Jeffries, T., Linnemann, U., and Storey, C., 2011, Provenance of Neoproterozoic and early Paleozoic siliciclastic rocks of the Teplá-Barrandian unit (Bohemian Massif): Evidence from U–Pb detrital zircon ages: Gondwana Research, v. 19, p. 213-231. doi:10.1016/j.gr.2010.05.003

Dumont, J.P., 1978, Karacahisar kubbesi içinde (Isparta Bölgesi, Türkiye) yüzeyleyen iki tip Paleozoyik taban ve bunların Orta Triyastan once meydana gelen eski tip tektonik hat tarafından ayrılmaları: Maden Tetkik ve Arama Dergisi, V. 90, p. 74–78 (in Turkish). (The Two Types of Paleozoic base in the Karacahisar Dome (Isparta Region, Turkey) and Their Separation by a Pre-Triassic Tectonic Lineament).

Dumont, J.P., and Kerey, E., 1975, Eğridir gölü güneyinin temel jeolojik etüdü: Türkiye Jeoloji Kurumu Bülteni v. 18, p. 169–174 (in Turkish). (Basic Geological Study of Southern Part of Lake Eğirdir).

Dumont, J.P., and Monod, O., 1976, Dipoyraz Dağ masifinin Triyasik karbonatlı serisi (Batı Toroslar, Türkiye): Maden Tetkik ve Arama Dergisi, v. 87, p. 26-38 (in Turkish). (Triassic Carbonate Series of Dipoyraz Dağ Massif (Western Taurides, Turkey)).

Eckelmann, K., Nesbor, H-D, Königshof, P., Linnemann, U., Hofmann, M., Lange, J-M., and Sagawe, A., 2014, Plate interactions of Laurussia and Gondwana during the formation of Pangaea — Constraints from U–Pb LA–SF–ICP–MS detrital zircon ages of Devonian and Early Carboniferous siliciclastics of the Rhenohercynian zone, Central European Variscides: Gondwana Research v. 25, p. 1484-1500. doi:10.1016/j.gr.2013.05.018

Erdoğan, B., 1990, Tectonic Relations Between İzmir-Ankara Zone and Karaburun Belt: Bulletin of the Mineral Research and Exploration, v. 110, p. 1-15.

Erdoğan, B., Altıner, D., Güngör, T., and Özer, S., 1990, The stratigraphy of the Karaburun Peninsula. Bulletin of the Mineral Research and Exploration, v. 111, p. 1–23.

Eren, Y., Kurt, H., Rosselet, F., and Stampfli, G., 2004, Palaeozoic deformation and magmatism in the northern area of the Anatolide block (Konya), witness of the Palaeotethys active margin: Eclogae Geologicae Helvetiae, v. 97, p. 293–306. doi:10.1007/s00015-003-1131-8

Fedo, C., M., Sircombe, K., N., and Rainbird, R., H., 2003, Detrital zircon analyses of the sedimentary record: in Hanchar, J., M., Hoskin, P., W., O., eds., Zircon. Reviews in Mineralogy and Geochemistry, v. 53, p. 277–303.doi:10.2113/0530277

Garfunkel, Z., 2004, Origin of the Eastern Mediterranean basin: A re-evaluation: Tectonophysics, v. 391, p. 11–34. doi:10.1016/j.tecto.2004.07.006

Gerdes, A., and Zeh, A., 2006, Combined U–Pb and Hf isotope LA-(MC-) ICP-MS analyses of detrital zircons: comparison with SHRIMP and new constraints for the

provenance and age of an Armorican metasediment in Central Germany: Earth Planet Science Letters, v. 249, p. 47–62.doi:10.1016/j.epsl.2006.06.039

Gerdes, A., and Zeh, A., 2009, Zircon formation versus zircon alteration-new insights from combined U–Pb and Lu–Hf in situ LA-ICP-MS analyses of Archean zircons from the Limpopo Belt: Chemical Geology, v. 261(3–4), p. 230–243. doi: 10.1016/j.chemgeo.2008.03.005

Göncüoğlu, M.C., Kozur, H., Turhan, N., and Göncüoğlu, Y., 2000, Stratigraphy of the Silurian-Lower Carboniferous rock units in Konya area. I Congresso Iberico de Palaeontologia/XVI Jornades le la Sociedad Española de Palaeontologia. VII International Meeting: International Geological Correlation Programme, v. 421, p. 227–228.

Göncüoğlu, M.C., Turhan, N., and Tekin, U.K., 2003, Evidence of Triassic rifting and opening of the Neotethyan İzmir–Ankara Ocean and discussion on the presence of Cimmerian events at the northern edge of the Tauride– Anatolide Platform, Turkey. Bolletino della Societa Geologica Italiana, Special volume, v. 2, p. 203–212.

~~**Göncüoğlu, M.C., Kozur, H., Turhan, N., and Göncüoğlu, Y., 2000**, Stratigraphy of the Silurian-Lower Carboniferous rock units in Konya area. I Congresso Iberico de Palaeontologia/XVI Jornades le la Sociedad Española de Palaeontologia. VII International Meeting: International Geological Correlation Programme, v. 421, p. 227–228.~~

Göncüoğlu, M.C., Çapkınoğlu, Ş., Gürsu, S., Noble, P., Turhan, N., Tekin, U.K., Okuyucu, C., and Göncüoğlu, Y., 2007, The Mississippian in the Central and Eastern Taurides (Turkey): constraints on the tectonic setting of the Tauride–Anatolide platform: Geologica Carpathica, v. 58, p. 427–442.

Gutnic, M., Monod, O., Poisson, A., and Dumont, J.-F., 1979, Géologie des Taurides Occidentales (Turquie): Mémoires de la Société Géologique de France, No. 137, 112 pp.

Gürsu, S., and Göncüoğlu, M.C. 2005, Early Cambrian back-arc volcanism in the western Taurides, Turkey: implications for rifting along the northern Gondwanan margin: Geological Magazine, v. 142, p. 617-631.

Gürsu, S., and Göncüoğlu, M.C., 2006, Petrogenesis and tectonic setting of Cadomian felsic igneous rocks, Sandıklı area of the western Taurides, Turkey: International Journal of Earth Sciences, v. 95, p. 741-757. doi:10.1007/s00531-005-0064-4

Gürsu, S., and Göncüoğlu, M.C., 2008, Petrogenesis and geodynamic evolution of the Late Neoproterozoic post-collisional felsic magmatism in NE Afyon area, western central Turkey. in Ennih, N., and Lie Geois, J.-P., eds., The Boundaries of the West African Craton. Geological Society, London, Special Publications, v. 297, p. 409–431.

Gürsu, S., Möller, A., Usta, D., Köksal, S., Ateş, Ş., Sunkari, E. D., and Göncüoğlu, M.C., 2017, Laser Ablation Inductively Coupled Plasma Mass Spectrometry U-Pb Dating of Detrital and Magmatic Zircons of Glacial Diamictites and Pebbles in Late Ordovician Sediments of the Taurides and Southeast Anatolian Autochthon Belt, Turkey: Indications for Their Arabian-Nubian Provenance: The Journal of Geology, v. 125-2, p. 165-202.doi: 10.1086/690199

Güven, A., Ustaömer, T., and Peytcheva, I., 2012, Late Triassic crustal extension in NW Konya (Afyon Zone): new finding from LAICP-MS U–Pb zircon dating of the Ladik dyke swarm and the Kadınhanı meta-volcanics, in 5th Geochemistry Symposium, 23–25 May 2012, Denizli, Abstracts, p. 122–123.

Hawkesworth, C., J., and Kemp, A.,I.,S., 2006a, Using hafnium and oxygen isotopes in zircon to unravel the record of crustal evolution: Chemical Geology, v. 226, p.144–162. doi: 10.1016/j.chemgeo.2005.09.018

Hawkesworth, C.J., and Kemp, A.I.S., 2006b. Evolution of the continental crust: Nature, v. 443, p. 811–817. doi:10.1038/nature05191

Henderson, B.J., Collins, W.J., Murphy, J.B., Gutierrez-Alonso, G., and Hand, M., 2016, Gondwanan basement terranes of the Variscan–Appalachian orogen: Baltican, Saharan and West African hafnium isotopic fingerprints in Avalonia, Iberia and the

Armorican Terranes: Tectonophysics, v. 681, p. 278-304. doi: 10.1016/j.tecto.2015.11.020

Himmerkus, F., Reischmann, T., and Kostopoulos, D., 2009, Serbo-Macedonian revisited: a Silurian basement terrane from northern Gondwana in the Internal Hellenides, Greece: Tectonophysics, v. 473, p. 20–35.

Karslı, O., Dokuz, A. and Kandemir, R., 2016, Subduction-related Late Carboniferous to Early Permian Magmatism in the Eastern Pontides, the Camlik and Casurluk plutons: Insights from geochemistry, whole-rock Sr–Nd and in situ zircon Lu–Hf isotopes, and U–Pb geochronology: Lithos, v. 266-267, p. 98-114. doi: 10.1016/j.lithos.2016.10.007

Keay, S., and Lister, G., 2002, African provenance for the metasediments and metaigneous rocks of the Cyclades, Aegean Sea, Greece: Geology, v. 30(3), p. 235-238.

Kemp, A.,I.,–S., Hawkesworth, C.,–J., Paterson, B.,A, and Kinny, B.D, 2006, Episodic growth of the Gondwana supercontinent from hafnium and oxygen isotopes in zircon: Nature, v. 439, p. 580–583. doi:10.1038/nature04505

Ketin, İ., 1966, Tectonic units of Anatolia (Asia Minor): Bulletin of the Mineral Research and Exploration, v. 66, p. 23–34.

Koralay, O.E., Satır, M., Dora, and O.Ö., 2001, Geochemical and geochronological evidence for Early Triassic calc-alkaline magmatism in the Menderes Massif, western Turkey: International Journal of Earth Sciences, v. 89, p. 822–835

Košler, J., Konopasek, J., Slama, J., and Vrana, S., 2014, U–Pb zircon provenance of Moldanubian metasediments in the Bohemian Masif: Journal of the Geological Society, London, v. 171, p. 83–95. doi:10.1144/jgs2013-059

Kozur, H.,–W., 1997, First discovery of Muellerisphaerida (inc. sedis) and Eoalbaillella (Radiolaria) in Turkey and the age of the siliciclastic sequence (clastic series) in Karaburun peninsula: Freiberger Forschungshefte, v. 466, p. 33–59.

Kozur, H.,W., 1998, The age of the siliciclastic series ("Karareis formation") of the western Karaburun peninsula, western Turkey: Paleontologica Polonica, v. 58, p. 172–187.

Kröner, A., and Şengör, A.M.C., 1990, Archean and Proterozoic ancestry in late Precambrian to early Paleozoic crustal elements of southern Turkey revealed by single-zircon dating:. Geology, v. **18,** p. 1186-1190.

Linnemann, U., McNaughton, N.J., Romer, R.L., Gehmlich, M., Drost, K., and Tonk, C., 2004. West African provenance for Saxo-Thuringia (Bohemian Massif): Did Armorica ever leave pre-Pangean Gondwana? – U/Pb-SHRIMP zircon evidence and the Nd-isotopic record: International Journal of Earth Sciences, v. 93, p. 683-705. doi:10.1007/s00531-004-0413-8

Linnemann, U., Gerdes, A., Drost, K., and Bushmann, B., 2007, The continuum between Cadomian orogenesis and opening of the Rheic Ocean: Constraints from LA-ICP-MS U-Pb zircon dating and analysis of plate-tectonic setting (Saxo-Thuringian zone, northeastern Bohemian Massif, Germany), in Linnemann, U., Nance, R.D., Kraft, P., and Zulauf, G., eds., The evolution of the Rheic Ocean: From Avalonian-Cadomian active margin to Alleghenian-Variscan collision: Geological Society of America Special Paper, v. 423, p. 61–96.

Linnemann, U., Gerdes, A., Hofmann, M., and Marko, L., 2014, The Cadomian Orogen: Neoproterozoic to Early Cambrian crustalgrowth and orogenic zoning along the periphery of the West African Craton—Constraints from U–Pb zircon ages and Hf isotopes (Schwarzburg Antiform, Germany): Precambrian Research, v. 244, p. 236-278. doi: 10.1016/j.precamres.2013.08.007

Löwen, K, Meinhold, G., Güngör, T., and Berndt, J., 2017, Palaeotethys-related sediments of the Karaburun Peninsula, western Turkey: constraints on provenance and stratigraphy from detrital zircon geochronology: International Journal of Earth Sciences, v. 106 (8), p. 2771-2796. doi:10.1007/s00531-017-1458-9

Löwen, K, Meinhold, G., Arslan, A., Güngör, T., and Berndt, J., 2018~~a~~, Evolution of the Palaeotethys in the Eastern Mediterranean: Age, provenance and tectonic setting of the Upper Palaeozoic Konya Complex and its Mesozoic cover sequence (south-central Turkey): GeoBonn 2018, 2-6 September 2018, Bonn, Germany, Abstracts, pp. 61.

Löwen, K, Meinhold, G., Arslan, A., Güngör, T., and Berndt, J., 2019, Evolution of the Paleotethys in the Eastern Mediterranean: a multi-method approach to unravel the age, provenance and tectonic setting of the Upper Paleozoic Konya Complex and its Mesozoic cover sequence (south-central Turkey): International Geology Review, doi: 10.1080/00206814.2019.1616619

~~**Löwen, K, Meinhold, G., Güngör, T., and Berndt, J., 2017,** Palaeotethys-related sediments of the Karaburun Peninsula, western Turkey: constraints on provenance and stratigraphy from detrital zircon geochronology: International Journal of Earth Sciences, v. 106 (8), p. 2771-2796. doi:10.1007/s00531-017-1458-9~~

Ludwig, K.R., 2003, Isoplot 3.00—a geochronological toolkit for Microsoft Excel: Berkeley Geochronological Center Special Publication 4.

Mackintosh, P.W., and Robertson, A.H.F., 2009, Structural and sedimentary evidence from the northern margin of the Tauride platform in south central Turkey used to test alternative models of Tethys during Early Mesozoic time: Tectonophysics, v. 473, p. 149–172. doi:10.1016/j.tecto.2008.10.031

Mackintosh, P.W., and Robertson, A.H.F., 2012, Late Devonian–Late Triassic sedimentary development of the central Taurides, S Turkey: Implications for the northern margin of Gondwana: Gondwana Research, v. 21, p. 1089-1114. doi:10.1016/j.gr.2011.07.016

Meinhold, G., and Frei, D., 2008, Detrital zircon ages from the islands of Inousses and Psara, Aegean Sea, Greece: constraints on depositional age and provenance: Geological Magazine, v. 145, p. 886-891. doi:10.1017/S0016756808005505

Meinhold, G., Reischmann, T., Kostopoulos, D., Lehnert, O., Matukov, D., and Sergeev, S., 2008, Provenance of sediments during subduction of Palaeotethys: Detrital

zircon ages and olistolith analysis in Palaeozoic sediments from Chios Island, Greece: Palaeogeography, Palaeoclimatology, Palaeoecology, v. 263, p. 71–91. doi:10.1016/j.palaeo.2008.02.013

Meinhold, G., Reischmann, T., Kostopoulos, D., Frei, D., and Larionov, A.N., 2010a, Mineral chemical and geochronological constraints on the age and provenance of the eastern Circum-Rhodope Belt low-grade metasedimentary rocks, NE Greece: Sedimentary Geology, v. 229, p. 207–223.doi:10.1016/j.sedgeo.2010.06.007

Meinhold, G., Kostopoulos, D., Frei, D., Himmerkus, F., and Reischmann, T., 2010b, U–Pb LA-SF-ICP-MS zircon geochronology of the Serbo-Macedonian Massif, Greece: palaeotectonic constraints for Gondwana-derived terranes in the Eastern Mediterranean: International Journal of Earth Sciences, v. 99, p. 813–832. doi:10.1007/s00531-009-0425-5

Millonig, L.J., Gerdes, A., and Groat, L.A., 2012, U–Th–Pb geochronology of metacarbonatites and meta-alkaline rocks in the southern Canadian Cordillera: a geodynamic perspective: Lithos, v. 152, p. 202–217.doi:10.1016/j.lithos.2012.06.016

Moix, P., Beccaletto, L., Kozur, H.W., Hochard, V., Rosselet, F., and Stampfli, G.M., 2008, A new classification of the Turkish terranes and sutures and its implication for the paleotectonic history of the region: Tectonophysics, v. 451, p. 7–39.doi: 10.1016/j.tecto.2007.11.044

Monod, O., 1977. Réchérches géologique dans le Taurus occidental au sud de Beyşehir (Turquie). PhD thesis, Université Paris-Sud Orsay, 442 pp.

Monod, O., and Akay, E., 1984, Evidence for a Late Triassic–Early Jurassic orogenic event in the Taurides, in Robertson, A.H.F., Dixon, J.E., eds., The Geological Evolution of the Eastern Mediterranean: Geological Society, London, Special Publication, v. 17, p. 113–122.

Morag, N., Avigad, D., Gerdes, A., Belousovac, E., and Harlavand, Y., 2011, Crustal evolution and recycling in the northern Arabian-Nubian Shield: New perspectives from

zircon Lu–Hf and U–Pb systematics: Precambrian Research, v. 186, p. 101-116. doi: 10.1016/j.precamres.2011.01.004

MTA, 2002. 1:500,000 Geological Map of Turkey. Maden Tektik ve Arama Enstitüsü (MTA), Ankara.

Muttoni, G., Kent, D.V., Garzanti, E., Brack, P., Nielss, A., and Gaetani, M., 2003, Early Permian 'B' to Late Permian 'A': Earth and Planetary Science Letters, v. 215, p. 379-394

Okay, A.I., Satır, M., Maluski, H., Siyako, M., Monie, P., Metzger, R., and Akyüz, S., 1996, Paleo- and Neo-Tethyan events in northwestern Turkey: geologic and geochronologic constraints: In: Yin, A., Harrison, T.M., Eds., The Tectonic Evolution of Asia., Cambridge University Press, p. 420–441.

Okay, A. I., and Tüysüz, O., 1999, Tethyan sutures of northern Turkey. In: Mascle, A., and Jolivet, L., eds., The Mediterranean Basin: Tertiary Extension within the Alpine Orogen. Geological Society, London, Special Publications, v. 156, p. 475–515.

Okay, A.İ., Satır, M., and Siebel, W., 2006, Pre-Alpide Palaeozoic and Mesozoic orogenic events in the Eastern Mediterranean region, in Gee, D., G., and Stephenson, R.A., eds., European Litosphere Dynamics. Geological Society, London, Memoirs, v. 32, p. 389-405.

Okay, A.İ., Satır, M., and Shang, C.K., 2008, Ordovician metagranite from the Anatolide–Tauride block, northwest Turkey—geodynamic implications: Terra Nova, v. 20, p. 280–288. doi:10.1111/j.1365-3121.2008.00818.x

Okay, A.İ., İşintek, İ., Altıner, D., Özkan-Altıner, S., and Okay, N., 2012. An olistostrome–mélange belt formed along a suture: Bornova Flysch zone, western Turkey. Tectonophysics 568-569, 282-295. doi:10.1016/j.tecto.2012.01.007

~~**Okay, A.İ., Satır, M. and Shang, C.K., 2008**, Ordovician metagranite from the Anatolide–Tauride block, northwest Turkey—geodynamic implications: Terra Nova, v. 20, p. 280–288. doi:10.1111/j.1365-3121.2008.00818.x~~

~~**Okay, A.İ., Satır, M., and Siebel, W., 2006,** Pre-Alpide Palaeozoic and Mesozoic orogenic events in the Eastern Mediterranean region, in Gee, D., G., and Stephenson, R.A., eds., European Litosphere Dynamics. Geological Society, London, Memoirs, v. 32, p. 389-405.~~

~~Okay, N., Zack, T., Okay, A.İ., and Barth, M., 2011, **Sinistral transport along the Trans-European Suture Zone: detrital zircon–rutile geochronology and sandstone petrography from the Carboniferous flysch of the Pontides. Geological Magazine , v. 148, p. 380-403. doi:10.1017/S0016756810000804**~~

Özbey, Z., Ustaömer, T., Robertson, A.H.F., and Ustaömer, P.A., 2013a, Tectonic significance of Late Ordovician granitic magmatism and clastic sedimentation on the northern margin of Gondwana (Tavşanlı Zone, NW Turkey): Journal of Geological Society, London, v. 170, p. 159–173. doi:10.1144/jgs2011-091

Özbey, Z., Ustaömer, T., and Robertson, A.H.F., 2013b, Mesozoic magmatic and sedimentary development of the Tavşanlı Zone (NW Turkey): implications for rifting, passive magrin development and ocean crust emplacement, in Robertson, A.,H.,F., Parlak, O., Ünlügenç, U.,C., eds., Geological Development of Anatolia and the Easternmost Mediterranean Region: Geological Society, London, Special Publications, v. 372, p. 141-165.

Özcan, A., Göncüoğlu, M., C., Turhan, N., Şentürk, K.C., and Uysal, Ş., 1990, Konya-Kadınhanı-Ilgın Dolayının Temel Jeolojisi: Maden Tetkik ve Arama Genel Müdürlüğü Rapor no: 9535, 132 s, Ankara. (Basic Geology of the Konya-Kadınhanı-Ilgın Region: MTA Report No: 9535, pp.132, Ankara, (unpublished)).

Özdamar, Ş., Billor, M.Z., Sunal, G., Esenli, F., and Roden, M.F., 2013, First U–Pb SHRIMP zircon and $^{40}Ar/^{39}Ar$ ages of metarhyolites from the Afyon–Bolkardag Zone, SW Turkey: Implications for the rifting and closure of the Neo-Tethys: Gondwana Research, v. 24, p. 377–391. doi:10.1016/j.gr.2012.10.006

Özer, S., Sözbilir, H., Özkar, İ., and Sarı, B., 2001, Stratigraphy of Upper Cretaceous–Palaeogene sequences in the southern and eastern Menderes Massif

(western Turkey): International Journal of Earth Sciences, v. 89 (4), p. 852-866. doi: 10.1007/s005310000142

~~**Özdamar, Ş., Billor, M.Z., Sunal, G., Esenli, F., and Roden, M.F., 2013**, First U–Pb SHRIMP zircon and $^{40}Ar/^{39}Ar$ ages of metarhyolites from the Afyon–Bolkardag Zone, SW Turkey: Implications for the rifting and closure of the Neo-Tethys: Gondwana Research, v. 24, p. 377–391. doi:10.1016/j.gr.2012.10.006~~

Özgül, N., 1976, Some geological aspects of the Taurus orogenic belt (Turkey): Bulletin of the Geological Society of Turkey, v. 19, p. 65–78.

Özgül, N., 1997, Stratigraphy of the tectono-stratigraphic units around Hadim-Bozkır-Taşkent region (northern part of the Central Taurides, Turkey): Bulletin of the Geological Society of Turkey, v. 119, p. 113–174.

Pickett E.A., and Robertson, A.H.F., 1996, Formation of the Late Palaeozoic-Early Mesozoic Karakaya Complex and related ophiolites in NW Turkey by Paleotethyan subduction-accretion: Journal of the Geological Society, London, v. 153, p. 995-1009.

Piper, D., J., W., von Huene, R., and ;Duncan, J., R., 1973, Late Quaternary sedimentation in the active eastern Aleutian trench: Geology, v. 1 (1), 19-22. doi: 10.1130/0091-7613

Poisson, A., 1977, Récherches Géologiques dans les Taurides Occidentales, Turquie. PhD thesis, University of Paris-Sud, Orsay, France.

Poisson, A., 1984, The extension of the Ionian trough into southwestern Turkey, in, Dixon, J., E., and Robertson, A., H.,F., eds., The geological evolution of the eastern Mediterranean: Geological Society of London Special Publication, v. 17, p. 241-249.

Pourteau, A., Candan, O., and Oberhansli, R., 2010, High-pressure metasediments in central Turkey: Constraints on the Neotethyan closure history: Tectonics, v. 29, TC5004. doi:10.1029/2009TC002650

Pourteau, A., Sudo, M., Candan, O., Lanari; P., Vidal, O. and Oberhansli, R., 2013, Neotethys closure history of Anatolia: insights from ^{40}Ar–^{39}Ar geochronology and *P*–*T* estimation in high - pressure metasedimentary rocks: Journal of Metamorphic Geology, v. 31, p. 585-606. doi:10.1111/jmg.12034

Porteau A., Oberhansli, R., Candan, O., and Barrier, E., 2016, Neotethyan closure history of western Anatolia: a geodynamic discussion: International Journal of Earth Science, v. 105, p. 203-224. doi:10.1007/s00531-015-1226-7

Robertson, A. H. F., and Dixon, J., E., 1984, Introduction: Aspects of the geological evolution of the Eastern Mediterranean, in: J., E., Dixon and A., H., F., Robertson, eds., The Geological Evolution of the Eastern Mediterranean, Geological Society, London, Special Publication: v. 17, p. 1-74.

Robertson, A,H.F., and Pickett, E.A., 2000, Palaeozoic-Early Tertiary Tethyan evolution of mélanges, rift and passive margin units in the Karaburun Peninsula (western Turkey) and Chios island (Greece), in Bozkurt, E., Winchester, J., A., Piper, J., D., A., eds., Tectonics and Magmatism in Turkey and the Surrounding Area: The Geological Society, London, Special Publication, v. 173, p. 43–82.

Robertson, A.H.F., Ustaömer, T., Pickett, E.A., Collins, A.S., Andrew, T., and Dixon, J.E. 2004, Testing models of Late Palaeozoic–Early Mesozoic orogeny in Western Turkey. Support for an evolving open-Tethyan model: Journal of the Geological Society, London, v. 161, p. 501–511. doi: 10.1144/0016-764903-080

~~**Robertson, A. H. F., Parlak, O., and Ustaömer, T., 2012,** Overview of the Palaeozoic-Neogene evolution of Neotethys in the Eastern Mediterranean region (southern Turkey, Cyprus, Syria): Petroleum Geoscience, v. 18, p. 381–404. doi: 10.1144/petgeo2011-091~~

~~**Robertson, A.H.F., Parlak, O., and Ustaömer, T., 2013,** Late Palaeozoic-Early Cenozoic tectonic development of Southern Turkey and the easternmost Mediterranean region: evidence from the inter-relations of continental and oceanic units. In: Robertson, A.H.F., Ustaömer, T., and Parlak, O., eds.,Geological Evolution of the Anatolia and the~~

~~Eastern Mediterranean Region: Geological Society, London, Special Publication, v. 372, p. 9-48.~~

~~**Robertson, A,H.F., and Pickett, E.A., 2000**, Palaeozoic-Early Tertiary Tethyan evolution of mélanges, rift and passive margin units in the Karaburun Peninsula (western Turkey) and Chios island (Greece), in Bozkurt, E., Winchester, J., A., Piper, J., D., A., eds., Tectonics and Magmatism in Turkey and the Surrounding Area: The Geological Society, London, Special Publication, v. 173, p. 43–82.~~

Robertson, A.,H.F., and Ustaömer, T., 2009a, Formation of the upper Palaeozoic Konya Complex and comparable units in southern Turkey subduction–accretion processes: implications for the tectonic development of Tethys in the Eastern Mediterranean region: Tectonophysics, v. 473, p. 113–148. doi: 10.1016/j.tecto.2008.10.027

Robertson, A.H.F., and Ustaömer, T., 2009b, Upper Palaeozoic subduction/accretion processes in the closure of Palaeotethys: evidence from the Chios Melange (E Greece), the Karaburun Melange (W Turkey) and the Teke Dere Unit (SW Turkey): Sedimentary Geology, v. 220, p. 29–59.doi:10.1016/j.sedgeo.2009.06.005

Robertson, A.H.F., and Ustaömer, T., 2011, Role of tectonic-sedimentary melange and Permian–Triassic cover units, central southern Turkey in Tethyan continental margin evolution: Journal of Asian Earth Sciences, v. 40, p. 98–120. doi: 10.1016/j.jseaes.2010.09.001

Robertson, A.H.F., Parlak, O., and Ustaömer, T., 2012, Overview of the Palaeozoic-Neogene evolution of Neotethys in the Eastern Mediterranean region (southern Turkey, Cyprus, Syria): Petroleum Geoscience, v. 18, p. 381–404. doi: 10.1144/petgeo2011-091

Robertson, A.H.F., Parlak, O., and Ustaömer, T., 2013, Late Palaeozoic-Early Cenozoic tectonic development of Southern Turkey and the easternmost Mediterranean region: evidence from the inter-relations of continental and oceanic units. In: Robertson, A.H.F., Ustaömer, T., and Parlak, O., eds.,Geological Evolution of the Anatolia and the

Eastern Mediterranean Region: Geological Society, London, Special Publication, v. 372, p. 9-48.

~~Robertson, A.H.F., Ustaömer, T., Pickett, E.A., Collins, A.S., Andrew, T., and Dixon, J.E. 2005, Testing models of Late Palaeozoic–Early Mesozoic orogeny in Western Turkey. Support for an evolving open-Tethyan model: Journal of the Geological Society, London, v. 161, p. 501–511. doi: 10.1144/0016-764903-080~~

Robinson, F.A., Foden, J.D., Collins, A.S., and Payne, J.L., 2014, Arabian Shield magmatic cycles and their relationship with Gondwana assembly: Insights from zircon U–Pb and Hf isotopes: Earth and Planetary Science Letters, v. 408, p. 207-225. doi: 10.1016/j.epsl.2014.10.010

Schweller, W.J., Kulm, L.D., and Prince, R.A. 1981, Tectonics structure, and sedimentary framework of the Peru-Chile Trench, in: Kulm, L.D., Dymond, J., Dasch, E.J., Hussong, D.M., eds., Submarine fans and related turbidite systems. Springer-Verlag, New York, p. 23–28.

Slama, J., Košler, J., Condon, D.J., Crowley, J.L., Gerdes, A., Hanchar, J.M., Horstwood, M.S.A., Morris, G.A., Nasdala, L., Norberg, N., Schaltegger, U., Schoene, B., Tubrett, M.N., and Whitehouse, M.J., 2008, Plešovice zircon—a new natural reference material for U–Pb and Hf isotopic microanalysis: Chemical Geology, v. 249, p. 1–35. doi: 10.1016/j.chemgeo.2007.11.005

Smith, A.G., 2006. Tethyan ophiolite emplacement, Africa to Eurasia motions, andAtlantic spreading. In: Robertson, A.H.F., Mountrakis, D. (Eds.), Tectonic Development of the Eastern Mediterranean Region. Geological Society of London SpecialPublication, vol. 260, pp. 11–35.

Stampfli, G.M., 2000, Tethyan Oceans, in Bozkurt, E., Winchester, J.A., Piper, J.D.A., eds., Tectonics and Magmatism in Turkey and the Surrounding Area. The Geological Society, London, Special Publication, v. 173, p. 1-23.

Stampfli, G.M., Mosar, J., Favre, P., Pellevuit, A., and Vannay, J.-C., 2001, Permo-Mesozoic evolution of the western Tethys realm: the Neo-Tethys East Mediterranean

Basin connection. in Ziegler, P., Cavazza, W., Robertson, A.H.F., and Crasquin-Soleau, A., eds., Peri-Tethyan Rift/Wrench Basins and Passive Margins: Peri-Tethys Memoire, v. 5, p. 51–108.

Sunal, G., 2012, Devonian magmatism in the western Sakarya Zone, Karacabey region, NW Turkey: Geodinamica Acta, v. 25 (3-4), p. 183-201.

Şenel, M., 1991, Palaeocene-Eocene sediments interbedded with volcanics within the Lycian Nappes: Faralya Formation: Bulletin of Mineral Research and Exploration (Turkey), v. 113, p. 1–14.

Şenel, M., Gedik, İ., Dalkılıç, H., Serdaroğlu, M., Bilgin, A.Z., Uğuz, M.F., Bölükbaşı, A.S., Korucu, M., and Özgül, N., 1996, Stratigraphy of the Autochthonous and Allochthonous Units at the Eastern Part of the Isparta Angle, Western Taurides-Turkey: MTA Bulletin, v. 118, p. 111-160.

~~**Şenel, M., 1991,** Palaeocene-Eocene sediments interbedded with volcanics within the Lycian Nappes: Faralya Formation: Bulletin of Mineral Research and Exploration (Turkey), v. 113, p. 1–14.~~

Şengör, A.M.C., and Yılmaz, Y., 1981, Tethyan evolution of Turkey: a plate tectonic approach: Tectonophysics, v. 75, p. 181–241. doi:10.1016/0040-1951(81)90275-4

Şengör, A.M.C., 1984, The Cimmeride Orogenic System and the Tectonics of Eurasia, in Sengör, A.M. C., ed., The Cimmeride Orogenic System and the Tectonics of Eurasia. Geological Society of America, 1–82. doi:10.1130/SPE195-p1

~~**Slama, J., Košler, J., Condon, D.J., Crowley, J.L., Gerdes, A., Hanchar, J.M., Horstwood, M.S.A., Morris, G.A., Nasdala, L., Norberg, N., Schaltegger, U., Schoene, B., Tubrett, M.N., and Whitehouse, M.J., 2008,** Plešovice zircon—a new natural reference material for U–Pb and Hf isotopic microanalysis: Chemical Geology, v. 249, p. 1–35. doi: 10.1016/j.chemgeo.2007.11.005~~

~~**Stampfli, G.M., 2000**, Tethyan Oceans, in Bozkurt, E., Winchester, J.A., Piper, J.D.A., eds., Tectonics and Magmatism in Turkey and the Surrounding Area. The Geological Society, London, Special Publication, v. 173, p. 1-23.~~

~~**Stampfli, G.M., Mosar, J., Favre, P., Pellevuit, A., and Vannay, J.-C.,** 2001, Permo-Mesozoic evolution of the western Tethys realm: the Neo-Tethys East Mediterranean Basin connection in Ziegler, P., Cavazza, W., Robertson, A.H.F., and Crasquin-Soleau, A., eds., Peri-Tethyan Rift/Wrench Basins and Passive Margins: Peri-Tethys Memoire, v. 5, p. 51–108.~~

Tekeli, O., 1980, Toroslarda Aladağların yapısal evrimi. Türkiye Jeoloji Kurumu Bülteni; v. 23, p. 11-14 (in Turkish). (Structural Evolution of Aladağ Mountains in Taurus Belt).

Tekeli, O., Aksay, A., Ürgün, B.M., and~~AND~~ Işık, A., 1984, Geology of the Aladağ Mountains, in Tekeli, O., Göncüoğlu, M.C., eds., Geology of the Taurus Belt: Proceedings of International Tauride Symposium. Mineral Research and Exploration Institute (MTA) of Turkey, Publications, p. 143-158.

Toker, V., Sonel, N., Ayyıldız, T., and Albayrak, M., 1993, Akseki kuzeyi-Üzümdere (Antalya) civarının Stratigrafisi: Türkiye Jeoloji Bülteni, v. 36, p. 56-71 (in Turkish) (Stratigraphy of the Northern Portion of Akseki-Üzümdere (Antalya) Vicinity).

Ustaömer, P.A., Mundil, R., and Renne, P.R.,~~and~~ 2005, U/Pb and Pb/Pb zircon ages for arc related intrusions of the Bolu Massif (W Pontides, NW Turkey): Evidence for Late Precambrian (Cadomian) age: Terra Nova, v. 17, p. 215-223. doi:10.1111/j.1365-3121.2005.00594.x

Ustaömer, P.A., Ustaömer, T., Gerdes, A., and Zulauf, G., 2011, Detrital zircon ages from a Lower Ordovician quartzite of the İstanbul exotic terrane (NW Turkey): evidence for Amazonian affinity: International Journal of Earth Sciences, v. 100, p. 23-41. doi:10.1007/s00531-009-0498-1

Ustaömer, P.A., Ustaömer, T., and Robertson, A.H.F., 2012a, Ion Probe U–Pb dating of the Central Sakarya basement: a peri-Gondwana terrane cut by late Lower

Carboniferous subduction/collision-related granitic magmatism: Turkish Journal of Earth Sciences, v. 21, p. 905-932. doi:10.3906/yer-1103-1

Ustaömer, P.A., Ustaömer, T., Gerdes A., Robertson A.H.F., and Collins, A.S., 2012b, Evidence of Precambrian sedimentation/magmatism and Cambrian metamorphism in the Bitlis Massif, SE Turkey utilising whole-rock geochemistry and U-Pb LA-ICP-MS zircon dating: Gondwana Research, v. 21, p. 1001-1018. doi:10.1016/j.gr.2011.07.012

Ustaömer, T., and Robertson, A.H.F., 1993, A Late Palaeozoic-Early Mesozoic marginal basin along the active southern continental margin of Eurasia: evidence from the Central Pontides (Turkey) and adjacent regions: Geological Journal, v. 28, p. 219-238.

~~**Ustaömer, P.A., Ustaömer, T., and Robertson, A.H.F., 2012a,** Ion Probe U–Pb dating of the Central Sakarya basement: a peri-Gondwana terrane cut by late Lower Carboniferous subduction/collision-related granitic magmatism: Turkish Journal of Earth Sciences, v. 21, p. 905-932. doi:10.3906/yer-1103-1~~

Ustaömer, T., and Robertson, A.H.F., 1997, Tectonic-sedimentary evolution of the eastern Mediterranean, in Robinson, A.G., ed., Regional and Petroleum Geology of the Black Sea and Surrounding Region. American Association of Petroleum Geologists Memoir, Tulsa, Oklahama, p, 68, p. 255-290.

Ustaömer, T., Gerdes, A., Ustaömer P.A., and Robertson, A.H.F., 2012. U-Pb LA-SF-ICP-MS dating of detrital zircons from an Upper Carboniferous quartzite in the Siyah Aladağ Nappe, Yahyalı-Kayseri, E Taurides: source area characteristics, in Yalçın, M.N., Çorbacıoğlu, H., Aksu, Ö., and Bozdoğan, N., eds., Palaeozoic of Northern Gondwana and its Petroleum Potential, a Field Workshop, 9-14 September 2012, Kayseri-Turkey, Extended Abstracts, p. 108-110.

Ustaömer, T., Robertson, A.H.F., Ustaömer, P.A., Gerdes, A., and Peytcheva, I., 2013. Constraints on Variscan and Cimmerian magmatism and metamorphism in the Pontides (Yusufeli–Artvin area), NE Turkey from U–Pb dating and granite

geochemistry: In Robertson, A. H. F., Parlak, O. & Ünlügenç, U. C. (eds) Geological Development of Anatolia and the Easternmost Mediterranean Region. Geological Society, London, Special Publications, v. 372, p. 49–74.

Ustaömer, T., Ustaömer, P.A., Robertson, A.H.F., and Gerdes, A., 2016a, Implications of U–Pb and Lu–Hf isotopic analysis of detrital zircons for the depositional age, provenance and tectonic setting of the Permian–Triassic Palaeotethyan Karakaya Complex, NW Turkey: International Journal of Earth Sciences, v. 105, p. 7-38. doi:10.1007/s00531-015-1225-8

Ustaömer, T., Ustaömer, P.A., Robertson, A.H.F., and Gerdes, A., 2016b, Testing alternative tectonic models of Palaeotethys in the E Mediterranean region: new U-Pb and Lu-Hf isotopic analyses of detrital zircons from Late Carboniferous and Late Triassic sandstones associated with the Anatolide and Tauride blocks (S Turkey): Geophysical Research Abstracts, Vol. 18, EGU2016-15469-1.

~~**Ustaömer, T., Ustaömer, P.A., Robertson, A.H.F., and Gerdes, A., 2016**, Implications of U–Pb and Lu–Hf isotopic analysis of detrital zircons for the depositional age, provenance and tectonic setting of the Permian–Triassic Palaeotethyan Karakaya Complex, NW Turkey: International Journal of Earth Sciences, v. 105, p. 7-38. doi:10.1007/s00531-015-1225-8~~

Ustaömer, T., Ustaömer, P.A., Robertson, A.H.F., and Gerdes, A., 2018, U-Pb and Lu-Hf isotopic data from detrital zircons in Late Carboniferous and Late Triassic sandstones used to determine provenance and test alternative tectonic models of the tectonic setting of the Anatolide and Taurides, S Turkey: GeoBonn 2018, 2-6 September 2018, Bonn, Germany, Abstracts, pp. 65.

Vermeesch, P., 2012, On the visualisation of detrital age distributions: Chemical Geology, v.312-313, 190-194.doi:10.1016/j.chemgeo.2012.04.021

Wehrmann, A., Yılmaz, I., Yalçın, M.N., Wilde, V., Schindler, E., Weddige, K., Saydam Demirtas, G., Özkan, R., Nazik, A., Nalcıoğlu, G., Kozlu, H., Karslıoğlu, Ö., Jansen, U., Ertuğ, K., Brocke, R., and Bozdoğan, N., 2010, Devonian shallow-

water sequences from the North Gondwana coastal margin (Central and Eastern Taurides, Turkey): sedimentology, facies and global events: Gondwana Research, v. 17, p. 546–560. doi:10.1016/j.gr.2009.09.011

Wiedenbeck, M., Allé, P., Corfu, F., Griffin, W.Lç, Meier, M., Oberli, F., von Quadt, A., Roddick, J.C., and Spiegel, W., 1995, Three natural zircon standards for U–Th–Pb, Lu–Hf, trace element and REE analyses: Geostandarts Newsletter, v. 19, p. 1–23. doi: 10.1111/j.1751-908X.1995.tb00147.x

Xiang, W., Griffin, W.L., Chen, J., Huang, P., and Ziang, L., 2011, U and Th contents and Th/U ratios of zircon in felsic and mafic magmatic rocks: improved zircon-melt distribution coefficients: Acta Geologica Sinica, v. 85, p. 164-174. doi:10.1111/j.1755-6724.2011.00387.x

Zanchi, A., Garzanti, E., Larghi, C., and Angiolini, L., 2003, The Variscan orogeny in Chios (Greece): Carboniferous accretion along a Palaeotethyan active margin: Terra Nova, v.15(3), p. 213-223. doi:10.1046/j.1365-3121.2003.00483.x

Zlatkin, O., Avigad, D., and Gerdes, A., 2013, Evolution and provenance of Neoproterozoic basement and Lower Paleozoic siliciclastic cover of the Menderes Massif (western Taurides): Coupled U–Pb–Hf zircon isotope geochemistry: Gondwana Research, v. 23, p. 682-700. doi:10.1016/j.gr.2012.05.006

Zlatkin, O., Avigad, D., and Gerdes, A., 2018, New Detrital Zircon Geochronology From the Cycladic Basement (Greece): Implications for the Paleozoic Accretion of Peri-Gondwanan Terranes to Laurussia: Tectonics, v. 37 (12), p. 4679-4699. doi: 10.1029/2018TC005046

Figure captions

Figure 1: Simplified tectonic map of southern Turkey showing the locations of the samples studied and the logs in~~on~~ Fig. 2 (MTA, 2002). The tectonic subdivisions of the metamorphic Anatolide continental units~~s~~ to the north~~N~~ and the non-metamorphic Tauride crustal ~~blocks~~ units to the south~~S~~ are indicated. The Anatolide continental unit ~~s~~ includ~~e~~ing the Tavşanlı Zone and the Afyon Zone~~s~~ that experienced HP/LT metamorphism during Late Cretaceous and Palaeocene times, respectively. The Menderes Massif to the west records orogenic events during the Ediacaran-Cambrian and Eocene-Recent periods. The Tauride continental units~~s~~ includes autochthonous successions, including ~~(~~ Bey Dağları, Geyik Dağ, Akseki-Anamas and Belemedik~~)~~, as shown in blue, and also fron overlying thrust sheets including the Lycian Nappes in the

west, the Beyşehir-Hoyran-Hadim Nappes in the centre, the Aladağ Nappes in the east and the Antalya and Alanya tectonic units the south of the region. Abbreviations: SP Sandıklı Porphyroid; BHHN Beyşehir-Hoyran-Hadim Nappes; Y Yahyalı; BG Beyşehir Lake; EG Eğirdir Lake. Inset: the wider distribution of suture zones throughout Turkey extending into Iran, Armenia, Georgia and the Russian Federation.

Figure 2: Stratigraphic logs of the successions sampled in the Tauride ~~Autochthon~~ continental unit and overlying allochthonous units. The sample locations and their stratigraphic position are indicated by red arrows. Sources of information: Aladağ Nappe: Tekeli *et al*. (1984), Özgül (1976), Ayhan and Lengeranlı (1986); Afyon Zone (Konya Region): Robertson and Ustaömer (2011); Karaburun Peninsula: Robertson and Ustaömer (2009a,b), Çapkınoğlu and Bilgin (2006), Erdoğan et al. (1990); Bey Dağları (Tauride Autochthon): Poisson (1984), Şenel 1996; Akseki (Tauride Autochthon): Monod (1977).

Figure 3: Selected cathodoluminescence images of detrital zircons from metasandstones ~~from~~ of the Konya Complex (~~,~~ Afyon Zone), Central Taurides. The circles marked on the zircons show the locations of the spots analysed~~;, whereas~~ the numbers within the circles indicate ~~the name of~~ the individual spots. S~~The s~~cale bars ~~are~~ 20 μm in panel a. $^{206}Pb/^{238}U$ ages are used for <1Ga and $^{206}Pb/^{207}Pb$ ages are used for >1 Ga. Errors are at 1σ level.

Figure 4: Age versus Th/U diagram for detrital zircons from all of the sandstones ~~studied~~discussed in the paper. Th/U=3.7 indicates the average Th/U ratios of zircons from mafic igneous source rocks; Th/U=0.93 indicates the average Th/U ratios of zircons from intermediate composition igneous source rocks; Th/U=0.59 indicates the average Th/U ratios of zircons from felsic igneous source rocks (Xiang *et al.* 2011).

Figure 5: Concordia (left) and density-kernel density estimates plot (right) for the ~~meta~~sandstones analysed during this work. a, b Köşkdere Formation; c, d Konya Complex; e, f Karaburun Melange. The numbers indicate the peak ages in Ma.

Figure 6: Pie charts showing different age spectra of the detrital zircons in the Carboniferous (left) and Triassic (right) sandstones analysed during this work.

Figure 7: Concordia plots for Triassic sandstones analysed during this work. a, b Kasımlar Formation; c Üzümdere Formation, d Güvercinlik Formation.

Figure 8: Histogram and kernel density estimate plots for Triassic sandstones analysed during this work. a, b Kasımlar Formation; c Üzümdere Formation, d Güvercinlik Formation. The numbers indicate peak ages in Ma.

Figure 9: Age versus $\varepsilon_{Hf(t)}$ plots of Triassic sandstones analysed during this work from ~~from.~~ ~~the~~ a-b Kasımlar Formation ~~(a, b)~~; c ~~the~~ Üzümdere Formation ~~(c)~~ and d~~the~~ Güvercinlik Formation ~~(d)~~. Curves are kernel density estimates for each of the samples. Arrow shows the crustal evolution path. DM Depleted Mantle, CHUR Chondritic Uniform Reservoir, ANS Arabian-Nubian Shield (Robinson *et al*. 2014).

Figure 10: Age versus $\varepsilon_{Hf(t)}$ plots of Carboniferous sandstones analysed during this work from a~~the~~ Konya Complex ~~(a)~~ and b Karaburun Melange ~~(b)~~. Arrow shows the crustal evolution path. See the caption of Figure 9 for the abbreviations.

Figure 11: Age versus $\varepsilon_{Hf(t)}$ plots of Carboniferous meta-granites of the Afyon Zone analysed during this work. The red dashed lines represent crustal evolution paths of TDM =1.3 and 2.1 Ga with $^{176}Lu/^{177}Hf$=0.0013. See the caption ~~for~~ to Figure 9 for abbreviations.

Figure 12: Normalised probability plot ~~of~~ for all of the samples analysed ~~in~~ during this study ranging in~~for the~~ age ~~range~~ from 0-1200 Ma. See text for explanation.

Figure 13: Cumulative probability plot of all the samples analysed in this study. The diagram shows that the sandstones from the Karaburun Peninsula (K.13.102 and K.13.104) are differ~~ent~~ in the ages of prominent zircon populations ~~from~~in the ~~remainder of the~~ samples from all of the other areas and units considered in this paper (both new and published data)~~in terms of the age of the prominent zircon populations~~. Common to all of the samples is the rarity or absence of Early to Mid- Mesoproterozoic zircons (horizontal lines between 1.1 to 1.6 Ga) and the abundance of the Neoproterozoic zircons. The samples from the Anatolide and Tauride ~~crustal~~continental ~~blocks~~ units (excluding the two samples from the Karaburun Peninsula) indicate a similar provenance as for the Precambrian zircons, irrespective of depositional age. Late Palaeozoic zircons in these sandstones appear in the Late Triassic sandstones and reach a maximum of 15% of the whole data set.

Figure 14: U-Pb age versus $\varepsilon_{Hf(t)}$ of Carboniferous granites from the Sakarya continental margin arc and the Afyon Zone. All of the Carboniferous detrital zircons in the Carboniferous and Triassic sandstones from the Anatolide~~s~~ and Tauride continental unit~~s~~s are plotted for comparison. Data from the Sakarya Zone are from Ustaömer *et al.* 2016 (KK.09.04) and our unpublished data (K.12.111); Karslı *et al.* 2016 (CM21, CS10). See text for explanation.

Figure 15: U-Pb age versus $\varepsilon_{Hf(t)}$ of: 1) Devonian metagranite from the Sakarya continental margin arc and 2) Devonian detrital zircons in the Late Carboniferous sandstone of the Karaburun Melange. The Devonian metagranite exhibits a tight cluster of $\varepsilon_{Hf(t)}$ values from -8.5 to -7.1, with corresponding Hf model ages of 1.5-1.4 Ga

(Ustaömer *et al.* 2016). In contrast, the Devonian detrital zircons in the Karaburun Melange sandstone differ significantly, with $\varepsilon_{Hf(t)}$ values straddling the CHUR line and Hf model ages of <1.1 Ga. Several other Devonian metagranites ~~in~~ of the Sakarya continental margin arc (Pontides) exhibit $\varepsilon_{Nd(401-389)}$ values of -9 to -8 with corresponding Nd model ages of 1.9-1.8 Ga (Aysal *et al.* 2012).

Figure 16: Palaeogeographic sketch map showing the inferred tectonic setting of the Aegean region and central and northern Turkey during the late Carboniferous (c. 310 Ma). Siliciclastic sediments were shed from the Anatolide and Tauride ~~crustal~~ continental units in the south and east, whereas in the west Devonian zircon-rich sand are ~~sediment is~~ inferred to have been come ~~derived~~ from the adjacent Aegean region or from the ~~the Armorican Terrane Assemblage of the~~ Variscan terranes in central Europe~~orogen in the west~~. The solid arrow indicates the inferred sedimentary transport direction

Electronic supplement

Supplementary Table 1: GPS coordinates of the samples analysed.

Supplementary Table 2: Summary of U-Pb and Lu-Hf data for Carboniferous sandstones.

Supplementary Table 3: Summary of U-Pb and Lu-Hf data for Triassic sandstones.

Supplementary Table 4: Uranium-lead analytical data.

Supplementary Table 5: Lutetium-hafnium analytical data.

Supplementary figure captions

Supplementary Figure 1: Geological map of the Aladağ region, Eastern Tauride continental unit, showing the location of the uUpper Carboniferous quartzite sample (S3) analysed for zircon U-Pb analysis. Thise map is a small part of a larger map that was, produced during the first author's joint field work with Esen Arpat and Necdet Özgül (both at Geomar) in 2008. Satellite image of the area was also used during the mapping.

Supplementary Figure 2: Selected cathodoluminescence images of detrital zircons from the uUpper Carboniferous quartzite of the Köşkdere Formation, Siyah Aladağ Nappe, Eastern Tauride continental units. The open circles on the zircons show the locations of the spots analysed;, whereas the numbers within the circles indicate the name of the individual spots;, and the red numbers above the zircons refer to the name of the zircon crystals. The ages obtained from the metamorphic zircon growths are indicated by the blue numbers and those from the igneous zircons by the black numbers. $^{206}Pb/^{238}U$ ages are used for <1Ga and $^{206}Pb/^{207}Pb$ ages are used for >1 Ga. Errors are at 1σ. The scale bars are 20 μm.

Supplementary Figure 3: Simplified geological map of the Karacahisar-Seydişehir area, central Tauride continental unit, showing the sample locations. None of the samples collected from the Cambro-Ordovician Seydişehir Formation yielded usable any zircons. Zircons from the samples 75 and 78 taken from the Kasımlar Formation were analysed for U-Pb-Hf isotopic analysis. Map modified after (Şenel 1997).

Supplementary Figure 4: Selected cathodoluminescence images of detrital zircons of from sandstone sample K.12.75 from of the Late Triassic Kasımlar Formation, Tauride continental unitAutochthon. The open circles on the zircons show the locations of the spots analysed;, whereas the numbers within the circles indicate the name of the

individual spots. $^{206}Pb/^{238}U$ ages are used for <1Ga and $^{206}Pb/^{207}Pb$ ages are used for >1 Ga. Errors are at 1σ level.

Supplementary Figure 5: Selected cathodoluminescence images of detrital zircons ~~of~~ from sandstone sample K.12.78 ~~from~~ of the Late Triassic Kasımlar Formation, Tauride ~~A~~continental unit~~utochthon~~. The open circles on the zircons show the locations of the spots analysed;~~,~~ ~~whereas~~ the numbers within the circles indicate the ~~name of the~~ individual spots. $^{206}Pb/^{238}U$ ages are used for <1Ga and $^{206}Pb/^{207}Pb$ ages are used for >1 Ga. Errors are at 1σ level.

Supplementary Figure 6: Simplified geological map of the Üzümdere area, Tauride continental unit, showing the location of the sandstone sample (K.13.77) analysed. Map ~~was~~ re-drawn after Monod (1977) and Toker *et al.* (1993).

Supplementary Figure 7: Selected cathodoluminescence images of detrital zircons ~~of~~ from sandstone ~~from~~ of the Late Triassic Üzümdere Formation, Tauride continental unit~~Autochthon~~. The open circles on the zircons show the locations of the spots analysed;~~,~~ ~~whereas~~ the numbers within the circles indicate the ~~name of the~~ individual spots. $^{206}Pb/^{238}U$ ages are used for <1Ga and $^{206}Pb/^{207}Pb$ ages are used for >1 Ga. Errors are at 1σ level.

Supplementary Figure 8: Geological map of the Sızma-Ladik area of Konya, showing the location of the meta-sandstone sample (K.13.75) analysed from the Konya Complex. See Robertson and Ustaömer (2009a) for data sources.

Supplementary Figure 9: Selected cathodoluminescence images of detrital zircons from metasandstone ~~from~~ of the Konya Complex, Afyon Zone, c~~C~~entral Anatolide continental unit~~Taurides~~. The open circles on the zircons show the locations of the spots

analysed;, whereas the numbers within the circles indicate the name of the individual spots. $^{206}Pb/^{238}U$ ages are used for <1Ga and $^{206}Pb/^{207}Pb$ ages are used for >1 Ga. Errors are at 1σ level.

Supplementary Figure 10: Simplified geological map of the Karaburun Peninsula, showing the locations of the samples (K.13.102 and K.13.104) analysed in during this study. See Robertson and Ustaömer (2009b) for the data sources.

Supplementary Figure 11: Selected cathodoluminescence images of detrital zircons of sandstone from the Karaburun Melange. The open circles on the zircons show the locations of the spots analysed;, whereas the numbers within the circles indicate the name of the individual spots. $^{206}Pb/^{238}U$ ages are used for <1Ga and $^{206}Pb/^{207}Pb$ ages are used for >1 Ga. Errors are at 1σ level.

Supplementary Figure 12: Selected cathodoluminescence images of detrital zircons of sandstone sample from the Late Triassic Güvercinlik Formation (Tauride continental unit). The open circles on the zircons show the locations of the spots analysed;, whereas the numbers within the circles indicate the name of the individual spots. $^{206}Pb/^{238}U$ ages are used for <1Ga and $^{206}Pb/^{207}Pb$ ages are used for >1 Ga. Errors are at 1σ level.

Supplementary Figure 13: Simplified geological map of the Simav-Alaçam area (after Candan *et al.* 2016), showing the locations of the meta-granite samples from the Afyon Zone, Anatolide continental unit (TM.17.33, TM.17.34 and TM.17.35) analysed in this study.

Supplementary Table 1: Uranium-lead analytical data.

Supplementary Table 2: Lutetium-hafnium analytical data.

Supplementary Table 3: GPS coordinates of the samples analysed.

~~**Table 2:** Summary of U-Pb and Lu-Hf data for Carboniferous sandstones.~~

~~**Table 3:** Summary of U-Pb and Lu-Hf data for Triassic sandstones.~~

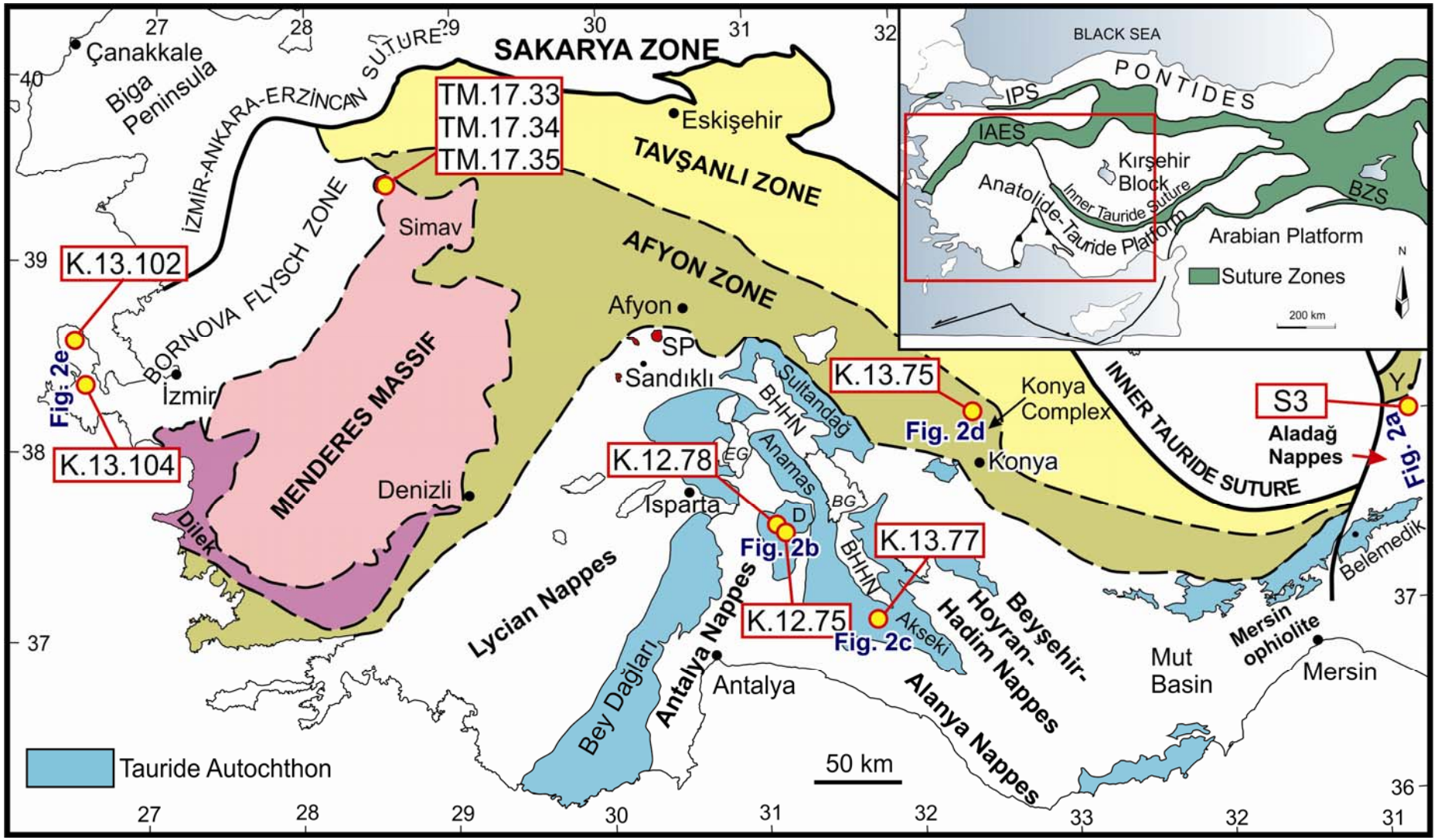
SAKARYA ZONE
TAVŞANLI ZONE
AFYON ZONE
İZMİR-ANKARA-ERZİNCAN SUTURE
BORNOVA FLYSCH ZONE
MENDERES MASSIF
INNER TAURIDE SUTURE
Lycian Nappes
Antalya Nappes
Bey Dağları
Beyşehir-Hoyran-Hadim Nappes
Alanya Nappes
Aladağ Nappes
Mersin ophiolite
Mut Basin
Çanakkale
Biga Peninsula
Eskişehir
Simav
Afyon
SP
Sandıklı
İzmir
Denizli
Dilek
Isparta
Sultandağ
Anamas
BHHN
EG
BG
D
Konya
Konya Complex
Akseki
Antalya
Belemedik
Mersin
TM.17.33
TM.17.34
TM.17.35
K.13.102
K.13.104
K.12.78
K.12.75
K.13.75
K.13.77
S3
Fig. 2a
Fig. 2b
Fig. 2c
Fig. 2d
Fig. 2e
Tauride Autochthon
50 km
BLACK SEA
PONTIDES
IPS
IAES
Kırşehir Block
Anatolide-Tauride Platform
Inner Tauride Suture
BZS
Arabian Platform
Suture Zones
200 km
N

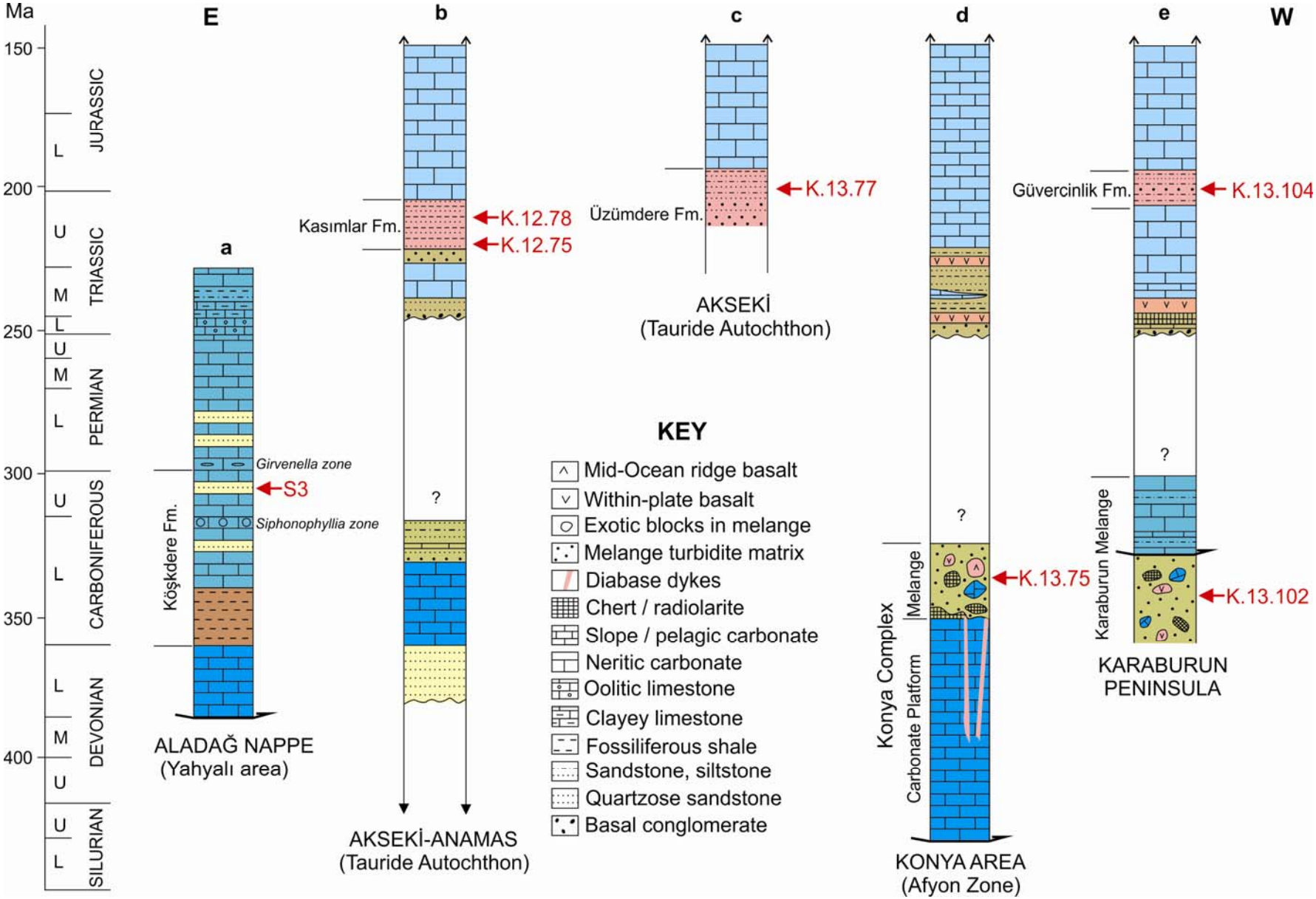
Ma
150
200
250
300
350
400
JURASSIC
TRIASSIC
PERMIAN
CARBONIFEROUS
DEVONIAN
SILURIAN
E
a
Girvenella zone
S3
Siphonophyllia zone
Köşkdere Fm.
ALADAĞ NAPPE
(Yahyalı area)
b
Kasımlar Fm.
K.12.78
K.12.75
?
AKSEKİ-ANAMAS
(Tauride Autochthon)
c
Üzümdere Fm.
K.13.77
AKSEKİ
(Tauride Autochthon)
KEY
Mid-Ocean ridge basalt
Within-plate basalt
Exotic blocks in melange
Melange turbidite matrix
Diabase dykes
Chert / radiolarite
Slope / pelagic carbonate
Neritic carbonate
Oolitic limestone
Clayey limestone
Fossiliferous shale
Sandstone, siltstone
Quartzose sandstone
Basal conglomerate
d
?
Melange
K.13.75
Konya Complex
Carbonate Platform
KONYA AREA
(Afyon Zone)
e
W
Güvercinlik Fm.
K.13.104
?
Karaburun Melange
K.13.102
KARABURUN
PENINSULA


33b
666±7
607±8
35c
601±9
620±9
13a
765±11
788±7
840±14
11d
1063±11
565±10
33d
563±8
718±7
812±8
27d
a
Köşkdere Fm. (S3)
900±7
318
2844±5
304
639±5
297
734±6
293
531±4
321
2742±9
305
376
629±5
2008±19
362
314±2
319
308
570±4
2530±6
296
971±7
392
1888±9
343
1933±12
406
b
Kasımlar Fm. (K.12.75 &78)
100 µm
837±7
207
456±4
214
828±7
272
544±5
211
452±4
205
230
659±5
c
Üzümdere Fm. (K.13.77)
100 µm
7
643±6
8
599±5
23
804±6
914±6
47
49
1923±8
101
592±6
2504±10
58
d
Konya Complex (K.13.75)
100 µm
1925±9
729
392±3
728
779
492±4
2158±14
686
675
408±6
720
513±4
679
395±3
e
Karaburun Melange (K.13.102)
100 µm
353±3
1262
1309
2015±18
1975±6
1291
603±5
658±5
1280
734±5
1244
310±3
317±3
1282
1283
587±6
1189
1227
558±4
606±5
1281
2502±6
1179
369±3
1188
f
Güvercinlik Fm. (K.13.104)
100 µm

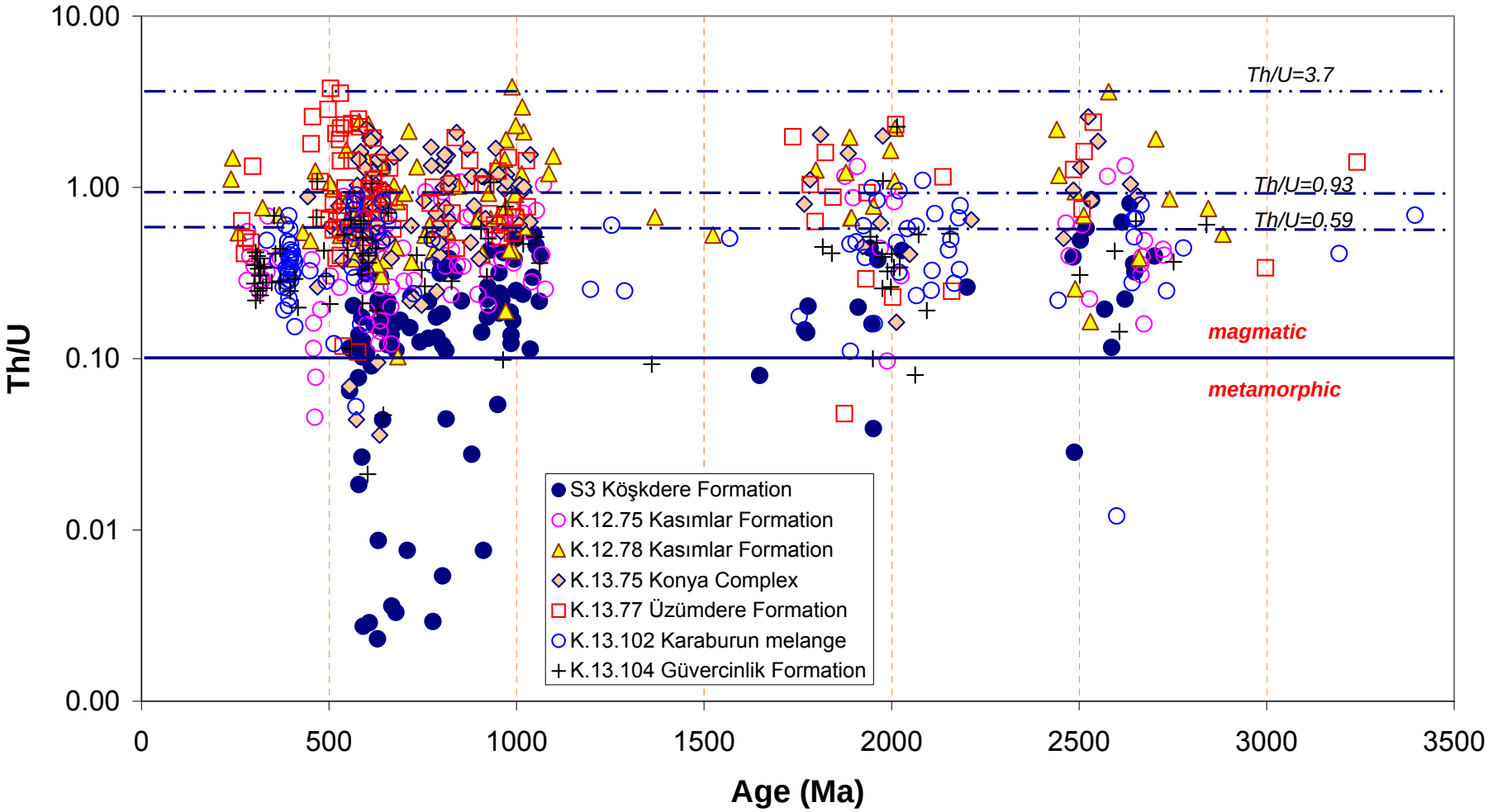
10.00
1.00
0.10
0.01
0.00
Th/U
0
500
1000
1500
2000
2500
3000
3500
Age (Ma)
Th/U=3.7
Th/U=0.93
Th/U=0.59
magmatic
metamorphic
S3 Köşkdere Formation
K.12.75 Kasımlar Formation
K.12.78 Kasımlar Formation
K.13.75 Konya Complex
K.13.77 Üzümdere Formation
K.13.102 Karaburun melange
K.13.104 Güvercinlik Formation

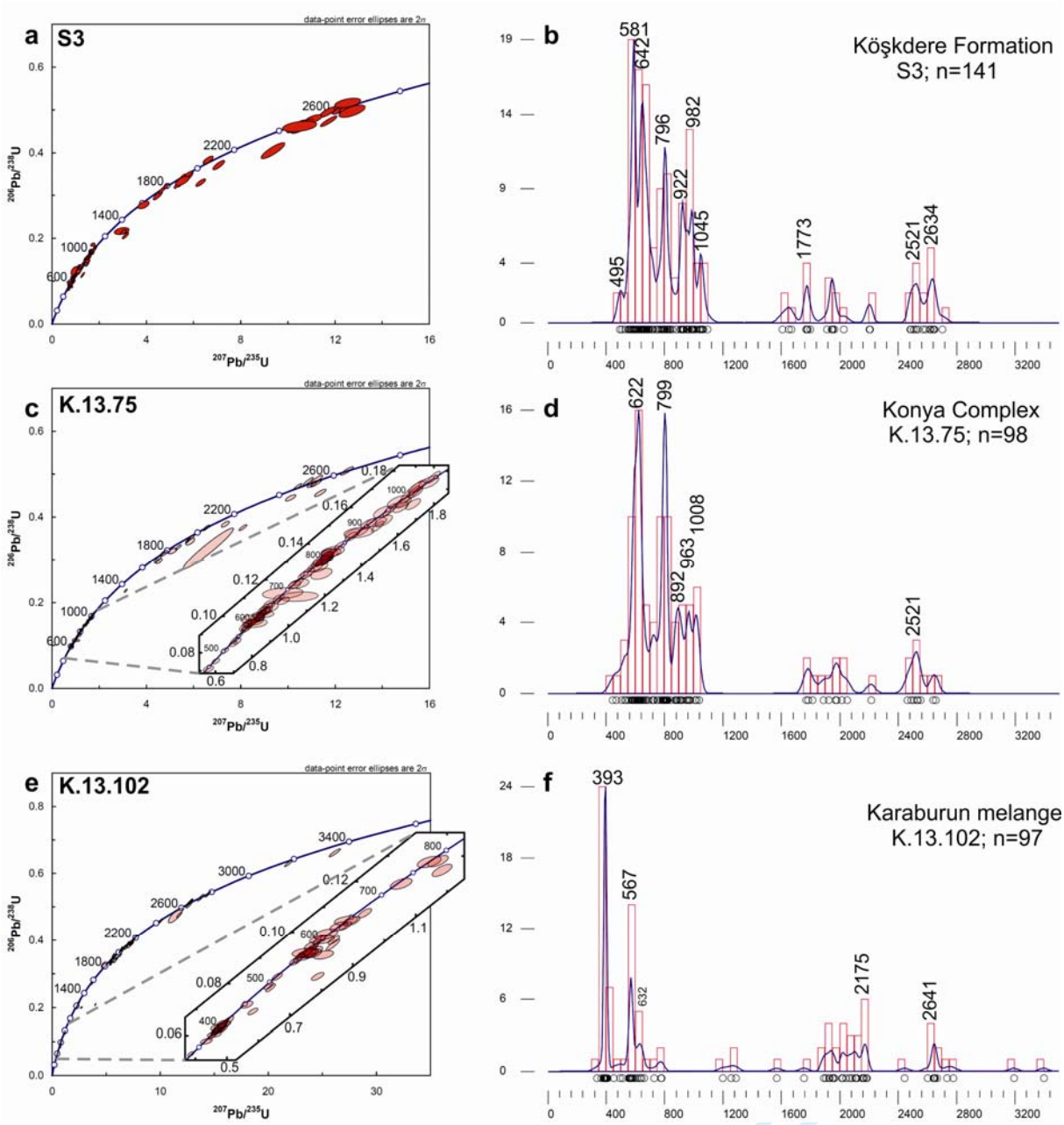
a
S3
data-point error ellipses are 2σ
$^{206}Pb/^{238}U$
$^{207}Pb/^{235}U$
b
Köşkdere Formation
S3; n=141
581
642
796
982
922
1045
495
1773
2521
2634
c
K.13.75
d
Konya Complex
K.13.75; n=98
622
799
1008
963
892
2521
e
K.13.102
f
Karaburun melange
K.13.102; n=97
393
567
632
2175
2641

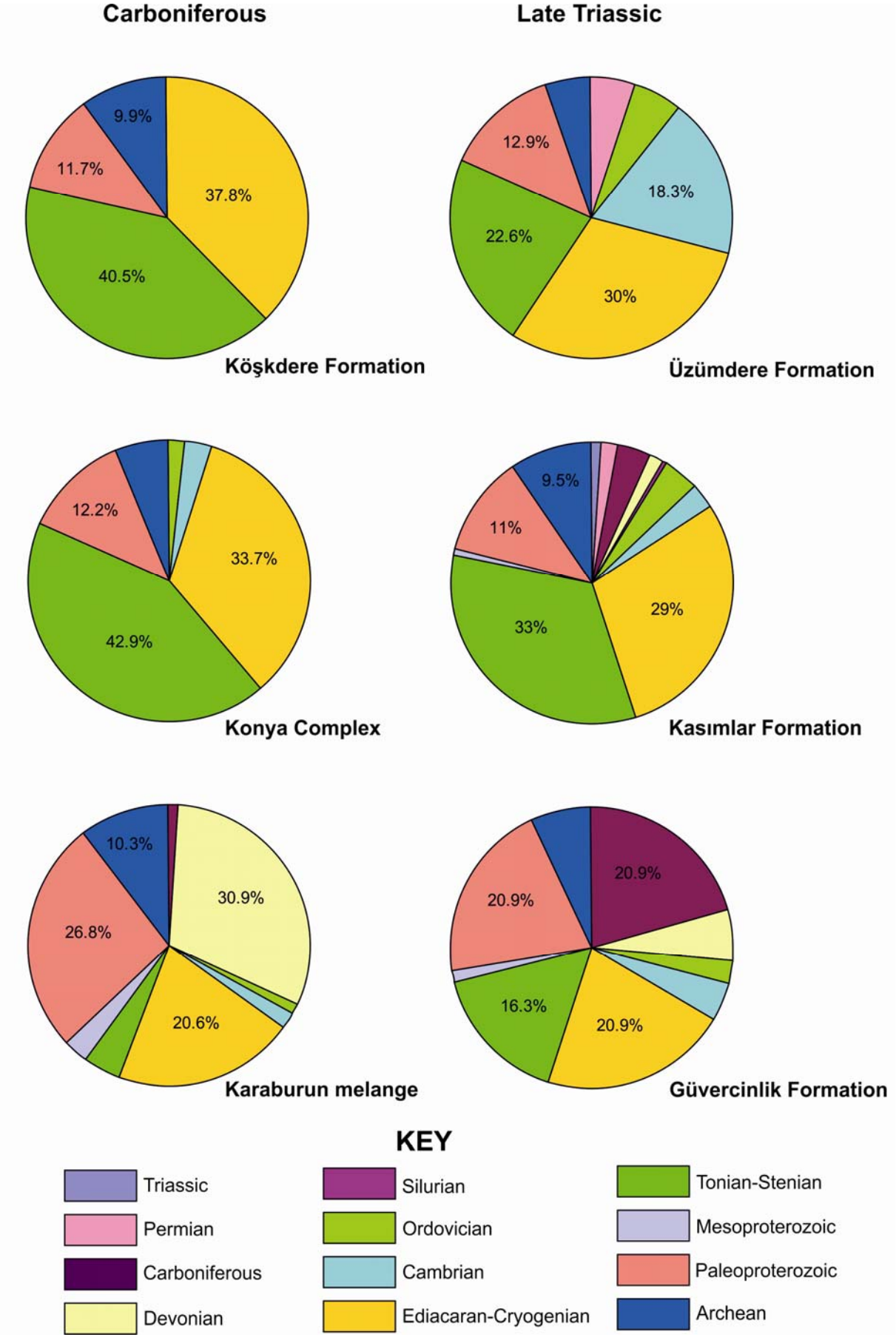
Carboniferous
9.9%
11.7%
37.8%
40.5%
Köşkdere Formation
Late Triassic
12.9%
18.3%
22.6%
30%
Üzümdere Formation
12.2%
33.7%
42.9%
Konya Complex
9.5%
11%
29%
33%
Kasımlar Formation
10.3%
30.9%
26.8%
20.6%
Karaburun melange
20.9%
20.9%
16.3%
20.9%
Güvercinlik Formation
KEY
Triassic
Permian
Carboniferous
Devonian
Silurian
Ordovician
Cambrian
Ediacaran-Cryogenian
Tonian-Stenian
Mesoproterozoic
Paleoproterozoic
Archean

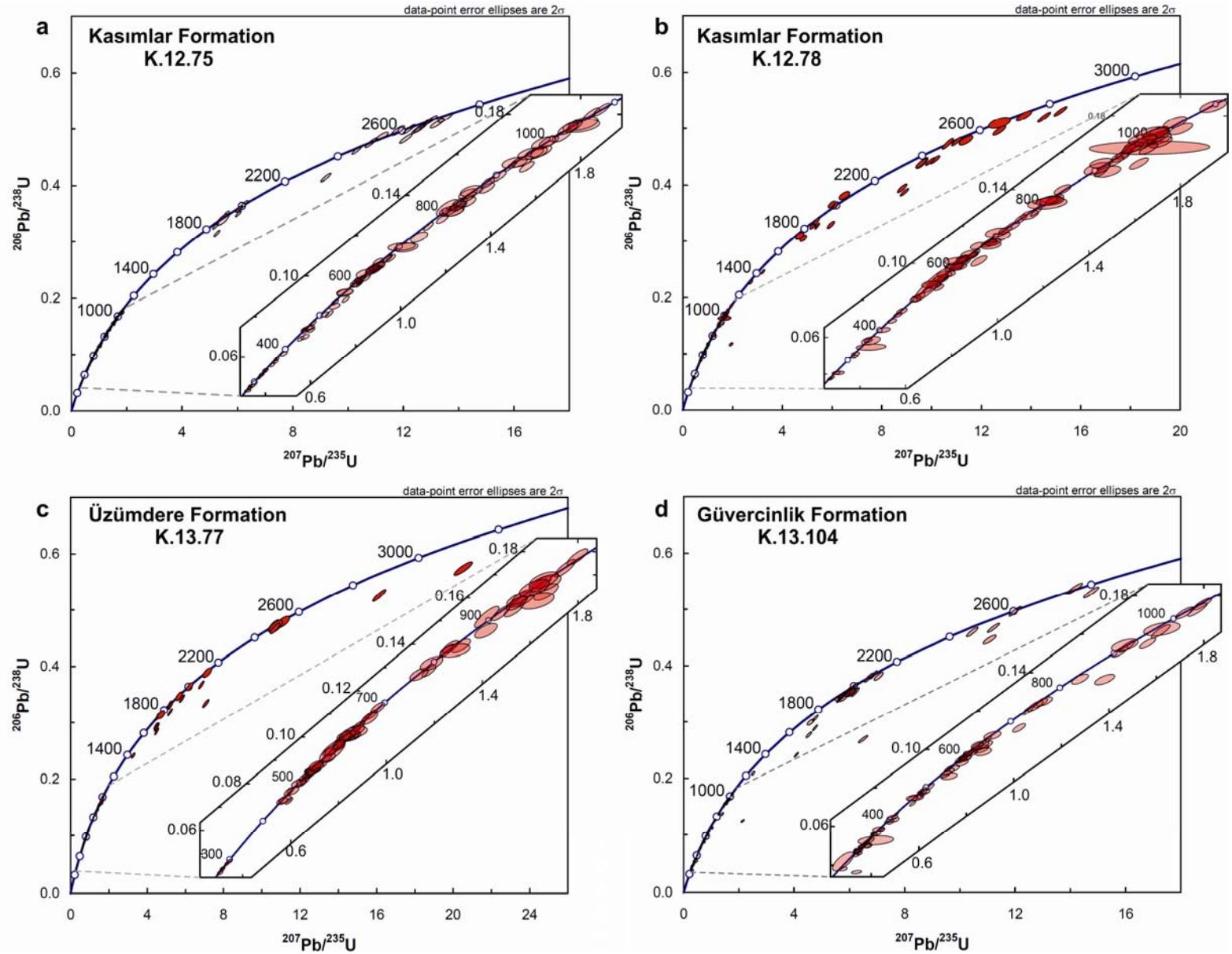
a
Kasımlar Formation
K.12.75
data-point error ellipses are 2σ
b
Kasımlar Formation
K.12.78
data-point error ellipses are 2σ
c
Üzümdere Formation
K.13.77
data-point error ellipses are 2σ
d
Güvercinlik Formation
K.13.104
data-point error ellipses are 2σ
$^{206}Pb/^{238}U$
$^{207}Pb/^{235}U$

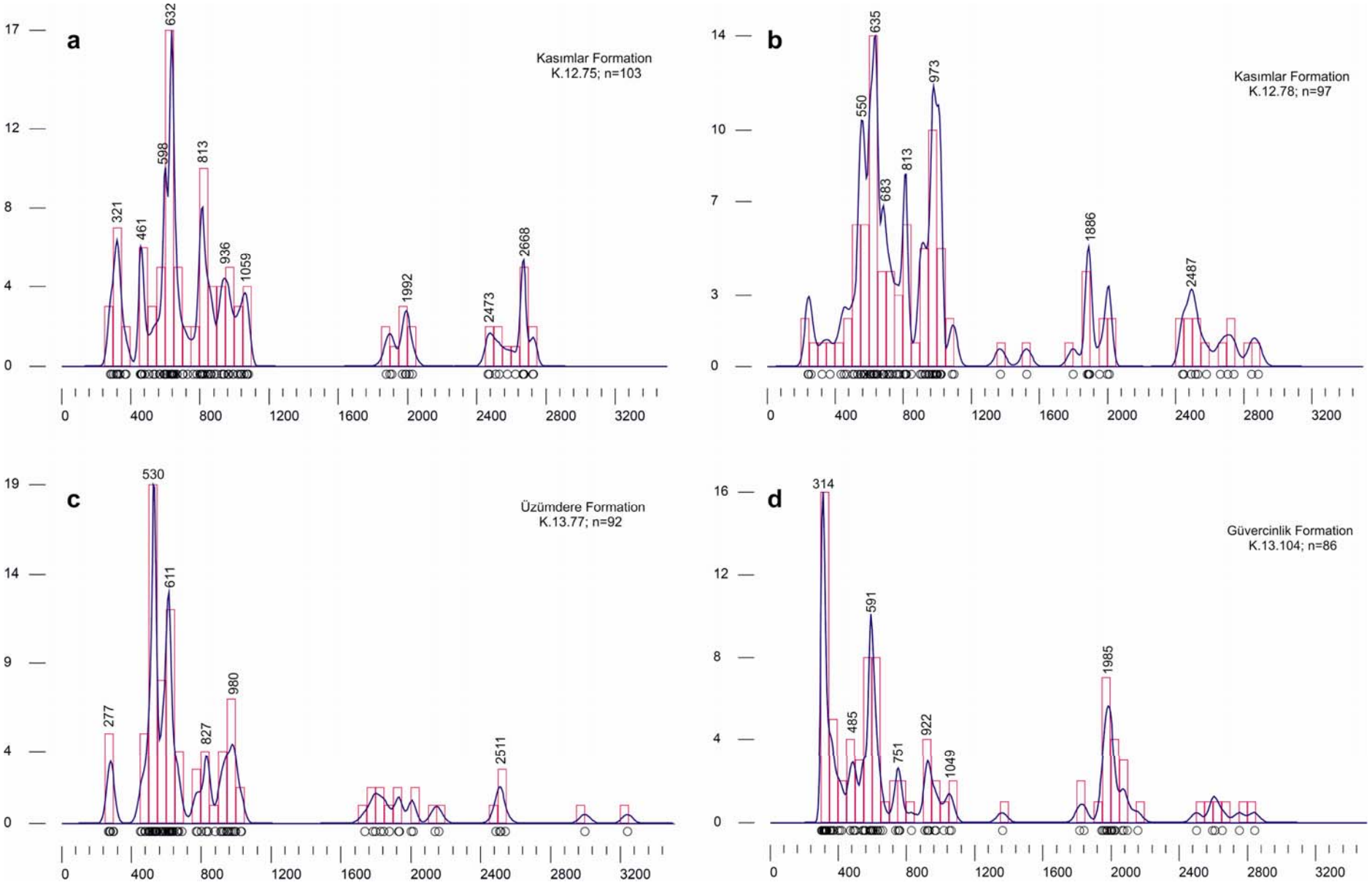
a
Kasımlar Formation
K.12.75; n=103
632
598
813
321
461
936
1059
1992
2473
2668
b
Kasımlar Formation
K.12.78; n=97
635
550
973
813
683
1886
2487
c
Üzümdere Formation
K.13.77; n=92
530
611
980
277
827
2511
d
Güvercinlik Formation
K.13.104; n=86
314
591
1985
485
751
922
1049
0
400
800
1200
1600
2000
2400
2800
3200

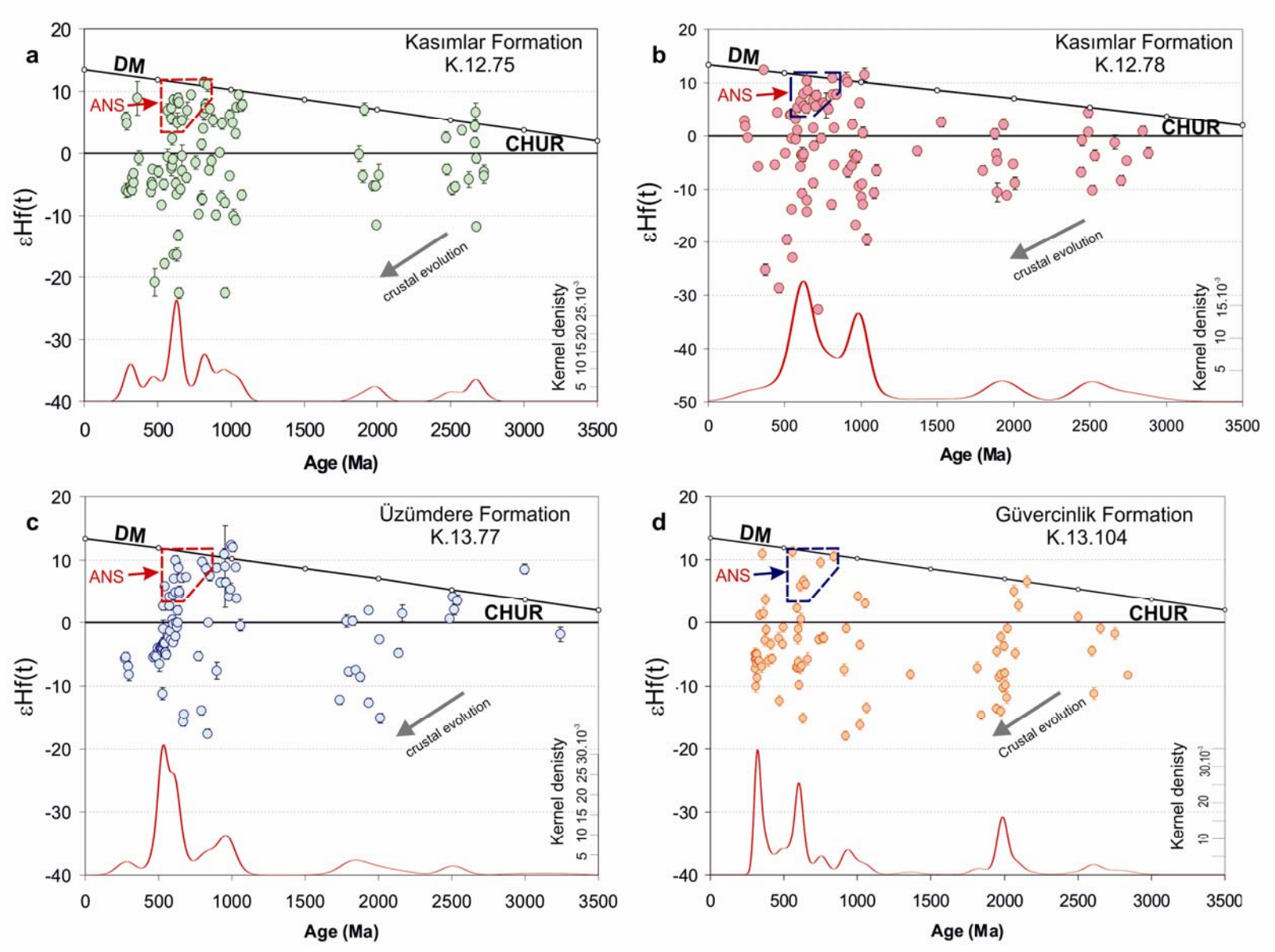
a
Kasımlar Formation
K.12.75
DM
ANS
CHUR
crustal evolution
εHf(t)
Kernel denisty
Age (Ma)
b
Kasımlar Formation
K.12.78
DM
ANS
CHUR
crustal evolution
εHf(t)
Kernel denisty
Age (Ma)
c
Üzümdere Formation
K.13.77
DM
ANS
CHUR
crustal evolution
εHf(t)
Kernel denisty
Age (Ma)
d
Güvercinlik Formation
K.13.104
DM
ANS
CHUR
Crustal evolution
εHf(t)
Kernel denisty
Age (Ma)

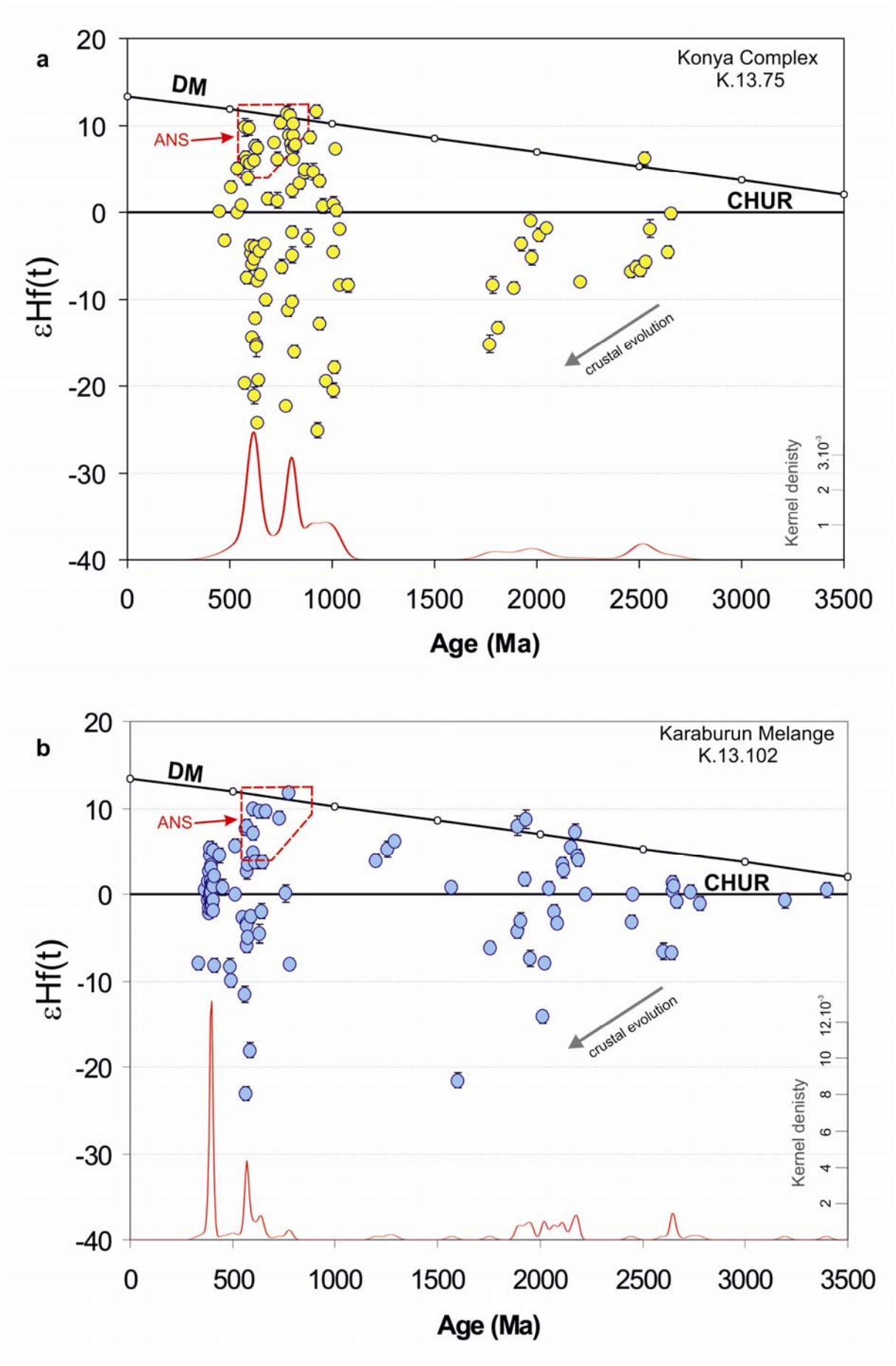
a
Konya Complex
K.13.75
DM
ANS
CHUR
crustal evolution
Kernel denisty
3.10-3
εHf(t)
Age (Ma)
b
Karaburun Melange
K.13.102
DM
ANS
CHUR
crustal evolution
Kernel denisty
12.10-3
εHf(t)
Age (Ma)

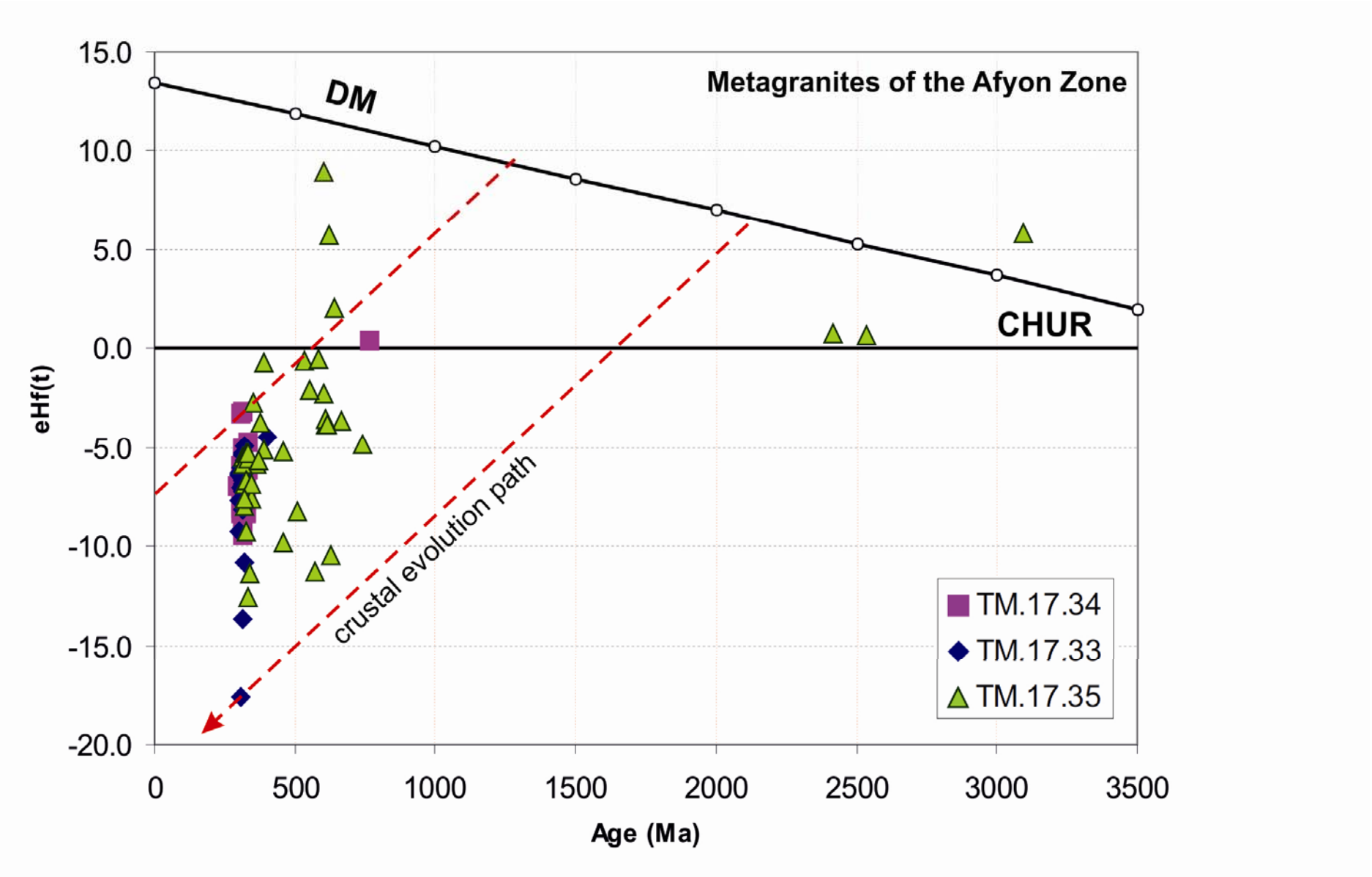
Metagranites of the Afyon Zone
DM
CHUR
crustal evolution path
TM.17.34
TM.17.33
TM.17.35
eHf(t)
Age (Ma)
15.0
10.0
5.0
0.0
-5.0
-10.0
-15.0
-20.0
0
500
1000
1500
2000
2500
3000
3500

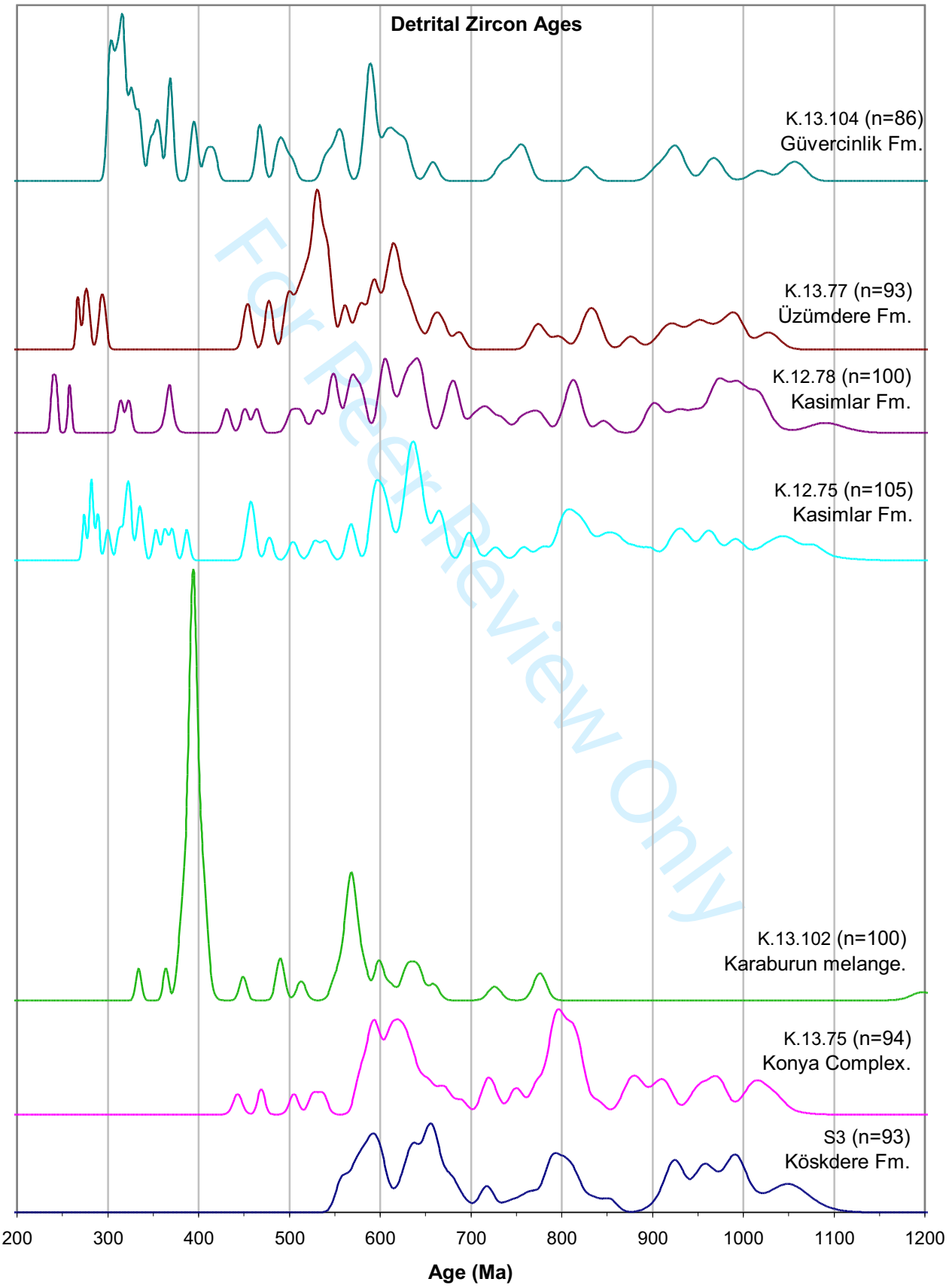

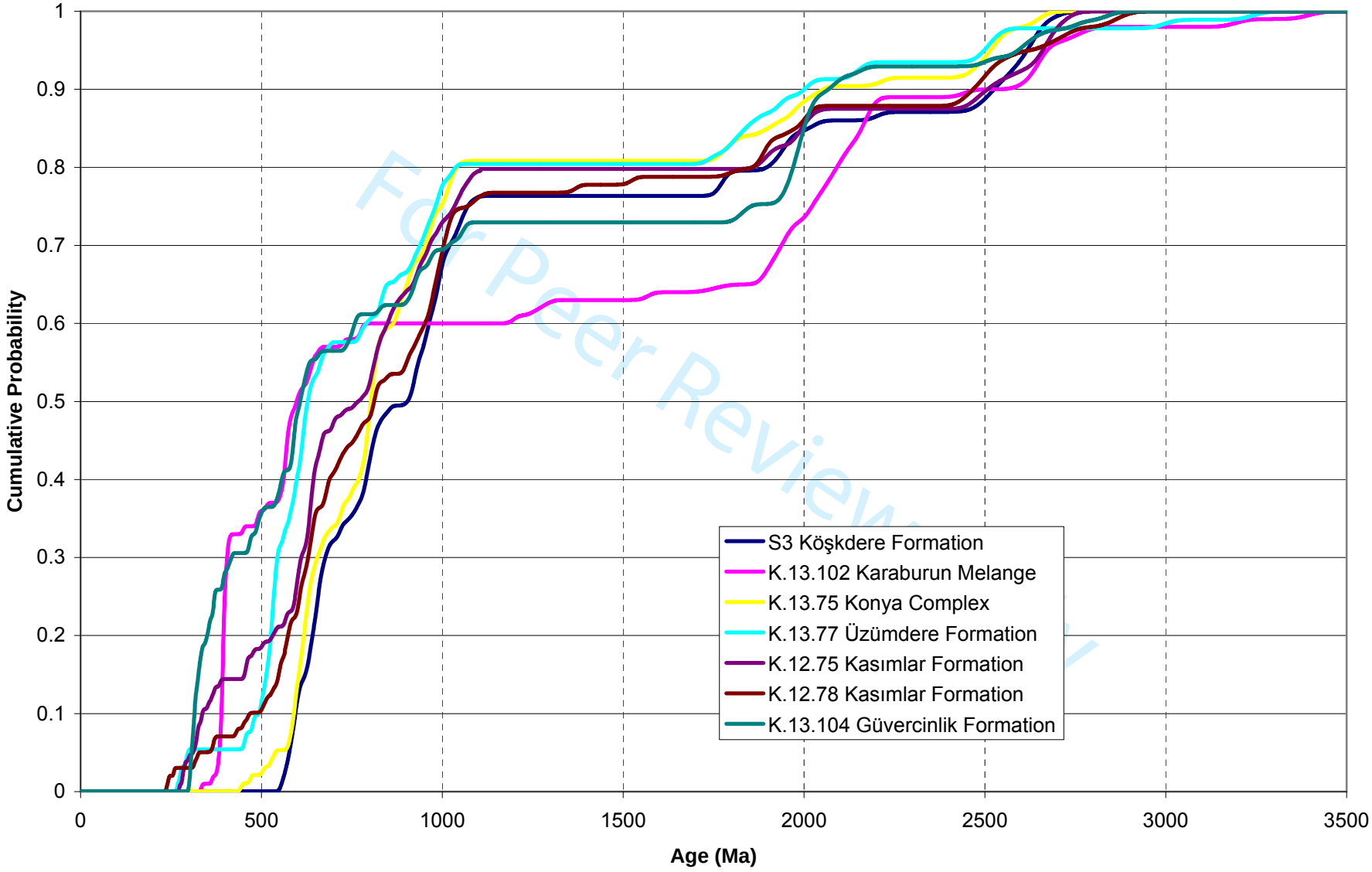

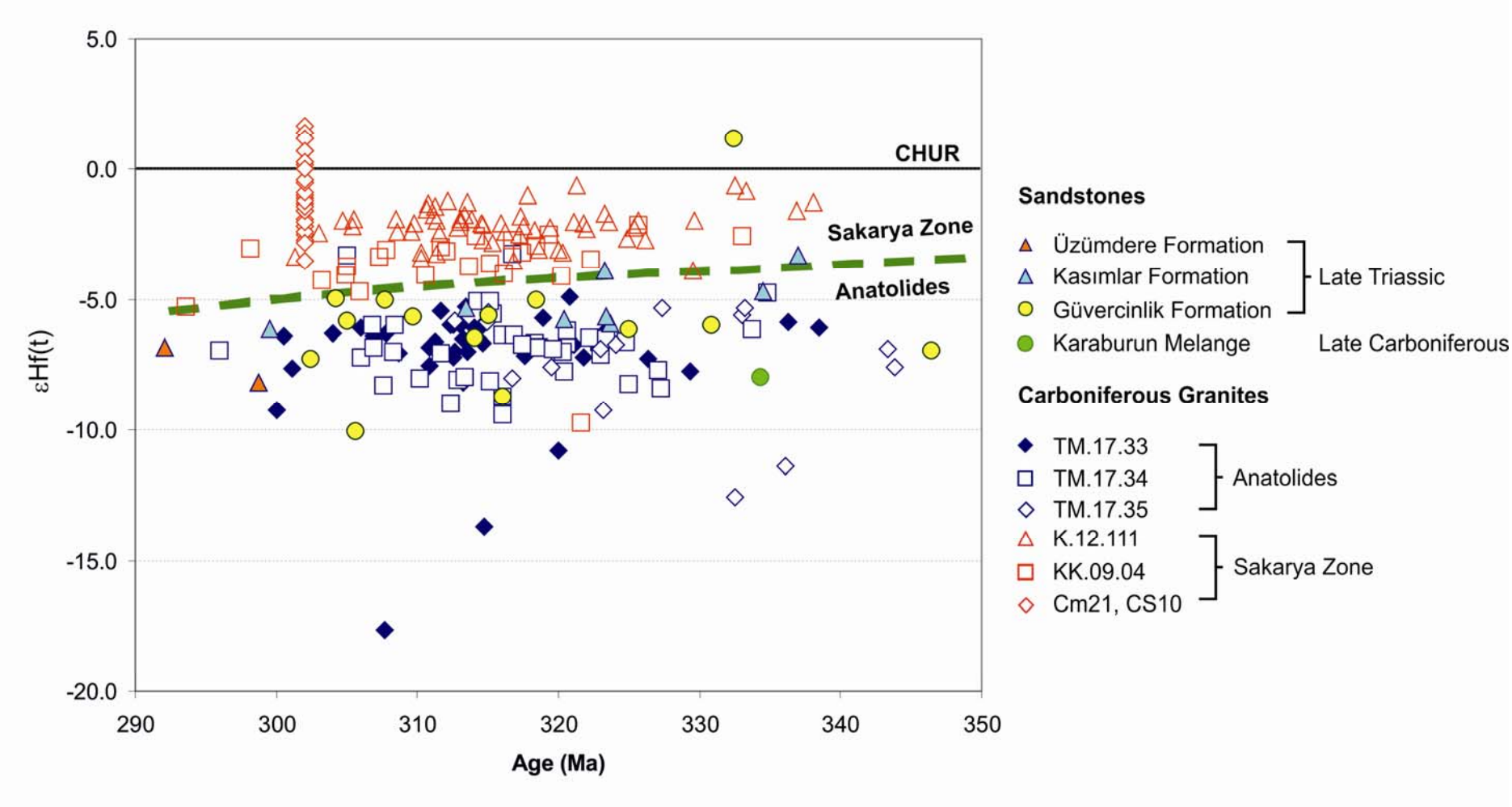
5.0
0.0
-5.0
-10.0
-15.0
-20.0
εHf(t)
290
300
310
320
330
340
350
Age (Ma)
CHUR
Sakarya Zone
Anatolides
Sandstones
Üzümdere Formation
Kasımlar Formation
Güvercinlik Formation
Late Triassic
Karaburun Melange
Late Carboniferous
Carboniferous Granites
TM.17.33
TM.17.34
TM.17.35
Anatolides
K.12.111
KK.09.04
Cm21, CS10
Sakarya Zone

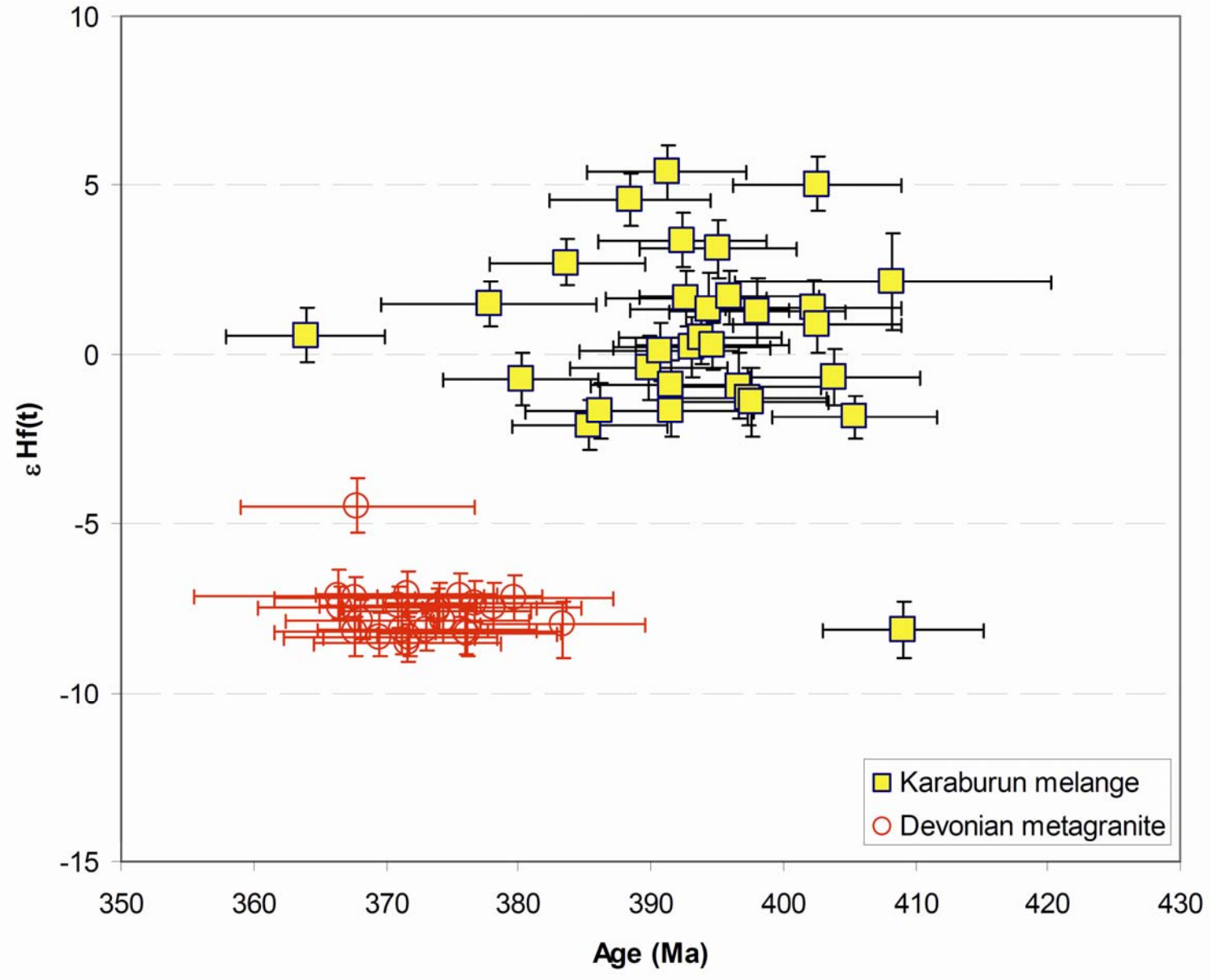
10
5
0
-5
-10
-15
εHf(t)
350
360
370
380
390
400
410
420
430
Age (Ma)
Karaburun melange
Devonian metagranite

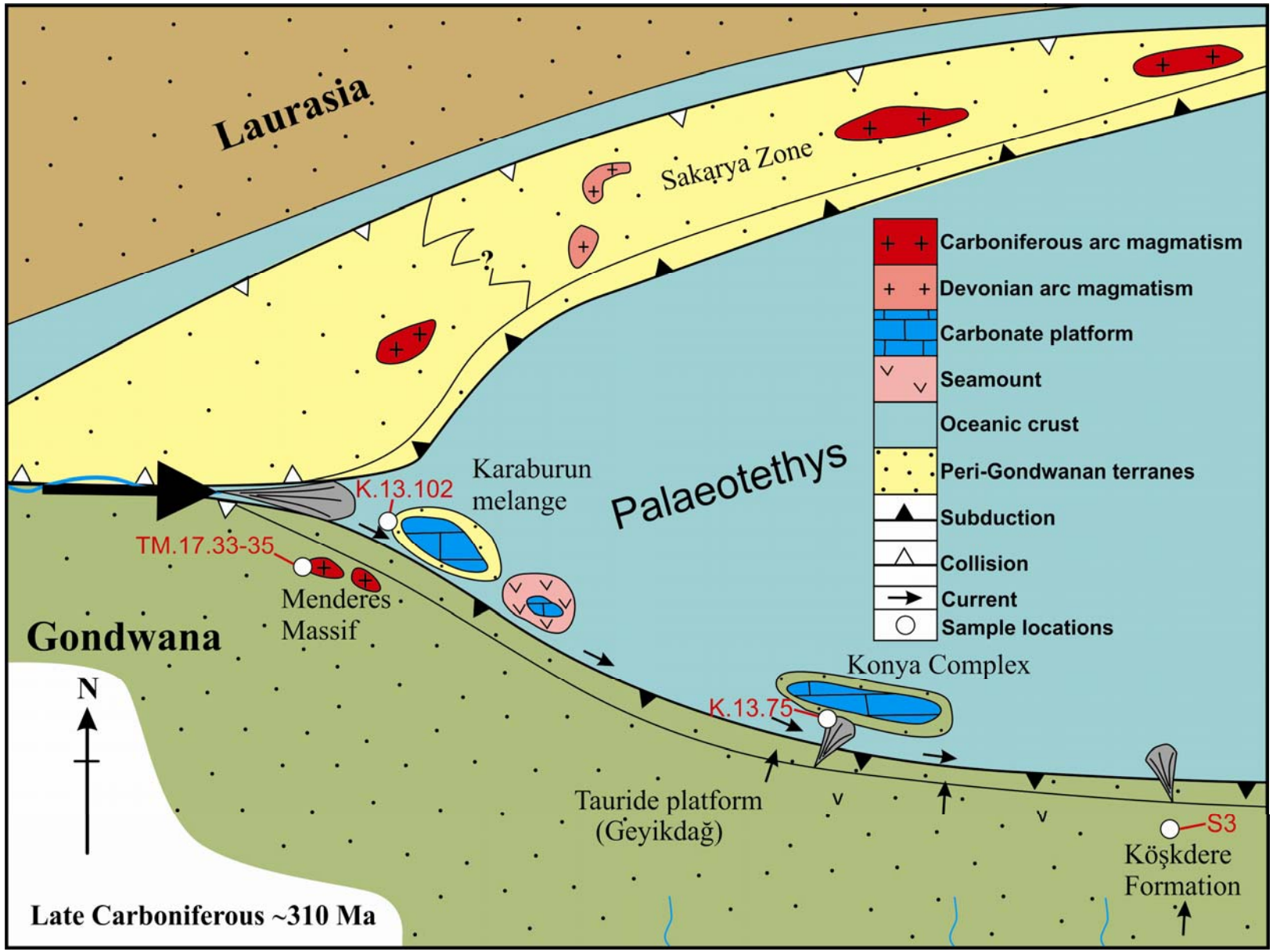
Laurasia
Sakarya Zone
?
Carboniferous arc magmatism
Devonian arc magmatism
Carbonate platform
Seamount
Oceanic crust
Peri-Gondwanan terranes
Subduction
Collision
Current
Sample locations
Karaburun
melange
K.13.102
Palaeotethys
TM.17.33-35
Menderes
Massif
Gondwana
Konya Complex
K.13.75
N
Tauride platform
(Geyikdağ)
S3
Köşkdere
Formation
Late Carboniferous ~310 Ma

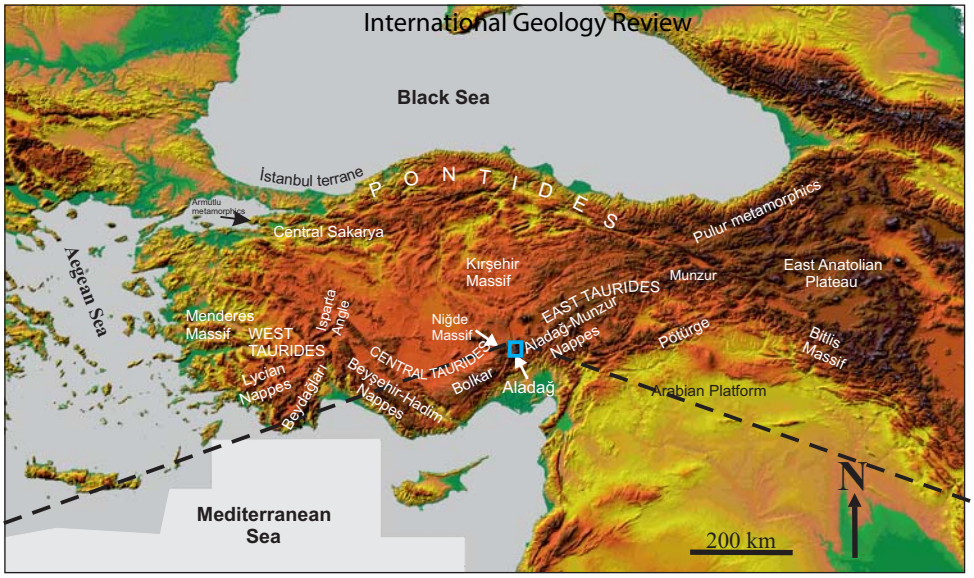

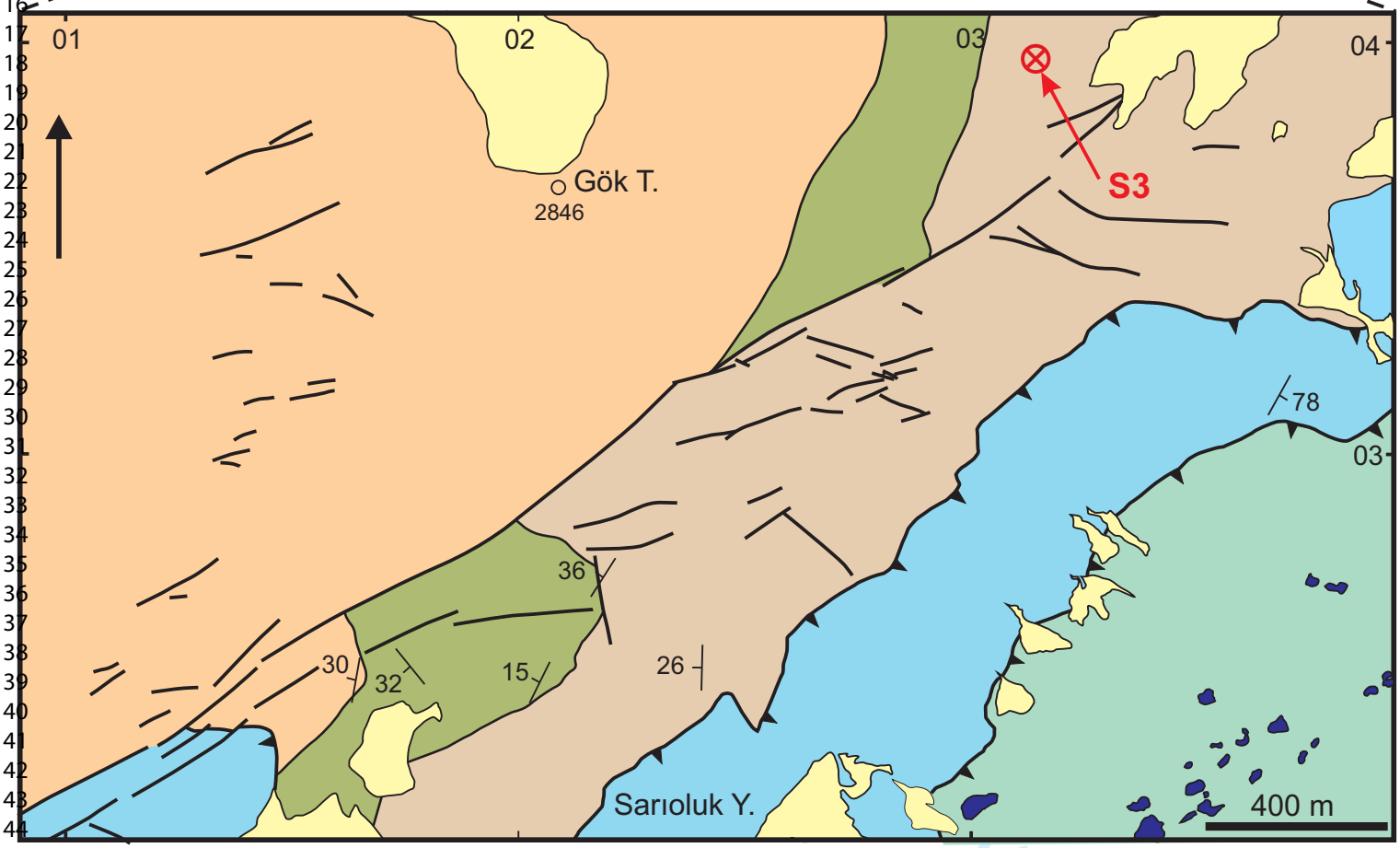

KEY

- Slope scree — Quaternary
- Matrix
- Limestone blocks
  - Aladağ ophiolitic melange – Senonian
- Çobankaya Formation - Jurassic
- Zindandere Formation - Upper Permian
- *Girvenella* limestone - Lower Permian
- Köşkdere Formation-Upper Carboniferous
  - Siyah Aladağ Nappe
- Thrust fault
- Fault
- 32 — Strike and dip of bedding
- 2846 — Peak and altitude


S3 33b
666±7
607±8
S3 35c
601±9
620±9
S3 13a
765±11
788±7
840±14
S3 11d
1063±11
565±10
S3 33d
563±8
718±7
S3 37d
690±9
S3 9a
907±12
922±10
S3 27a
686±8
1053±10
631±6
S3 23d
827±11
S3 25a
799±13
766±10
950±12
S3 11c
966±11
671±12
S3 45b
1026±12
S3 33a
587±7
S3 19b
686±11
990±9
S3 17b
2533±19
2568±13
1797±18
S315b
555±6
853±8
S3 31b
S3 19d
1774±19
1777±13
S3 21c
1963±23
1943±18
812±8
S3 27d
S3 19c
709±7
591±5
S3 21a
667±6
608±8
2533±18
S3 25b
2519±18
931±11
S3 15d
S3 (Köşkdere Fm.)

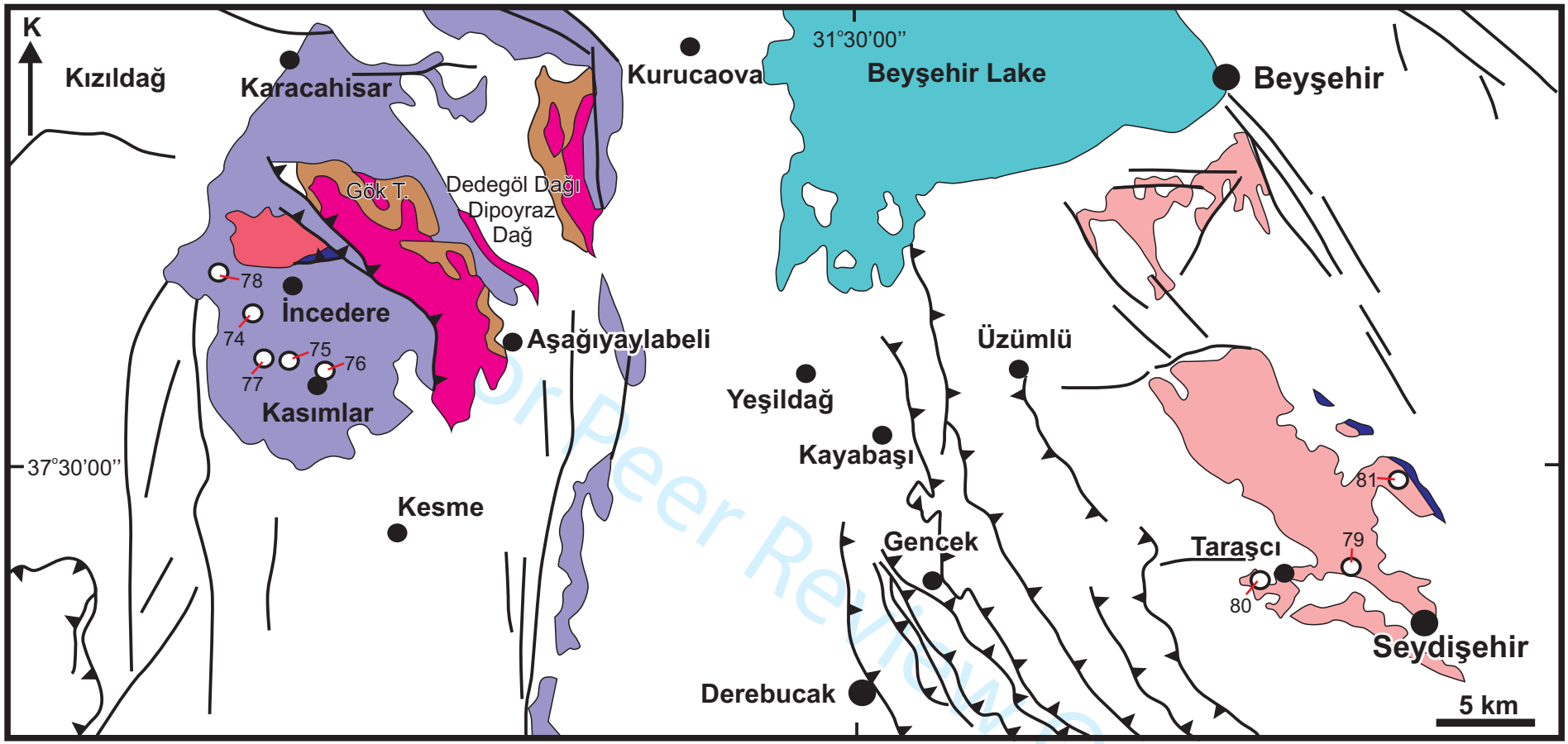

LEGEND

- 77 Sample location
- Triassic and younger
- Kasımlar Formation Upper Triassic
- Gökdağ limestone & Karlık Formation, Carboniferous
- Seydişehir Formation, Cambrian-Ordovician
- Çaltepe Formation, Cambrian
- Bozburun & Sarıçiçek schists, Pre-Carboniferous


478±4
977
1053±9
1002
462±3
1001
283±2
991
1031
632±5
2576±8
974
1009
437±3
432±3
978
2508±6
993
647±5
1029
2623±5
990
816±6
1012
947
665±5
637±4
979
622±5
1010
960±7
992
1027
926
697±6
923
1040±11
950
966±7
880±6
281±2
1004
540±4
969
921
938
459±3
971
454±3
949
458±3
1011
2665±5
802±7
337±3
960
595±5
964
972
2528±8
940
957
289±2
988
637±5
1031±11
942
951
962
2668±5
610±4
300±3
958
938±6
320±2
944
927
2465±5
897±6
1025
963
1876±7
642±4
842±7
1017
1015
1018
465±4
858±6
936
994
1031±14
601±4
999
827±6
916
1028
1016
779±5
371±3
200 µm
K.12.75 (Kasımlar Formation)


566±7
603±5
295
294
368±3
347
464±4
324
239±2
412
816±6
327
323±3
340
1997±8
395
1796±22
389
603±6
359
925±6
367
702±6
299
2705±8
320
1878±17
346
1016±8
804±7
313
317
981±8
311
531±4
321
2742±9
305
734±6
293
900±7
318
639±5
297
2008±19
362
1524±11
380
2844±5
304
2530±6
296
1933±12
406
314±2
319
1888±9
343
308
300
846±7
303
370
673±5
972±8
338
570±4
607±5
2513±7
342
992±7
410
971±7
392
1013±19
376
629±5
2579±12
363
292
546±4
323
679±5
373
998±7
360
431±3
306
682±5
337
768±6
713±6
312
581±5
316
502±4
344
335
258±2
988±7
2441±8
374
1020±17
378
302
365
815±6
309
100 µm
K.12.78 (Kasımlar Formation)

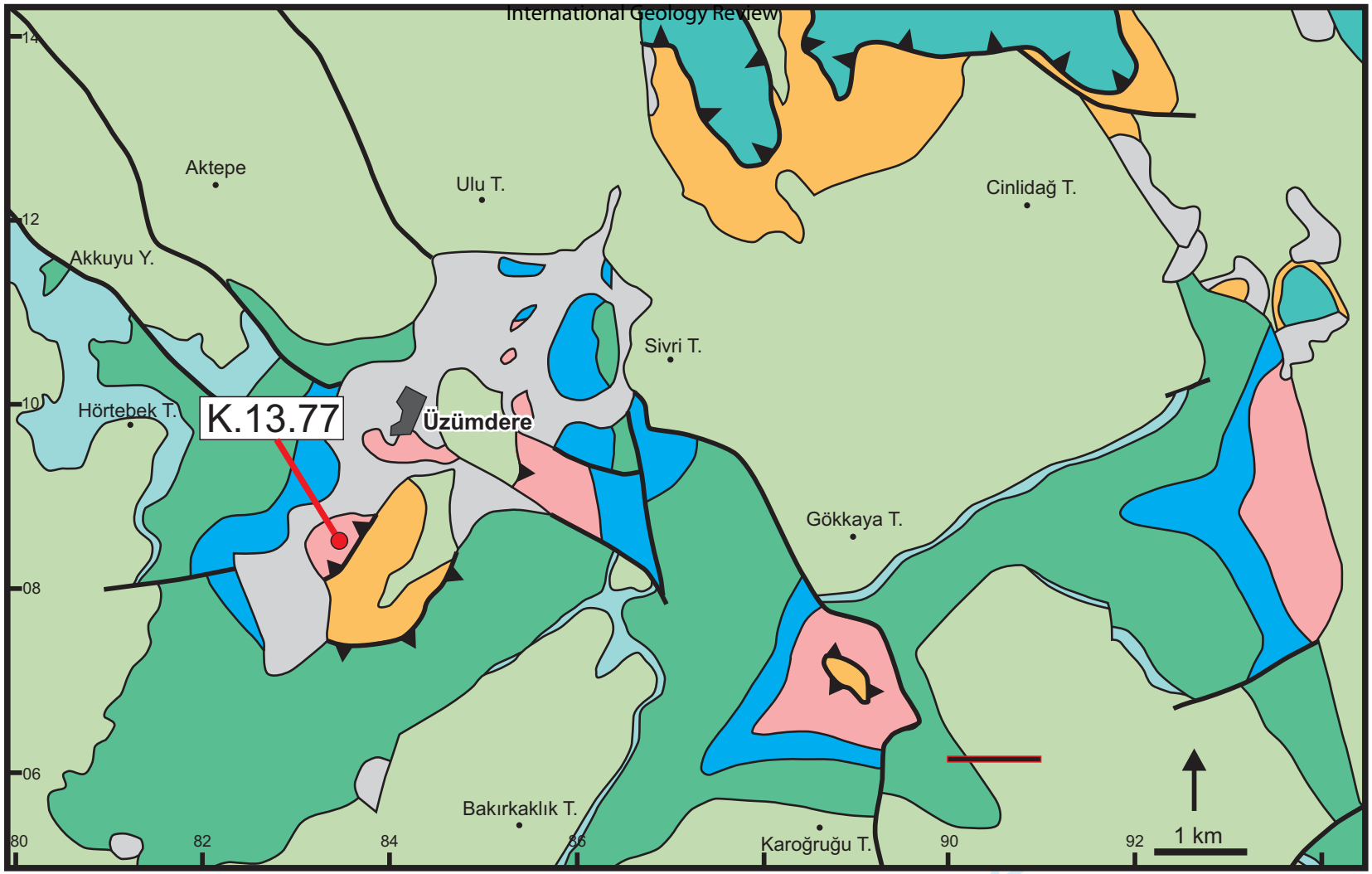

KEY

Alluvium, slope scree	Quaternary	Akkuyu Formation	Late Jurassic
Beyşehir-Hoyran Nappes	Paleozoic	Hendos Formation	Mid Jurassic
Gümüşdamla Formation	Eocene	Pisarçukuru Formation	Mid Jurassic
Akseki & Seyrandağı Formations	Cretaceous	Üzümdere Formation	Late Triassic-Early Jurassic

URL: https://mc.manuscriptcentral.com/tigr E-mail: rjstern@utdallas.edu

Thrust fault

Fault


2137±17
223
279
918±8
989±8
247
519±4
222
543±5
192
2003±8
233
969±8
248
479±4
212
229
611±6
541±5
210
497±4
262
257
2513±9
1026±12
220
521±4
250
607±5
246
189
827±7
951±8
243
292±3
228
2485±12
190
616±6
209
837±7
207
275±3
245
231
770±7
452±4
205
456±4
214
265
476±4
978±9
281
828±7
272
276
996±8
296±3
266
226
1844±9
2997±6
252
542±5
291
500±4
300
889±7
255
230
659±5
561±5
249
1590±13
188
593±5
253
626±6
219
544±5
211
532±5
208
519±5
224
236
1934±18
579±12
259
2538±16
216
1824±10
227
631±6
213
3241±7
263
100 µm
K.13.77 (Üzümdere Formation)

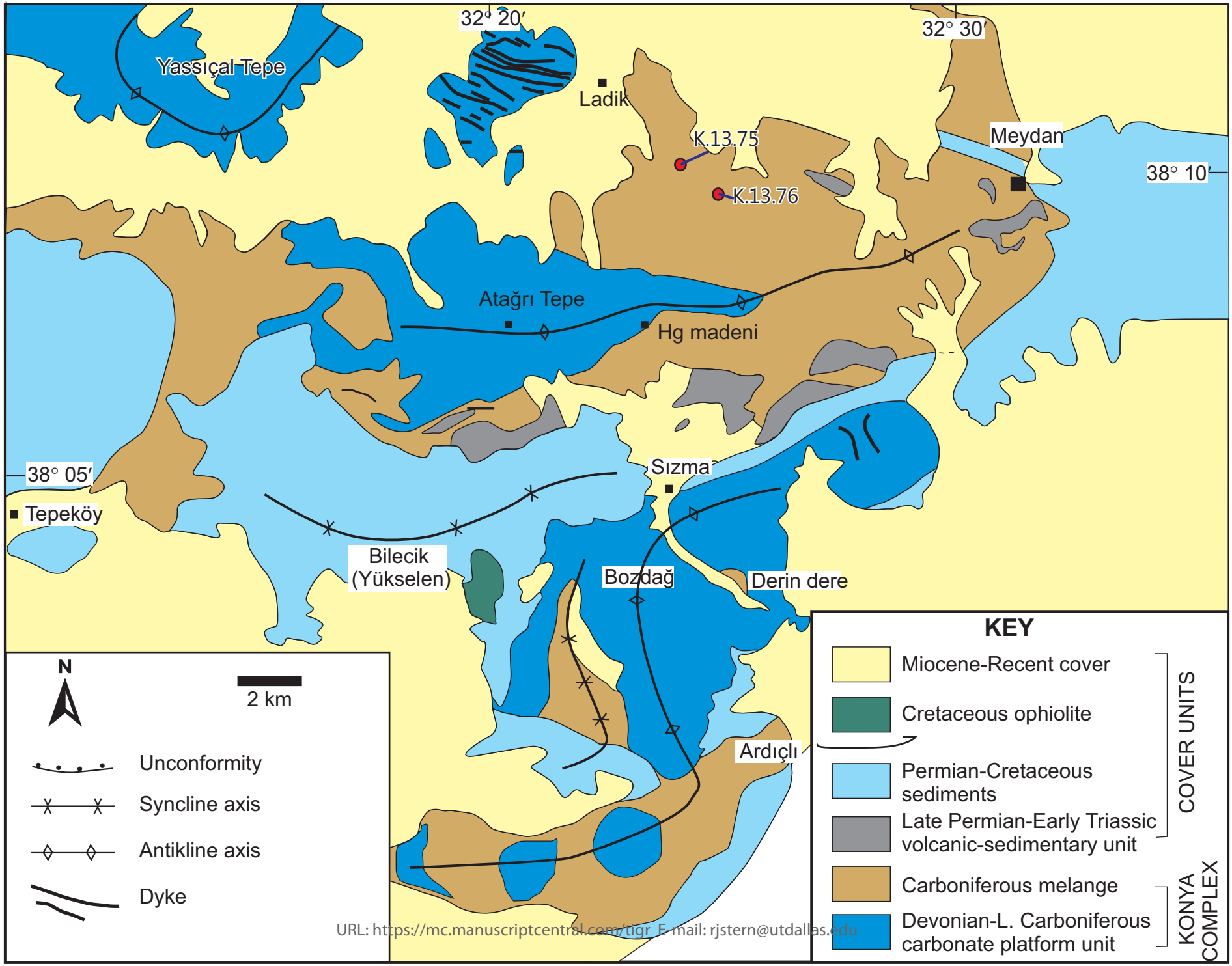


917±7
29
592±5
18
98
2485±6
96
97
804±6
23
7
643±6
8
599±5
607±6
19
28
573±5
975±8
2459±5
914±6
47
49
1923±8
2504±10
58
795±7
100
1017±14
10
592±6
101
2655±9
94
772±7
20
613±5
112
108
630±5
945±8
115
585±4
117
11
797±6
881±7
73
630±5
43
1811±16
1782±16
14
107
2551±7
129
31
469±4
785±5
95
809±6
116
59
636±5
726±5
76
2533±7
92
64
1019±8
1037±21
46
2637±7
113
443±5
16
51
907±7
2212±12
42
969±7
90
952±8
121
83
753±7
6
589±5
840±6
75
42
2212±12
127
716±6
624±5
109
812±6
41
1970±7
55
2013±17
26
974±7
126
72
580±5
747±6
80
65
818±6
617±5
39
2524±7
44
537±5
86
794±7
130
719±6
12
635±5
30
795±6
13
1885±21
88
806±5
40
1008±7
24
81
1767±11
9
773±6
114
650±5
200 µm
K.13.75 (Konya Complex)

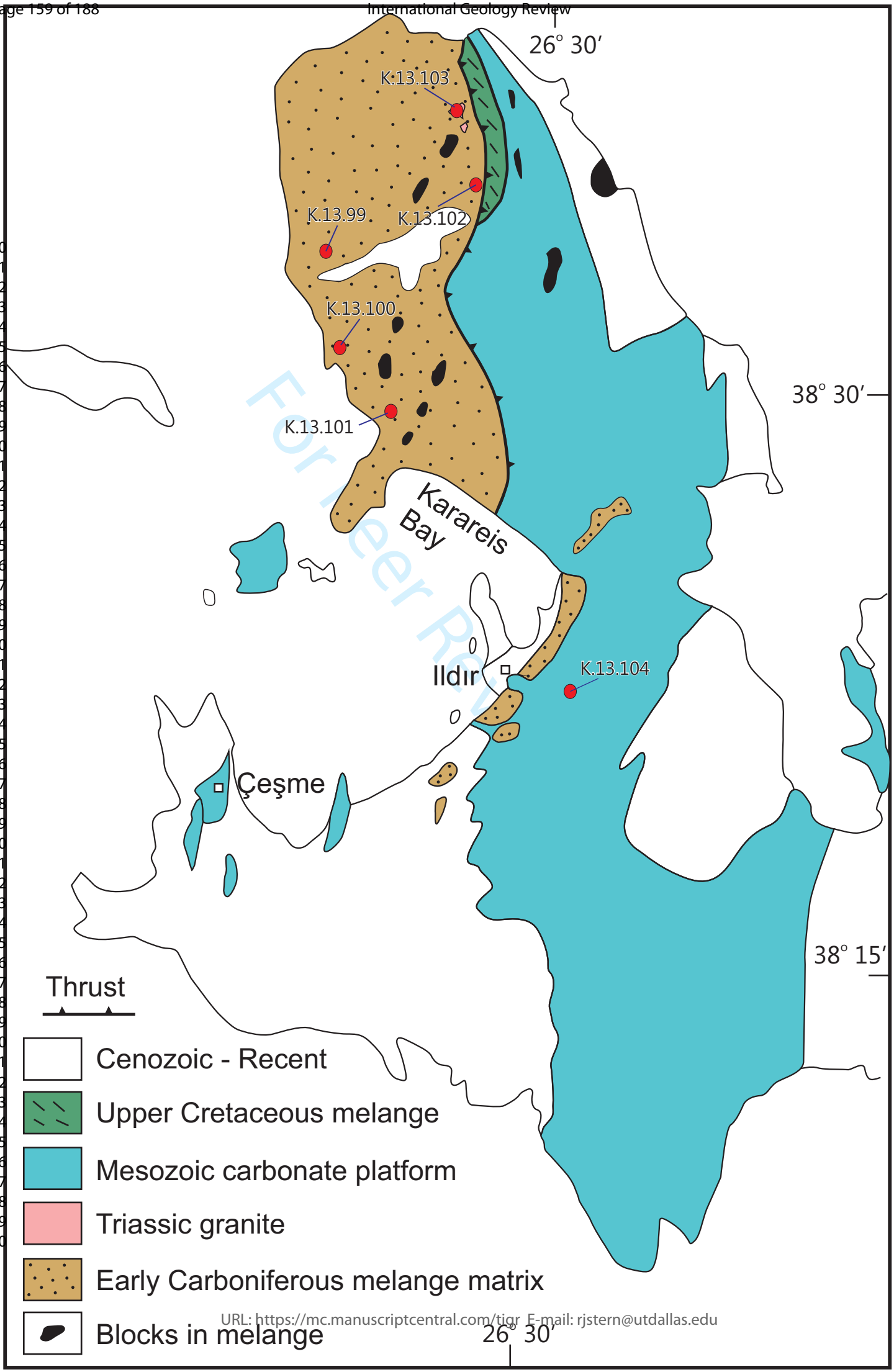


2115±7
759
760
1954±6
1961±11
742
743
2042±7
753
752
2020±14
2066±8
1889±8
673
777±6
718
398±3
781
2665±7
767
385±3
754
397±3
755
772
558±4
1948±9
768
1197±12
740
561±4
684
692
693
584±5
687
775±5
737
2183±6
392±3
735
364±3
711
2083±7
745
3396±5
701
2013±6
751
395±3
756
641±5
698
393±3
763
642±4
680
405±3
776
659±4
674
569±4
769
378±4
724
598±5
682
1254±18
689
395±3
679
629±5
712
630±4
723
579±4
719
398±3
766
716
388±3
380±3
681
392±3
728
779
492±4
1925±9
729
726
568±4
676
2645±5
2158±14
686
675
408±6
677
2733±7
720
513±4
K.13.102 (Karaburun Melange)
200 µm


1309
1975±6
1310
2015±18
310±3
1282
317±3
1283
587±6
1189
417±3
1247
353±3
1262
734±5
1244
1281
606±5
502±4
1230
1998±6
1224
1361±15
1213
658±5
1280
2502±6
1179
369±3
1188
558±4
1227
1291
603±5
357±3
1215
925±7
1290
2752±6
1284
1214
317±3
747±7
1257
617±6
1194
556±4
1199
2022±6
1297
980±8
1292
1816±14
1216
370±3
1249
1288
326±3
397±3
1293
1051±10
1222
2840±5
1285
645±5
1187
468±4
1307
2607±5
1218
315±3
1229
1943±16
1221
2094±6
1184
2595±5
1241
1989±6
1206
1287
1977±16
905±6
1211
301±2
1185
1178
1177
755±6
2604±7
760±6
1294
200 µm
K.13.104 (Güvercinlik Formation)

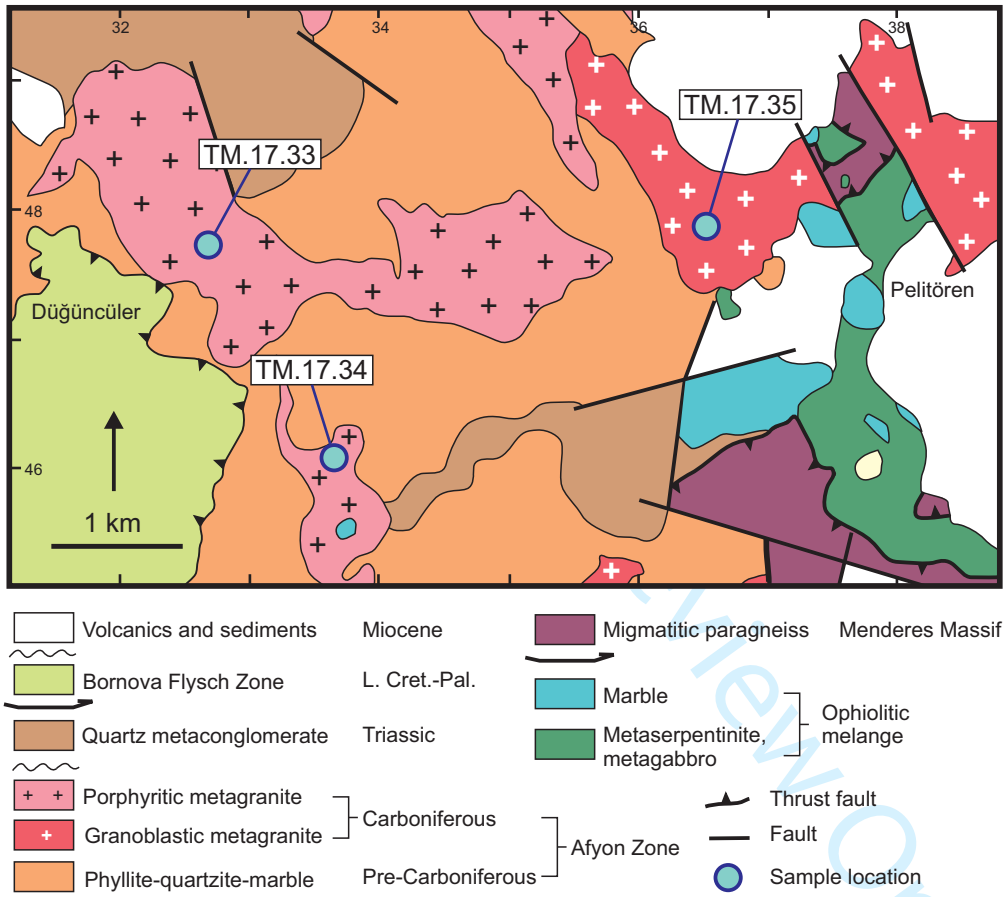

Formation	Sample No	GPS Coordinates	
		E	N
Köşkdere Formation	S3	705350	4206728
Konya Complex	K.13.75	448483	4223804
Karaburun Melange	K.12.102	455134	4273058
Kasımlar Formation	K.12.75	339360	4156502
	K.12.78	334109	4161226
Üzümdere Formation	K.13.77	393386	4109271
Güvercinlik Formation	K.12.104	459162	4109271
Meta-Granites	TM.17.33	632847	4347832
	TM.17.34	633784	4346330
	TM.17.35	636558	4347763

		LATE PALAEOZOIC								
		Köşkdere Formation S3			Konya Complex K.13.75			Karaburun Melange K.13.102		
Number of spots	U-Pb	141			112			111		
	Lu-Hf	0			97			101		
No of concordant results		112			98			97		
Age range (Ma)		2701-555			2637-443			3396-334		
Maximum age of deposition (Ma) (Youngest Graphical Peak)		558			505			384		
Prominent Populations (Ma)		720-555	850-740	1086-880	689-573	821-747	1037-945	409-364	659-550	2220-2013
% of whole data		38	15	13	31	20	12	31	21	13
Peak Ages (Ma)		587, 646	796	980, 1045	622	799	963, 1008	393	567	2175
εHf (t)					-24.2 to +9.8	-22.3 to +11.4	-25 to +11.6	-8.1 to +5.4	-23.1 to +9.9	-14.1 to +8.7
% of zircons with positive εHf(t)					34	65	38	61	50	67
Small clusters (Ga)		2..7-2.4	2.0-1.9	1.8-1.6	2.55-2.45	0.92-0.87	0.55-0.50	1.97-1.89	2.67-2.64	1.29-1.20
Peak Ages (Ga)		2.6, 2.5	1.94	1.76	2.52	0.89	0.55	1.91, 1.94	2.64	1.26
εHf (t)					-6.8 to +6.2	-25.0 to +11.6	+2.9 to +5.1	-7.4 to +8.7	-6.8 to +1.3	+3.9 to +6.1

Age		LATE TRIASSIC											
Formation Name / Sample Number		Üzümdere Formation K.13.77			Kasımlar Formation						Güvercinlik Formation K.13.104		
					K.12.75			K.12.78					
Number of spots	U-Pb	101			111			111			113		
	Lu-Hf	90			98			93			79		
No of concordant results		90			108			93			80		
Age range (Ma)		3241-267			2727-281			2884-239			2840-301		
Maximum age of deposition (Ma)		272			283			246			304		
Prominent Populations (Ma)		687-561	544-497	1029-876	667-592	1077-923	880-779	1020-889	816-673	648-603	333-301	2094-1943	629-585
Peak Ages (Ma)		611	530	980	632, 598	1059, 936	813	973, 915	683	635	314	1985	591
eHf (t)		-15.7 to +9.9	-11.2 to +5.8	-7.6 to +12.3	-22.6 to +8.9	-22.5 to +9.5	-9.9 to +11.4	-19.5 to +11.5	-14.3 to +10.5	-22.8 to +5.3	-10.0 to +1.2	-14.6 to +5.1	-15.2 to +11.2
% of zircons with positive εHf(t)		63	10	85	45	56	56	35	63	43	7	13	31
Small clusters (Ga)		2.01-1.74	2.54-2.49	0.48-0.45	2.72-2.46	2.03-1.97	0.48-0.45	0.58-0.53	1.95-1.87	2.53-2.44	0.93-0.9	0.76-0.73	0.50-0.46
Peak Ages (Ga)		1.79, 1,9, 2.0	2.51	0.45	2.66, 2.47	1.99	0.45	0.55	1.89	2.49	0.92	0.75	0.48
eHf (t)		**-15.1 to +2.0**	+0.7 to +4.1	-5.5 to -5.2	-11.9 to +6.6	-11.7 to +7.1	-20.8 to -2.5	-22.8 to +4.0	-11.2 to +2.1	-10.2 to +4.4	-17.9 to -0.9	-2.6 to +9.6	-12.3 to -0.7

S3 Koşkdere Formation

grain		$^{207}Pb^{a}$ (cps)	U^{b} (ppm)	Pb^{b} (ppm)	$\frac{Th^{b}}{U}$	$^{206}Pbc^{c}$ (%)	$\frac{^{206}Pb^{d}}{^{238}U}$	±2σ (%)	$\frac{^{207}Pb^{d}}{^{235}U}$	±2σ (%)	$\frac{^{207}Pb^{d}}{^{206}Pb}$	±2σ (%)	rho^{e}	$\frac{^{206}Pb}{^{238}U}$	±2σ (Ma)	$\frac{^{207}Pb}{^{235}U}$	±2σ (Ma)	$\frac{^{207}Pb}{^{206}Pb}$	±2σ (Ma)	conc. (%)
A01	S3-9d1	1681	48	8	0.22	0.3	0.1537	2.3	1.481	3.7	0.06991	2.9	0.63	922	20	923	23	926	59	100
A02	S3-9d2	1370	34	6	0.18	0.2	0.1595	2.3	1.571	4.1	0.07146	3.5	0.55	954	20	959	26	971	71	98
A03	S3-9d3	390	21	2	0.62	0.0	0.08932	3.8	0.7846	7.2	0.06371	6	0.52	552	20	588	33	732	130	75
A04	S3-9a1	875	25	4	0.14	0.4	0.1511	2.7	1.422	4.2	0.06825	3.2	0.64	907	23	898	25	876	66	104
A05	S3-9a2	1685	43	7	0.17	0.2	0.1538	2.2	1.458	4.0	0.06876	3.3	0.56	922	19	913	24	891	68	103
A06	S3-9b	81	4.7	0.5	0.00	2.5	0.1237	6.4	0.949	12.4	0.05564	11	0.52	752	46	678	63	438	236	172
A07	S3-9c1	1946	85	10	0.20	0.3	0.1069	2.1	0.9064	3.8	0.06147	3.1	0.56	655	13	655	18	656	67	100
A08	S3-9c2	10904	638	57	0.03	0.2	0.09546	2.0	0.7722	3.1	0.05867	2.4	0.65	588	11	581	14	555	52	106
A09	S3-11d1	1541	39	8	0.40	b.d.	0.1753	2.5	1.808	3.2	0.07480	2.1	0.77	1041	24	1048	21	1063	41	98
A10	S3-11d2	3131	116	23	3.07	0.0	0.1392	3.4	1.500	4.0	0.07817	2.1	0.85	840	27	930	25	1151	42	73
A11	S3-11c3	341	16	2	0.00	0.5	0.1098	3.7	0.8563	7.3	0.05657	6.3	0.51	671	24	628	35	475	140	141
A12	S3-11c1	3868	109	17	0.05	0.0	0.1587	2.7	1.531	3.6	0.06995	2.4	0.74	950	24	943	23	927	50	102
A13	S3-11c2	7952	232	47	0.42	0.0	0.1617	2.4	1.590	2.9	0.0713	1.7	0.82	966	21	966	18	966	34	100
A14	S3-11a1	9405	52	23	0.26	0.1	0.3714	2.4	7.062	2.9	0.1379	1.7	0.81	2036	41	2119	26	2201	29	92
A15	S3-11a2	23069	585	63	0.01	0.1	0.1139	4.5	1.298	5.1	0.08260	2.4	0.88	696	30	845	30	1260	48	55
A16	S3-13c1	819	52	6	0.37	b.d.	0.09682	2.3	0.797	6.7	0.05970	6.3	0.34	596	13	595	31	593	137	101
A17	S3-13c2	3139	183	20	0.16	0.4	0.1065	1.8	0.8461	3.1	0.05764	2.6	0.56	652	11	622	15	516	57	126
A18	S3-13c3	1057	67	8	0.31	b.d.	0.09760	2.3	0.8062	3.8	0.05991	3.0	0.61	600	13	600	17	600	65	100
A19	S3-13b2	4552	129	28	0.50	0.0	0.1670	1.9	1.664	2.8	0.07227	2.1	0.67	995	17	995	18	993	43	100
A20	S3-13b1	3462	101	19	0.43	0.1	0.1548	2.1	1.533	3.8	0.07182	3.2	0.55	928	18	944	24	981	64	95
A21	S3-13a2	1705	69	9	0.13	b.d.	0.1260	2.9	1.119	3.8	0.06441	2.5	0.75	765	21	763	21	755	53	101
A22	S3-13a1	3435	128	17	0.13	0.0	0.13	1.9	1.174	2.7	0.06551	2.0	0.68	788	14	789	15	791	42	100
A23	S3-15d1	2561	75	13	0.25	0.0	0.1554	2.4	1.531	3.5	0.07145	2.6	0.67	931	21	943	22	970	53	96
A25	S3-15c1	2309	109	13	0.16	b.d.	0.1108	2.2	0.9585	4.1	0.06274	3.4	0.53	677	14	683	20	700	73	97
A26	S3-15c3	2235	109	12	0.11	0.1	0.1110	2.4	0.9600	3.9	0.06271	3.1	0.61	679	15	683	19	698	65	97
A27	S3-15c2	3705	205	25	0.15	b.d.	0.1174	2.6	1.031	3.6	0.06368	2.5	0.72	716	17	719	19	731	53	98
A28	S3-15b2	4593	347	30	0.06	0.2	0.08989	2.3	0.7253	3.8	0.05852	3.0	0.60	555	12	554	16	549	66	101
A29	S3-15b1	13836	226	45	0.02	0.0	0.2052	2.9	3.109	3.5	0.1099	1.9	0.83	1203	32	1435	27	1797	35	67
A30	S3-15a3	91	9	2	1.29	b.d.	0.1049	5.4	0.8769	7.8	0.06064	5.6	0.69	643	33	639	38	626	121	103
A31	S3-15a1	2232	134	15	0.22	0.1	0.1029	2.4	0.8683	3.9	0.06119	3.0	0.62	631	14	635	18	646	65	98
A32	S3-15a2	909	57	6	0.18	0.4	0.1064	2.4	0.8984	6.7	0.06122	6.3	0.35	652	15	651	33	647	135	101
A33	S3-17a1	2642	94	17	0.22	0.1	0.1608	2.5	1.598	3.8	0.07207	2.8	0.66	961	22	969	24	988	57	97
A34	S3-17a2	3549	111	21	0.22	0.0	0.1764	3.4	1.817	4.2	0.07472	2.5	0.80	1047	33	1052	28	1061	51	99
A35	S3-17a3	3584	139	26	0.25	0.0	0.1676	2.6	1.638	3.9	0.07089	2.9	0.67	999	24	985	25	954	59	105
A36	S3-17b1	56096	284	163	0.19	0.5	0.4953	2.0	11.68	2.5	0.1711	1.5	0.81	2594	43	2579	24	2568	25	101
A37	S3-17b2	21914	99	57	0.50	0.8	0.4053	3.8	9.362	4.4	0.1675	2.3	0.86	2193	70	2374	41	2533	38	87
A38	S3-17c1	721	21	4	0.38	0.5	0.1667	3.0	1.666	3.9	0.07245	2.4	0.78	994	28	996	25	999	49	100
A39	S3-17c2	1300	40	10	0.53	b.d.	0.1785	2.3	1.826	3.7	0.07418	2.9	0.62	1059	23	1055	25	1046	59	101
A41	S3-19a1	8236	331	55	0.31	0.0	0.1541	2.4	1.580	3.2	0.07437	2.1	0.76	924	21	962	20	1052	42	88
A42	S3-19a2	10916	459	74	0.14	0.0	0.1652	5.4	1.665	5.6	0.0731	1.5	0.96	985	49	995	36	1017	30	97
A43	S3-19b1	3777	241	28	0.15	b.d.	0.1123	3.4	1.011	4.9	0.06529	3.5	0.70	686	22	709	25	784	73	88
A44	S3-19b2	10693	546	89	0.17	0.0	0.1661	1.8	1.691	2.7	0.07388	2.0	0.68	990	17	1005	17	1038	40	95
A45	S3-19c2	4803	332	36	0.01	0.0	0.1162	2.0	0.9965	3.2	0.06219	2.4	0.63	709	13	702	16	681	52	104
A46	S3-19c1	1362	36	9	0.89	0.1	0.2165	3.1	2.955	8.5	0.09903	7.9	0.36	1263	35	1396	66	1606	147	79
A47	S3-19d2	17318	245	86	0.20	b.d.	0.3193	2.4	4.784	2.8	0.1087	1.4	0.86	1786	38	1782	24	1777	26	101
A48	S3-19d1	17389	281	90	0.14	0.4	0.3001	2.9	4.488	3.6	0.1085	2.1	0.81	1692	43	1729	30	1774	38	95
A49	S3-21a1	3267	305	27	0.00	0.0	0.09603	1.7	0.7805	3.3	0.05894	2.8	0.52	591	10	586	15	565	61	105
A50	S3-21a3	2840	243	24	0.00	0.0	0.1091	2.0	0.9237	3.6	0.06142	3.0	0.54	667	12	664	18	654	65	102
A51	S3-21a2	2767	242	22	0.00	0.0	0.09883	2.6	0.8092	3.7	0.05938	2.7	0.70	608	15	602	17	581	58	105
A52	S3-21b2	1632	137	13	0.13	0.1	0.09610	2.3	0.8248	4.6	0.06225	4.0	0.50	592	13	611	21	683	85	87
A53	S3-21b1	1947	173	16	0.12	0.4	0.09374	2.3	0.7826	5.3	0.06055	4.7	0.44	578	13	587	24	623	101	93
A54	S3-21b3	844	91	9	0.10	b.d.	0.09563	2.9	0.7726	7.6	0.05860	7.0	0.39	589	17	581	34	552	152	107
A55	S3-21b4	1763	185	17	0.12	0.1	0.09003	2.3	0.7368	4.1	0.05935	3.4	0.55	556	12	561	18	580	75	96
B01	S3-21d1	4920	100	18	0.24	0.0	0.1597	2.7	1.580	4.0	0.07174	2.9	0.69	955	24	962	25	978	59	98
B02	S3-21d2	3855	140	14	0.04	0.0	0.1049	2.1	0.8973	3.5	0.06202	2.8	0.61	643	13	650	17	675	59	95
B03	S3-21c1	702	4	2	0.38	0.7	0.3427	3.3	5.694	4.2	0.1205	2.5	0.80	1900	55	1930	37	1963	45	97
B04	S3-21c2	1123	7	3	0.44	0.2	0.3309	3.5	5.434	4.0	0.1191	2.0	0.87	1843	56	1890	35	1943	36	95
B05	S3-23b2	6631	202	30	0.54	0.2	0.1178	2.2	1.129	3.3	0.06947	2.4	0.67	718	15	767	18	913	50	79
B06	S3-23b1	7100	197	33	0.50	0.1	0.1348	2.3	1.302	3.3	0.07006	2.4	0.68	815	17	847	19	930	50	88
B07	S3-23b3	1517	56	6	0.15	b.d.	0.1045	4.1	0.8742	5.9	0.06068	4.3	0.69	641	25	638	28	628	92	102
B09	S3-23c	3829	93	16	0.26	0.0	0.154	2.2	1.48	2.8	0.06967	1.8	0.79	923	19	922	17	919	36	101
B10	S3-23d2	5682	285	27	0.01	0.1	0.1029	1.9	0.8570	2.9	0.06040	2.2	0.67	631	12	628	14	618	47	102
B11	S3-23d1	1756	52	8	0.21	b.d.	0.1368	2.7	1.332	4.4	0.07061	3.5	0.61	827	21	860	26	946	71	87
B12	S3-25c1	31713	89	55	0.32	b.d.	0.5036	1.7	12.47	3.0	0.1795	2.5	0.57	2629	38	2640	29	2649	41	99
B13	S3-25c2	30589	88	52	0.36	0.1	0.4742	2.1	11.72	2.4	0.1792	1.1	0.90	2502	44	2582	23	2645	18	95
B14	S3-25c3	15316	47	28	0.22	b.d.	0.5030	2.1	12.26	2.4	0.1767	1.2	0.86	2627	45	2624	23	2622	20	100
B15	S3-25d4	2027	58	7	0.01	0.1	0.1326	2.3	1.198	4.1	0.06552	3.3	0.58	803	18	800	23	791	70	102
B16	S3-25d2	2252	58	8	0.01	0.0	0.1519	2.7	1.483	3.9	0.07079	2.9	0.69	912	23	923	24	951	58	96
B17	S3-25d1	1578	46	6	0.04	0.1	0.1343	2.7	1.226	5.0	0.06621	4.2	0.53	812	20	812	28	813	88	100
B18	S3-25a1	2435	79	13	0.37	0.0	0.1319	3.5	1.205	4.5	0.06629	2.9	0.77	799	26	803	25	816	60	98
B19	S3-25a2	3670	124	17	0.22	b.d.	0.1261	2.8	1.141	3.9	0.06562	2.7	0.73	766	20	773	21	794	56	96
B20	S3-25b1	5546	21	16	0.85	b.d.	0.4790	1.8	11.07	2.7	0.1675	2.1	0.64	2523	37	2529	26	2533	35	100

B21	S3-25b2	4969	18	12	0.58	b.d.	0.4624	2.9	10.59	3.6	0.1661	2.1	0.81	2450	60	2488	34	2519	36	97
B22	S3-27c	31440	257	85	0.15	0.4	0.3110	1.9	4.637	2.3	0.1081	1.3	0.83	1746	29	1756	19	1768	23	99
B23	S3-27d2	1517	50	7	0.11	0.2	0.1342	2.1	1.203	4.5	0.06505	4.0	0.46	812	16	802	26	776	85	105
B24	S3-27a3	4965	167	18	0.05	0.1	0.1124	2.7	1.027	3.2	0.06628	1.7	0.85	686	18	717	17	815	35	84
B25	S3-27a1	6573	166	30	0.11	0.0	0.1775	2.0	1.806	2.8	0.07382	2.0	0.72	1053	20	1048	19	1036	40	102
B26	S3-27b2	2084	94	9	0.14	0.1	0.09411	2.9	0.7645	4.7	0.05892	3.7	0.61	580	16	577	21	564	81	103
B27	S3-27b1	1315	61	11	1.01	0.0	0.1045	3.0	0.9182	4.9	0.06372	3.8	0.61	641	18	661	24	732	81	87
B28	S3-29d	50466	177	100	0.12	0.2	0.5143	1.8	12.27	2.2	0.1730	1.2	0.82	2675	40	2625	21	2587	21	103
B29	S3-29c	6793	26	15	0.39	b.d.	0.4618	2.7	10.36	3.4	0.1627	2.0	0.80	2447	55	2467	32	2484	34	99
B30	S3-29b	5320	105	17	0.32	0.0	0.1594	2.1	1.557	2.9	0.07085	1.9	0.74	953	19	953	18	953	39	100
B31	S3-29a	7215	167	38	0.46	0.1	0.1703	3.6	1.747	3.9	0.0744	1.5	0.92	1014	34	1026	25	1052	31	96
B32	S3-31a	537	24	3	0.00	b.d.	0.1281	3.9	1.149	8.0	0.06506	7.0	0.48	777	29	777	45	776	148	100
B33	S3-31b	1736	54	8	0.22	0.3	0.1415	2.1	1.353	4.7	0.06937	4.3	0.44	853	16	869	28	910	88	94
B34	S3-31c	11236	590	52	0.14	0.0	0.09311	2.6	0.8272	3.7	0.06443	2.6	0.72	574	14	612	17	756	54	76
B35	S3-31d	5860	1810	158	0.02	0.0	0.0941	2.3	0.7639	3.0	0.05888	1.9	0.78	580	13	576	13	563	40	103
B36	S3-33d1	520	172	22	0.65	b.d.	0.0912	2.8	0.7248	6.7	0.05764	6.1	0.41	563	15	554	29	516	135	109
B37	S3-33d2	1070	292	29	0.20	b.d.	0.09161	3.4	0.7596	6.3	0.06014	5.3	0.54	565	19	574	28	609	115	93
B38	S3-33c	1292	252	39	0.31	b.d.	0.1315	2.7	1.190	5.1	0.06561	4.2	0.54	796	21	796	28	794	89	100
B39	S3-33b1	3518	878	96	0.14	0.1	0.1088	2.1	0.9183	3.7	0.06119	3.0	0.57	666	13	661	18	646	65	103
B40	S3-33b3	2462	804	78	0.23	0.0	0.09869	2.8	0.9226	4.3	0.06780	3.3	0.64	607	16	664	21	862	69	70
B41	S3-33a1	4468	1725	174	0.17	0.0	0.09539	2.4	0.7913	3.6	0.06017	2.7	0.66	587	13	592	16	610	58	96
B44	S3-35b1	969	292	40	0.12	b.d.	0.1327	2.8	1.194	6.1	0.06524	5.4	0.46	803	21	798	34	782	114	103
B45	S3-35c1	1695	786	124	0.75	0.0	0.09774	3.1	0.8167	4.5	0.06060	3.3	0.68	601	18	606	21	625	72	96
B46	S3-35c2	1305	776	81	0.16	b.d.	0.1010	2.9	0.8544	5.2	0.06134	4.3	0.56	620	17	627	25	651	93	95
B47	S3-35d	1208	541	83	0.33	b.d.	0.1319	2.5	1.196	4.2	0.06576	3.4	0.59	799	19	799	24	799	71	100
B48	S3-37a1	1002	679	80	0.22	b.d.	0.1073	2.6	0.9243	5.5	0.06248	4.9	0.46	657	16	665	27	691	104	95
B49	S3-37a2	875	660	74	0.20	b.d.	0.1027	2.9	0.8627	5.5	0.0609	4.7	0.53	630	18	632	26	636	101	99
B50	S3-37b1	2815	2422	264	0.12	0.2	0.1071	2.0	0.8955	3.8	0.06062	3.2	0.54	656	13	649	18	626	69	105
B51	S3-37b2	1494	1830	179	0.13	0.1	0.09593	1.9	0.7740	4.4	0.05852	4.0	0.44	590	11	582	20	549	87	107
B52	S3-37c1	772	1047	115	0.16	0.3	0.1059	2.8	0.8806	6.3	0.0603	5.6	0.45	649	17	641	30	614	122	106
B53	S3-37d1	3443	7330	951	0.23	b.d.	0.1178	2.1	1.028	3.8	0.06327	3.2	0.55	718	14	718	20	717	68	100
B54	S3-37d2	3459	15992	1880	0.17	0.2	0.1129	2.8	0.9602	4.2	0.06166	3.1	0.67	690	18	683	21	662	67	104
B55	S3-39d	14969	#####	-61821	0.12	0.0	0.1652	3.3	1.689	3.6	0.07416	1.4	0.92	985	30	1004	23	1046	28	94
C01	S3-39c1	4072	254	25	0.09	0.2	0.09979	2.0	0.8233	3.2	0.05984	2.5	0.62	613	12	610	15	598	55	103
C02	S3-39c2	2126	103	10	0.11	0.1	0.09766	2.4	0.8014	4.0	0.05952	3.2	0.60	601	14	598	18	586	70	102
C03	S3-39b1	5289	278	26	0.00	0.0	0.1025	2.2	0.8591	3.6	0.06076	2.9	0.60	629	13	630	17	631	62	100
C04	S3-39b2	4392	175	18	0.00	0.1	0.111	1.7	0.9437	3.0	0.06166	2.5	0.56	678	11	675	15	663	54	102
C05	S3-39a1	17959	121	47	0.20	0.2	0.3422	2.0	5.52	2.3	0.1170	1.3	0.84	1897	33	1904	20	1911	23	99
C06	S3-41a1	7177	43	21	0.43	0.3	0.3835	1.9	6.606	2.7	0.1249	1.8	0.72	2093	35	2060	24	2028	33	103
C07	S3-41a2	32638	264	92	0.04	0.3	0.3494	1.8	5.766	2.4	0.1197	1.5	0.78	1932	31	1941	21	1952	26	99
C08	S3-41b	2355	58	12	0.19	1.0	0.1849	1.8	1.724	4.4	0.06762	4.1	0.41	1094	18	1018	29	857	84	128
C09	S3-41d1	1186	49	7	0.17	b.d.	0.1297	2.1	1.188	5.0	0.06640	4.5	0.43	786	16	795	28	819	94	96
C10	S3-41d2	829	29	4	0.13	0.5	0.1221	2.8	1.121	8.6	0.06656	8.1	0.33	743	20	763	47	824	169	90
C11	S3-41c1	4502	35	13	0.16	0.6	0.3347	2.7	5.511	4.2	0.1194	3.2	0.65	1861	45	1902	37	1948	58	96
C12	S3-43c1	15710	48	39	0.81	0.0	0.5071	1.7	12.46	1.9	0.1782	0.9	0.87	2644	37	2640	18	2636	16	100
C13	S3-43c2	3527	12	8	0.40	0.3	0.4973	2.3	12.71	3.6	0.1853	2.8	0.65	2602	50	2658	35	2701	45	96
C14	S3-43d	2132	55	10	0.24	0.0	0.1703	1.9	1.717	4.2	0.07312	3.8	0.45	1014	18	1015	28	1017	77	100
C15	S3-43a	1004	51	5	0.22	0.8	0.09723	2.4	0.6839	7.6	0.05101	7.2	0.31	598	14	529	32	241	165	248
C16	S3-43b	1660	65	9	0.32	0.0	0.1383	1.9	1.317	4.8	0.06909	4.5	0.38	835	15	853	28	901	92	93
C17	S3-45b	4411	105	21	0.30	0.0	0.1725	2.5	1.762	3.2	0.07407	2.0	0.78	1026	23	1032	21	1044	40	98
C18	S3-45a	12797	93	36	0.42	0.0	0.3305	2.2	6.299	2.7	0.1382	1.6	0.81	1841	35	2018	24	2205	28	83
C19	S3-45d	742	45	4	0.25	0.3	0.08176	2.7	0.7052	5.7	0.06256	5.0	0.48	507	13	542	24	693	106	73
C20	S3-45c	13997	380	66	0.19	0.0	0.1648	2.2	1.724	2.6	0.07588	1.5	0.82	983	20	1018	17	1092	30	90
C21	S3-47c	3849	175	19	0.14	0.1	0.1081	2.2	0.9191	3.2	0.06167	2.3	0.69	662	14	662	16	663	50	100
C22	S3-47d	1549	43	6	0.03	0.2	0.1464	2.7	1.440	5.4	0.07133	4.7	0.49	881	22	906	33	967	95	91
C23	S3-47a1	9831	520	47	0.05	0.2	0.09412	3.2	0.8665	4.5	0.06677	3.2	0.71	580	18	634	22	831	67	70
C24	S3-47a2	1354	86	8	0.30	0.1	0.07967	2.3	0.6582	4.5	0.05992	3.9	0.52	494	11	514	18	601	84	82
C25	S3-47b2	795	45	4	0.32	0.0	0.07957	3.0	0.6879	6.6	0.06270	5.9	0.45	494	14	532	28	698	126	71
C26	S3-49a	2590	149	17	0.30	0.0	0.1038	1.8	0.8731	4.3	0.06101	3.9	0.42	637	11	637	20	640	83	100
C28	S3-51a1	552	20	3	0.18	0.2	0.1324	2.6	1.204	5.7	0.06592	5.1	0.46	802	20	802	32	804	106	100
C29	S3-51a2	1582	51	8	0.38	0.0	0.1355	2.0	1.247	4.2	0.06677	3.7	0.48	819	16	822	24	831	77	99
C30	S3-51b	2377	116	12	0.64	0.0	0.08564	2.4	0.8366	4.6	0.07085	3.9	0.52	530	12	617	22	953	80	56
C31	S3-53a2	1095	56	5	0.08	0.4	0.09393	2.4	0.7846	6.5	0.06059	6.0	0.37	579	13	588	29	625	129	93
C32	S3-53a1	4609	55	15	0.41	0.2	0.2149	2.2	3.032	3.2	0.1023	2.4	0.67	1255	25	1416	25	1667	44	75
C34	S3-55a2	9463	117	33	0.08	0.5	0.2776	2.57	3.878	5.0	0.1013	4.3	0.51	1579	36	1609	41	1648	80	96
C35	S3-55b1	44568	177	84	0.03	b.d.	0.4623	1.6	10.39	2.3	0.1630	1.6	0.70	2450	33	2470	21	2487	28	98
C36	S3-55b2	10490	41	27	0.49	b.d.	0.4621	2.2	10.49	5.6	0.1646	5.2	0.39	2449	45	2479	53	2503	87	98
C37	S3-57b	1028	34	5	0.20	0.0	0.1464	2.1	1.507	5.1	0.07466	4.6	0.41	881	17	933	32	1059	94	83
C38	S3-57a1	5565	16	12	0.63	0.5	0.5169	1.78	12.53	3.6	0.1758	3.1	0.49	2686	39	2645	35	2614	52	103
Felix [g]		2686	53	5	1.02	0.22	0.08039	6.2	0.6371	6.5	0.05748	1.4	0.52	460	290	500	26	510	31	90
91500 [g]		6925	50	9	0.41	0.30	0.17937	1.7	1.8558	1.8	0.07504	1.6	0.57	1064	17	1065	12	1070	32	99

Spot size = 20 µm; depth of crater ~15µm. $^{206}Pb/^{238}U$ error is the quadratic additions of the within run precision (2 SE) and the external reproducibility (2 SD) of the reference zircon. $^{207}Pb/^{206}Pb$ error propagation (^{207}Pb signal dependent) following Gerdes & Zeh (2009). $^{207}Pb/^{235}U$ error is the quadratic addition of the $^{207}Pb/^{206}Pb$ and $^{206}Pb/^{238}U$ uncertainty.
[a]Within run background-corrected mean ^{207}Pb signal in cps (counts per second).

[b] U and Pb content and Th/U ratio were calculated relative to GJ-1 reference zircon.
[c] percentage of the common Pb on the ^{206}Pb. b.d. = below dectection limit.
[d] corrected for background, within-run Pb/U fractionation (in case of ^{206}Pb/^{238}U) and common Pb using Stacy and Kramers (1975) model Pb composition and subsequently normalised to GJ-1 (ID-TIMS value/measured value); ^{207}Pb/^{235}U calculated using ^{207}Pb/^{206}Pb/(^{238}U/^{206}Pb*1/137.88)
[e] rho is the ^{206}Pb/^{238}U/^{207}Pb/^{235}U error correlation coefficient.
[f] degree of concordance = ^{206}Pb/^{238}U age / ^{207}Pb/^{206}Pb age x 100
[g] Accuracy and reproducibilty was checked by repeated analyses (n = 10) of reference zircon Felix and 91500; data given as mean with 2 standard deviation uncertainties

Konya Complex grain		^{207}Pb[a] (cps)	U[b] (ppm)	Pb[b] (ppm)	Th[b]/U	^{206}Pbc[c] (%)	^{206}Pb[d]/^{238}U	±2σ (%)	^{207}Pb[d]/^{235}U	±2σ (%)	^{207}Pb[d]/^{206}Pb	±2σ (%)	rho[e]	^{206}Pb/^{238}U	±2σ (Ma)	^{207}Pb/^{235}U	±2σ (Ma)	^{207}Pb/^{206}Pb	±2σ (Ma)	conc. (%)
A06	K.13.75	8231	238	26.1	0.91	0.0	0.09568	1.6	0.7898	2.1	0.05987	1.4	0.76	589	9	591	9	599	29	98
A07		1524	43	5.7	1.55	0.3	0.1048	2	0.8892	4.6	0.06152	4.2	0.43	643	12	646	22	657	89	98
A08		1827	53	7.3	2.20	b.d.	0.09735	1.8	0.8176	4.1	0.06091	3.7	0.44	599	10	607	19	636	79	94
A09		4188	93	14.4	1.34	0.0	0.1274	1.7	1.145	3	0.06515	2.5	0.55	773	12	775	16	779	52	99
A10		12376	176	33.8	0.96	0.1	0.1684	1.4	1.698	2	0.07313	1.4	0.72	1004	13	1008	13	1017	28	99
A11		4717	102	16.3	1.34	0.0	0.1317	1.6	1.207	2.6	0.06651	2.1	0.61	797	12	804	15	822	43	97
A12		2341	55	6.9	0.60	b.d.	0.1181	1.7	1.055	4.2	0.06482	3.9	0.40	719	11	731	22	769	81	94
A13		5397	103	14.4	0.62	0.4	0.1313	1.6	1.192	2.4	0.06583	1.8	0.65	795	12	797	13	801	39	99
A14		3510	17	6.6	1.11	b.d.	0.3155	1.8	4.741	2.5	0.109	1.7	0.72	1768	28	1775	21	1782	31	99
A15		12937	206	31.0	0.38	0.1	0.1498	1.6	1.490	1.9	0.07212	1.1	0.82	900	13	926	12	989	23	91
A16		14476	472	39.2	0.88	1.5	0.07117	2	0.5534	4.3	0.0564	3.8	0.47	443	9	447	16	468	84	95
A17		5692	99	16.1	0.78	b.d.	0.1475	1.5	1.409	2	0.0693	1.3	0.77	887	13	893	12	908	26	98
A18		3394	93	9.2	0.46	0.6	0.09614	1.6	0.7773	3.8	0.05864	3.4	0.43	592	9	584	17	554	74	107
A19		33201	326	41.9	0.40	15	0.09873	1.9	0.7976	6.7	0.05859	6.4	0.28	607	11	595	31	552	140	110
A20		1584	33	5.8	1.72	0.2	0.1273	1.8	1.164	3.5	0.06632	3	0.52	772	13	784	19	817	63	95
A21		5604	202	17.5	0.59	0.6	0.08141	1.5	0.6438	2.7	0.05736	2.2	0.56	505	7	505	11	505	49	100
A22		12372	118	19.7	1.59	10	0.1128	2.2	0.9638	9.5	0.06194	9.2	0.23	689	14	685	48	672	197	103
A23		5039	93	14.5	1.00	0.1	0.1328	1.6	1.205	2.4	0.06576	1.8	0.65	804	12	803	14	799	38	101
A24		25572	401	76.9	1.04	0.0	0.1692	1.4	1.687	1.7	0.07231	0.87	0.86	1008	13	1004	11	995	18	101
A25		7781	203	28.6	1.87	0.7	0.0994	1.9	0.8246	4.1	0.06017	3.6	0.46	611	11	611	19	610	78	100
A26		103908	464	162.0	0.16	2.5	0.3424	1.9	5.847	2.7	0.1239	1.9	0.70	1898	31	1953	24	2013	34	94
A27		14958	264	42.4	1.12	0.5	0.1355	1.3	1.215	2.8	0.06503	2.4	0.48	819	10	807	16	775	51	106
A28		8926	281	24.3	0.04	0.8	0.09292	1.8	0.7559	2.5	0.059	1.8	0.70	573	10	572	11	567	39	101
A29		3872	127	21.2	0.66	b.d.	0.1528	1.7	1.524	2.5	0.07232	1.8	0.68	917	14	940	15	995	37	92
A30		4167	232	26.6	0.82	0.0	0.1035	1.7	0.8668	2.7	0.06072	2	0.65	635	10	634	13	629	44	101
A31		2067	154	11.5	0.26	0.6	0.07548	1.6	0.5943	2.9	0.05711	2.3	0.57	469	7	474	11	496	52	95
A39		7683	217	26.0	1.23	0.4	0.1005	1.5	0.8348	3.2	0.06026	2.9	0.46	617	9	616	15	613	62	101
A40		17244	327	45.7	0.55	0.2	0.1333	1.4	1.221	1.9	0.06645	1.3	0.74	806	10	810	10	820	26	98
A41		3534	69	10.2	0.76	0.1	0.1342	1.5	1.224	3.1	0.06612	2.6	0.50	812	12	812	17	810	55	100
A42		54479	174	74.8	0.65	0.1	0.3836	1.5	7.341	2	0.1388	1.3	0.74	2093	26	2154	18	2212	23	95
A43		7100	194	24.7	1.45	0.2	0.1027	1.5	0.8694	2.4	0.06138	1.8	0.64	630	9	635	11	653	39	97
A44		47435	97	70.9	2.58	0.0	0.4882	1.6	11.22	1.8	0.1667	0.85	0.88	2563	34	2541	17	2524	14	102
A45		3777	109	12.4	1.07	0.3	0.09775	1.6	0.8123	2.7	0.06027	2.1	0.61	601	9	604	12	613	46	98
A46		5392	76	16.7	1.55	0.3	0.1741	1.6	1.772	2.6	0.07383	2.1	0.62	1035	16	1035	17	1037	42	100
A47		7127	203	34.0	1.15	0.3	0.1523	1.4	1.483	3.1	0.07062	2.7	0.46	914	12	924	19	947	56	97
A48		5678	100	15.1	0.48	0.2	0.1458	1.5	1.350	2.6	0.06712	2.1	0.57	877	12	867	15	842	44	104
A49		38366	178	62.1	0.45	0.0	0.3294	1.4	5.350	1.7	0.1178	0.82	0.87	1835	23	1877	14	1923	15	95
A50		12972	356	48.3	1.95	0.6	0.09938	1.4	0.8357	3	0.06099	2.7	0.47	611	8	617	14	639	58	96
A51		13045	210	37.7	1.16	0.5	0.1511	1.6	1.439	2.5	0.06907	1.9	0.65	907	14	905	15	901	39	101
A52		16319	391	49.3	0.25	b.d.	0.1299	1.5	1.171	1.9	0.06534	1.2	0.78	787	11	787	10	785	25	100
A55		77218	330	123.6	0.62	0.2	0.345	1.4	5.752	1.6	0.1209	0.7	0.90	1911	24	1939	14	1970	13	97
A56		14474	356	44.2	1.29	1.0	0.09661	1.8	0.7851	3.6	0.05894	3.1	0.51	595	10	588	16	565	67	105
A57		7357	179	24.7	1.50	0.8	0.1101	1.4	0.9425	2.6	0.06207	2.2	0.53	674	9	674	13	676	48	100
A58		34207	85	47.6	1.31	b.d.	0.4449	1.4	10.10	1.8	0.1647	1.2	0.78	2372	28	2444	17	2504	20	95
A59		5307	136	15.5	0.71	0.2	0.1036	1.4	0.852	2.5	0.05964	2	0.58	636	9	626	12	590	44	108
A60		8239	168	24.0	0.73	b.d.	0.1307	1.5	1.204	2	0.06678	1.3	0.77	792	11	802	11	831	26	95
A61		7107	138	23.5	1.53	b.d.	0.1349	1.8	1.229	2.2	0.06605	1.4	0.80	816	14	814	13	808	28	101
A63		8685	231	26.8	1.06	3.0	0.1011	1.5	0.8545	5.9	0.06133	5.7	0.26	621	9	627	28	651	122	95
A64		14891	205	40.6	1.01	0.2	0.1713	1.6	1.706	2.2	0.07222	1.5	0.73	1019	15	1011	14	992	31	103
A65		10458	151	24.8	1.01	3.1	0.1352	1.4	1.231	3.6	0.06602	3.3	0.39	818	11	815	20	807	69	101
A66		7883	79	11.1	0.50	10.2	0.1109	1.9	1.054	8.3	0.06897	8	0.23	678	12	731	44	898	166	76
A72		6192	199	24.0	1.46	0.2	0.09411	1.7	0.7591	2.4	0.0585	1.6	0.73	580	10	573	10	549	36	106
A73		7339	108	19.0	1.15	3.0	0.1465	1.6	1.386	4.9	0.0686	4.7	0.32	881	13	883	30	887	97	99
A74		11451	215	39.6	1.68	0.1	0.1443	1.4	1.345	2.1	0.06762	1.5	0.68	869	12	865	12	857	32	101
A75		10934	215	40.6	2.09	0.1	0.1392	1.4	1.283	2.1	0.06684	1.6	0.66	840	11	838	12	833	33	101
A76		8309	241	28.1	0.23	b.d.	0.1191	1.4	1.052	2	0.06402	1.5	0.69	726	10	730	11	742	31	98
A77		71091	541	214.6	0.49	3.9	0.3264	12	6.625	13	0.1472	3.5	0.96	1821	197	2063	119	2313	60	79
A79		17263	425	46.5	0.39	0.2	0.1089	1.4	0.9394	1.9	0.06257	1.3	0.74	666	9	673	9	694	27	96
A80		4684	107	12.7	0.21	0.3	0.1228	1.6	1.086	2.7	0.06414	2.1	0.61	747	11	747	14	746	44	100
A81		27670	140	47.8	0.80	0.1	0.3015	2.5	4.492	2.8	0.1081	1.2	0.90	1699	38	1729	23	1767	22	96
A83		1826	40	5.5	0.84	0.9	0.1239	1.9	1.101	2.9	0.06443	2.2	0.66	753	14	754	15	756	46	100
A85		20552	1284	104.0	0.08	0.2	0.08644	1.5	0.715	2.2	0.05999	1.5	0.69	534	8	548	9	603	34	89
A86		3912	123	10.9	0.37	0.4	0.08687	1.9	0.6966	2.4	0.05816	1.5	0.78	537	10	537	10	536	33	100
A87		147879	421	168.3	0.32	0.1	0.3752	1.5	8.081	1.7	0.1562	0.82	0.87	2054	26	2240	15	2415	14	85
A88		10711	52	22.3	1.58	0.7	0.3208	1.7	5.100	2.9	0.1153	2.3	0.61	1794	27	1836	24	1885	41	95
A89		80061	340	165.5	2.00	0.3	0.3532	1.5	5.912	1.9	0.1214	1	0.83	1950	26	1963	16	1977	19	99
A90		18945	290	53.2	0.97	0.0	0.1621	1.5	1.686	2	0.07541	1.4	0.72	969	13	1003	13	1079	28	90
A091		5778	116	19.3	1.43	0.1	0.1332	1.6	1.212	2.2	0.06597	1.6	0.71	806	12	806	13	805	33	100
A92		49555	110	62.0	0.84	b.d.	0.4773	1.4	11.02	1.6	0.1675	0.78	0.87	2516	29	2525	15	2533	13	99
A93		11045	314	34.1	0.62	0.1	0.1023	1.6	0.8539	1.9	0.06053	1.1	0.83	628	10	627	9	623	23	101

A94	22550	46	25.3	0.89	0.1	0.4569	1.5	11.36	1.8	0.1803	1	0.84	2426	31	2553	17	2655	17	91
A95	8243	175	24.3	0.71	0.1	0.1295	1.4	1.155	2.2	0.06469	1.6	0.65	785	10	780	12	764	35	103
A96	123168	301	156.8	0.50	b.d.	0.4706	1.3	10.40	1.5	0.1603	0.61	0.91	2486	27	2471	14	2459	10	101
A97	64270	149	86.5	0.96	0.0	0.4834	1.5	10.85	1.6	0.1628	0.64	0.92	2542	31	2510	15	2485	11	102
A98	2354	33	6.4	1.08	0.6	0.1634	1.7	1.604	3.1	0.0712	2.5	0.57	975	16	972	19	963	52	101
A100	3564	74	9.8	0.40	0.2	0.1312	1.8	1.195	3	0.06608	2.4	0.60	795	14	798	17	809	50	98
A101	720	21	2.3	0.86	0.0	0.09621	1.9	0.8152	6.4	0.06145	6.1	0.30	592	11	605	30	655	131	90
A107	7831	42	17.7	2.03	0.1	0.2967	1.7	4.528	2.4	0.1107	1.8	0.68	1675	25	1736	21	1811	32	93
A108	3644	102	9.9	0.10	0.1	0.1026	1.5	0.8691	3	0.06144	2.5	0.51	630	9	635	14	655	55	96
A109	10034	284	31.7	0.76	0.3	0.1017	1.6	0.8436	2.4	0.06015	1.8	0.65	624	9	621	11	609	40	103
A110	13694	362	49.0	1.96	0.4	0.1013	1.6	0.8478	2.4	0.06067	1.8	0.65	622	9	623	11	628	40	99
A111	4624	124	13.8	0.50	0.3	0.1071	1.4	0.888	2.6	0.06011	2.2	0.55	656	9	645	13	607	48	108
A112	9023	251	26.2	0.55	0.2	0.09977	1.6	0.8363	2.2	0.06079	1.5	0.72	613	9	617	10	632	33	97
A113	41985	84	52.4	1.04	0.1	0.5081	1.6	12.49	1.8	0.1783	0.79	0.90	2648	35	2642	17	2637	13	100
A114	6419	174	21.0	0.96	0.2	0.1061	1.4	0.8962	2.3	0.06126	1.9	0.60	650	9	650	11	648	40	100
A115	3305	61	12.2	1.69	b.d.	0.1578	1.7	1.518	2.8	0.06976	2.2	0.61	945	15	938	17	921	46	103
A116	9304	196	32.9	1.55	0.1	0.1336	1.5	1.206	2.3	0.06547	1.7	0.67	809	12	803	13	789	36	102
A117	7245	219	27.2	1.61	0.3	0.09493	1.5	0.7769	1.9	0.05935	1.2	0.79	585	8	584	8	580	26	101
A118	3975	166	24.7	0.64	0.5	0.1359	1.8	1.24	4.3	0.06616	3.9	0.42	821	14	819	24	811	81	101
A119	1702	53	7.4	2.32	0.6	0.09443	2	0.7518	2.9	0.05775	2.1	0.69	582	11	569	13	520	47	112
A120	9858	140	23.6	0.55	b.d.	0.1603	1.5	1.617	2.2	0.07317	1.6	0.68	959	13	977	14	1019	32	94
A121	42525	661	125.2	1.19	0.3	0.1591	1.8	1.559	2.1	0.07108	1.1	0.84	952	16	954	13	960	23	99
A122	43977	1372	115.2	0.07	0.5	0.08984	1.4	0.7286	1.8	0.05882	1.1	0.79	555	8	556	8	560	24	99
A123	36545	135	53.7	0.41	0.2	0.3748	1.4	6.53	1.7	0.1264	0.84	0.86	2052	26	2050	15	2048	15	100
A124	58651	462	104.2	0.11	0.5	0.227	1.4	3.113	1.7	0.0995	1	0.80	1319	17	1436	14	1615	19	82
A125	7030	171	19.4	0.52	0.4	0.1087	1.5	0.9693	2.8	0.06468	2.3	0.55	665	10	688	14	764	49	87
A126	15048	220	42.7	1.19	0.2	0.163	1.5	1.633	2.2	0.07265	1.6	0.69	974	14	983	14	1004	32	97
A127	3128	74	8.5	0.22	0.2	0.1174	1.6	1.029	2.9	0.06353	2.4	0.56	716	11	718	15	726	51	99
A128	1382	29	4.0	1.01	b.d.	0.1235	2	1.178	4.1	0.06919	3.6	0.48	751	14	791	23	904	75	83
A129	59309	129	84.4	1.86	0.0	0.4796	1.6	11.19	1.8	0.1693	0.86	0.88	2525	34	2539	17	2551	14	99
A130	1668	34	4.6	0.48	0.1	0.131	1.8	1.181	3.3	0.06539	2.8	0.56	794	14	792	18	787	58	101
A131	11044	337	36.3	1.03	0.2	0.09337	1.4	0.7639	2.5	0.05934	2.1	0.57	575	8	576	11	580	45	99
A133	30140	427	80.0	0.63	0.1	0.1769	1.5	1.800	1.7	0.0738	0.91	0.85	1050	14	1045	11	1036	18	101
A134	9758	368	67.8	0.60	b.d.	0.1691	3.1	1.685	3.5	0.07227	1.6	0.89	1007	29	1003	22	994	32	101
A135	20193	738	70.2	0.78	0.9	0.085	1.4	0.6913	2.8	0.05899	2.4	0.49	526	7	534	12	567	53	93
A136	3082	84	8.1	0.04	0.2	0.1035	1.5	0.8765	2.8	0.0614	2.4	0.53	635	9	639	14	653	52	97
A32	2343	132	12.2	0.20	2.0	0.09047	3.2	0.6283	22	0.05037	22	0.15	558	17	495	90	212	506	263
A53	6754	288	12.8	0.18	11	0.03525	11	0.2234	14	0.04596	9.3	0.75	223	23	205	27			
A62	8706	65	10.2	2.14	16.2	0.0788	2.8	0.8379	12	0.07712	12	0.24	489	13	618	57	1124	231	43
A82	13774	469	24.5	0.19	0.1	0.05366	4.7	0.4623	4.9	0.06248	1.5	0.95	337	15	386	16	691	33	49
A84	15602	1400	61.6	0.19	0.1	0.04504	3.8	0.3966	4.2	0.06387	1.6	0.92	284	11	339	12	737	34	39
A132	32378	1297	66.4	0.61	0.7	0.04618	1.6	0.3774	2.4	0.05927	1.8	0.68	291	5	325	7	577	38	50
Felix [g]	7816	600	76.5	2.87	0.31	0.08115	2.3	0.6438	4.4	0.05754	3.1	0.57	503.0	11.3	504.6	17.5	512	68	99
Ples. [g]	9451	1185	60	0.14	0.22	0.05360	1.8	0.3961	3.2	0.05359	1.9	0.68	337	6	339	9	354	42	95
91500 [g]	11681	70	13	0.46	0.20	0.1774	1.3	1.8341	2.1	0.07500	1.5	0.66	1053	12	1058	14	1068	30	99

Spot size = 33 and 50 µm, respectively; depth of crater ~15µm. $^{206}Pb/^{238}U$ error is the quadratic additions of the within run precision (2 SE) and the external reproducibility (2 SD) of the reference zircon. $^{207}Pb/^{206}Pb$ error propagation (^{207}Pb signal dependent) following Gerdes & Zeh (2009). $^{207}Pb/^{235}U$ error is the quadratic addition of the $^{207}Pb/^{206}Pb$ and $^{206}Pb/^{238}U$ uncertainty.

[a] Within run background-corrected mean ^{207}Pb signal in cps (counts per second).

[b] U and Pb content and Th/U ratio were calculated relative to GJ-1 reference zircon.

[c] percentage of the common Pb on the ^{206}Pb. b.d. = below dectection limit.

[d] corrected for background, within-run Pb/U fractionation (in case of $^{206}Pb/^{238}U$) and common Pb using Stacy and Kramers (1975) model Pb composition and subsequently normalised to GJ-1 (ID-TIMS value/measured value); $^{207}Pb/^{235}U$ calculated using $^{207}Pb/^{206}Pb/(^{238}U/^{206}Pb*1/137.88)$

[e] rho is the $^{206}Pb/^{238}U/^{207}Pb/^{235}U$ error correlation coefficient.

[f] degree of concordance = $^{206}Pb/^{238}U$ age / $^{207}Pb/^{206}Pb$ age x 100

[g] Accuracy and reproducibilty was checked by repeated analyses (n = 13) of reference zircon Plesovice, Felix and 91500; data given as mean with 2 standard deviation uncertainties

grain	Karaburun Melange	^{207}Pb (cps)	U [b] (ppm)	Pb [b] (ppm)	Th/U [b]	^{206}Pbc [c] (%)	$^{206}Pb/^{238}U$ [d]	±2σ (%)	$^{207}Pb/^{235}U$ [d]	±2σ (%)	$^{207}Pb/^{206}Pb$ [d]	±2σ (%)	rho [e]	$^{206}Pb/^{238}U$	±2σ (Ma)	$^{207}Pb/^{235}U$	±2σ (Ma)	$^{207}Pb/^{206}Pb$	±2σ (Ma)	conc. (%)
A662	K.13.102	43200	1269	71.3	0.49	1.5	0.05323	1.4	0.3852	2.3	0.05249	1.7	0.64	334	5	331	6	307	40	109
A663		727549	479	370.5	0.41	b.d.	0.6302	1.3	21.84	1.5	0.2514	0.56	0.92	3150	33	3177	14	3193	9	99
A664		3785	105	7.9	0.33	0.2	0.07215	1.5	0.5632	2.8	0.05661	2.4	0.53	449	6	454	10	476	52	94
A665		7101	126	12.6	0.27	0.1	0.09731	1.4	0.8028	4.0	0.05984	3.7	0.35	599	8	598	18	598	81	100
A666		36241	83	34.2	0.33	b.d.	0.3788	1.5	6.829	1.8	0.1308	1.1	0.80	2071	26	2090	16	2108	19	98
A672		292960	303	187.7	0.51	0.1	0.5097	1.7	12.6	1.8	0.1793	0.6	0.94	2655	36	2650	17	2647	10	100
A673		36262	96	37.4	0.47	0.2	0.339	1.4	5.402	1.6	0.1156	0.9	0.84	1882	22	1885	14	1889	16	100
A674		12728	201	25.7	0.68	0.1	0.1077	1.4	0.9394	1.8	0.06327	1.2	0.74	659	8	673	9	717	26	92
A675		26950	831	56.0	0.37	0.4	0.06539	2.9	0.5	3.5	0.05546	1.9	0.84	408	12	412	12	431	43	95
A676		94884	108	70.0	0.65	0.1	0.5146	1.5	12.71	1.6	0.1792	0.61	0.93	2676	33	2659	15	2645	10	101
A677		57883	62	36.9	0.25	b.d.	0.5279	1.6	13.75	1.8	0.189	0.79	0.90	2733	36	2733	17	2733	13	100
A678		38535	76	33.1	0.28	0.1	0.4	1.4	7.459	1.7	0.1353	0.88	0.85	2169	27	2168	15	2167	15	100
A679		7760	233	16.9	0.57	0.1	0.06321	1.4	0.4822	2.3	0.05532	1.8	0.62	395	5	400	8	425	40	93
A680		10097	97	11.8	0.82	0.3	0.1048	1.3	0.8784	3.5	0.0608	3.2	0.39	642	8	640	17	632	69	102
A681		11479	340	20.7	0.19	0.3	0.06075	1.4	0.459	4.0	0.05479	3.7	0.37	380	5	384	13	404	82	94
A682		23147	710	67.9	0.32	0.0	0.09716	1.5	0.7944	2.0	0.0593	1.3	0.77	598	9	594	9	578	28	103
A683		16874	443	45.4	0.46	3.8	0.09939	1.8	0.8148	3.8	0.05945	3.3	0.47	611	10	605	17	584	72	105
A684		4172	36	3.4	0.34	0.2	0.0909	1.6	0.7466	3.1	0.05957	2.7	0.50	561	8	566	13	588	58	95
A685		11682	217	22.7	0.59	0.2	0.08901	1.5	0.7187	2.2	0.05856	1.6	0.67	550	8	550	9	551	35	100

A686	23876	50	22.5	0.50	1.3	0.3835	1.5	7.114	2.2	0.1345	1.6	0.70	2092	27	2126	20	2158	27	97
A687	5860	74	10.5	0.50	0.1	0.1277	1.4	1.144	2.7	0.06499	2.3	0.52	775	10	775	15	774	48	100
A688	5145	96	11.5	0.90	1.8	0.09309	1.5	0.7751	3.2	0.06039	2.8	0.46	574	8	583	14	618	61	93
A689	20110	115	27.9	0.60	0.1	0.2031	1.8	2.306	2.5	0.08235	1.8	0.71	1192	19	1214	18	1254	35	95
A690	9556	49	5.9	0.74	4.0	0.09175	1.5	0.7572	3.4	0.05985	3.1	0.42	566	8	572	15	598	67	95
A691	13269	392	26.5	0.32	0.1	0.06444	1.5	0.4847	2.1	0.05456	1.6	0.68	403	6	401	7	394	35	102
A692	67794	149	-7.6	0.29	1.4	-0.09114	4.0	-2.006	5.7	0.1596	4	0.71	-616	-26	######	####	2452	68	-25
A693	18727	295	28.4	0.16	1.7	0.09489	1.5	0.7696	2.5	0.05883	1.9	0.62	584	9	580	11	561	42	104
A694	3378	25	3.4	1.29	0.4	0.09134	1.5	0.8075	3.2	0.06412	2.9	0.46	563	8	601	15	745	61	76
A695	33724	2059	56.8	0.64	1.8	0.02272	3.5	0.1718	4.2	0.05484	2.3	0.84	145	5	161	6	406	51	36
A696	3842	63	6.7	0.55	0.7	0.09196	1.6	0.7686	3.4	0.06061	3	0.46	567	9	579	15	626	65	91
A697	660507	1597	772.6	0.01	8.2	0.4739	3.8	11.4	4.7	0.1744	2.8	0.81	2501	79	2556	45	2600	46	96
A698	6750	109	12.9	0.49	0.2	0.1046	1.5	0.8961	2.5	0.06213	2	0.60	641	9	650	12	679	42	95
A699	19420	561	36.6	0.34	0.7	0.06174	1.4	0.4676	2.4	0.05493	2	0.56	386	5	390	8	410	45	94
A700	20535	604	41.9	0.48	0.1	0.06234	1.4	0.4699	1.9	0.05466	1.2	0.76	390	5	391	6	399	27	98
A701	672367	564	484.1	0.69	0.1	0.6623	1.5	26.11	1.7	0.2859	0.65	0.92	3276	39	3351	16	3396	10	96
A707	26203	771	79.3	0.59	0.0	0.09708	1.4	0.8398	1.8	0.06274	1.1	0.77	597	8	619	8	699	24	85
A708	132667	182	90.6	0.22	0.0	0.4578	1.4	10.03	1.5	0.1589	0.61	0.92	2430	28	2438	14	2444	10	99
A709	22366	677	35.4	0.63	0.0	0.044	1.9	0.4165	2.5	0.06864	1.6	0.77	278	5	354	8	888	33	31
A710	244218	290	152.1	0.28	1.1	0.4757	1.3	11.73	1.5	0.1788	0.72	0.88	2509	28	2583	14	2641	12	95
A711	6548	81	5.1	0.37	1.6	0.05808	1.6	0.4347	3.5	0.05428	3.2	0.44	364	6	367	11	383	71	95
A712	6676	108	13.0	0.59	0.3	0.1024	1.4	0.856	2.7	0.0606	2.3	0.53	629	9	628	13	625	50	101
A713	164973	426	168.2	0.48	0.0	0.3446	1.4	5.541	1.5	0.1166	0.57	0.92	1909	22	1907	13	1905	10	100
A714	37597	104	38.8	0.39	0.3	0.3323	1.7	5.417	2.0	0.1182	1.2	0.82	1850	27	1888	18	1929	21	96
A715	16736	318	30.6	0.30	0.2	0.09219	1.5	0.7508	2.0	0.05907	1.4	0.72	568	8	569	9	570	31	100
A716	13487	409	26.1	0.26	0.3	0.06211	1.4	0.4646	2.2	0.05425	1.6	0.66	388	5	387	7	381	37	102
A717	58512	913	146.5	1.51	0.0	0.1244	1.6	1.185	2.2	0.06913	1.6	0.70	756	11	794	12	903	33	84
A718	11130	140	19.1	0.35	0.1	0.128	1.5	1.173	2.3	0.06644	1.8	0.64	777	11	788	13	820	37	95
A719	13143	248	27.1	0.61	0.1	0.09406	1.4	0.7714	1.9	0.05948	1.3	0.74	579	8	581	9	585	28	99
A720	11485	256	20.5	0.12	0.1	0.08291	1.4	0.6603	2.0	0.05776	1.5	0.68	513	7	515	8	521	33	99
A721	13743	83	18.6	0.25	b.d.	0.215	1.5	2.484	2.3	0.08382	1.8	0.65	1255	17	1268	17	1288	35	97
A722	4383	127	8.7	0.38	0.1	0.06357	1.4	0.4842	2.4	0.05524	2	0.57	397	5	401	8	422	44	94
A723	13505	101	11.8	0.54	0.1	0.1027	1.3	0.8771	1.8	0.06195	1.2	0.74	630	8	639	9	672	26	94
A724	29458	976	60.2	0.26	0.7	0.06036	2.1	0.4555	2.5	0.05474	1.3	0.85	378	8	381	8	401	29	94
A725	17247	534	36.5	0.40	0.5	0.06335	1.6	0.4696	3.7	0.05377	3.3	0.44	396	6	391	12	361	76	110
A726	12004	237	27.5	0.84	b.d.	0.09208	1.4	0.7686	2.6	0.06054	2.2	0.53	568	7	579	11	623	47	91
A727	24560	754	51.1	0.38	0.2	0.0631	1.4	0.474	1.9	0.05448	1.3	0.72	394	5	394	6	391	30	101
A728	14549	430	28.2	0.33	0.4	0.06262	1.5	0.4744	3.3	0.05494	3	0.44	392	6	394	11	410	67	96
A729	46494	119	50.1	0.60	0.1	0.35	1.6	5.691	1.8	0.1179	1	0.84	1935	26	1930	16	1925	18	101
A730	190763	212	137.2	0.66	b.d.	0.5141	1.5	12.76	1.6	0.1799	0.57	0.94	2674	34	2662	16	2652	9	101
A731	85462	87	56.4	0.44	b.d.	0.5383	1.4	14.41	1.5	0.1942	0.63	0.91	2776	31	2777	15	2778	10	100
A732	45222	846	73.7	0.05	0.2	0.09276	1.4	0.7598	1.9	0.0594	1.3	0.74	572	8	574	8	582	28	98
A733	27303	55	23.8	0.33	b.d.	0.3902	1.4	7.334	1.9	0.1363	1.2	0.76	2124	26	2153	17	2181	21	97
A734	54111	1217	100.8	0.44	0.7	0.07861	1.6	0.639	1.9	0.05896	1.1	0.83	488	8	502	8	565	23	86
A735	8301	254	15.9	0.20	0.2	0.06262	1.5	0.4686	2.3	0.05427	1.8	0.64	392	6	390	8	382	41	102
A736	19661	75	23.9	0.50	1.5	0.2712	1.5	3.63	2.4	0.09706	1.8	0.64	1547	21	1556	19	1568	34	99
A737	77837	155	79.9	0.78	b.d.	0.4063	1.4	7.645	1.5	0.1365	0.68	0.90	2198	26	2190	14	2183	12	101
A738	30163	550	62.9	0.87	0.0	0.09522	1.9	0.8375	2.1	0.06379	0.96	0.89	586	11	618	10	735	20	80
A739	103790	206	99.5	0.66	b.d.	0.3925	1.4	7.368	1.6	0.1361	0.73	0.89	2134	26	2157	14	2179	13	98
A740	25697	173	35.5	0.25	b.d.	0.1973	1.5	2.176	1.9	0.08002	1.2	0.79	1161	16	1174	14	1197	23	97
A741	20001	608	39.2	0.29	0.4	0.06257	1.4	0.475	2.5	0.05506	2.1	0.57	391	5	395	8	415	46	94
A742	67561	163	67.2	0.57	0.0	0.3459	1.4	6.007	1.6	0.1259	0.77	0.87	1915	23	1977	14	2042	14	94
A743	27653	132	58.9	0.84	0.5	0.3379	1.6	5.607	2.1	0.1203	1.2	0.80	1877	27	1917	18	1961	22	96
A744	12869	392	29.5	0.68	0.2	0.06281	1.4	0.4708	2.3	0.05437	1.8	0.63	393	6	392	7	386	40	102
A745	80465	80	39.8	1.10	0.0	0.3561	1.3	6.33	1.6	0.1289	0.77	0.87	1964	23	2023	14	2083	14	94
A751	114831	267	113.2	0.48	b.d.	0.3663	1.4	6.259	1.5	0.1239	0.67	0.90	2012	24	2013	14	2013	12	100
A752	47609	119	52.1	0.59	0.2	0.3716	1.6	6.542	1.8	0.1277	0.86	0.88	2037	28	2052	16	2066	15	99
A753	17903	40	15.3	0.32	0.7	0.3399	1.9	5.828	2.5	0.1244	1.6	0.78	1886	32	1951	22	2020	28	93
A754	4349	123	7.9	0.28	0.4	0.0616	1.4	0.4625	2.8	0.05445	2.4	0.51	385	5	386	9	390	53	99
A755	6126	183	12.3	0.34	0.2	0.06347	1.5	0.4785	2.4	0.05468	1.9	0.61	397	6	397	8	399	42	99
A756	15884	465	31.2	0.37	b.d.	0.06313	1.3	0.4772	2.0	0.05482	1.4	0.69	395	5	396	6	405	32	97
A757	13503	394	25.3	0.15	0.2	0.06552	1.4	0.4953	1.8	0.05483	1.2	0.75	409	5	409	6	405	27	101
A758	11141	323	21.8	0.32	0.2	0.06465	1.5	0.4903	2.1	0.055	1.4	0.72	404	6	405	7	412	32	98
A759	48352	102	48.5	0.70	b.d.	0.3851	1.4	6.971	1.6	0.1313	0.81	0.86	2100	25	2108	14	2115	14	99
A760	166195	514	184.9	0.16	0.2	0.3522	1.6	5.82	1.7	0.1199	0.61	0.93	1945	27	1949	15	1954	11	100
A761	109978	589	127.8	0.23	0.0	0.2075	1.5	3.991	1.7	0.1395	0.8	0.88	1216	16	1632	14	2220	14	55
A762	55315	275	57.1	0.17	0.3	0.199	1.3	2.7	1.8	0.09841	1.2	0.75	1170	14	1329	13	1594	22	73
A763	12686	389	24.7	0.22	0.3	0.06288	1.4	0.4697	2.0	0.05417	1.4	0.70	393	5	391	6	378	32	104
A764	5688	33	4.0	0.24	0.3	0.1192	1.5	1.055	2.7	0.06421	2.2	0.55	726	10	731	14	748	47	97
A765	235029	753	266.8	0.11	b.d.	0.3539	1.4	5.644	1.6	0.1156	0.82	0.87	1953	24	1923	14	1890	15	103
A766	7772	225	16.0	0.47	0.3	0.06364	1.4	0.4733	2.5	0.05394	2	0.57	398	5	393	8	369	46	108
A767	64618	33	21.7	0.79	0.0	0.5059	1.4	12.65	1.7	0.1813	0.86	0.86	2639	31	2654	16	2665	14	99
A768	51593	73	30.0	0.99	0.4	0.3293	1.4	5.423	1.7	0.1194	0.97	0.82	1835	22	1888	15	1948	17	94
A769	5673	88	10.3	0.80	1.3	0.09225	1.4	0.7458	4.2	0.05863	3.9	0.34	569	8	566	18	554	86	103
A770	110171	246	99.7	0.23	0.0	0.379	1.4	6.673	1.6	0.1277	0.72	0.89	2072	25	2069	14	2067	13	100
A771	21615	689	47.2	0.41	0.3	0.06445	1.5	0.5	2.1	0.05627	1.4	0.72	403	6	412	7	463	32	87
A772	14811	303	30.4	0.48	0.1	0.09034	1.4	0.7321	1.9	0.05877	1.2	0.75	558	8	558	8	559	27	100
A773	137168	284	125.7	0.43	0.1	0.3925	1.7	7.255	1.8	0.134	0.59	0.95	2135	31	2143	16	2152	10	99
A774	63633	148	73.6	0.95	0.1	0.3733	1.4	6.402	1.6	0.1244	0.86	0.85	2045	24	2032	14	2020	15	101
A775	32049	1058	74.2	0.30	0.0	0.06946	1.6	0.5825	2.2	0.06082	1.5	0.73	433	7	466	8	633	32	68
A776	6414	199	13.8	0.38	0.2	0.0649	1.4	0.4844	2.7	0.05413	2.3	0.53	405	6	401	9	377	51	108
A777	22752	707	47.7	0.60	0.0	0.06133	1.4	0.4602	1.9	0.05442	1.2	0.77	384	5	384	6	389	27	99
A778	20090	637	43.1	0.38	0.1	0.06299	1.5	0.4724	2.1	0.05439	1.4	0.71	394	6	393	7	387	32	102
A779	22522	463	38.6	0.28	0.3	0.07938	1.4	0.6334	1.9	0.05787	1.3	0.74	492	7	498	8	525	28	94
A780	64599	316	104.1	0.18	b.d.	0.3261	2.3	4.823	4.4	0.1073	3.7	0.53	1819	36	1789	37	1754	68	104
A781	9308	129	8.9	0.43	0.1	0.06362	1.3	0.4822	2.1	0.05496	1.7	0.62	398	5	400	7	411	38	97

A782	25235	696	49.9	0.61	0.2	0.06276	1.5	0.4884	2.1	0.05644	1.4	0.73	392	6	404	7	470	31	84
A783	47693	851	95.5	1.07	0.1	0.08299	1.5	0.7885	2.0	0.06891	1.4	0.73	514	7	590	9	896	29	57
A784	70179	152	63.3	0.25	0.0	0.3885	1.4	6.995	1.7	0.1306	0.86	0.85	2116	25	2111	15	2106	15	100
A785	8952	257	17.1	0.29	0.6	0.06369	1.6	0.4831	2.1	0.055	1.4	0.74	398	6	400	7	412	32	97
A786	17585	543	35.5	0.31	0.1	0.06247	1.4	0.4686	2.0	0.05441	1.4	0.72	391	5	390	6	388	31	101
A787	3119	91	6.4	0.42	0.3	0.0644	1.5	0.4845	2.6	0.05457	2.1	0.60	402	6	401	9	395	46	102
BB [g]	18314	746	66.3	0.11	0.09	0.09203	1.9	0.7496	2.6	0.05907	1.4	0.82	568	10	568	11	570	30	100
Ples. [g]	18680	1443	75	0.08	0.76	0.05401	1.7	0.3963	2.1	0.05322	1.0	0.80	339	5	339	6	338	23	100
91500 [g]	25044	71	14	0.45	1.01	0.1807	1.4	1.8462	3.4	0.07412	2.6	0.46	1070	13	1062	22	1044	53	103

Spot size = 33 and 50 µm, respectively; depth of crater ~15µm. $^{206}Pb/^{238}U$ error is the quadratic additions of the within run precision (2 SE) and the external reproducibility (2 SD) of the reference zircon. $^{207}Pb/^{206}Pb$ error propagation (^{207}Pb signal dependent) following Gerdes & Zeh (2009). $^{207}Pb/^{235}U$ error is the quadratic addition of the $^{207}Pb/^{206}Pb$ and $^{206}Pb/^{238}U$ uncertainty.

[a] Within run background-corrected mean ^{207}Pb signal in cps (counts per second).

[b] U and Pb content and Th/U ratio were calculated relative to GJ-1 reference zircon.

[c] percentage of the common Pb on the ^{206}Pb. b.d. = below dectection limit.

[d] corrected for background, within-run Pb/U fractionation (in case of $^{206}Pb/^{238}U$) and common Pb using Stacy and Kramers (1975) model Pb composition and subsequently normalised to GJ-1 (ID-TIMS value/measured value); $^{207}Pb/^{235}U$ calculated using $^{207}Pb/^{206}Pb/(^{238}U/^{206}Pb*1/137.88)$

[e] rho is the $^{206}Pb/^{238}U/^{207}Pb/^{235}U$ error correlation coefficient.

[f] degree of concordance = $^{206}Pb/^{238}U$ age / $^{207}Pb/^{206}Pb$ age x 100

[g] Accuracy and reproducibilty was checked by repeated analyses (n = 30) of reference zircon Plesovice, BB and 91500; data given as mean with 2 standard deviation uncertainties

Uzumdere Formation

grain		^{207}Pb (cps) [a]	U (ppm) [b]	Pb (ppm) [b]	Th/U [b]	^{206}Pbc (%) [c]	$^{206}Pb/^{238}U$ [d]	±2σ (%)	$^{207}Pb/^{235}U$ [d]	±2σ (%)	$^{207}Pb/^{206}Pb$ [d]	±2σ (%)	rho [e]	$^{206}Pb/^{238}U$	±2σ (Ma)	$^{207}Pb/^{235}U$	±2σ (Ma)	$^{207}Pb/^{206}Pb$	±2σ (Ma)	conc. (%)
A188	K.13.77	6370	115	19.4	0.70	b.d.	0.1547	1.7	1.5340	2.2	0.07189	1.4	0.76	927	14	944	14	983	29	94
A189		6700	147	23.5	1.05	b.d.	0.1369	1.7	1.252	2	0.06637	1.2	0.81	827	13	825	12	818	25	101
A190		12815	14	8.5	1.27	0.1	0.4729	1.8	10.62	2.3	0.1628	1.4	0.80	2496	38	2490	22	2485	23	100
A191		6882	180	20.7	0.57	0.4	0.1096	1.6	0.9363	2.1	0.06198	1.3	0.78	670	10	671	10	673	27	100
A192		5971	227	22.3	0.84	0.2	0.0878	1.6	0.7051	2.1	0.05824	1.4	0.77	543	9	542	9	539	30	101
A193		8344	45	20.1	1.97	0.6	0.3118	1.8	4.57	2.2	0.1063	1.3	0.81	1750	27	1744	18	1737	24	101
A199		1054	16	1.4	0.40	0.3	0.08573	2	0.688	3.3	0.0582	2.6	0.60	530	10	532	14	537	57	99
A200		5275	40	7.5	1.44	0.1	0.1455	1.8	1.416	2.7	0.07061	2	0.65	876	15	896	16	946	42	93
A201		8174	186	27.8	1.00	0.1	0.1283	1.6	1.177	2.1	0.06656	1.3	0.79	778	12	790	11	824	26	94
A202		4329	134	16.8	2.22	1.8	0.08584	1.9	0.6893	3.6	0.05824	3.1	0.51	531	9	532	15	539	68	99
A203		4820	180	23.8	2.36	0.0	0.09093	1.7	0.7499	2.4	0.05982	1.7	0.70	561	9	568	11	597	37	94
A204		3477	131	14.1	1.43	0.5	0.08579	1.7	0.691	4.1	0.05842	3.7	0.42	531	9	533	17	546	82	97
A205		7117	270	26.6	1.80	0.6	0.0727	1.7	0.5626	3.3	0.05613	2.8	0.51	452	7	453	12	457	63	99
A206		6495	181	29.6	1.05	0.0	0.1514	2.5	1.419	3	0.06797	1.6	0.84	909	21	897	18	868	33	105
A207		9818	189	35.6	1.95	0.1	0.1386	1.6	1.268	2.2	0.06634	1.5	0.73	837	13	831	13	817	32	102
A208		5005	188	17.5	0.72	0.2	0.08609	1.7	0.6956	2.7	0.05861	2.1	0.62	532	9	536	11	553	47	96
A209		9114	139	17.2	0.80	6.2	0.1004	1.9	0.8423	4.9	0.06088	4.5	0.40	616	11	620	23	635	96	97
A210		1820	25	3.2	2.32	1.3	0.0876	1.8	0.7077	2.8	0.05859	2.1	0.65	541	9	543	12	552	46	98
A211		5146	71	6.5	0.54	1.4	0.088	1.7	0.7204	3.2	0.05937	2.7	0.54	544	9	551	14	581	58	94
A212		7397	271	22.2	0.66	1.1	0.07711	1.8	0.6072	3.3	0.05711	2.8	0.54	479	8	482	13	496	61	97
A213		3103	41	4.8	0.96	0.2	0.1028	1.8	0.8605	3	0.06068	2.4	0.60	631	11	630	14	628	52	100
A214		7666	292	32.8	2.59	0.9	0.07332	1.8	0.5751	3.7	0.05689	3.2	0.49	456	8	461	14	487	70	94
A215		5672	204	29.8	3.54	0.7	0.08573	1.7	0.6845	3.2	0.05791	2.8	0.51	530	8	529	13	526	61	101
A216		17028	39	28.3	2.40	1.5	0.4791	1.7	11.1	2.5	0.168	1.8	0.69	2523	36	2531	24	2538	31	99
A217		24326	24	13.4	0.75	0.8	0.4706	1.9	10.71	2.8	0.165	2.1	0.67	2486	39	2498	27	2508	35	99
A218		37766	261	71.4	0.70	1.0	0.2412	1.7	3.266	2.2	0.09819	1.3	0.79	1393	21	1473	17	1590	25	88
A219		2079	27	3.0	0.66	0.5	0.102	2	0.8666	4.9	0.06161	4.5	0.41	626	12	634	24	660	96	95
A220		11940	172	35.0	1.43	0.0	0.1725	1.8	1.747	2.1	0.07344	1.1	0.84	1026	17	1026	14	1026	23	100
A221		5005	351	16.1	0.50	0.6	0.04403	1.7	0.3138	2.7	0.05169	2.2	0.62	278	5	277	7	272	50	102
A222		14681	543	45.6	0.39	0.1	0.08385	1.6	0.6791	2.2	0.05874	1.5	0.73	519	8	526	9	558	33	93
A223		29230	106	51.2	1.15	1.4	0.3891	1.8	7.132	2.6	0.1329	1.9	0.69	2119	32	2128	23	2137	33	99
A224		4012	145	17.3	2.06	0.3	0.08381	1.9	0.6682	2.5	0.05783	1.7	0.73	519	9	520	10	523	38	99
A225		15664	419	37.2	0.11	0.9	0.09352	1.6	0.7606	3.2	0.05898	2.8	0.50	576	9	574	14	566	61	102
A226		42548	213	82.0	0.88	0.4	0.3322	1.7	5.163	1.9	0.1127	0.93	0.87	1849	27	1847	16	1844	17	100
A227		17639	109	37.2	1.60	0.0	0.2921	2.1	4.49	2.4	0.1115	1.1	0.89	1652	31	1729	20	1824	20	91
A228		4974	321	15.4	0.48	0.3	0.04627	1.8	0.3333	2.5	0.05224	1.8	0.70	292	5	292	6	296	41	98
A229		24301	567	65.5	0.95	0.6	0.09935	1.8	0.8276	2.2	0.06041	1.3	0.82	611	11	612	10	618	27	99
A230		22796	632	75.3	0.87	0.2	0.1077	1.6	0.9098	1.8	0.06127	0.88	0.88	659	10	657	9	649	19	102
A231		7890	158	22.6	0.81	1.2	0.1268	1.7	1.136	2.8	0.06497	2.2	0.62	770	13	771	15	773	47	100
A232		6233	226	20.6	0.58	0.4	0.08573	1.8	0.6839	2.8	0.05786	2.2	0.63	530	9	529	12	524	48	101
A233		61816	272	95.2	0.23	0.0	0.3429	1.6	5.824	1.8	0.1232	0.83	0.89	1900	27	1950	16	2003	15	95
A234		4490	104	14.3	1.30	0.5	0.1081	2	0.9274	3	0.0622	2.2	0.67	662	13	666	15	681	47	97
A235		3979	130	17.4	1.94	0.0	0.1004	1.6	0.8577	2.7	0.06195	2.1	0.61	617	10	629	13	672	45	92
A236		10861	44	18.4	0.93	1.4	0.3471	1.8	5.674	2.7	0.1185	2	0.68	1921	30	1927	23	1934	35	99
A237		6378	238	21.9	0.82	0.3	0.08259	1.7	0.6545	2.5	0.05748	1.8	0.69	512	9	511	10	510	40	100
A243		6078	107	20.4	1.24	b.d.	0.159	1.8	1.561	3	0.07121	2.3	0.62	951	16	955	19	963	47	99
A244		12745	351	35.5	0.46	0.5	0.09802	1.7	0.8002	2.4	0.05921	1.7	0.71	603	10	597	11	575	37	105
A245		4890	335	14.8	0.41	0.2	0.04355	1.8	0.3135	2.5	0.05222	1.8	0.70	275	5	277	6	295	41	93
A246		7325	225	25.9	0.98	0.4	0.09876	1.6	0.815	2.9	0.05986	2.4	0.56	607	9	605	13	598	52	101
A247		9510	148	25.9	0.54	0.1	0.1658	1.7	1.644	2.1	0.07191	1.3	0.79	989	16	987	14	983	26	101
A248		5225	31	5.5	0.62	b.d.	0.1622	1.8	1.668	2.5	0.07459	1.7	0.72	969	16	996	16	1058	35	92
A249		2548	37	3.8	1.43	0.5	0.09099	1.7	0.7596	2.8	0.06055	2.2	0.59	561	9	574	12	623	48	90
A250		6205	237	21.4	0.64	0.1	0.0842	1.6	0.6823	2	0.05877	1.2	0.78	521	8	528	8	559	27	93

A251	131453	475	178.8	0.64	0.1	0.3344	1.8	7.058	2	0.1531	0.94	0.88	1860	29	2119	18	2381	16	78
A252	178976	396	231.3	0.34	b.d.	0.5266	1.6	16.13	1.8	0.2222	0.72	0.91	2727	36	2885	17	2997	12	91
A253	6093	190	19.2	0.51	0.1	0.09631	1.8	0.7978	2.7	0.06008	2	0.66	593	10	596	12	606	44	98
A254	4864	104	14.5	0.57	0.3	0.1315	1.9	1.188	3.3	0.06552	2.6	0.59	797	15	795	18	791	55	101
A255	8491	170	24.3	0.44	0.0	0.1391	1.7	1.311	2.5	0.06839	1.8	0.67	839	13	851	14	880	38	95
A256	3715	118	14.0	1.11	b.d.	0.1005	1.7	0.847	2.6	0.06112	2	0.64	617	10	623	12	644	43	96
A257	23395	64	38.4	1.62	0.0	0.4674	1.7	10.67	2	0.1656	1	0.85	2472	34	2495	18	2513	17	98
A258	10580	326	33.0	0.62	0.0	0.09597	1.7	0.8024	2.5	0.06064	1.8	0.70	591	10	598	11	626	38	94
A259	5414	199	27.3	2.50	2.1	0.09393	4.2	0.7727	5.7	0.05966	3.9	0.73	579	23	581	26	591	84	98
A260	118122	646	204.8	0.29	0.1	0.3185	1.7	5.197	1.9	0.1183	0.79	0.91	1782	26	1852	16	1931	14	92
A261	94853	554	178.7	0.05	0.1	0.3312	1.9	5.236	2.1	0.1147	0.84	0.91	1844	30	1858	18	1874	15	98
A262	4156	152	18.8	2.85	1.0	0.08022	1.7	0.632	3.8	0.05714	3.4	0.45	497	8	497	15	497	75	100
A263	418657	1402	923.2	1.41	2.2	0.5744	1.7	20.52	1.9	0.2591	0.91	0.88	2926	39	3116	19	3241	14	90
A264	94391	342	130.2	0.25	0.3	0.3675	1.6	6.827	1.8	0.1347	0.85	0.89	2018	28	2089	16	2160	15	93
A265	7454	285	24.6	1.08	1.0	0.07662	1.8	0.591	2.6	0.05594	1.9	0.69	476	8	471	10	450	42	106
A266	23770	1209	67.7	1.33	0.8	0.04704	1.7	0.342	2.5	0.05273	1.8	0.70	296	5	299	6	317	40	93
A267	9022	337	26.9	1.07	0.0	0.07279	1.6	0.5919	2.1	0.05898	1.3	0.80	453	7	472	8	566	27	80
A268	7988	288	41.5	3.78	0.0	0.08137	1.6	0.6591	2.3	0.05875	1.6	0.72	504	8	514	9	558	34	90
A269	2582	18	3.3	0.83	0.3	0.166	1.9	1.663	3.3	0.07263	2.6	0.58	990	17	994	21	1004	54	99
A270	1926	13	2.2	0.42	0.1	0.1583	1.8	1.629	3.6	0.07465	3.2	0.50	947	16	982	23	1059	63	89
A271	11087	431	37.1	0.56	0.0	0.08252	1.6	0.6619	2	0.05818	1.1	0.84	511	8	516	8	536	23	95
A272	2904	28	4.1	0.71	0.3	0.1371	1.7	1.287	4	0.06808	3.6	0.42	828	13	840	23	871	75	95
A273	20889	545	64.1	0.91	0.4	0.1047	1.7	0.8831	2.3	0.06116	1.5	0.76	642	11	643	11	645	32	100
A274	7374	260	29.6	1.90	0.4	0.08536	1.6	0.6933	3	0.05891	2.5	0.55	528	8	535	12	564	54	94
A276	8884	145	24.4	0.52	0.2	0.1599	1.7	1.564	2.3	0.07096	1.5	0.76	956	15	956	14	956	30	100
A277	128555	1042	315.5	1.08	0.2	0.2837	1.7	4.496	1.9	0.1149	0.88	0.88	1610	24	1730	16	1879	16	86
A278	10690	233	26.2	1.05	1.0	0.1008	1.7	0.8354	3.3	0.06009	2.8	0.53	619	10	617	15	607	60	102
A279	16417	259	42.5	1.03	0.0	0.1531	1.7	1.48	2.1	0.07011	1.2	0.82	918	15	922	13	931	24	99
A280	2240	36	7.2	0.67	0.1	0.1673	1.7	1.66	3	0.07188	2.5	0.58	997	16	993	19	982	50	102
A281	3880	63	13.0	1.49	0.5	0.1638	1.9	1.618	3.2	0.07165	2.5	0.60	978	17	977	20	976	52	100
A282	8972	152	25.6	0.60	0.2	0.1572	1.6	1.545	2.3	0.07125	1.5	0.73	941	14	948	14	965	32	98
A289	2122	74	9.8	2.25	0.3	0.09433	1.9	0.7687	3	0.0591	2.4	0.62	581	10	579	13	571	52	102
A290	12685	596	48.5	0.12	0.4	0.08696	1.8	0.7121	2.8	0.05939	2.2	0.64	538	9	546	12	581	47	92
A291	21469	824	77.6	0.99	0.5	0.08779	1.8	0.7039	3.4	0.05815	2.8	0.55	542	10	541	14	535	62	101
A292	8065	247	26.5	0.71	0.2	0.09961	1.7	0.828	2.3	0.06029	1.6	0.74	612	10	613	11	614	34	100
A293	3841	111	14.4	1.39	0.0	0.103	1.7	0.8783	2.8	0.06182	2.2	0.60	632	10	640	13	668	48	95
A294	23990	572	69.7	0.71	0.4	0.1125	1.7	0.9641	2.4	0.06215	1.8	0.69	687	11	685	12	679	38	101
A296	28025	115	62.2	2.33	0.2	0.3645	1.7	6.22	2.4	0.1238	1.6	0.73	2004	30	2007	21	2011	29	100
A297	58945	308	98.2	0.63	0.4	0.2935	1.6	4.444	1.9	0.1098	0.92	0.87	1659	24	1721	16	1796	17	92
A298	10009	502	22.8	0.64	1.7	0.04234	1.7	0.304	3.3	0.05208	2.8	0.50	267	4	270	8	289	65	92
A300	3652	138	12.0	0.65	0.4	0.08067	1.7	0.6443	2.5	0.05792	1.8	0.68	500	8	505	10	527	40	95
A301	5132	149	16.2	0.78	0.3	0.09674	1.7	0.8009	2.4	0.06004	1.7	0.70	595	10	597	11	605	37	98
A302	15670	233	45.5	0.77	0.0	0.1773	1.6	1.798	2	0.07354	1.2	0.82	1052	16	1045	13	1029	24	102
A303	15652	84	32.1	1.04	0.4	0.3143	1.9	4.725	3.4	0.109	2.8	0.57	1762	29	1772	29	1783	50	99
A275	16122	627	51.9	1.83	0.5	0.06858	1.8	0.7142	3	0.07553	2.4	0.59	428	7	547	13	1083	48	39
A288	82715	572	133.3	1.22	0.7	0.1895	1.9	2.944	2.2	0.1127	1.1	0.86	1119	19	1393	17	1843	20	61
A295	90880	877	130.7	1.03	2.1	0.1201	1.9	2.142	2.9	0.1294	2.2	0.66	731	13	1163	20	2090	38	35
A299	5080	167	21.0	2.43	b.d.	0.0878	1.7	0.8367	3	0.06911	2.5	0.55	543	9	617	14	902	52	60
Felix [g]	7816	600	76.5	2.87	0.31	0.08115	2.3	0.6438	4.4	0.05754	3.1	0.57	503	11	505	17	512	68	99
Ples. [g]	4606	553	28	0.15	0.89	0.05361	2.0	0.3938	2.4	0.05328	2.3	0.56	337	7	337	7	341	52	99
91500 [g]	12259	78	14	0.47	0.35	0.1783	2.3	1.8315	2.4	0.07450	1.0	0.74	1058	22	1057	16	1055	21	100

Spot size = 33 and 50 µm, respectively; depth of crater ~15µm. $^{206}Pb/^{238}U$ error is the quadratic additions of the within run precision (2 SE) and the external reproducibility (2 SD) of the reference zircon. $^{207}Pb/^{206}Pb$ error propagation (^{207}Pb signal dependent) following Gerdes & Zeh (2009). $^{207}Pb/^{235}U$ error is the quadratic addition of the $^{207}Pb/^{206}Pb$ and $^{206}Pb/^{238}U$ uncertainty.

[a] Within run background-corrected mean ^{207}Pb signal in cps (counts per second).

[b] U and Pb content and Th/U ratio were calculated relative to GJ-1 reference zircon.

[c] percentage of the common Pb on the ^{206}Pb. b.d. = below dectection limit.

[d] corrected for background, within-run Pb/U fractionation (in case of $^{206}Pb/^{238}U$) and common Pb using Stacy and Kramers (1975) model Pb composition and subsequently normalised to GJ-1 (ID-TIMS value/measured value); $^{207}Pb/^{235}U$ calculated using $^{207}Pb/^{206}Pb/(^{238}U/^{206}Pb*1/137.88)$

[e] rho is the $^{206}Pb/^{238}U/^{207}Pb/^{235}U$ error correlation coefficient.

[f] degree of concordance = $^{206}Pb/^{238}U$ age / $^{207}Pb/^{206}Pb$ age x 100

[g] Accuracy and reproducibilty was checked by repeated analyses (n = 13) of reference zircon Plesovice, Felix and 91500; data given as mean with 2 standard deviation uncertainties

Kasimlar Formation

grain		^{207}Pb (cps)	U (ppm)	Pb (ppm)	Th/U	^{206}Pbc (%)	$^{206}Pb/^{238}U$	±2σ (%)	$^{207}Pb/^{235}U$	±2σ (%)	$^{207}Pb/^{206}Pb$	±2σ (%)	rho	$^{206}Pb/^{238}U$	±2σ (Ma)	$^{207}Pb/^{235}U$	±2σ (Ma)	$^{207}Pb/^{206}Pb$	±2σ (Ma)	conc. (%)
A915	K.12.75	10667	92	17.6	0.40	0.5	0.1755	1.5	1.814	3.0	0.07497	2.6	0.52	1042	15	1051	20	1068	52	98
A916		10831	362	23.2	0.39	0.3	0.05918	1.4	0.4425	2.2	0.05424	1.7	0.63	371	5	372	7	381	38	97
A917		7939	296	16.5	0.39	0.4	0.05143	1.5	0.3756	2.5	0.05296	2	0.60	323	5	324	7	327	45	99
A918		2630	47	5.6	0.82	0.6	0.09191	1.7	0.7489	4.0	0.0591	3.6	0.42	567	9	568	17	571	78	99
A919		4899	49	8.8	0.57	0.8	0.1561	1.4	1.507	3.0	0.07004	2.7	0.46	935	12	933	19	929	55	101
A920		11888	146	25.2	0.94	0.2	0.1327	1.4	1.222	2.0	0.06678	1.5	0.68	803	11	811	11	831	31	97
A921		17057	443	34.7	0.38	0.1	0.07301	1.4	0.5719	1.9	0.05681	1.3	0.75	454	6	459	7	484	28	94
A922		10375	371	22.3	0.13	0.3	0.06182	1.6	0.4754	2.5	0.05577	1.9	0.64	387	6	395	8	443	43	87
A923		5217	43	8.4	0.61	1.2	0.1606	1.5	1.578	2.9	0.07124	2.5	0.52	960	14	961	18	964	51	100
A924		16783	289	36.3	0.61	0.2	0.1072	1.4	0.8977	2.1	0.06074	1.6	0.64	656	8	651	10	630	35	104
A925		19894	847	42.8	0.25	0.0	0.04983	1.3	0.3654	1.8	0.05318	1.2	0.75	313	4	316	5	336	26	93

A926	2617	39	4.9	0.44	0.5	0.1143	1.6	1.022	4.2	0.06489	3.9	0.38	697	11	715	22	771	82	91
A927	10720	446	22.8	0.35	0.6	0.04756	1.8	0.342	2.9	0.05215	2.3	0.62	300	5	299	7	292	51	103
A933	3996	49	9.3	1.08	0.1	0.1408	1.5	1.299	2.6	0.06689	2.2	0.57	849	12	845	15	834	45	102
A934	16914	289	34.2	0.55	0.1	0.1027	1.4	0.8616	2.0	0.06083	1.5	0.69	630	8	631	10	633	32	100
A935	3154	25	6.0	1.03	0.7	0.1743	1.5	1.806	3.7	0.07514	3.4	0.41	1036	15	1048	25	1072	68	97
A936	7997	87	13.2	0.43	0.8	0.1368	1.5	1.296	2.3	0.06869	1.8	0.64	827	12	844	14	889	37	93
A937	18417	224	31.2	0.24	b.d.	0.1367	1.4	1.263	2.2	0.067	1.7	0.62	826	11	829	13	838	36	99
A938	278330	350	198.6	0.31	0.0	0.4996	1.4	12.49	1.5	0.1813	0.53	0.93	2612	30	2642	14	2665	9	98
A939	35879	697	77.5	0.52	0.1	0.09799	1.5	0.8118	1.8	0.06008	1.1	0.80	603	8	603	8	607	23	99
A940	29848	534	57.6	0.40	b.d.	0.09924	1.4	0.8429	1.9	0.0616	1.3	0.73	610	8	621	9	660	28	92
A941	100252	112	68.8	0.40	0.0	0.5207	1.4	13.52	1.6	0.1882	0.73	0.89	2702	31	2716	15	2727	12	99
A942	198516	333	173.2	0.62	b.d.	0.4143	1.4	9.193	1.6	0.1609	0.6	0.92	2235	27	2357	14	2465	10	91
A943	5588	99	10.3	0.51	0.4	0.0922	1.4	0.7491	4.2	0.05893	3.9	0.34	569	8	568	18	565	85	101
A944	20865	225	34.5	0.24	0.0	0.1494	1.5	1.434	2.0	0.06964	1.4	0.72	897	12	903	12	918	29	98
A945	36731	103	46.8	0.87	b.d.	0.3494	1.4	5.594	1.7	0.1161	0.93	0.83	1932	23	1915	14	1897	17	102
A946	13208	126	22.0	0.38	0.5	0.1607	1.5	1.604	2.5	0.07236	2	0.59	961	13	972	16	996	41	96
A947	23052	362	39.7	0.20	0.0	0.1087	1.5	0.9373	1.7	0.06255	0.95	0.84	665	9	671	9	693	20	96
A948	19790	302	33.9	0.26	0.1	0.1089	1.4	0.9544	1.8	0.06357	1.2	0.76	666	9	680	9	727	24	92
A949	7720	99	15.0	0.53	b.d.	0.1324	1.7	1.226	3.8	0.06716	3.3	0.45	802	13	813	21	843	70	95
A950	10208	269	19.6	0.16	0.1	0.07381	1.4	0.5675	2.2	0.05576	1.6	0.67	459	6	456	8	443	36	104
A951	3122	139	6.9	0.40	0.6	0.04582	1.5	0.3304	3.7	0.05229	3.4	0.40	289	4	290	9	298	77	97
A952	88854	99	60.0	0.43	0.0	0.5102	1.4	13.22	1.6	0.1879	0.74	0.88	2657	30	2695	15	2724	12	98
A953	75341	192	90.1	0.83	0.0	0.3672	1.6	6.252	1.8	0.1235	0.91	0.86	2016	27	2012	16	2007	16	100
A954	4307	56	9.3	0.85	0.0	0.1321	1.4	1.238	2.5	0.06797	2.1	0.56	800	11	818	14	868	43	92
A955	10828	180	20.5	0.38	0.2	0.1053	1.5	0.8921	2.4	0.06146	1.8	0.63	645	9	648	11	656	39	98
A956	6323	74	12.8	0.67	0.0	0.1437	1.4	1.383	2.0	0.06982	1.4	0.72	865	11	882	12	923	28	94
A957	18989	314	33.2	0.12	0.0	0.109	1.4	0.9404	1.8	0.06258	1.1	0.80	667	9	673	9	694	23	96
A958	20121	205	33.7	0.32	0.0	0.154	1.4	1.563	1.7	0.07363	1.1	0.79	923	12	956	11	1031	21	90
A959	123896	185	98.8	0.40	b.d.	0.4628	1.4	10.32	1.5	0.1617	0.56	0.93	2452	29	2464	14	2473	9	99
A960	10872	270	21.2	0.34	0.1	0.07362	1.4	0.5997	2.1	0.05908	1.5	0.69	458	6	477	8	570	33	80
A961	6865	221	29.7	0.35	0.0	0.134	2.5	1.206	3.3	0.06526	2.2	0.75	811	19	803	19	783	47	104
A962	103599	123	72.8	0.39	b.d.	0.5111	1.4	12.8	1.5	0.1816	0.56	0.92	2661	30	2665	14	2668	9	100
A963	10971	130	19.7	0.35	0.2	0.1423	1.5	1.315	3.2	0.06704	2.8	0.48	858	12	852	18	839	58	102
A964	218267	325	172.7	0.22	0.2	0.4867	1.3	11.21	1.6	0.167	0.92	0.83	2556	28	2540	15	2528	15	101
A965	26052	446	44.7	0.12	b.d.	0.1032	1.5	0.8839	1.9	0.06214	1.3	0.74	633	9	643	9	679	28	93
A966	131703	168	94.0	0.36	b.d.	0.4833	1.4	12.08	1.6	0.1813	0.63	0.91	2542	30	2611	15	2665	10	95
A967	5223	122	10.4	0.30	b.d.	0.08132	1.4	0.6582	2.3	0.0587	1.8	0.63	504	7	514	9	556	39	91
A968	26044	454	48.8	0.30	0.0	0.1029	1.4	0.8851	1.6	0.06238	0.87	0.84	631	8	644	8	687	19	92
A969	7850	158	18.2	0.89	0.3	0.08733	1.4	0.7043	2.0	0.05849	1.4	0.72	540	7	541	8	548	30	98
A970	177114	210	114.5	0.16	0.0	0.5018	1.5	12.6	1.6	0.1822	0.57	0.93	2621	31	2651	15	2673	9	98
A971	4880	49	9.3	0.65	b.d.	0.1616	1.5	1.627	2.3	0.073	1.8	0.64	966	14	981	15	1014	36	95
A972	12200	487	31.2	0.68	0.1	0.05366	1.5	0.393	2.8	0.05312	2.3	0.53	337	5	337	8	334	53	101
A973	7660	134	15.5	0.48	0.4	0.1048	1.5	0.8921	3.1	0.06176	2.7	0.48	642	9	647	15	666	57	96
A974	37488	50	36.3	1.16	b.d.	0.4975	1.4	11.79	1.7	0.1719	0.94	0.83	2603	30	2588	16	2576	16	101
A975	43223	797	76.3	0.56	0.5	0.08156	1.8	0.6788	2.3	0.06036	1.3	0.81	505	9	526	9	617	29	82
A976	10941	237	20.7	0.26	b.d.	0.08539	1.4	0.7011	2.9	0.05955	2.6	0.47	528	7	539	12	587	56	90
A977	11075	287	21.9	0.19	0.1	0.07693	1.5	0.6069	2.0	0.05722	1.3	0.75	478	7	482	8	500	29	96
A978	22209	545	36.3	0.06	0.8	0.06934	1.5	0.551	2.2	0.05763	1.7	0.66	432	6	446	8	516	37	84
A979	16740	294	31.4	0.26	0.0	0.1038	1.4	0.8954	1.8	0.06258	1.2	0.76	637	8	649	9	694	25	92
A980	3937	51	6.4	0.29	0.3	0.1193	1.7	1.08	2.9	0.06563	2.3	0.60	727	12	744	15	795	49	91
A981	6669	236	14.2	0.35	0.2	0.05626	1.6	0.4246	2.2	0.05473	1.6	0.71	353	5	359	7	401	35	88
A982	4785	214	10.1	0.38	1.0	0.04335	1.4	0.314	3.4	0.05254	3.1	0.41	274	4	277	8	309	70	88
A988	8374	79	14.1	0.50	1.0	0.1566	1.4	1.539	2.4	0.07125	2	0.58	938	12	946	15	965	40	97
A989	31389	465	74.7	0.94	0.1	0.1247	1.4	1.123	1.7	0.06532	0.92	0.84	758	10	765	9	785	19	97
A990	5548	67	10.3	0.49	b.d.	0.135	1.5	1.255	2.4	0.06744	1.9	0.61	816	11	826	14	851	40	96
A991	3336	176	8.9	0.55	0.4	0.04489	1.5	0.3226	2.9	0.05213	2.4	0.54	283	4	284	7	291	55	97
A992	34403	300	54.6	0.28	0.1	0.1739	1.4	1.773	1.7	0.07394	1	0.81	1034	13	1036	11	1040	21	99
A993	103070	145	85.3	0.60	0.0	0.4759	1.5	10.83	1.6	0.165	0.63	0.92	2510	31	2509	15	2508	11	100
A994	21746	199	38.9	0.55	0.0	0.1692	1.4	1.717	2.0	0.07363	1.4	0.71	1008	13	1015	13	1031	28	98
A995	22682	199	42.1	0.71	0.0	0.173	1.5	1.746	2.1	0.07317	1.5	0.70	1029	14	1026	14	1019	30	101
A996	41644	803	78.0	0.19	0.0	0.0977	1.4	0.8194	1.6	0.06083	0.83	0.86	601	8	608	7	633	18	95
A997	8860	362	19.3	0.29	0.1	0.05149	1.4	0.3772	2.1	0.05313	1.5	0.69	324	5	325	6	334	34	97
A998	172106	205	127.5	0.49	0.0	0.5162	1.4	12.98	1.5	0.1824	0.59	0.92	2683	30	2678	14	2674	10	100
A999	16704	303	23.0	0.08	2.9	0.07473	1.5	0.5915	3.0	0.0574	2.6	0.49	465	7	472	11	507	58	92
A1000	91570	248	90.6	0.44	0.2	0.3151	1.4	5.254	1.6	0.1209	0.72	0.89	1766	22	1861	13	1970	13	90
A1001	16247	402	28.1	0.05	0.1	0.07435	1.4	0.5859	2.5	0.05715	2	0.56	462	6	468	9	497	45	93
A1002	27807	271	59.1	0.73	b.d.	0.1803	1.5	1.85	1.7	0.07443	0.87	0.86	1069	14	1064	11	1053	17	101
A1003	13611	541	30.0	0.32	0.0	0.05325	1.4	0.3948	1.8	0.05377	1.2	0.74	334	4	338	5	361	28	93
A1004	11644	446	21.1	0.29	0.8	0.04463	1.5	0.3222	2.5	0.05236	2	0.61	281	4	284	6	301	45	93
A1005	179760	518	188.0	0.10	0.1	0.3584	1.3	6.037	1.6	0.1222	0.86	0.84	1974	23	1981	14	1988	15	99
A1006	42627	769	77.2	0.27	0.0	0.09631	1.4	0.8146	1.5	0.06134	0.69	0.89	593	8	605	7	651	15	91
A1007	8233	125	14.9	0.28	0.1	0.1147	1.5	1.001	5.0	0.06331	4.7	0.29	700	10	704	25	719	101	97
A1008	46140	807	83.0	0.17	0.0	0.1038	1.4	0.8858	1.7	0.06189	1	0.80	637	8	644	8	670	22	95
A1009	13527	359	25.8	0.25	b.d.	0.07021	1.4	0.5702	2.6	0.0589	2.2	0.53	437	6	458	10	564	49	78
A1010	5868	97	13.2	1.00	0.6	0.1013	1.7	0.8365	3.8	0.05988	3.3	0.46	622	10	617	18	599	72	104
A1011	7733	142	16.6	0.67	0.5	0.0967	1.5	0.7981	2.6	0.05986	2.1	0.58	595	9	596	12	598	46	99
A1012	289518	367	276.2	1.34	b.d.	0.5	1.4	12.19	1.5	0.1768	0.54	0.93	2614	29	2619	14	2623	9	100
A1013	5979	103	10.5	0.14	0.1	0.1038	1.5	0.873	2.5	0.06102	2.1	0.58	636	9	637	12	640	45	99
A1014	4878	82	29.2	1.33	0.7	0.3399	2.4	5.477	3.2	0.1169	2.1	0.76	1886	40	1897	28	1909	37	99
A1015	59782	179	83.8	1.16	0.1	0.3285	1.4	5.196	1.6	0.1147	0.75	0.88	1831	22	1852	14	1876	13	98
A1016	13009	252	24.3	0.16	0.2	0.09769	1.5	0.8004	2.0	0.05942	1.3	0.75	601	8	597	9	583	28	103
A1017	35967	413	61.7	0.35	0.1	0.1396	1.4	1.307	1.8	0.06791	1.2	0.75	842	11	849	11	866	25	97
A1018	9357	166	21.6	0.77	0.3	0.1047	1.4	0.879	2.0	0.06086	1.5	0.68	642	8	640	10	634	32	101
A1019	6025	55	11.3	0.74	0.3	0.1658	1.6	1.637	2.7	0.07164	2.2	0.59	989	14	985	17	976	44	101
A1020	161997	410	156.7	0.30	0.0	0.35	1.3	6.021	1.5	0.1248	0.62	0.91	1935	22	1979	13	2026	11	96
A1021	19446	369	38.0	0.35	0.2	0.09617	1.4	0.797	1.9	0.06011	1.3	0.72	592	8	595	9	607	29	97

A1022	17924	305	31.7	0.27	0.3	0.09867	1.4	0.8215	2.1	0.06038	1.5	0.68	607	8	609	10	617	33	98
A1023	12916	120	21.6	0.36	0.2	0.1665	1.4	1.66	2.1	0.07232	1.5	0.68	993	13	993	13	995	31	100
A1024	4539	161	10.0	0.38	0.3	0.05786	1.5	0.4372	2.6	0.05481	2.1	0.57	363	5	368	8	404	47	90
A1025	17960	727	38.4	0.28	0.3	0.05096	1.4	0.3741	1.9	0.05325	1.3	0.72	320	4	323	5	339	30	94
A1026	12372	336	23.9	0.11	0.2	0.07377	1.4	0.5688	1.9	0.05593	1.2	0.74	459	6	457	7	449	28	102
A1027	16775	187	32.9	0.69	0.0	0.1462	1.4	1.386	1.9	0.06875	1.2	0.75	880	12	883	11	891	26	99
A1028	31672	419	62.6	0.59	b.d.	0.1284	1.4	1.184	1.8	0.0669	1.2	0.76	779	10	793	10	835	25	93
A1029	6260	108	12.8	0.51	0.2	0.1056	1.4	0.9001	2.6	0.0618	2.2	0.54	647	9	652	13	667	47	97
A1030	17880	401	65.5	1.94	0.0	0.08868	1.4	0.7531	1.7	0.0616	1	0.79	548	7	570	8	660	22	83
A1031	4629	82	11.0	0.94	0.2	0.103	1.6	0.8722	3.0	0.06143	2.5	0.53	632	9	637	14	654	54	97
A1032	56105	660	108.8	0.66	0.0	0.1347	1.4	1.265	1.6	0.06815	0.73	0.89	814	11	830	9	873	15	93
A1033	41168	441	68.9	0.21	b.d.	0.1543	1.3	1.49	1.5	0.07001	0.69	0.89	925	12	926	9	929	14	100
A1034	16404	156	29.5	0.25	b.d.	0.1825	1.4	1.895	1.6	0.07531	0.89	0.84	1080	14	1079	11	1077	18	100
A1035	39208	100	48.5	0.98	0.0	0.3588	1.4	6.052	1.7	0.1223	0.86	0.85	1977	24	1983	14	1990	15	99
BB [g]	18314	746	66.3	0.11	0.09	0.09203	1.9	0.7496	2.6	0.05907	1.4	0.82	568	10	568	11	570	30	100
Ples. [g]	18680	1443	75	0.08	0.76	0.05401	1.7	0.3963	2.1	0.05322	1.0	0.80	339	5	339	6	338	23	100
91500 [g]	25044	71	14	0.45	1.01	0.1807	1.4	1.8462	3.4	0.07412	2.6	0.46	1070	13	1062	22	1044	53	103

Spot size = 33 and 50 µm, respectively; depth of crater ~15µm. $^{206}Pb/^{238}U$ error is the quadratic additions of the within run precision (2 SE) and the external reproducibility (2 SD) of the reference zircon. $^{207}Pb/^{206}Pb$ error propagation (^{207}Pb signal dependent) following Gerdes & Zeh (2009). $^{207}Pb/^{235}U$ error is the quadratic addition of the $^{207}Pb/^{206}Pb$ and $^{206}Pb/^{238}U$ uncertainty.

[a] Within run background-corrected mean ^{207}Pb signal in cps (counts per second).

[b] U and Pb content and Th/U ratio were calculated relative to GJ-1 reference zircon.

[c] percentage of the common Pb on the ^{206}Pb. b.d. = below dectection limit.

[d] corrected for background, within-run Pb/U fractionation (in case of $^{206}Pb/^{238}U$) and common Pb using Stacy and Kramers (1975) model Pb composition and subsequently normalised to GJ-1 (ID-TIMS value/measured value); $^{207}Pb/^{235}U$ calculated using $^{207}Pb/^{206}Pb/(^{238}U/^{206}Pb*1/137.88)$

[e] rho is the $^{206}Pb/^{238}U/^{207}Pb/^{235}U$ error correlation coefficient.

[f] degree of concordance = $^{206}Pb/^{238}U$ age / $^{207}Pb/^{206}Pb$ age x 100

[g] Accuracy and reproducibilty was checked by repeated analyses (n = 30) of reference zircon Plesovice, BB and 91500; data given as mean with 2 standard deviation uncertainties

Kasimlar Formation

grain		^{207}Pb (cps)	U^b (ppm)	Pb^b (ppm)	$\frac{Th}{U}^b$	^{206}Pbc (%)	$\frac{^{206}Pb}{^{238}U}^d$	±2σ (%)	$\frac{^{207}Pb}{^{235}U}^d$	±2σ (%)	$\frac{^{207}Pb}{^{206}Pb}^d$	±2σ (%)	rho[e]	$\frac{^{206}Pb}{^{238}U}$	±2σ (Ma)	$\frac{^{207}Pb}{^{235}U}$	±2σ (Ma)	$\frac{^{207}Pb}{^{206}Pb}$	±2σ (Ma)	conc. (%)
A292	**K.12.78**	3110	106	12.2	1.65	0.2	0.0884	1.6	0.7199	3.6	0.05906	3.3	0.44	546	8	551	16	569	71	96
A293		8868	204	30.0	1.32	0.3	0.1207	1.6	1.065	2.3	0.06403	1.8	0.66	734	11	736	12	742	37	99
A294		7912	232	26.7	1.10	0.1	0.09803	1.5	0.8257	2.3	0.06109	1.7	0.65	603	9	611	11	642	37	94
A295		1846	88	9.1	0.68	2.7	0.09173	2.3	0.7458	4.1	0.05896	3.3	0.57	566	13	566	18	566	72	100
A296		115719	278	138.5	0.16	0.2	0.4771	1.4	11.00	1.6	0.1672	0.71	0.90	2515	30	2523	15	2530	12	99
A297		5813	157	18.1	0.80	0.0	0.1043	1.4	0.8858	2.3	0.06162	1.8	0.62	639	9	644	11	661	39	97
A298		4355	117	13.9	0.89	0.4	0.1053	1.6	0.8748	3.6	0.06024	3.3	0.44	646	10	638	17	612	71	105
A299		2913	76	9.9	0.92	b.d.	0.1150	1.7	1.012	3.4	0.06383	2.9	0.50	702	11	710	17	736	62	95
A300		10483	136	22.1	1.02	0.4	0.1403	1.6	1.284	2.4	0.06638	1.7	0.68	846	13	839	14	818	36	103
A301		12658	345	36.7	0.37	0.2	0.1058	1.4	0.8984	2	0.0616	1.4	0.70	648	9	651	10	660	31	98
A302		1934	163	6.9	0.54	0.2	0.04086	1.6	0.2901	4.9	0.0515	4.6	0.32	258	4	259	11	263	107	98
A303		4662	134	18.8	2.14	0.8	0.09879	1.5	0.8069	4	0.05923	3.7	0.38	607	9	601	18	576	80	106
A304		190375	316	197.7	0.75	0.0	0.5204	1.4	14.51	1.5	0.2022	0.62	0.92	2701	31	2784	15	2844	10	95
A305		48181	89	55.9	0.86	b.d.	0.5232	1.4	13.70	1.8	0.1899	1	0.81	2713	31	2729	17	2742	17	99
A306		4371	197	14.2	0.55	0.2	0.06908	1.5	0.5349	3.1	0.05616	2.7	0.48	431	6	435	11	459	61	94
A307		11747	355	39.1	0.85	0.2	0.09921	1.4	0.8162	2.3	0.05967	1.8	0.61	610	8	606	11	591	40	103
A308		5163	149	14.7	0.54	0.9	0.09249	1.5	0.7506	3.2	0.05886	2.9	0.46	570	8	569	14	562	62	101
A309		10687	208	29.5	0.55	0.3	0.1347	1.4	1.244	2.1	0.06696	1.6	0.67	815	11	821	12	837	33	97
A310		6555	201	19.5	0.50	0.4	0.09374	1.5	0.7736	2.5	0.05985	1.9	0.62	578	8	582	11	598	42	97
A311		7200	112	18.9	0.43	0.4	0.1643	1.7	1.614	3.1	0.07125	2.7	0.53	981	15	976	20	965	54	102
A312		3336	103	14.1	2.41	1.1	0.09429	1.6	0.7727	4.3	0.05944	4	0.37	581	9	581	19	583	86	100
A313		1219	23	3.3	0.69	0.8	0.1328	1.9	1.217	5.8	0.06648	5.5	0.32	804	14	809	33	822	115	98
A314		175679	1395	157.5	1.51	20.1	0.05851	3.1	0.4438	7.6	0.05501	7	0.41	367	11	373	24	413	155	89
A315		10943	195	14.7	0.64	17.0	0.05513	2.4	0.4424	12	0.05819	11	0.20	346	8	372	37	537	248	64
A316		4699	168	16.0	1.06	0.4	0.08099	1.6	0.6385	3.1	0.05718	2.6	0.53	502	8	501	12	498	58	101
A317		5913	83	22.4	2.95	0.7	0.1706	1.7	1.677	3.6	0.07128	3.2	0.46	1016	16	1000	23	966	65	105
A318		3224	50	8.3	0.69	0.3	0.1498	1.6	1.482	3.1	0.07174	2.7	0.52	900	14	923	19	979	55	92
A319		4424	290	15.5	0.68	0.2	0.04992	1.5	0.3711	3.3	0.05393	3	0.44	314	4	321	9	368	67	85
A320		47270	93	65.2	1.92	0.1	0.4964	1.4	12.71	1.7	0.1857	0.94	0.84	2598	31	2659	16	2705	15	96
A321		14160	482	43.4	0.52	0.4	0.08581	1.4	0.6911	2.4	0.05841	2	0.58	531	7	533	10	545	43	97
A322		43754	111	62.1	0.94	b.d.	0.4729	1.7	10.64	1.8	0.1633	0.8	0.90	2496	35	2493	17	2490	13	100
A323		12661	289	33.5	0.44	1.4	0.1111	1.5	0.961	3	0.06273	2.5	0.51	679	10	684	15	699	54	97
A324		2319	92	8.7	1.25	0.6	0.07457	1.8	0.5786	3.3	0.05627	2.7	0.56	464	8	464	12	463	60	100
A325		20070	568	72.3	1.34	0.1	0.1045	1.4	0.8892	2.2	0.0617	1.7	0.64	641	9	646	11	664	36	97
A326		7341	107	20.3	0.91	0.2	0.1673	1.5	1.705	2.7	0.07392	2.3	0.55	997	14	1010	18	1039	46	96
A327		5427	113	17.4	1.01	0.1	0.1350	1.5	1.250	2.5	0.06717	2.1	0.58	816	11	823	14	843	43	97
A333		1432	78	3.7	0.81	4.3	0.04097	1.9	0.3011	7.1	0.05329	6.9	0.27	259	5	267	17	341	156	76
A334		6241	159	16.9	0.10	0.2	0.1119	1.4	0.9664	2.4	0.06266	1.9	0.60	684	9	687	12	697	41	98
A335		4668	104	17.6	2.13	0.7	0.1169	1.7	0.9943	4.1	0.06167	3.7	0.41	713	11	701	21	663	79	108
A336		7415	172	22.2	0.53	0.1	0.1244	1.6	1.100	2.1	0.06414	1.5	0.73	756	11	754	11	746	31	101
A337		4570	119	14.7	0.83	0.4	0.1116	1.5	0.9796	2.9	0.06366	2.5	0.50	682	10	693	15	730	53	93
A338		33982	563	120.9	1.90	11.7	0.1627	1.8	1.664	13	0.07419	13	0.14	972	16	995	86	1047	260	93
A339		38236	100	54.9	1.17	0.3	0.4382	1.8	9.614	2	0.1591	1.1	0.86	2343	35	2399	19	2446	18	96
A340		2745	189	10.5	0.76	0.0	0.0514	1.5	0.375	3.9	0.05292	3.6	0.39	323	5	323	11	325	82	99
A341		1628	42	4.9	1.00	0.4	0.1009	2.1	0.842	3.7	0.06054	3	0.56	620	12	620	17	623	66	99
A342		69899	178	90.2	0.69	0.0	0.4443	1.4	10.14	1.6	0.1655	0.84	0.86	2370	28	2447	15	2513	14	94

A343	27278	131	60.0	1.96	0.0	0.3339	1.3	5.319	1.6	0.1155	0.92	0.82	1857	22	1872	14	1888	17	98
A344	3978	88	11.8	0.60	0.2	0.1266	1.6	1.137	2.8	0.06516	2.3	0.55	768	11	771	15	780	49	99
A345	3442	100	14.1	2.34	0.1	0.09836	1.5	0.8309	3.2	0.06127	2.8	0.47	605	9	614	15	649	61	93
A346	53516	253	96.8	1.22	2.0	0.3054	1.5	4.838	2.3	0.1149	1.8	0.63	1718	22	1791	20	1878	33	91
A347	3867	223	14.0	0.69	0.3	0.05873	1.5	0.4305	3.4	0.05317	3	0.44	368	5	364	10	336	69	109
A348	5237	109	17.1	1.13	0.1	0.1346	1.5	1.221	2.7	0.06582	2.3	0.55	814	12	810	15	801	48	102
A349	19179	92	33.1	0.66	0.0	0.3276	1.5	5.227	1.9	0.1157	1.3	0.76	1827	24	1857	17	1891	23	97
A350	6823	234	21.4	0.71	b.d.	0.08726	1.6	0.7404	2.5	0.06154	1.9	0.66	539	9	563	11	658	40	82
A351	36831	627	100.5	0.66	0.1	0.1496	1.4	1.451	1.7	0.07033	1.1	0.78	899	11	910	10	938	22	96
A352	3799	73	11.3	0.41	0.1	0.1514	1.8	1.435	3.3	0.06877	2.8	0.55	909	15	904	20	892	57	102
A353	7280	240	22.8	0.63	0.9	0.08909	1.5	0.7105	2.8	0.05784	2.4	0.53	550	8	545	12	524	52	105
A354	50591	854	145.7	0.68	0.2	0.1592	1.4	1.551	1.9	0.07068	1.3	0.73	952	12	951	12	948	26	100
A355	14887	226	53.3	2.11	0.2	0.1713	1.4	1.704	2.2	0.07213	1.7	0.65	1019	13	1010	14	990	34	103
A356	6672	192	17.8	0.38	0.1	0.09218	1.5	0.7580	2.3	0.05964	1.7	0.66	568	8	573	10	591	38	96
A357	252335	415	253.2	0.53	0.0	0.5306	1.3	15.16	1.4	0.2072	0.58	0.91	2744	29	2825	14	2884	9	95
A358	4992	137	15.4	0.46	0.3	0.1098	1.4	0.9083	2.7	0.05997	2.4	0.49	672	9	656	13	603	52	111
A359	1572	49	6.0	1.43	0.3	0.09803	1.9	0.8066	4	0.05967	3.5	0.48	603	11	601	18	592	75	102
A360	8118	114	21.6	0.67	0.3	0.1765	1.5	1.776	2.4	0.07298	1.9	0.61	1048	14	1037	16	1013	38	103
A361	4363	206	15.1	0.49	0.6	0.07243	1.5	0.5606	2.6	0.05614	2.1	0.58	451	7	452	9	458	47	98
A362	5813	22	10.2	1.09	0.5	0.3810	1.6	6.489	2.6	0.1235	2.1	0.62	2081	29	2044	24	2008	37	104
A363	35165	76	63.5	3.62	0.5	0.4788	1.4	11.37	2	0.1722	1.4	0.71	2522	29	2554	19	2579	23	98
A364	100157	402	147.2	0.61	0.4	0.3293	1.6	5.951	2	0.1311	1.1	0.81	1835	26	1969	17	2113	20	87
A365	5978	84	24.7	3.86	0.0	0.1657	1.5	1.714	2.4	0.07503	1.9	0.63	988	14	1014	15	1069	37	92
A366	2720	237	11.3	1.48	0.5	0.03842	1.7	0.2707	3.7	0.05111	3.3	0.46	243	4	243	8	246	75	99
A367	12931	194	34.1	0.92	1.0	0.1544	1.4	1.453	2.9	0.06827	2.6	0.48	925	12	911	18	877	53	106
A368	1973	91	6.1	0.58	0.7	0.06436	1.7	0.4997	4.7	0.05631	4.4	0.35	402	7	411	16	464	98	87
A369	5352	207	19.6	0.98	0.1	0.08274	1.5	0.657	2.7	0.05759	2.2	0.56	512	7	513	11	514	49	100
A370	14983	506	61.2	1.03	1.9	0.1100	1.5	0.9703	3.7	0.06396	3.4	0.39	673	9	689	19	740	72	91
A371	30655	502	95.6	1.33	0.3	0.1578	1.4	1.537	2.1	0.07063	1.6	0.64	945	12	945	13	947	33	100
A372	155	93	9.5	0.85	0.8	0.08868	8.5	0.7088	9.3	0.05797	3.8	0.91	548	45	544	40	529	83	104
A373	7739	112	26.9	2.30	0.7	0.1674	1.5	1.633	3.1	0.07074	2.7	0.49	998	14	983	20	950	56	105
A374	21801	58	35.9	2.18	0.1	0.4377	1.6	9.57	1.8	0.1586	0.9	0.87	2340	31	2394	17	2441	15	96
A375	61736	160	84.9	1.55	0.0	0.3942	1.6	8.808	1.8	0.162	0.89	0.87	2142	29	2318	17	2477	15	86
A376	6871	203	23.4	0.93	0.3	0.1024	1.4	0.848	2.8	0.06004	2.5	0.50	629	9	624	13	605	53	104
A377	43495	988	127.5	0.42	0.0	0.1283	1.6	1.168	1.8	0.06603	0.82	0.89	778	11	786	10	807	17	96
A378	7709	114	20.3	0.59	0.2	0.1687	1.7	1.703	2.4	0.07321	1.7	0.71	1005	16	1010	16	1020	34	99
A379	96356	465	172.9	0.67	0.6	0.3354	1.6	5.358	2	0.1159	1.2	0.81	1864	26	1878	17	1893	21	98
A380	28292	231	60.2	0.53	0.1	0.2452	1.4	3.204	1.8	0.09478	1.1	0.79	1413	18	1458	14	1524	21	93
A381	4753	136	15.5	0.85	0.5	0.1028	1.5	0.8452	2.9	0.05965	2.5	0.51	631	9	622	13	591	54	107
A382	19653	331	55.4	0.66	0.1	0.1554	1.4	1.518	1.8	0.07088	1.1	0.79	931	12	938	11	954	23	98
A388	24980	450	79.6	0.76	b.d.	0.1626	1.4	1.585	1.6	0.07068	0.85	0.85	971	13	964	10	948	17	102
A389	47413	244	92.7	1.26	3.0	0.3092	1.7	4.686	2.9	0.1099	2.4	0.57	1737	25	1765	25	1798	44	97
A390	2303	65	8.0	1.24	1.2	0.1016	1.6	0.8181	5.3	0.05841	5	0.31	624	10	607	25	545	110	114
A391	11049	168	34.2	1.46	0.0	0.1621	1.5	1.661	2	0.07433	1.3	0.75	969	13	994	13	1050	26	92
A392	7924	125	19.8	0.19	0.3	0.1626	1.5	1.591	2.4	0.07095	1.8	0.64	971	14	967	15	956	37	102
A393	57799	570	73.7	0.27	3.1	0.1168	1.9	1.935	3.2	0.1201	2.5	0.60	712	13	1093	21	1958	45	36
A394	11487	309	36.4	0.37	0.1	0.1182	1.4	1.032	2.3	0.06334	1.8	0.62	720	10	720	12	720	38	100
A395	42870	173	82.8	1.64	0.3	0.3631	1.3	6.148	1.6	0.1228	0.87	0.84	1997	23	1997	14	1997	15	100
A396	73121	208	88.9	0.45	0.3	0.3875	1.4	8.902	1.6	0.1666	0.72	0.89	2111	26	2328	15	2524	12	84
A397	10835	305	31.4	0.30	0.2	0.1043	1.4	0.8829	2	0.06137	1.5	0.68	640	8	643	10	652	32	98
A398	4125	135	13.4	0.84	1.3	0.08896	1.6	0.7015	4.2	0.05719	3.9	0.38	549	8	540	18	499	86	110
A399	20832	190	46.8	0.67	0.2	0.2271	1.4	2.737	2	0.08738	1.4	0.70	1319	17	1338	15	1369	27	96
A400	221610	587	273.2	0.26	0.0	0.4411	1.3	9.929	1.5	0.1632	0.62	0.91	2356	27	2428	14	2489	10	95
A401	56297	1054	121.0	0.63	1.2	0.1015	2.3	0.9165	3.1	0.06551	2.1	0.75	623	14	661	15	791	43	79
A402	7407	108	22.0	1.20	0.5	0.1703	1.5	1.692	2.7	0.07206	2.3	0.55	1014	14	1005	18	988	46	103
A403	15170	221	37.8	0.82	0.0	0.1541	1.6	1.618	2.1	0.07618	1.3	0.78	924	14	977	13	1100	26	84
A404	14981	196	45.3	1.52	0.3	0.1854	1.5	1.945	2.5	0.0761	2.1	0.58	1096	15	1097	17	1098	41	100
A405	15543	462	47.3	0.36	0.3	0.1023	1.7	0.8465	2.2	0.06003	1.4	0.78	628	10	623	10	605	29	104
A406	30607	137	71.1	2.22	0.3	0.3658	1.4	5.974	1.9	0.1184	1.3	0.73	2010	25	1972	17	1933	24	104
A407	4199	81	11.7	0.66	0.3	0.1341	1.5	1.227	4.1	0.06639	3.8	0.37	811	12	813	23	819	79	99
A408	139931	513	282.5	0.39	0.7	0.5105	1.6	12.73	2.8	0.1808	2.3	0.56	2659	34	2660	27	2660	39	100
A409	8955	124	25.7	1.20	0.0	0.1729	1.5	1.804	2.3	0.07565	1.7	0.67	1028	15	1047	15	1086	34	95
A410	7330	111	19.0	0.42	0.3	0.1664	1.5	1.649	2.4	0.07183	1.9	0.63	992	14	989	15	981	38	101
A411	64305	312	114.2	0.78	0.0	0.3269	1.3	5.396	1.5	0.1197	0.73	0.88	1824	21	1884	13	1952	13	93
A412	5209	470	20.7	1.12	0.4	0.03771	1.4	0.2629	3.5	0.05057	3.2	0.41	239	3	237	7	221	73	108
Felix [g]	7816	600	76.5	2.87	0.31	0.08115	2.3	0.6438	4.4	0.05754	3.1	0.57	503.0	11.3	504.6	17.5	512	68	99
Ples. [g]	9451	1185	60	0.14	0.22	0.05360	1.8	0.3961	3.2	0.05359	1.9	0.68	337	6	339	9	354	42	95
91500 [g]	11681	70	13	0.46	0.20	0.1774	1.3	1.8341	2.1	0.07500	1.5	0.66	1053	12	1058	14	1068	30	99

Spot size = 33 and 50 µm, respectively; depth of crater ~15µm. $^{206}Pb/^{238}U$ error is the quadratic additions of the within run precision (2 SE) and the external reproducibility (2 SD) of the reference zircon. $^{207}Pb/^{206}Pb$ error propagation (^{207}Pb signal dependent) following Gerdes & Zeh (2009). $^{207}Pb/^{235}U$ error is the quadratic addition of the $^{207}Pb/^{206}Pb$ and $^{206}Pb/^{238}U$ uncertainty.

[a] Within run background-corrected mean ^{207}Pb signal in cps (counts per second).

[b] U and Pb content and Th/U ratio were calculated relative to GJ-1 reference zircon.

[c] percentage of the common Pb on the ^{206}Pb. b.d. = below dectection limit.

[d] corrected for background, within-run Pb/U fractionation (in case of $^{206}Pb/^{238}U$) and common Pb using Stacy and Kramers (1975) model Pb composition and subsequently normalised to GJ-1 (ID-TIMS value/measured value); $^{207}Pb/^{235}U$ calculated using $^{207}Pb/^{206}Pb/(^{238}U/^{206}Pb*1/137.88)$

[e] rho is the $^{206}Pb/^{238}U/^{207}Pb/^{235}U$ error correlation coefficient.

[f] degree of concordance = $^{206}Pb/^{238}U$ age / $^{207}Pb/^{206}Pb$ age x 100

[g] Accuracy and reproducibilty was checked by repeated analyses (n = 13) of reference zircon Plesovice, Felix and 91500; data given as mean with 2 standard deviation uncertainties

Guvercinlik Formation

grain		$^{207}Pb^{a}$ (cps)	U^{b} (ppm)	Pb^{b} (ppm)	$\frac{Th^{b}}{U}$	$^{206}Pbc^{c}$ (%)	$\frac{^{206}Pb^{d}}{^{238}U}$	±2σ (%)	$\frac{^{207}Pb^{d}}{^{235}U}$	±2σ (%)	$\frac{^{207}Pb^{d}}{^{206}Pb}$	±2σ (%)	rho[e]	$\frac{^{206}Pb}{^{238}U}$	±2σ (Ma)	$\frac{^{207}Pb}{^{235}U}$	±2σ (Ma)	$\frac{^{207}Pb}{^{206}Pb}$	±2σ (Ma)	conc. (%)
A1177	K.13.104	298594	638	246.9	1.09	b.d.	0.2692	2.1	6.487	2.2	0.1748	0.86	0.92	1537	28	2044	20	2604	14	59
A1178		26878	351	47.5	0.12	1.9	0.1242	1.7	2.135	2.2	0.1247	1.3	0.80	755	12	1160	15	2025	24	37
A1179		37115	56	29.1	0.31	b.d.	0.4603	1.5	10.44	1.7	0.1644	0.71	0.90	2441	31	2474	16	2502	12	98
A1180		8138	207	17.6	0.43	0.2	0.07839	1.4	0.6262	3.5	0.05794	3.1	0.41	487	7	494	14	527	69	92
A1181		20816	665	33.7	0.22	2.7	0.04838	1.6	0.3504	4.5	0.05253	4.2	0.36	305	5	305	12	308	95	99
A1182		5208	224	11.9	0.40	0.2	0.0491	1.6	0.3565	2.5	0.05267	1.9	0.63	309	5	310	7	314	44	98
A1183		8146	365	18.7	0.35	0.1	0.048	1.6	0.3493	2.5	0.05278	1.9	0.64	302	5	304	6	319	43	95
A1184		119254	268	108.0	0.19	0.1	0.3843	1.5	6.872	1.6	0.1297	0.65	0.91	2096	26	2095	14	2094	11	100
A1185		22831	793	40.5	0.27	1.5	0.04786	1.5	0.3469	3.1	0.05257	2.7	0.49	301	4	302	8	310	62	97
A1186		20296	388	34.0	0.67	2.1	0.0751	1.5	0.5809	3.1	0.0561	2.7	0.48	467	7	465	12	456	60	102
A1187		18721	327	32.3	0.05	0.1	0.1052	1.5	0.8915	1.9	0.06145	1.1	0.80	645	9	647	9	655	24	98
A1188		7537	260	17.0	0.44	0.7	0.05897	1.5	0.4462	2.8	0.05487	2.3	0.54	369	5	375	9	407	52	91
A1189		18147	369	37.1	0.31	0.2	0.0953	2.1	0.7798	2.5	0.05935	1.4	0.84	587	12	585	11	580	30	101
A1190		3124	104	7.1	0.35	0.0	0.06407	1.5	0.5049	2.8	0.05715	2.3	0.55	400	6	415	10	498	52	80
A1191		23058	346	35.2	0.21	2.5	0.0957	1.5	0.8039	2.4	0.06093	1.9	0.60	589	8	599	11	637	41	93
A1192		30462	78	30.9	0.41	0.1	0.3523	1.5	5.975	1.7	0.123	0.84	0.87	1945	25	1972	15	2000	15	97
A1193		41925	106	37.7	0.08	0.0	0.3535	1.7	6.211	1.9	0.1274	0.78	0.91	1951	29	2006	17	2063	14	95
A1194		17819	361	40.7	0.49	0.1	0.1004	1.8	0.8414	2.2	0.06078	1.2	0.83	617	11	620	10	632	26	98
A1195		12509	437	27.6	0.37	0.0	0.05864	1.5	0.4504	2.0	0.05571	1.4	0.73	367	5	378	6	441	30	83
A1196		104524	378	99.3	0.28	0.0	0.2417	1.4	4.082	1.6	0.1225	0.69	0.90	1396	18	1651	13	1992	12	70
A1197		17215	469	32.1	0.07	b.d.	0.07242	1.5	0.5808	1.8	0.05817	0.97	0.84	451	6	465	7	536	21	84
A1198		48098	158	21.3	0.24	39.7	0.05348	3.6	0.4244	14.4	0.05756	14	0.25	336	12	359	45	513	307	65
A1199		18800	403	35.1	0.11	0.1	0.09008	1.5	0.7287	1.9	0.05867	1.1	0.82	556	8	556	8	555	24	100
A1206		93232	251	96.1	0.32	0.0	0.3611	1.5	6.085	1.6	0.1222	0.61	0.92	1987	26	1988	14	1989	11	100
A1207		2092	82	4.4	0.29	0.6	0.0507	1.7	0.385	5.0	0.05508	4.7	0.34	319	5	331	14	415	104	77
A1208		2617	55	5.5	0.54	0.5	0.0864	1.6	0.7351	3.7	0.06171	3.3	0.43	534	8	560	16	664	72	80
A1209		6734	99	13.2	0.64	b.d.	0.1114	1.7	1.027	2.2	0.06687	1.4	0.75	681	11	718	11	834	30	82
A1210		63675	158	70.4	0.53	0.1	0.3793	1.7	6.7	1.9	0.1281	0.82	0.90	2073	30	2073	17	2072	14	100
A1211		14338	157	27.2	0.57	0.0	0.1508	1.5	1.451	1.9	0.06981	1.2	0.79	905	12	910	11	923	24	98
A1212		1901	35	4.6	0.95	b.d.	0.1005	1.7	0.8664	3.0	0.06251	2.5	0.55	617	10	634	14	692	54	89
A1213		6879	49	9.7	0.09	0.0	0.2085	1.5	2.502	2.2	0.08701	1.6	0.68	1221	16	1273	16	1361	30	90
A1214		5159	213	11.7	0.38	0.1	0.05037	1.6	0.3683	3.1	0.05303	2.6	0.53	317	5	318	8	330	59	96
A1215		9669	194	13.3	0.41	5.8	0.05698	1.7	0.4244	4.1	0.05403	3.8	0.40	357	6	359	13	372	85	96
A1216		11659	39	13.5	0.45	0.8	0.2996	1.6	4.586	2.2	0.111	1.5	0.73	1689	23	1747	18	1816	27	93
A1217		18066	713	37.8	0.26	0.4	0.05143	1.7	0.3781	2.1	0.05332	1.3	0.79	323	5	326	6	342	30	94
A1218		158126	216	114.4	0.14	0.0	0.4966	1.4	11.99	1.5	0.1751	0.55	0.93	2599	31	2604	15	2607	9	100
A1219		10080	418	22.9	0.28	0.1	0.05299	1.6	0.3873	2.0	0.05302	1.3	0.77	333	5	332	6	330	30	101
A1220		2659	83	4.2	0.75	3.3	0.03733	1.8	0.3425	4.9	0.06655	4.6	0.37	236	4	299	13	824	95	29
A1221		21334	62	24.9	0.51	b.d.	0.3438	1.5	5.647	2.3	0.1191	1.7	0.65	1905	24	1923	20	1943	31	98
A1222		29558	259	51.5	0.51	0.1	0.1755	1.5	1.799	1.8	0.07437	0.96	0.84	1042	14	1045	12	1051	19	99
A1223		15572	316	35.1	0.61	0.0	0.09496	1.6	0.7886	2.0	0.06023	1.3	0.78	585	9	590	9	612	27	96
A1224		122693	330	126.3	0.26	0.0	0.3559	1.5	6.028	1.6	0.1229	0.64	0.92	1963	25	1980	14	1998	11	98
A1225		12570	176	22.7	0.26	0.2	0.1244	1.5	1.119	2.0	0.06527	1.3	0.76	756	11	763	11	783	28	96
A1226		6655	117	12.3	0.26	0.0	0.1027	1.5	0.8917	2.3	0.06296	1.7	0.68	630	9	647	11	707	35	89
A1227		4347	95	10.3	0.64	b.d.	0.0904	1.6	0.7537	2.5	0.06047	2	0.62	558	8	570	11	620	42	90
A1228		1841	100	4.9	0.85	0.7	0.03894	2.0	0.2869	5.3	0.05342	4.8	0.39	246	5	256	12	347	110	71
A1229		3329	146	7.6	0.31	0.1	0.05002	1.5	0.3638	3.3	0.05275	2.9	0.46	315	5	315	9	318	67	99
A1230		16621	397	32.4	0.21	0.1	0.08106	1.7	0.6537	2.1	0.05849	1.2	0.83	502	8	511	8	548	25	92
A1231		156933	692	205.8	0.17	0.3	0.2894	1.5	4.748	1.7	0.119	0.65	0.92	1639	22	1776	14	1941	12	84
A1232		11881	452	25.4	0.33	0.1	0.05348	1.9	0.4059	2.3	0.05505	1.4	0.80	336	6	346	7	414	31	81
A1238		20024	399	45.6	0.64	0.1	0.09634	1.6	0.7921	2.0	0.05963	1.3	0.78	593	9	592	9	590	27	100
A1239		8568	173	18.0	0.41	0.1	0.09588	1.6	0.7956	2.1	0.06018	1.4	0.73	590	9	594	10	610	31	97
A1240		2405	46	6.1	1.06	0.0	0.09897	1.6	0.8775	3.2	0.0643	2.8	0.50	608	9	640	16	752	59	81
A1241		176467	252	137.7	0.42	0.1	0.4676	1.4	11.21	1.5	0.1738	0.57	0.93	2473	29	2541	14	2595	10	95
A1242		47862	167	57.1	0.41	0.1	0.3064	1.5	4.755	1.7	0.1125	0.73	0.90	1723	23	1777	14	1841	13	94
A1243		110420	298	117.9	0.34	0.0	0.3638	1.5	6.189	1.6	0.1234	0.58	0.93	2000	25	2003	14	2006	10	100
A1244		24944	373	48.9	0.40	0.1	0.1206	1.5	1.065	1.8	0.06405	1	0.83	734	10	736	10	743	22	99
A1245		4948	167	10.9	0.31	b.d.	0.06287	1.5	0.4874	2.3	0.05623	1.7	0.66	393	6	403	8	461	38	85
A1246		2729	110	6.1	0.45	0.2	0.05037	1.5	0.3902	3.4	0.05619	3	0.45	317	5	335	10	460	67	69
A1247		17702	597	39.6	0.20	0.0	0.06683	1.5	0.5102	1.8	0.05537	0.99	0.83	417	6	419	6	427	22	98
A1248		9659	239	18.5	0.23	0.0	0.07639	1.6	0.6131	2.1	0.05821	1.4	0.75	475	7	486	8	538	30	88
A1249		3553	73	4.9	0.28	5.1	0.05904	1.7	0.4366	4.9	0.05364	4.6	0.35	370	6	368	15	356	104	104
A1250		95929	271	106.1	0.47	0.0	0.3404	1.4	5.645	1.6	0.1203	0.68	0.90	1889	24	1923	14	1960	12	96
A1251		68365	316	90.6	0.22	0.0	0.277	1.6	4.525	1.8	0.1185	0.92	0.86	1576	22	1735	15	1933	16	82
A1252		16715	158	30.9	0.77	4.9	0.1625	1.7	1.628	3.9	0.07265	3.5	0.45	971	16	981	25	1004	70	97
A1253		23469	460	49.1	0.40	0.1	0.09844	1.4	0.821	1.9	0.06049	1.2	0.76	605	8	609	9	621	27	97
A1254		12971	255	18.8	0.29	4.3	0.06543	1.5	0.4962	3.5	0.055	3.2	0.43	409	6	409	12	412	71	99
A1255		11472	220	29.5	1.05	0.1	0.09988	1.5	0.8344	2.0	0.06059	1.3	0.77	614	9	616	9	625	28	98
A1256		15737	582	28.6	0.27	1.8	0.04595	1.4	0.3437	2.6	0.05424	2.2	0.55	290	4	300	7	381	50	76
A1257		10984	164	21.3	0.33	0.2	0.1229	1.9	1.096	2.4	0.06467	1.5	0.77	747	13	751	13	764	32	98
A1258		6331	122	13.3	0.51	0.1	0.09583	1.5	0.8034	2.4	0.0608	1.9	0.61	590	8	599	11	632	41	93
A1259		47269	66	37.5	0.63	1.5	0.4465	1.5	11.07	1.7	0.1798	0.95	0.84	2380	29	2529	16	2651	16	90
A1260		25002	240	51.0	1.07	b.d.	0.1552	1.4	1.568	1.8	0.07323	1.1	0.80	930	12	957	11	1020	22	91
A1261		10710	129	20.2	0.53	0.0	0.1365	1.6	1.388	2.4	0.07374	1.8	0.67	825	13	884	15	1034	37	80
A1262		4400	174	11.6	0.68	0.1	0.05631	1.5	0.4171	2.7	0.05372	2.3	0.55	353	5	354	8	359	51	98
A1263		11752	110	21.1	0.47	0.1	0.1709	1.5	1.724	1.8	0.07315	1.1	0.81	1017	14	1017	12	1018	22	100
A1264		3926	80	7.9	0.43	0.5	0.08889	1.6	0.7319	2.6	0.05971	2	0.60	549	8	558	11	593	44	93
A1265		4117	90	8.9	0.53	0.3	0.08742	1.6	0.7168	2.5	0.05947	1.9	0.64	540	8	549	11	584	42	92
A1266		20902	826	46.0	0.34	0.6	0.05212	1.5	0.3851	2.1	0.05359	1.5	0.70	328	5	331	6	354	34	93
A1272		82863	235	93.4	0.39	0.1	0.3559	1.5	5.949	1.7	0.1212	0.73	0.90	1963	26	1968	15	1974	13	99
A1273		26820	61	27.9	0.54	0.2	0.381	1.6	7.055	1.9	0.1343	1.1	0.83	2081	29	2118	17	2155	19	97

A1274	20072	545	44.8	0.30	0.2	0.07943	1.5	0.6217	1.9	0.05677	1.2	0.78	493	7	491	7	483	26	102
A1275	21313	550	41.5	0.21	0.0	0.07735	1.5	0.626	1.7	0.05869	0.91	0.85	480	7	494	7	556	20	86
A1276	20482	842	47.9	0.28	0.1	0.05537	1.6	0.4066	1.9	0.05326	1	0.84	347	5	346	5	340	23	102
A1277	6097	273	14.2	0.34	0.1	0.04957	1.5	0.3624	2.6	0.05302	2.1	0.59	312	5	314	7	330	47	95
A1278	2407	45	4.6	0.19	0.3	0.1024	1.7	0.8622	3.5	0.06106	3.1	0.49	629	10	631	17	641	66	98
A1279	328322	451	115.0	0.56	56.8	0.04268	9.1	0.2877	12.6	0.04888	8.7	0.72	269	24	257	29	142	204	189
A1280	3446	60	7.8	0.71	0.5	0.1074	1.7	0.9156	3.2	0.06181	2.7	0.52	658	10	660	16	668	59	99
A1281	9572	180	19.0	0.36	0.2	0.09855	1.6	0.8289	2.4	0.06101	1.9	0.65	606	9	613	11	639	40	95
A1282	17043	714	35.9	0.25	0.8	0.04919	1.5	0.3539	2.1	0.05218	1.5	0.72	310	5	308	6	293	33	105
A1283	8173	579	30.6	0.23	2.4	0.05035	1.6	0.3642	3.2	0.05246	2.8	0.50	317	5	315	9	306	64	104
A1284	73519	87	54.3	0.37	0.2	0.537	1.5	14.15	1.6	0.1911	0.65	0.92	2771	34	2760	16	2752	11	101
A1285	140830	155	103.5	0.60	0.1	0.5302	1.5	14.74	1.6	0.2016	0.62	0.92	2742	33	2799	15	2840	10	97
A1286	4391	190	9.9	0.31	0.4	0.0504	1.6	0.3652	3.1	0.05255	2.7	0.52	317	5	316	9	309	60	102
A1287	25848	67	32.4	1.09	1.4	0.3437	1.6	5.754	2.4	0.1214	1.8	0.67	1905	26	1939	21	1977	31	96
A1288	17185	729	39.7	0.34	0.2	0.05187	1.5	0.3771	2.0	0.05273	1.3	0.74	326	5	325	6	317	30	103
A1289	25017	270	43.1	0.30	0.1	0.1536	1.6	1.481	1.9	0.06993	0.98	0.86	921	14	923	12	926	20	99
A1290	6434	65	11.5	0.50	0.8	0.1542	1.7	1.472	3.1	0.0692	2.7	0.53	925	14	919	19	905	55	102
A1291	13420	267	24.3	0.02	0.1	0.09801	1.5	0.8097	2.0	0.05992	1.4	0.74	603	9	602	9	601	29	100
A1292	21303	212	33.0	0.10	0.0	0.1613	1.7	1.624	2.0	0.07306	1	0.86	964	16	980	13	1016	21	95
A1293	20540	692	44.5	0.25	0.2	0.06349	1.5	0.4726	1.8	0.05398	1.1	0.79	397	6	393	6	370	25	107
A1294	9358	132	18.7	0.51	0.4	0.1252	1.6	1.133	2.5	0.06565	1.9	0.63	760	11	769	13	795	40	96
A1295	5450	113	10.8	0.27	0.2	0.09344	1.6	0.7885	2.7	0.0612	2.2	0.59	576	9	590	12	646	47	89
A1296	7498	136	15.4	0.44	0.5	0.1019	1.5	0.8533	2.3	0.06072	1.8	0.66	626	9	626	11	629	38	99
A1297	161402	420	164.5	0.34	0.2	0.3543	1.6	6.082	1.7	0.1245	0.65	0.93	1955	27	1988	15	2022	11	97
A1298	5631	249	13.2	0.42	0.3	0.04835	1.7	0.3512	2.6	0.05268	2	0.64	304	5	306	7	315	46	97
A1299	5926	233	12.3	0.56	0.0	0.04667	1.5	0.3574	2.4	0.05555	1.8	0.64	294	4	310	6	434	41	68
A1300	48589	451	82.5	0.36	b.d.	0.1725	1.6	1.778	1.8	0.07475	0.89	0.88	1026	15	1037	12	1062	18	97
A1301	7034	89	12.5	0.28	0.1	0.1368	1.5	1.284	2.3	0.06807	1.7	0.68	827	12	839	13	871	35	95
A1307	17473	272	28.6	1.08	4.8	0.07538	1.6	0.5891	5.0	0.05668	4.8	0.32	468	7	470	19	479	105	98
A1308	106398	313	108.9	0.10	0.1	0.345	1.5	5.688	1.6	0.1196	0.76	0.89	1911	24	1930	14	1950	14	98
A1309	149960	428	160.7	0.26	0.1	0.352	1.5	5.887	1.6	0.1213	0.59	0.93	1944	25	1959	14	1975	11	98
A1310	2649	7	4.5	2.26	0.0	0.3528	1.8	6.032	2.8	0.124	2	0.67	1948	31	1981	24	2015	36	97
Griedel [g]	51614	605	15.8	1.95	57.52	0.00412	8.1	0.0274	26.2	0.04809	20.6	0.32	26	2	27	7			
Ples. [g]	10456	734	37	0.13	0.13	0.05393	1.5	0.3959	1.6	0.05324	1.3	0.68	339	5	339	5	339	30	100
91500 [g]	25044	71	14	0.45	1.01	0.1807	1.4	1.8462	3.4	0.07412	2.6	0.46	1070	13	1062	22	1044	53	103

Spot size = 33 and 50 µm, respectively; depth of crater ~15µm. $^{206}Pb/^{238}U$ error is the quadratic additions of the within run precision (2 SE) and the external reproducibility (2 SD) of the reference zircon. $^{207}Pb/^{206}Pb$ error propagation (^{207}Pb signal dependent) following Gerdes & Zeh (2009). $^{207}Pb/^{235}U$ error is the quadratic addition of the $^{207}Pb/^{206}Pb$ and $^{206}Pb/^{238}U$ uncertainty.

[a] Within run background-corrected mean ^{207}Pb signal in cps (counts per second).

[b] U and Pb content and Th/U ratio were calculated relative to GJ-1 reference zircon.

[c] percentage of the common Pb on the ^{206}Pb. b.d. = below dectection limit.

[d] corrected for background, within-run Pb/U fractionation (in case of $^{206}Pb/^{238}U$) and common Pb using Stacy and Kramers (1975) model Pb composition and subsequently normalised to GJ-1 (ID-TIMS value/measured value); $^{207}Pb/^{235}U$ calculated using $^{207}Pb/^{206}Pb/(^{238}U/^{206}Pb*1/137.88)$

[e] rho is the $^{206}Pb/^{238}U/^{207}Pb/^{235}U$ error correlation coefficient.

[f] degree of concordance = $^{206}Pb/^{238}U$ age / $^{207}Pb/^{206}Pb$ age x 100

[g] Accuracy and reproducibilty was checked by repeated analyses (n = 7) of reference zircon Plesovice, Griedel and 91500; data given as mean with 2 standard deviation uncertainties

META-GRANITES

grain		$^{207}Pb_a$ (cps)	Ub (ppm)	Pbb (ppm)	Thb / U	$^{206}Pb_{cc}$ (%)	$^{206}Pb_d/^{238}U$	±2s (%)	$^{207}Pb_d/^{235}U$	±2s (%)	$^{207}Pb_d/^{206}Pb$	±2s (%)	rhoe	$^{206}Pb/^{238}U$	±2s (Ma)	$^{207}Pb/^{235}U$	±2s (Ma)	$^{207}Pb/^{206}Pb$	±2s (Ma)	conc. (%)
A141	TM.17.33	9908	375	20	0.55	7.1	0.05241	1.6	0.4952	5.8	0.06854	5.6	0.27	329	5	408	20	884	116	37
A142		3782	387	19	0.35	0.0	0.0494	1.2	0.3605	2.7	0.05295	2.4	0.45	311	4	313	7	326	55	95
A143		4871	455	23	0.28	0.0	0.05102	1.3	0.4005	2.5	0.05694	2.2	0.51	321	4	342	7	489	48	66
A144		2969	301	15	0.46	0.0	0.05106	1.3	0.3707	2.5	0.05267	2.1	0.53	321	4	320	7	314	48	102
A145		5367	551	26	0.33	0.0	0.04875	1.3	0.3537	2.3	0.05263	1.9	0.55	307	4	307	6	312	43	98
A151		12699	1265	61	0.13	0.0	0.0494	1.2	0.3657	1.8	0.05371	1.3	0.68	311	4	316	5	358	30	87
A152		5198	531	27	0.47	0.0	0.05102	1.2	0.3716	2.4	0.05285	2	0.52	321	4	321	6	322	46	100
A153		3934	372	18	0.36	0.0	0.0483	2.3	0.3491	3.3	0.05244	2.3	0.70	304	7	304	9	304	53	100
A154		3647	393	19	0.37	0.0	0.04861	1.3	0.3443	2.3	0.0514	1.9	0.56	306	4	300	6	258	43	119
A155		4479	393	20	0.32	0.3	0.05072	1.3	0.3696	3.1	0.05286	2.8	0.42	319	4	319	9	322	64	99
A156		3950	193	9	0.40	0.2	0.04888	1.9	0.3535	3.8	0.05246	3.3	0.50	308	6	307	10	305	75	101
A157		2451	259	13	0.62	0.0	0.04979	1.4	0.362	3.6	0.05275	3.4	0.38	313	4	314	10	317	76	99
A158		10366	1084	53	0.17	0.0	0.04969	1.2	0.361	1.6	0.0527	1	0.76	313	4	313	4	315	24	99
A159		12890	1343	66	0.26	0.0	0.05002	1.2	0.3681	1.7	0.05338	1.2	0.71	315	4	318	5	344	27	91
A160		4963	500	25	0.57	0.0	0.05119	1.2	0.3712	2.2	0.0526	1.8	0.56	322	4	321	6	311	42	103
A161		14735	1524	80	0.20	0.0	0.05355	1.3	0.3896	1.8	0.05278	1.2	0.73	336	4	334	5	319	27	106
A162		4254	453	22	0.40	0.0	0.04875	1.2	0.3493	2.1	0.05197	1.8	0.56	307	4	304	6	284	41	108
A163		5268	517	25	0.34	0.0	0.05003	1.3	0.3613	2.6	0.05239	2.3	0.48	315	4	313	7	302	52	104
A164		1632	164	8	0.41	b.d.	0.04968	1.3	0.3599	2.9	0.05256	2.6	0.46	313	4	312	8	309	58	101
A165		6190	650	33	0.47	0.0	0.05193	1.2	0.3767	2.2	0.05262	1.9	0.55	326	4	325	6	312	42	105
A166		8974	955	46	0.39	0.0	0.04947	1.2	0.3599	1.9	0.05278	1.4	0.66	311	4	312	5	319	32	98
A167		3240	353	17	0.40	0.0	0.04964	1.2	0.3641	2.6	0.05321	2.3	0.46	312	4	315	7	337	53	93
A168		2874	297	15	0.57	0.0	0.05067	1.3	0.3649	2.9	0.05224	2.5	0.46	319	4	316	8	295	58	108
A169		2667	285	14	0.60	0.0	0.04906	1.5	0.3526	3.2	0.05215	2.9	0.45	309	4	307	9	291	66	106
A170		5128	541	25	0.38	0.0	0.04782	1.2	0.3437	2.0	0.05215	1.6	0.61	301	4	300	5	291	36	103
A171		5584	536	26	0.57	0.0	0.04982	1.4	0.3592	2.3	0.0523	1.7	0.64	313	4	312	6	298	40	105
A172		7047	751	37	0.10	0.0	0.04977	1.3	0.3651	1.7	0.05322	1.2	0.74	313	4	316	5	338	26	93
A173		18176	1803	96	0.58	0.0	0.05391	2.0	0.3958	2.4	0.05327	1.2	0.86	338	7	339	7	340	27	100
A174		2991	299	15	0.28	0.0	0.04979	1.3	0.3657	3.2	0.05329	2.9	0.40	313	4	316	9	340	66	92

A175	26680	3116	146	0.28	0.1	0.04764	1.2	0.3469	1.5	0.05283	0.96	0.78	300	4	302	4	321	22	93
A176	5920	458	29	0.41	0.0	0.06407	1.2	0.491	2.3	0.0556	2	0.52	400	5	406	8	436	45	92
A177	4368	469	23	0.32	0.0	0.04985	1.3	0.3661	2.6	0.05328	2.3	0.49	314	4	317	7	340	51	92
A178	5381	515	24	0.33	0.4	0.04772	1.4	0.3414	1.9	0.0519	1.3	0.72	300	4	298	5	280	30	107
A179	2593	274	14	0.42	0.0	0.05051	1.4	0.3677	2.8	0.05282	2.4	0.49	318	4	318	8	320	56	99
A180	9444	1006	50	0.18	0.0	0.05089	2.4	0.3699	3.1	0.05273	1.9	0.79	320	8	320	8	317	43	101
A181	9507	1033	51	0.27	0.0	0.04999	1.2	0.3622	1.7	0.05256	1.3	0.69	314	4	314	5	309	29	102
A182	6193	673	33	0.22	0.0	0.04968	1.7	0.3618	2.2	0.05283	1.5	0.75	313	5	314	6	321	34	97
A183	4123	448	22	0.41	0.0	0.04991	1.3	0.3636	2.7	0.05284	2.3	0.50	314	4	315	7	321	53	98
A184	9804	1045	53	0.25	0.0	0.05146	1.2	0.3809	1.9	0.0537	1.5	0.64	324	4	328	5	358	33	90
A185	3634	387	19	0.57	0.0	0.0489	1.2	0.3547	2.5	0.05263	2.1	0.50	308	4	308	7	312	49	99
A186	2771	299	15	0.48	0.0	0.04954	1.4	0.3627	2.6	0.05312	2.2	0.52	312	4	314	7	333	51	94
BB-16 g	8991	623	55.9	0.25	0.00	0.0913	2.8	0.7463615	2.6	0.05929	1.6	0.82	563	15	566.1	11.4	576.9	34.2	97.7
Ples. g	8536	1109	55.4	0.09	0.00	0.0534	3.6	0.3937154	4.1	0.05351	1.5	0.81	335	12	337.1	11.6	350.0	34.7	96.0
91500 g	11140	142	26.7	0.35	1.51	0.17992	2.0	1.8447	2.0	0.07439	2.0	0.79	1066	20	1061.5	13	1051.4	39.1	99.1

Spot size = 30 µm; depth of crater ~15µm. 206Pb/238U error is the quadratic additions of the within run precision (2 SE) and the external reproducibility 2 SD) of the reference zircon. 207Pb/206Pb error propagation (207Pb signal dependent) following Gerdes & Zeh (2009). 207Pb/235U error is the quadratic addition of the 207Pb/206Pb and 206Pb/238U uncertainty.

[a] Within run background-corrected mean 207Pb signal in cps (counts per second).

[b] U and Pb content and Th/U ratio were calculated relative to GJ-1 reference zircon.

[c] percentage of the common Pb on the 206Pb. b.d. = below dectection limit.

[d] corrected for background, within-run Pb/U fractionation (in case of 206Pb/238U) and common Pb using Stacy and Kramers (1975) model Pb composition and subsequently normalised to GJ-1 (ID-TIMS value/measured value); 207Pb/235U calculated using 207Pb /206Pb/(238U/206Pb*1/137.88).

[e] rho is the 206Pb/238U /207Pb/235U error correlation coefficient.

grain	$^{207}Pb^{a}$ (cps)	U^{b} (ppm)	Pb^{b} (ppm)	$\frac{Th^{b}}{U}$	$^{206}Pbc^{c}$ (%)	$\frac{^{206}Pb^{d}}{^{238}U}$	±2σ (%)	$\frac{^{207}Pb^{d}}{^{235}U}$	±2σ (%)	$\frac{^{207}Pb^{d}}{^{206}Pb}$	±2σ (%)	rho[e]	$\frac{^{206}Pb}{^{238}U}$	±2σ (Ma)	$\frac{^{207}Pb}{^{235}U}$	±2σ (Ma)	$\frac{^{207}Pb}{^{206}Pb}$	±2σ (Ma)	conc. (%)
A548 TM.17.34	3029	214	11	0.90	0.00	0.05061	0.9	0.3659	3.1	0.05245	2.9	0.30	318	3	317	8	304	66	105
A554	18197	1321	61	0.20	0.00	0.04698	0.9	0.3404	1.3	0.05256	0.93	0.70	296	3	297	3	309	21	96
A555	10795	728	38	0.18	0.00	0.05313	0.8	0.3854	1.3	0.05262	1.1	0.59	334	3	331	4	312	24	107
A556	9324	631	32	0.28	0.00	0.05099	0.8	0.3753	1.7	0.0534	1.5	0.46	321	2	324	5	345	33	93
A557	4941	354	18	0.80	0.00	0.05025	0.7	0.3714	2.2	0.05363	2.1	0.33	316	2	321	6	355	47	89
A558	3695	262	13	0.60	0.00	0.05067	0.8	0.3661	2.4	0.05241	2.3	0.32	319	2	317	7	303	52	105
A559	3300	238	11	0.66	0.01	0.04899	0.9	0.3591	2.6	0.05318	2.5	0.33	308	3	312	7	336	56	92
A560	3493	255	13	0.34	0.00	0.05094	0.8	0.367	1.9	0.05227	1.7	0.45	320	3	317	5	296	38	108
A561	4679	335	16	0.55	0.00	0.04861	0.8	0.3526	1.8	0.05263	1.5	0.47	306	2	307	5	312	35	98
A562	2142	153	7	0.52	0.00	0.04974	1.0	0.3667	2.7	0.05349	2.5	0.36	313	3	317	7	349	57	90
A563	7003	462	23	0.26	0.01	0.04996	0.7	0.3627	1.8	0.05267	1.6	0.39	314	2	314	5	314	37	100
A564	3481	229	12	0.41	0.00	0.05136	1.3	0.3788	2.5	0.05351	2.2	0.52	323	4	326	7	350	49	92
A565	4268	332	17	0.77	0.00	0.05095	0.9	0.3668	2.4	0.05223	2.3	0.38	320	3	317	7	295	52	109
A566	2707	173	9	0.32	0.05	0.05208	0.9	0.3852	2.3	0.05366	2.1	0.40	327	3	331	7	356	48	92
A567	2680	187	9	0.76	0.00	0.04954	0.8	0.3602	2.6	0.05275	2.5	0.29	312	2	312	7	318	58	98
A568	3886	279	14	0.67	0.00	0.04981	0.9	0.3591	2.4	0.0523	2.2	0.38	313	3	312	6	298	50	105
A569	6241	456	22	0.53	0.00	0.0493	0.9	0.3537	1.9	0.05206	1.6	0.48	310	3	308	5	287	37	108
A570	8977	632	31	0.22	0.00	0.05035	0.9	0.3629	2.0	0.05229	1.7	0.47	317	3	314	5	298	39	106
A571	4707	321	16	0.31	0.01	0.05014	0.9	0.3627	1.9	0.05248	1.7	0.45	315	3	314	5	306	39	103
A572	5127	346	18	0.34	0.04	0.05137	0.9	0.3781	2.3	0.05339	2.1	0.38	323	3	326	6	345	48	94
A573	4002	319	16	0.38	0.00	0.05204	0.8	0.3781	2.2	0.05271	2.1	0.35	327	2	326	6	316	47	104
A574	10499	722	37	0.29	0.00	0.05168	2.3	0.373	2.8	0.05237	1.7	0.81	325	7	322	8	301	38	108
A575	4006	280	14	0.32	b.d.	0.04965	0.8	0.3648	2.0	0.0533	1.8	0.41	312	3	316	5	341	41	92
A576	2213	157	8	0.47	b.d.	0.05082	0.9	0.3722	2.4	0.05312	2.2	0.37	320	3	321	7	333	51	96
A577	2523	188	9	0.68	0.00	0.05024	0.9	0.3639	3.1	0.05255	3	0.28	316	3	315	9	309	69	102
A578	11764	408	21	0.15	0.83	0.05332	1.4	0.3934	2.0	0.05353	1.4	0.70	335	5	337	6	351	32	95
A579	15222	1152	55	0.17	0.00	0.04888	0.8	0.3589	1.5	0.05327	1.2	0.54	308	2	311	4	340	28	91
A580	10698	765	37	0.30	0.00	0.04875	0.8	0.355	1.4	0.05284	1.1	0.60	307	3	309	4	321	26	96
A581	6040	426	21	0.34	0.00	0.05099	0.7	0.3681	1.9	0.05237	1.8	0.35	321	2	318	5	301	40	106
A582	11123	798	39	0.34	0.00	0.05024	0.7	0.3656	1.6	0.05279	1.4	0.48	316	2	316	4	319	31	99
A583	155192	108																	
A584	8213	178	22	1.09	0.00	0.1256	0.9	1.15	1.7	0.06638	1.5	0.54	763	7	777	9	818	31	93
A585	2851	205	10	0.85	0.00	0.049	1.0	0.3533	2.6	0.05232	2.4	0.37	308	3	307	7	299	56	103
A586	2928	207	10	0.49	0.00	0.05125	0.8	0.3714	2.3	0.05257	2.2	0.33	322	2	321	6	310	50	104
A587	5351	388	19	0.60	0.00	0.0501	0.8	0.3615	2.4	0.05235	2.2	0.35	315	3	313	6	300	51	105
A588	5238	372	18	0.28	0.00	0.05037	0.7	0.3689	2.1	0.05312	1.9	0.35	317	2	319	6	333	44	95
A589	7024	455	23	0.25	0.02	0.05144	0.8	0.3797	1.8	0.05355	1.7	0.43	323	2	327	5	351	37	92
A590	8655	640	30	0.24	0.00	0.04844	1.0	0.3462	2.0	0.05184	1.7	0.52	305	3	302	5	278	38	110
A591	2847	207	10	0.35	1.17	0.04874	0.9	0.3502	3.8	0.05212	3.7	0.23	307	3	305	10	290	84	106
A592	1602	111	6	0.67	0.01	0.0517	1.1	0.3705	3.6	0.05199	3.4	0.31	325	4	320	10	284	78	114
A593	4169	299	15	0.55	0.00	0.05047	0.9	0.3662	2.3	0.05265	2.1	0.39	317	3	317	6	313	48	101
A594	3380	244	12	0.25	0.01	0.0501	0.7	0.3572	2.4	0.05172	2.2	0.31	315	2	310	6	272	51	116
BB-16 g	9506	295	26.9	0.30	0.00	0.0913	1.2	0.7438154	2.5	0.05912	1.8	0.61	563	6	564.6	11.0	570.7	39.6	98.8
Ples. g	8662	502	25.3	0.09	0.01	0.0537	3.3	0.3939231	3.8	0.05321	1.3	0.63	337	11	337.2	10.8	336.9	30.5	100.3
91500 g	10236	56	10.4	0.32	1.78	0.18002	2.2	1.8702	2.0	0.07536	1.5	0.53	1067	22	1070.5	13	1077.6	29.3	99.0

Spot size = 30 µm; depth of crater ~15µm. 206Pb/238U error is the quadratic additions of the within run precision (2 SE) and the external reproducibility 2 SD) of the reference zircon. 207Pb/206Pb error propagation (207Pb signal dependent) following Gerdes & Zeh (2009). 207Pb/235U error is the quadratic addition of the 207Pb/206Pb and 206Pb/238U uncertainty.
[a] Within run background-corrected mean 207Pb signal in cps (counts per second).
[b] U and Pb content and Th/U ratio were calculated relative to GJ-1 reference zircon.
[c] percentage of the common Pb on the 206Pb. b.d. = below dectection limit.
[d] corrected for background, within-run Pb/U fractionation (in case of 206Pb/238U) and common Pb using Stacy and Kramers (1975) model Pb composition and subsequently normalised to GJ-1 (ID-TIMS value/measured value); 207Pb/235U calculated using 207Pb /206Pb/(238U/206Pb*1/137.88).
[e] rho is the 206Pb/238U /207Pb/235U error correlation coefficient.

grain		$^{207}Pb_a$ (cps)	Ub (ppm)	Pbb (ppm)	Thb/U	$^{206}Pb_{cc}$ (%)	$^{206}Pb_d/^{238}U$	±2s (%)	$^{207}Pb_d/^{235}U$	±2s (%)	$^{207}Pb_d/^{206}Pb$	±2s (%)	rhoe	$^{206}Pb/^{238}U$	±2s (Ma)	$^{207}Pb/^{235}U$	±2s (Ma)	$^{207}Pb/^{206}Pb$	±2s (Ma)	conc. (%)
A157	TM.17.35	18576	329	35	0.39	0.2	0.1088	0.9	0.9399	1.7	0.0627	1.5	0.54	666	6	673	9	697	31	95
A158		5605	245	12	0.15	1.6	0.05141	1.2	0.3711	2.1	0.05236	1.7	0.58	323	4	320	6	300	39	108
A159		26581	1294	65	0.10	0.0	0.05138	1.0	0.3723	1.3	0.05257	0.89	0.73	323	3	321	4	310	20	104
A160		6985	205	15	0.28	0.3	0.07323	1.0	0.5734	1.7	0.05681	1.4	0.60	456	5	460	6	484	31	94
A161		17870	855	42	0.06	0.0	0.04969	0.9	0.3623	1.5	0.05289	1.1	0.62	313	3	314	4	323	26	97
A162		3616	82	8	0.96	0.0	0.09881	1.1	0.8213	2.1	0.0603	1.8	0.52	607	6	609	10	614	39	99
A163		24174	996	59	0.03	0.1	0.06024	0.9	0.4481	1.4	0.05396	1.1	0.63	377	3	376	4	369	24	102
A164		16055	47	15	0.79	0.0	0.3083	3.5	6.636	3.8	0.1562	1.6	0.91	1732	53	2064	34	2414	27	72
A165		9241	461	23	0.29	0.0	0.05008	1.3	0.3687	2.6	0.05341	2.3	0.48	315	4	319	7	346	52	91
A166		4284	106	9	0.64	0.3	0.08638	1.5	0.7069	3.3	0.05937	2.9	0.45	534	8	543	14	580	64	92
A167		10889	496	25	0.01	0.1	0.05209	0.9	0.3831	1.8	0.05335	1.5	0.52	327	3	329	5	343	34	95
A168		28584	1412	80	0.01	0.0	0.05762	0.9	0.4237	1.2	0.05335	0.83	0.74	361	3	359	4	343	19	105
A169		4275	205	10	0.38	0.0	0.05036	1.0	0.3663	2.0	0.05276	1.7	0.53	317	3	317	5	318	39	100
A170		20017	446	43	0.55	0.0	0.09747	1.1	0.8105	1.6	0.06032	1.1	0.71	600	6	603	7	615	24	98
A171		29695	1346	72	0.01	0.1	0.05479	0.9	0.3997	1.4	0.05293	1.1	0.63	344	3	341	4	325	24	106
A172		5688	140	14	0.60	0.0	0.09873	1.2	0.8098	4.6	0.0595	4.4	0.27	607	7	602	21	585	95	104
A173		9175	293	21	0.21	b.d.	0.07363	0.9	0.5694	1.4	0.0561	1.1	0.65	458	4	458	5	456	24	100
A174		42699	1090	88	0.30	0.1	0.08187	1.0	0.6623	1.5	0.05869	1.1	0.66	507	5	516	6	555	24	91
A175		194616	196	122	0.44	0.1	0.5429	1.0	17.69	1.2	0.2364	0.6	0.87	2796	23	2973	11	3095	9	90
A176		95352	169	81	0.49	0.5	0.4409	0.9	10.18	1.1	0.1675	0.67	0.80	2355	18	2451	11	2533	11	93
A177		9320	432	21	0.18	0.0	0.05007	1.0	0.3658	1.7	0.05299	1.4	0.59	315	3	317	5	328	31	96
A178		6529	298	16	0.15	b.d.	0.05301	0.9	0.3923	1.6	0.05368	1.3	0.58	333	3	336	4	357	28	93
A179		13878	651	36	0.44	0.0	0.05582	1.0	0.4134	2.0	0.05373	1.7	0.52	350	4	351	6	359	38	97
A180		21774	765	47	0.23	8.2	0.0625	1.0	0.4768	6.4	0.05535	6.4	0.16	391	4	396	21	426	142	92
A181		8638	195	19	0.67	1.2	0.0997	1.3	0.8251	3.8	0.06004	3.6	0.35	613	8	611	17	604	77	101
A182		12480	602	31	0.41	0.0	0.05305	1.1	0.3853	1.7	0.0527	1.3	0.64	333	4	331	5	315	31	106
A183		51122	817	99	0.46	0.2	0.122	1.2	1.107	1.4	0.06579	0.75	0.84	742	8	757	7	799	16	93
A184		18164	360	35	0.41	b.d.	0.09801	0.9	0.8036	1.4	0.05948	1	0.67	603	5	599	6	584	22	103
A185		2679	135	7	0.69	0.0	0.05155	1.0	0.3719	2.4	0.05233	2.2	0.42	324	3	321	7	299	49	108
A186		16515	517	30	0.24	1.2	0.05954	0.8	0.4473	2.0	0.05451	1.9	0.41	373	3	375	6	391	42	95
A187		12871	386	24	0.14	0.7	0.0625	1.2	0.4691	2.3	0.05445	2	0.50	391	4	391	8	389	45	100
A188		12290	240	24	0.39	0.1	0.1016	0.9	0.843	1.5	0.06022	1.2	0.60	624	5	621	7	611	26	102
A189		15940	302	28	0.31	0.3	0.09234	1.5	0.7565	2.2	0.05943	1.7	0.66	569	8	572	10	582	36	98
A190		3916	165	9	0.13	0.3	0.05471	1.7	0.4083	2.6	0.05414	2	0.63	343	6	348	8	376	46	91
A191		26900	867	81	0.51	0.1	0.09476	2.2	0.7683	2.4	0.05882	0.93	0.92	584	12	579	10	560	20	104
A192		16632	354	36	0.96	0.0	0.1024	0.9	0.8575	1.6	0.06077	1.3	0.56	628	5	629	8	631	29	100
A193		20324	380	39	0.45	0.0	0.1046	1.1	0.8878	1.5	0.06155	1	0.74	642	7	645	7	658	22	97
A199		44965	2123	112	0.01	b.d.	0.05352	1.0	0.3921	1.2	0.05314	0.67	0.82	336	3	336	3	334	15	101
A200		3427	163	9	0.35	0.2	0.05294	1.1	0.3826	2.9	0.05243	2.7	0.39	333	4	329	8	303	61	110
A201		9023	277	14	0.86	0.0	0.05081	1.2	0.3748	1.9	0.05352	1.6	0.60	319	4	323	5	350	35	91
A202		35866	792	70	0.06	0.0	0.089	1.0	0.7363	1.3	0.06002	0.91	0.73	550	5	560	6	604	20	91
BB-16 g		12562	302	27.7	0.29	0.01	0.0909	1.6	0.7388769	1.8	0.05897	0.7	0.57	561	9	561.7	7.9	565.1	16.0	99.3
Ples. g		11154	501	25.3	0.08	0.05	0.0538	1.2	0.3954769	1.4	0.05335	0.8	0.58	338	4	338.4	4.1	343.2	17.2	98.4
91500 g		25512	62	20.2	0.33	3.59	0.17943	2.0	1.8525	2.4	0.07491	1.4	0.51	1064	19	1064.3	16	1065.4	27.9	99.9

Spot size = 30 µm; depth of crater ~15µm. 206Pb/238U error is the quadratic additions of the within run precision (2 SE) and the external reproducibility 2 SD) of the reference zircon. 207Pb/206Pb error propagation (207Pb signal dependent) following Gerdes & Zeh (2009). 207Pb/235U error is the quadratic addition of the 207Pb/206Pb and 206Pb/238U uncertainty.
[a] Within run background-corrected mean 207Pb signal in cps (counts per second).
[b] U and Pb content and Th/U ratio were calculated relative to GJ-1 reference zircon.
[c] percentage of the common Pb on the 206Pb. b.d. = below dectection limit.
[d] corrected for background, within-run Pb/U fractionation (in case of 206Pb/238U) and common Pb using Stacy and Kramers (1975) model Pb composition and subsequently normalised to GJ-1 (ID-TIMS value/measured value); 207Pb/235U calculated using 207Pb /206Pb/(238U/206Pb*1/137.88).
[e] rho is the 206Pb/238U /207Pb/235U error correlation coefficient.

Table 2
LA-MC-ICPMS Lu-Hf isotope data of zircon from sample K.13.75 (Konya Complex)

	$^{176}Yb/^{177}Hf$ [a]	±2σ	$^{176}Lu/^{177}Hf$	±2σ	$^{178}Hf/^{177}Hf$	$^{180}Hf/^{177}Hf$	Sig_{Hf} [b] (V)	$^{176}Hf/^{177}Hf$	±2σ [c]	$^{176}Hf/^{177}Hf_{(t)}$ [c]	εHf(t) [d]	±2σ [c]	T_{DM} [e] (Ga)	age [f] (Ma)	±2σ
seq1															
K.13.75_seq1_6	0.0652	55	0.00166	10	1.46718	1.88663	10	0.282706	24	0.282687	10	0.9	0.69	591	9
K.13.75_seq1_7	0.0349	33	0.00099	8	1.46717	1.88676	13	0.282262	19	0.282250	-4	0.7	1.53	646	22
K.13.75_seq1_8	0.0434	36	0.00121	8	1.46711	1.88666	12	0.282249	19	0.282235	-6	0.7	1.57	607	19
K.13.75_seq1_9	0.0668	55	0.00182	11	1.46716	1.88641	13	0.281693	17	0.281667	-22	0.6	2.60	775	16
K.13.75_seq1_10	0.0406	35	0.00119	8	1.46712	1.88640	14	0.282370	16	0.282347	7	0.6	1.18	1017	28
K.13.75_seq1_11	0.0289	28	0.00076	6	1.46720	1.88683	12	0.282225	18	0.282214	-2	0.6	1.53	804	15
K.13.75_seq1_12	0.0217	18	0.00052	3	1.46719	1.88641	10	0.282505	23	0.282498	6	0.8	1.01	731	22
K.13.75_seq1_13	0.0375	33	0.00104	7	1.46726	1.88622	9	0.282521	27	0.282505	8	1.0	0.96	797	13
K.13.75_seq1_14	0.0154	13	0.00046	3	1.46715	1.88678	13	0.281429	28	0.281414	-8	1.0	2.67	1782	31
K.13.75_seq1_15	0.0215	18	0.00074	5	1.46715	1.88681	16	0.281505	25	0.281492	-25	0.9	2.87	926	12
K.13.75_seq1_16	0.0335	29	0.00094	6	1.46717	1.88658	15	0.282514	17	0.282506	0	0.6	1.11	447	16
K.13.75_seq1_17	0.0462	52	0.00126	12	1.46713	1.88671	12	0.282486	22	0.282465	9	0.8	1.00	893	12
K.13.75_seq1_18	0.0400	37	0.00101	7	1.46723	1.88657	11	0.282595	23	0.282584	6	0.8	0.90	584	17
K.13.75_seq1_19	0.0344	35	0.00088	7	1.46730	1.88627	10	0.282580	29	0.282570	6	1.0	0.92	595	31
K.13.75_seq1_20	0.0136	11	0.00041	3	1.46719	1.88666	9	0.281979	19	0.281973	-11	0.7	2.01	784	19
K.13.75_seq1_21	0.0294	38	0.00075	7	1.46722	1.88697	13	0.282557	19	0.282550	3	0.7	1.00	505	11
K.13.75_seq1_22	0.0306	26	0.00074	5	1.46719	1.88649	12	0.282406	20	0.282397	2	0.7	1.22	685	48
K.13.75_seq1_23	0.0424	36	0.00108	7	1.46716	1.88711	12	0.282006	20	0.281990	-10	0.7	1.97	803	14
K.13.75_seq1_24	0.0315	32	0.00086	7	1.46725	1.88657	13	0.281588	25	0.281572	-20	0.9	2.69	1004	11
K.13.75_seq1_25	0.0428	34	0.00115	7	1.46720	1.88683	13	0.282008	19	0.281995	-14	0.7	2.03	611	19
K.13.75_seq1_26	0.0204	43	0.00035	6	1.46719	1.88650	20	0.281438	22	0.281425	-3	0.8	2.54	2013	34
K.13.75_seq1_27	0.1223	113	0.00245	17	1.46716	1.88688	16	0.282562	28	0.282525	9	1.0	0.92	807	16
K.13.75_seq1_28	0.0314	118	0.00069	22	1.46722	1.88609	14	0.281876	19	0.281868	-20	0.7	2.29	572	11
K.13.75_seq1_29	0.0104	15	0.00030	4	1.46723	1.88680	13	0.281836	21	0.281831	-13	0.7	2.22	940	15
K.13.75_seq1_30	0.0208	25	0.00049	5	1.46720	1.88665	15	0.282171	17	0.282166	-8	0.6	1.70	634	13
K.13.75_seq1_31	0.0738	60	0.00197	12	1.46723	1.88632	14	0.282412	19	0.282395	-3	0.7	1.31	474	11
K.13.75_seq1_39	0.0261	43	0.00062	8	1.46718	1.88600	16	0.281807	27	0.281800	-21	0.9	2.41	616	15
K.13.75_seq1_40	0.0199	23	0.00062	7	1.46721	1.88706	13	0.282457	15	0.282448	6	0.5	1.07	810	10
K.13.75_seq1_41	0.0244	21	0.00065	5	1.46721	1.88645	13	0.282572	17	0.282562	10	0.6	0.84	812	17
K.13.75_seq1_42	0.0141	17	0.00033	3	1.46715	1.88644	14	0.281158	15	0.281144	-8	0.5	3.00	2212	23
K.13.75_seq1_43	0.0317	33	0.00077	6	1.46725	1.88669	12	0.282606	20	0.282596	8	0.7	0.85	635	11
K.13.75_seq1_44	0.0654	56	0.00161	11	1.46719	1.88635	9	0.281417	22	0.281339	6	0.8	2.47	2524	14
K.13.75_seq1_45	0.0340	28	0.00089	5	1.46721	1.88661	13	0.282282	18	0.282272	-5	0.6	1.50	604	12
K.13.75_seq1_46	0.0563	129	0.00130	22	1.46717	1.88640	13	0.281920	17	0.281894	-8	0.6	2.06	1037	42
K.13.75_seq1_47	0.0934	78	0.00253	17	1.46716	1.88620	11	0.282573	22	0.282529	12	0.8	0.86	924	19
K.13.75_seq1_48	0.0322	30	0.00088	6	1.46717	1.88700	12	0.282390	20	0.282375	5	0.7	1.19	867	15
K.13.75_seq1_49	0.0720	61	0.00202	13	1.46721	1.88678	14	0.281528	22	0.281454	-4	0.8	2.53	1923	15
K.13.75_seq1_50	0.0455	39	0.00120	8	1.46719	1.88617	12	0.282261	22	0.282247	-5	0.8	1.54	617	14
K.13.75_seq1_51	0.1315	186	0.00282	31	1.46721	1.88649	10	0.282394	27	0.282346	5	1.0	1.23	905	15
K.13.75_seq1_52	0.0592	71	0.00137	14	1.46724	1.88601	15	0.282561	18	0.282541	9	0.6	0.90	787	10
K.13.75_seq1_55	0.0282	25	0.00067	4	1.46714	1.88602	14	0.281524	17	0.281499	-1	0.6	2.42	1970	13
K.13.75_seq1_56	0.0928	75	0.00244	15	1.46719	1.88666	11	0.282553	22	0.282526	4	0.8	1.01	588	16
K.13.75_seq1_57	0.0304	26	0.00076	5	1.46721	1.88659	12	0.282086	18	0.282076	-10	0.6	1.85	674	13
K.13.75_seq1_58	0.0163	13	0.00039	2	1.46727	1.88680	11	0.281008	20	0.280989	-7	0.7	3.17	2504	20
K.13.75_seq1_59	0.0179	15	0.00046	3	1.46722	1.88676	12	0.282614	19	0.282609	8	0.7	0.83	626	12
K.13.75_seq1_60	0.0306	25	0.00079	5	1.46715	1.88645	10	0.282360	22	0.282348	2	0.8	1.27	802	11
K.13.75_seq1_61	0.0267	22	0.00072	5	1.46713	1.88663	12	0.281830	19	0.281819	-16	0.7	2.29	814	13
K.13.75_seq1_63	0.0827	77	0.00220	16	1.46719	1.88602	6	0.281978	32	0.281952	-15	1.1	2.11	627	28
K.13.75_seq1_64	0.0359	29	0.00108	7	1.46720	1.88661	12	0.281663	21	0.281642	-18	0.7	2.55	1011	14
K.13.75_seq1_65	0.0612	58	0.00154	12	1.46721	1.88683	10	0.282511	22	0.282487	8	0.8	0.99	815	20
K.13.75_seq1_72	0.0927	79	0.00234	15	1.46716	1.88670	10	0.282727	29	0.282701	10	1.0	0.67	573	10
K.13.75_seq1_73	0.1032	154	0.00216	29	1.46722	1.88605	10	0.282179	29	0.282143	-3	1.0	1.64	883	30
K.13.75_seq1_74	0.0386	31	0.00127	8	1.46720	1.88664	13	0.282387	20	0.282367	5	0.7	1.21	865	12
K.13.75_seq1_75	0.0570	48	0.00188	12	1.46717	1.88718	10	0.282379	18	0.282350	3	0.6	1.25	838	12
K.13.75_seq1_76	0.0520	65	0.00123	13	1.46716	1.88633	12	0.282380	24	0.282363	1	0.9	1.27	730	11
K.13.75_seq1_79	0.0228	33	0.00053	7	1.46720	1.88669	16	0.282264	16	0.282258	-4	0.6	1.50	673	9
K.13.75_seq1_80	0.0241	24	0.00061	6	1.46727	1.88645	11	0.282616	22	0.282607	10	0.8	0.78	747	14
K.13.75_seq1_81	0.0722	219	0.00154	43	1.46722	1.88620	11	0.281283	29	0.281231	-15	1.0	3.03	1767	22
K.13.75_seq1_83	0.0155	13	0.00043	3	1.46719	1.88632	8	0.282139	23	0.282133	-6	0.8	1.71	754	15
K.13.75_seq1_86	0.0131	12	0.00034	3	1.46720	1.88660	11	0.282593	21	0.282589	5	0.7	0.91	537	10
K.13.75_seq1_88	0.0115	9	0.00031	2	1.46721	1.88694	11	0.281350	19	0.281339	-9	0.7	2.77	1885	41
K.13.75_seq1_89	0.0346	48	0.00090	11	1.46723	1.88707	10	0.281410	25	0.281376	-5	0.9	2.66	1977	19
K.13.75_seq1_90	0.0299	25	0.00080	5	1.46723	1.88601	11	0.281882	21	0.281866	-8	0.8	2.09	1079	28
K.13.75_seq1_91	0.0482	50	0.00132	13	1.46719	1.88622	11	0.282157	26	0.282137	-5	0.9	1.68	806	13
K.13.75_seq1_92	0.0219	18	0.00056	4	1.46720	1.88671	10	0.281025	19	0.280998	-6	0.7	3.14	2533	13
K.13.75_seq1_93	0.0293	24	0.00078	5	1.46719	1.88656	13	0.281970	17	0.281961	-15	0.6	2.09	627	9
K.13.75_seq1_94	0.0323	30	0.00103	8	1.46719	1.88663	10	0.281125	18	0.281073	0	0.6	2.93	2655	17
K.13.75_seq1_95	0.0640	69	0.00186	16	1.46719	1.88667	10	0.282642	24	0.282615	11	0.8	0.75	780	12
K.13.75_seq1_96	0.0148	12	0.00038	2	1.46719	1.88667	14	0.281033	17	0.281016	-7	0.6	3.14	2459	10
K.13.75_seq1_97	0.0298	24	0.00075	5	1.46717	1.88662	11	0.281048	20	0.281013	-6	0.7	3.13	2485	11
K.13.75_seq1_98	0.0309	26	0.00091	6	1.46722	1.88663	10	0.281639	19	0.281622	-19	0.7	2.61	972	19
K.13.75_seq1_100	0.0160	14	0.00046	3	1.46717	1.88644	11	0.282513	18	0.282506	8	0.6	0.96	798	17
K.13.75_seq1_101	0.0122	10	0.00032	2	1.46716	1.88655	8	0.282297	22	0.282293	-4	0.8	1.46	605	30
K.13.75_seq1_107	0.0308	25	0.00076	5	1.46721	1.88690	10	0.281283	18	0.281257	-13	0.7	2.96	1811	32
K.13.75_seq1_108	0.0125	11	0.00036	2	1.46718	1.88662	12	0.281706	16	0.281702	-24	0.6	2.59	635	14
K.13.75_seq1_109	0.0681	182	0.00133	28	1.46717	1.88650	15	0.282296	22	0.282281	-4	0.8	1.48	621	11
K.13.75_seq1_110	0.0285	31	0.00057	6	1.46717	1.88641	13	0.282056	20	0.282049	-12	0.7	1.92	623	11
K.13.75_seq1_112	0.0304	24	0.00080	5	1.46717	1.88665	13	0.282576	19	0.282567	6	0.7	0.92	617	10
K.13.75_seq1_113	0.0340	39	0.00087	8	1.46718	1.88674	11	0.281005	20	0.280961	-5	0.7	3.16	2637	13
K.13.75_seq1_114	0.0201	17	0.00051	3	1.46722	1.88695	12	0.282181	17	0.282175	-7	0.6	1.67	650	11
K.13.75_seq1_115	0.0260	22	0.00067	4	1.46723	1.88673	9	0.282306	21	0.282294	4	0.7	1.32	938	17
K.13.75_seq1_116	0.0619	52	0.00170	12	1.46722	1.88651	9	0.282510	23	0.282484	7	0.8	1.00	803	13
K.13.75_seq1_117	0.0249	25	0.00059	5	1.46719	1.88666	11	0.282214	20	0.282207	-7	0.7	1.63	584	8
K.13.75_seq1_118	0.0228	21	0.00059	4	1.46723	1.88624	12	0.282497	22	0.282488	8	0.8	0.99	819	24
K.13.75_seq1_120	0.0194	19	0.00048	4	1.46720	1.88641	13	0.282157	23	0.282148	0	0.8	1.57	1019	32

K.13.75_seq1_121	0.0794	129	0.00215	28	1.46721	1.88681	10	0.282240	25	0.282201	1	0.9	1.49	954	13
K.13.75_seq1_122	0.0151	13	0.00044	3	1.46719	1.88661	17	0.282461	17	0.282457	1	0.6	1.16	556	8
K.13.75_seq1_123	0.0497	46	0.00125	10	1.46724	1.88665	14	0.281472	17	0.281423	-2	0.6	2.53	2048	15
K.13.75_seq1_126	0.1159	106	0.00300	21	1.46723	1.88658	10	0.282232	25	0.282175	1	0.9	1.52	1004	32
K.13.75_seq1_127	0.0201	17	0.00054	3	1.46719	1.88689	10	0.282567	16	0.282560	8	0.6	0.89	718	15
K.13.75_seq1_129	0.0085	8	0.00019	1	1.46720	1.88651	9	0.281102	29	0.281093	-2	1.0	2.94	2551	14
K.13.75_seq1_130	0.0276	23	0.00086	5	1.46721	1.88688	14	0.282613	20	0.282601	11	0.7	0.78	792	18
K.13.75_seq1_131	0.0282	28	0.00075	6	1.46724	1.88615	13	0.282612	19	0.282604	6	0.7	0.86	576	11
K.13.75_seq1_133	0.0286	23	0.00074	5	1.46724	1.88659	14	0.282088	17	0.282073	-2	0.6	1.71	1036	18
K.13.75_seq1_134	0.0585	54	0.00178	15	1.46721	1.88614	12	0.282055	19	0.282021	-5	0.7	1.82	1003	22
K.13.75_seq1_135	0.0000	0	0.00000	0	0.00000	0.00000	0	0.000000	0	0.000000	0	0.0	0.00	534	12
K.13.75_seq1_136	0.0057	5	0.00013	1	1.46717	1.88597	12	0.281838	18	0.281836	-19	0.6	2.33	639	14

LA-MC-ICPMS Lu-Hf isotope data of zircon from sample K.13.102 (Karaburun Melange)

K.13.102_662	0.0600	57	0.00161	12	1.46717	1.88663	8	0.282360	21	0.282350	-8	0.8	1.46	334	5
K.13.102_663	0.0269	22	0.00080	5	1.46711	1.88674	8	0.280750	23	0.280701	-1	0.8	3.40	3193	9
K.13.102_664	0.0216	19	0.00060	5	1.46711	1.88590	7	0.282531	26	0.282526	1	0.9	1.07	449	7
K.13.102_665	0.0370	31	0.00106	7	1.46709	1.88656	8	0.282699	21	0.282687	10	0.8	0.69	599	9
K.13.102_672	0.0151	35	0.00038	9	1.46709	1.88669	10	0.281115	22	0.281096	0	0.8	2.89	2647	10
K.13.102_673	0.0208	17	0.00059	4	1.46714	1.88644	8	0.281479	21	0.281458	-4	0.7	2.53	1889	16
K.13.102_674	0.0443	36	0.00144	9	1.46710	1.88659	9	0.282659	21	0.282641	10	0.7	0.75	659	9
K.13.102_675	0.0542	63	0.00128	15	1.46716	1.88619	11	0.282599	41	0.282589	2	1.4	0.96	408	12
K.13.102_676	0.0164	14	0.00042	3	1.46711	1.88683	10	0.281141	25	0.281120	1	0.9	2.84	2645	10
K.13.102_677	0.0205	16	0.00059	4	1.46712	1.88658	9	0.281066	20	0.281035	0	0.7	2.97	2733	13
K.13.102_678	0.0577	47	0.00161	10	1.46711	1.88620	9	0.281670	27	0.281603	7	0.9	2.12	2167	15
K.13.102_679	0.0288	24	0.00085	5	1.46715	1.88723	9	0.282631	24	0.282624	3	0.9	0.90	395	6
K.13.102_680	0.0231	20	0.00072	5	1.46716	1.88693	10	0.282494	21	0.282486	4	0.7	1.07	642	9
K.13.102_681	0.0271	22	0.00073	5	1.46713	1.88686	9	0.282530	22	0.282525	-1	0.8	1.10	380	6
K.13.102_682	0.0408	41	0.00104	8	1.46712	1.88681	9	0.282555	20	0.282544	5	0.7	0.97	598	10
K.13.102_683	0.0407	39	0.00114	9	1.46711	1.88670	10	0.282520	25	0.282507	4	0.9	1.04	611	11
K.13.102_684	0.0318	26	0.00097	6	1.46715	1.88641	8	0.282658	23	0.282647	8	0.8	0.78	561	9
K.13.102_685	0.0358	31	0.00116	8	1.46719	1.88700	9	0.282375	20	0.282363	-3	0.7	1.35	550	8
K.13.102_687	0.0334	29	0.00102	7	1.46718	1.88638	8	0.282642	23	0.282627	12	0.8	0.73	775	11
K.13.102_688	0.0393	49	0.00114	13	1.46715	1.88671	9	0.282534	24	0.282521	3	0.8	1.03	574	9
K.13.102_689	0.0644	69	0.00179	16	1.46716	1.88704	8	0.282180	27	0.282137	5	0.9	1.49	1254	35
K.13.102_690	0.0194	18	0.00057	4	1.46714	1.88643	9	0.282266	22	0.282260	-6	0.8	1.54	566	9
K.13.102_691	0.0217	18	0.00075	5	1.46717	1.88668	8	0.282562	23	0.282556	1	0.8	1.03	403	6
K.13.102_692	0.0190	17	0.00054	4	1.46717	1.88628	7	0.281082	0	0.000000	0	0.0	0.00	2452	68
K.13.102_693	0.0166	13	0.00048	3	1.46714	1.88649	10	0.281910	24	0.281905	-18	0.9	2.22	584	9
K.13.102_694	0.0237	23	0.00068	5	1.46718	1.88641	8	0.281784	24	0.281777	-23	0.8	2.47	563	9
K.13.102_695	0.0482	48	0.00139	11	1.46715	1.88617	9	0.282610	0	0.000000	0	0.0	0.00	145	5
K.13.102_696	0.0208	18	0.00059	4	1.46720	1.88674	9	0.282658	23	0.282652	8	0.8	0.77	567	9
K.13.102_697	0.0497	49	0.00145	13	1.46713	1.88684	10	0.281002	27	0.280929	-7	1.0	3.24	2600	46
K.13.102_698	0.0151	12	0.00039	2	1.46713	1.88654	9	0.282329	24	0.282325	-2	0.9	1.38	641	10
K.13.102_699	0.0236	20	0.00069	5	1.46718	1.88701	10	0.282500	23	0.282495	-2	0.8	1.16	386	6
K.13.102_700	0.0279	23	0.00089	5	1.46717	1.88681	9	0.282534	27	0.282528	0	1.0	1.09	390	6
K.13.102_701	0.0620	55	0.00171	13	1.46720	1.88711	8	0.280712	24	0.280601	1	0.9	3.50	3396	10
K.13.102_707	0.0418	34	0.00125	8	1.46711	1.88686	9	0.282623	23	0.282609	7	0.8	0.84	597	9
K.13.102_708	0.0025	3	0.00003	0	1.46717	1.88666	10	0.281129	21	0.281127	-3	0.8	2.93	2444	10
K.13.102_709	0.0368	31	0.00109	8	1.46715	1.88656	9	0.282575	0	0.000000	0	0.0	0.00	278	6
K.13.102_710	0.0127	11	0.00033	2	1.46717	1.88615	11	0.280913	20	0.280896	-7	0.7	3.28	2641	12
K.13.102_711	0.0253	21	0.00073	5	1.46712	1.88614	8	0.282577	22	0.282572	1	0.8	1.01	364	6
K.13.102_712	0.0372	30	0.00107	7	1.46714	1.88640	9	0.282271	31	0.282259	-5	1.1	1.52	629	9
K.13.102_713	0.0571	46	0.00150	9	1.46718	1.88650	9	0.281534	26	0.281480	-3	0.9	2.48	1905	10
K.13.102_714	0.0460	37	0.00129	8	1.46717	1.88607	7	0.281845	31	0.281798	9	1.1	1.85	1929	21
K.13.102_715	0.0302	24	0.00082	5	1.46719	1.88706	10	0.282333	20	0.282324	-4	0.7	1.41	568	9
K.13.102_716	0.0370	32	0.00104	7	1.46715	1.88673	8	0.282677	22	0.282670	5	0.8	0.81	388	6
K.13.102_717	0.0363	30	0.00095	6	1.46713	1.88683	10	0.282323	28	0.282310	0	1.0	1.36	756	12
K.13.102_718	0.0203	17	0.00065	4	1.46718	1.88672	9	0.282077	19	0.282067	-8	0.7	1.83	777	12
K.13.102_720	0.0446	37	0.00132	8	1.46716	1.88623	8	0.282635	21	0.282622	6	0.7	0.85	513	8
K.13.102_721	0.0150	12	0.00040	2	1.46719	1.88676	10	0.282149	19	0.282139	6	0.7	1.47	1288	35
K.13.102_722	0.0229	19	0.00066	4	1.46722	1.88649	8	0.282504	24	0.282499	-1	0.9	1.14	397	6
K.13.102_723	0.0382	37	0.00122	10	1.46719	1.88637	11	0.282673	22	0.282659	10	0.8	0.73	630	9
K.13.102_724	0.0793	69	0.00180	14	1.46715	1.88633	13	0.282602	19	0.282589	1	0.7	0.98	378	8
K.13.102_725	0.0382	31	0.00115	7	1.46714	1.88672	10	0.282592	23	0.282583	2	0.8	0.98	396	7
K.13.102_726	0.0121	11	0.00034	2	1.46720	1.88656	11	0.282335	20	0.282331	-3	0.7	1.40	568	8
K.13.102_727	0.0293	31	0.00079	6	1.46714	1.88716	11	0.282580	31	0.282575	1	1.1	1.00	394	6
K.13.102_728	0.0329	27	0.00096	6	1.46721	1.88616	11	0.282520	21	0.282513	-1	0.8	1.12	392	6
K.13.102_729	0.0333	27	0.00090	6	1.46718	1.88666	9	0.281638	22	0.281605	2	0.8	2.23	1925	18
K.13.102_730	0.0477	44	0.00122	9	1.46717	1.88643	10	0.281168	20	0.281106	1	0.7	2.87	2652	9
K.13.102_731	0.0212	18	0.00057	4	1.46713	1.88685	10	0.280996	24	0.280965	-1	0.8	3.08	2778	10
K.13.102_732	0.0341	31	0.00096	7	1.46712	1.88642	12	0.282295	24	0.282285	-5	0.9	1.49	572	9
K.13.102_733	0.0130	11	0.00036	2	1.46715	1.88642	8	0.281529	21	0.281514	4	0.8	2.29	2181	21
K.13.102_734	0.0286	25	0.00078	5	1.46713	1.88605	9	0.282249	27	0.282242	-8	0.9	1.61	488	8
K.13.102_735	0.0332	27	0.00093	6	1.46713	1.88652	8	0.282498	23	0.282492	-2	0.8	1.16	392	6
K.13.102_736	0.0347	38	0.00096	10	1.46708	1.88624	8	0.281837	21	0.281808	1	0.8	1.99	1568	34
K.13.102_737	0.0498	41	0.00148	9	1.46708	1.88680	9	0.281562	22	0.281500	4	0.8	2.32	2183	12
K.13.102_738	0.0256	24	0.00083	6	1.46721	1.88694	9	0.282351	21	0.282341	-3	0.7	1.37	586	11
K.13.102_739	0.0089	7	0.00024	1	1.46718	1.88677	9	0.281526	17	0.281516	4	0.6	2.29	2179	13
K.13.102_740	0.0176	16	0.00051	4	1.46714	1.88678	9	0.282148	20	0.282136	4	0.7	1.51	1197	23
K.13.102_741	0.0458	43	0.00124	9	1.46718	1.88657	8	0.282700	22	0.282691	5	0.8	0.77	391	6
K.13.102_742	0.0276	29	0.00089	8	1.46710	1.88706	9	0.281535	21	0.281500	1	0.7	2.38	2042	14
K.13.102_744	0.0259	31	0.00072	7	1.46715	1.88697	9	0.282589	23	0.282584	2	0.8	0.98	393	6
K.13.102_745	0.0245	20	0.00071	4	1.46715	1.88649	8	0.281385	19	0.281357	-3	0.7	2.64	2083	14
K.13.102_751	0.0099	8	0.00027	2	1.46715	1.88677	8	0.281110	22	0.281100	-14	0.8	3.18	2013	12
K.13.102_754	0.0215	21	0.00069	6	1.46717	1.88649	8	0.282488	21	0.282483	-2	0.8	1.18	385	6
K.13.102_755	0.0338	27	0.00099	6	1.46722	1.88653	7	0.282516	28	0.282509	-1	1.0	1.12	397	6
K.13.102_756	0.0174	15	0.00059	4	1.46711	1.88678	9	0.282548	20	0.282544	0	0.7	1.06	395	6
K.13.102_757	0.0336	27	0.00095	6	1.46719	1.88637	7	0.282304	23	0.282297	-8	0.8	1.53	409	6
K.13.102_758	0.0288	26	0.00096	7	1.46714	1.88688	9	0.282519	24	0.282512	-1	0.8	1.11	404	6
K.13.102_759	0.0206	23	0.00065	6	1.46713	1.88708	9	0.281535	24	0.281509	3	0.9	2.33	2115	14

K.13.102_761	0.0332	36	0.00088	7	1.46713	1.88620	9	0.281190	0	0.000000	0	0.0	0.00	2220	14
K.13.102_762	0.0164	14	0.00046	3	1.46713	1.88709	8	0.281177	23	0.281163	-22	0.8	3.23	1594	22
K.13.102_763	0.0307	26	0.00096	7	1.46714	1.88688	8	0.282551	25	0.282544	0	0.9	1.06	393	6
K.13.102_764	0.0137	11	0.00043	3	1.46706	1.88673	10	0.282583	21	0.282577	9	0.8	0.85	726	11
K.13.102_765	0.0303	30	0.00096	9	1.46721	1.88594	11	0.281836	32	0.281802	8	1.1	1.86	1890	15
K.13.102_767	0.0332	27	0.00091	6	1.46720	1.88650	8	0.281094	23	0.281048	-1	0.8	2.98	2665	14
K.13.102_768	0.0229	20	0.00062	4	1.46710	1.88668	8	0.281355	28	0.281332	-7	1.0	2.75	1948	17
K.13.102_769	0.0370	33	0.00106	7	1.46718	1.88642	7	0.282513	27	0.282502	3	0.9	1.07	569	9
K.13.102_770	0.0430	48	0.00108	9	1.46711	1.88640	9	0.281448	25	0.281406	-2	0.9	2.56	2067	13
K.13.102_771	0.0494	53	0.00129	13	1.46711	1.88663	9	0.282684	23	0.282674	5	0.8	0.80	403	6
K.13.102_772	0.0413	33	0.00112	7	1.46718	1.88661	8	0.282119	28	0.282108	-12	1.0	1.84	558	8
K.13.102_773	0.0373	33	0.00100	7	1.46717	1.88664	10	0.281602	20	0.281561	5	0.7	2.21	2152	10
K.13.102_774	0.0271	22	0.00068	4	1.46711	1.88675	8	0.281295	19	0.281269	-8	0.7	2.84	2020	15
K.13.102_775	0.0592	53	0.00152	10	1.46722	1.88630	9	0.282652	25	0.282639	4	0.9	0.85	433	7
K.13.102_776	0.0257	21	0.00069	4	1.46716	1.88670	9	0.282482	18	0.282477	-2	0.6	1.18	405	6
K.13.102_777	0.0378	33	0.00106	8	1.46715	1.88647	9	0.282628	20	0.282620	3	0.7	0.91	384	6
K.13.102_778	0.0293	24	0.00090	6	1.46717	1.88659	10	0.282558	23	0.282551	0	0.8	1.04	394	6
K.13.102_779	0.0325	29	0.00086	6	1.46717	1.88678	11	0.282200	20	0.282192	-10	0.7	1.70	492	8
K.13.102_780	0.0147	12	0.00036	2	1.46716	1.88669	12	0.281504	19	0.281493	-6	0.7	2.53	1754	68
K.13.102_781	0.0350	31	0.00101	7	1.46713	1.88657	7	0.282502	29	0.282495	-1	1.0	1.15	398	6
K.13.102_782	0.0348	29	0.00095	6	1.46718	1.88669	10	0.282641	22	0.282634	3	0.8	0.88	392	6
K.13.102_783	0.0719	58	0.00185	11	1.46723	1.88691	9	0.282179	0	0.000000	0	0.0	0.00	514	8
K.13.102_784	0.0357	31	0.00093	6	1.46718	1.88633	10	0.281572	24	0.281535	3	0.9	2.28	2106	15
K.13.102_785	0.0220	18	0.00060	4	1.46715	1.88654	10	0.282575	28	0.282570	1	1.0	1.00	398	7
K.13.102_786	0.0366	34	0.00099	8	1.46720	1.88658	10	0.282549	24	0.282541	0	0.8	1.06	391	6
K.13.102_787	0.0169	14	0.00044	3	1.46716	1.88616	9	0.282574	24	0.282571	1	0.8	1.00	402	7

LA-MC-ICPMS Lu-Hf isotope data of zircon from sample K.13.77 (Uzumdere Formation)

K.13.77_seq2_189	0.1009	82	0.00243	15	1.46716	1.88701	11	0.282545	23	0.282507	9	0.8	0.95	825	12
K.13.77_seq2_190	0.0092	7	0.00024	1	1.46717	1.88689	12	0.281219	18	0.281208	1	0.6	2.75	2485	23
K.13.77_seq2_191	0.0262	21	0.00070	4	1.46716	1.88686	14	0.281962	18	0.281953	-14	0.6	2.09	671	10
K.13.77_seq2_192	0.0421	35	0.00108	7	1.46722	1.88685	12	0.282362	22	0.282351	-3	0.8	1.37	542	9
K.13.77_seq2_193	0.0327	28	0.00078	5	1.46715	1.88681	14	0.281359	18	0.281333	-12	0.6	2.84	1737	24
K.13.77_seq2_199	0.0139	14	0.00032	2	1.46722	1.88675	11	0.282528	21	0.282525	3	0.7	1.04	532	14
K.13.77_seq2_200	0.0166	33	0.00043	8	1.46718	1.88721	14	0.282473	19	0.282466	9	0.7	1.00	896	16
K.13.77_seq2_201	0.0305	29	0.00081	6	1.46720	1.88680	12	0.281905	19	0.281893	-14	0.7	2.16	790	11
K.13.77_seq2_202	0.0493	41	0.00125	8	1.46713	1.88701	13	0.282344	21	0.282331	-4	0.7	1.42	532	15
K.13.77_seq2_203	0.0485	45	0.00119	9	1.46722	1.88665	13	0.282374	19	0.282362	-2	0.7	1.34	568	11
K.13.77_seq2_204	0.0543	44	0.00141	9	1.46715	1.88696	12	0.282373	22	0.282359	-3	0.8	1.36	533	17
K.13.77_seq2_206	0.0312	68	0.00056	9	1.46713	1.88707	14	0.282012	37	0.282002	-8	1.3	1.90	897	18
K.13.77_seq2_207	0.0527	43	0.00143	9	1.46717	1.88675	10	0.281785	20	0.281763	-18	0.7	2.39	831	13
K.13.77_seq2_208	0.0895	72	0.00234	14	1.46716	1.88652	17	0.282383	22	0.28236	-3	0.8	1.36	536	11
K.13.77_seq2_209	0.0000	0	0.00000	0	0.00000	0.00000	0	#SAYI/0!	0	0	0	0.0	0.00	620	23
K.13.77_seq2_210	0.0391	32	0.00104	6	1.46720	1.88697	12	0.282322	19	0.282311	-5	0.7	1.45	543	12
K.13.77_seq2_211	0.1120	96	0.00295	23	1.46718	1.88604	11	0.282327	22	0.282297	-5	0.8	1.47	551	14
K.13.77_seq2_212	0.1010	83	0.00284	21	1.46723	1.88603	14	0.282359	19	0.282334	-5	0.7	1.43	482	13
K.13.77_seq2_213	0.0497	44	0.00120	10	1.46718	1.88704	11	0.282458	20	0.282444	2	0.7	1.16	630	14
K.13.77_seq2_214	0.0923	78	0.00257	19	1.46714	1.88651	13	0.282362	20	0.28234	-5	0.7	1.43	461	14
K.13.77_seq2_215	0.0546	60	0.00135	12	1.46718	1.88609	9	0.282438	39	0.282425	-1	1.4	1.23	529	13
K.13.77_seq2_216	0.0186	15	0.00044	3	1.46722	1.88695	11	0.281277	21	0.281256	4	0.7	2.63	2538	31
K.13.77_seq2_217	0.0297	26	0.00078	6	1.46716	1.88681	12	0.281329	21	0.281291	4	0.8	2.57	2508	35
K.13.77_seq2_219	0.0314	33	0.00083	8	1.46723	1.88667	13	0.282641	25	0.282632	9	0.9	0.78	634	24
K.13.77_seq2_220	0.0431	40	0.00124	11	1.46712	1.88647	13	0.282408	18	0.282384	9	0.6	1.10	1026	23
K.13.77_seq2_222	0.0208	19	0.00044	3	1.46712	1.88677	11	0.28214	28	0.282136	-11	1.0	1.80	526	9
K.13.77_seq2_223	0.0233	22	0.00061	6	1.46715	1.88637	14	0.281309	19	0.281284	-5	0.7	2.76	2137	33
K.13.77_seq2_224	0.0526	54	0.00139	13	1.46721	1.88698	13	0.282355	17	0.282341	-4	0.6	1.40	520	10
K.13.77_seq2_225	0.0041	6	0.00006	1	1.46722	1.88690	17	0.28254	17	0.282539	4	0.6	0.99	574	14
K.13.77_seq2_226	0.0247	23	0.00058	4	1.46718	1.88688	15	0.281418	16	0.281398	-7	0.6	2.67	1844	17
K.13.77_seq2_227	0.0219	18	0.00060	4	1.46715	1.88678	14	0.281649	20	0.281629	0	0.7	2.23	1824	20
K.13.77_seq2_228	0.0491	45	0.00127	9	1.46716	1.88679	13	0.282415	20	0.282408	-7	0.7	1.36	292	6
K.13.77_seq2_229	0.0499	43	0.00131	9	1.46715	1.88674	14	0.282353	19	0.282338	-2	0.7	1.37	612	10
K.13.77_seq2_230	0.0978	82	0.00241	16	1.46721	1.88664	12	0.282602	18	0.282572	7	0.7	0.89	657	9
K.13.77_seq2_231	0.0304	25	0.00076	5	1.46722	1.88664	14	0.28216	20	0.282149	-5	0.7	1.67	771	15
K.13.77_seq2_232	0.1060	86	0.00283	18	1.46713	1.88642	16	0.282365	20	0.282337	-4	0.7	1.40	529	12
K.13.77_seq2_233	0.0310	25	0.00085	5	1.46721	1.88689	15	0.281464	18	0.281431	-3	0.6	2.54	2003	15
K.13.77_seq2_234	0.0575	49	0.00141	9	1.46719	1.88625	8	0.28194	21	0.281922	-16	0.7	2.15	666	15
K.13.77_seq2_235	0.0606	49	0.00149	9	1.46719	1.88684	14	0.282406	18	0.282388	0	0.6	1.26	629	13
K.13.77_seq2_236	0.0143	12	0.00035	2	1.46718	1.88692	14	0.281207	20	0.281194	-13	0.7	3.03	1934	35
K.13.77_seq2_237	0.0634	53	0.00174	11	1.46716	1.88714	14	0.282369	21	0.282352	-4	0.7	1.38	511	10
K.13.77_seq2_243	0.0634	51	0.00089	5	1.46723	1.88619	2	0.282449	182	0.282433	9	6.4	1.04	955	19
K.13.77_seq2_244	0.0350	31	0.00089	6	1.46716	1.88640	9	0.282544	24	0.282534	4	0.8	0.99	597	11
K.13.77_seq2_245	0.0422	35	0.00120	7	1.46719	1.88682	12	0.282465	22	0.282458	-5	0.8	1.27	277	6
K.13.77_seq2_246	0.0279	24	0.00074	6	1.46723	1.88679	13	0.28261	17	0.282601	7	0.6	0.86	605	13
K.13.77_seq2_247	0.0287	26	0.00069	5	1.46716	1.88646	13	0.282325	26	0.282312	5	0.9	1.26	987	14
K.13.77_seq2_248	0.0685	56	0.00177	12	1.46712	1.88696	9	0.282138	26	0.282103	0	0.9	1.64	1058	35
K.13.77_seq2_249	0.0378	31	0.00100	6	1.46717	1.88677	11	0.282512	22	0.282501	3	0.8	1.07	574	12
K.13.77_seq2_250	0.0712	57	0.00189	11	1.46716	1.88687	14	0.282341	18	0.282322	-5	0.6	1.43	528	8
K.13.77_seq2_252	0.0460	43	0.00112	8	1.46717	1.88681	16	0.281156	22	0.281092	9	0.8	2.73	2997	12
K.13.77_seq2_253	0.0209	17	0.00052	3	1.46717	1.88598	15	0.282429	17	0.282423	1	0.6	1.21	596	12
K.13.77_seq2_254	0.0432	36	0.00118	7	1.46720	1.88685	13	0.282575	22	0.282557	10	0.8	0.86	795	18
K.13.77_seq2_255	0.0280	23	0.00081	5	1.46716	1.88664	12	0.282472	22	0.282459	8	0.8	1.03	851	14
K.13.77_seq2_256	0.0024	3	0.00004	0	1.46716	1.88658	15	0.282375	15	0.282374	-1	0.5	1.29	623	12
K.13.77_seq2_257	0.0178	16	0.00046	3	1.46713	1.88694	13	0.281252	23	0.28123	2	0.8	2.69	2513	17
K.13.77_seq2_258	0.0057	5	0.00011	1	1.46722	1.88671	16	0.282322	17	0.282321	-3	0.6	1.41	598	11
K.13.77_seq2_259	0.0706	59	0.00181	12	1.46718	1.88683	15	0.28236	19	0.282341	-3	0.7	1.38	581	26
K.13.77_seq2_260	0.0195	16	0.00050	3	1.46715	1.88722	17	0.281626	17	0.281608	2	0.6	2.22	1931	14
K.13.77_seq2_261	0.0584	48	0.00159	10	1.46717	1.88662	17	0.281403	18	0.281346	-9	0.6	2.76	1874	15
K.13.77_seq2_262	0.0816	66	0.00216	14	1.46719	1.88703	14	0.28238	18	0.28236	-4	0.6	1.37	497	15
K.13.77_seq2_263	0.0717	103	0.00162	19	1.46715	1.88712	15	0.280739	31	0.280638	-2	1.1	3.50	3241	14
K.13.77_seq2_264	0.0493	61	0.00117	9	1.46722	1.88673	15	0.281492	37	0.281444	1	1.3	2.44	2160	15
K.13.77_seq2_265	0.1174	103	0.00301	20	1.46714	1.88696	12	0.282369	20	0.282342	-5	0.7	1.42	471	10

K.13.77_seq2_266	0.1081	95	0.00283	18	1.46716	1.88592	8	0.282383	27	0.282367	-8	1.0	1.44	299	6
K.13.77_seq2_268	0.0452	38	0.00122	9	1.46718	1.88726	13	0.282358	16	0.282346	-4	0.6	1.39	514	9
K.13.77_seq2_269	0.0289	24	0.00077	5	1.46721	1.88679	11	0.282503	21	0.282489	12	0.7	0.90	1004	54
K.13.77_seq2_271	0.0865	95	0.00227	20	1.46722	1.88698	14	0.282364	16	0.282343	-4	0.6	1.40	516	8
K.13.77_seq2_272	0.0000	0	0.00000	0	0.00000	0.00000	0	#SAYI/0!	0	0	0	0.0	0.00	840	23
K.13.77_seq2_273	0.0590	90	0.00146	19	1.46714	1.88702	12	0.28254	21	0.282522	5	0.8	1.00	643	11
K.13.77_seq2_274	0.0623	51	0.00162	10	1.46718	1.88701	16	0.282377	17	0.28236	-3	0.6	1.36	535	12
K.13.77_seq2_275	0.0188	17	0.00055	4	1.46719	1.88665	13	0.28183	17	0.281819	-10	0.6	2.18	1083	48
K.13.77_seq2_276	0.0110	11	0.00028	2	1.46714	1.88683	16	0.282368	20	0.282363	6	0.7	1.17	956	14
K.13.77_seq2_278	0.0249	22	0.00073	6	1.46719	1.88613	11	0.282685	22	0.282677	10	0.8	0.70	617	15
K.13.77_seq2_279	0.0738	66	0.00178	13	1.46722	1.88651	12	0.282414	21	0.282383	6	0.7	1.15	922	13
K.13.77_seq2_280	0.0194	16	0.00061	4	1.46716	1.88692	17	0.282516	15	0.282504	12	0.5	0.88	993	19
K.13.77_seq2_281	0.0487	42	0.00130	9	1.46720	1.88673	12	0.282309	18	0.282285	4	0.6	1.32	977	20
K.13.77_seq2_282	0.0308	25	0.00081	5	1.46716	1.88661	10	0.282509	22	0.282495	11	0.8	0.92	948	14
K.13.77_seq2_289	0.0393	35	0.00101	8	1.46711	1.88678	12	0.282394	22	0.282383	-1	0.8	1.30	579	13
K.13.77_seq2_290	0.0603	51	0.00143	10	1.46719	1.88600	14	0.282325	21	0.28231	-5	0.8	1.45	546	12
K.13.77_seq2_291	0.0543	58	0.00141	11	1.46715	1.88705	15	0.282623	18	0.282609	6	0.6	0.87	541	14
K.13.77_seq2_292	0.0282	29	0.00062	5	1.46717	1.88719	14	0.282542	18	0.282535	5	0.6	0.98	613	11
K.13.77_seq2_293	0.0509	42	0.00126	8	1.46715	1.88698	11	0.282528	23	0.282513	5	0.8	1.02	640	13
K.13.77_seq2_294	0.0582	54	0.00140	10	1.46716	1.88683	18	0.282575	16	0.282557	7	0.6	0.91	685	12
K.13.77_seq2_296	0.0305	25	0.00077	5	1.46720	1.88704	10	0.281103	23	0.281074	-15	0.8	3.23	2011	29
K.13.77_seq2_297	0.0102	10	0.00023	2	1.46719	1.88675	14	0.281428	18	0.281421	-8	0.6	2.65	1796	17
K.13.77_seq2_298	0.0243	22	0.00067	6	1.46714	1.88667	13	0.282459	18	0.282455	-6	0.6	1.28	270	8
K.13.77_seq2_300	0.0894	79	0.00255	25	1.46713	1.88641	13	0.282306	34	0.282282	-7	1.2	1.52	505	10
K.13.77_seq2_301	0.0242	21	0.00064	4	1.46719	1.88708	13	0.282409	19	0.282401	0	0.7	1.25	597	11
K.13.77_seq2_302	0.0360	29	0.00093	6	1.46717	1.88660	15	0.282262	18	0.282244	4	0.6	1.38	1029	24
K.13.77_seq2_303	0.0263	22	0.00076	5	1.46721	1.88660	6	0.281681	28	0.281656	0	1.0	2.20	1783	50

LA-MC-ICPMS Lu-Hf isotope data of zircon from sample K.12.75 (Kasimlar Formation)

K.12.75_915	0.0179	16	0.00059	4	1.46712	1.88698	8	0.282336	26	0.282324	8	0.9	1.20	1068	52
K.12.75_916	0.0452	43	0.00127	9	1.46718	1.88697	7	0.282538	31	0.282529	-1	1.1	1.10	371	5
K.12.75_917	0.0554	49	0.00152	11	1.46713	1.88655	9	0.282481	26	0.282472	-4	0.9	1.23	323	5
K.12.75_918	0.0287	23	0.00085	5	1.46709	1.88644	8	0.28242	36	0.282411	-1	1.3	1.25	567	10
K.12.75_919	0.0282	26	0.00087	6	1.46717	1.88641	8	0.282006	32	0.281991	-7	1.1	1.91	935	14
K.12.75_920	0.0209	18	0.00059	4	1.46720	1.88674	9	0.282079	21	0.28207	-7	0.8	1.81	803	12
K.12.75_921	0.0376	31	0.00111	7	1.46716	1.88680	9	0.282334	22	0.282325	-6	0.8	1.46	454	7
K.12.75_922	0.0560	47	0.00147	9	1.46711	1.88635	11	0.282407	26	0.282396	-5	0.9	1.35	387	7
K.12.75_923	0.0194	16	0.00057	3	1.46716	1.88703	9	0.281552	22	0.281541	-23	0.8	2.77	960	15
K.12.75_924	0.0266	26	0.00065	5	1.46719	1.88671	10	0.282214	23	0.282206	-6	0.8	1.61	656	9
K.12.75_925	0.0295	24	0.00086	5	1.46720	1.88629	10	0.282442	24	0.282437	-5	0.8	1.30	313	5
K.12.75_926	0.0179	16	0.00049	4	1.46714	1.88691	9	0.282239	21	0.282233	-4	0.7	1.54	697	11
K.12.75_927	0.0461	38	0.00125	8	1.46714	1.88667	9	0.28243	25	0.282423	-6	0.9	1.33	300	6
K.12.75_933	0.0248	20	0.00070	4	1.46715	1.88640	8	0.282183	25	0.282172	-3	0.9	1.59	849	13
K.12.75_935	0.0168	20	0.00049	5	1.46722	1.88676	9	0.281925	22	0.281915	-7	0.8	2.00	1072	68
K.12.75_936	0.0207	20	0.00062	5	1.46718	1.88683	10	0.282478	24	0.282469	7	0.8	1.02	827	13
K.12.75_937	0.0140	11	0.00047	3	1.46715	1.88691	10	0.282491	25	0.282484	8	0.9	0.99	826	12
K.12.75_938	0.0321	27	0.00097	6	1.46716	1.88696	8	0.281167	22	0.281118	2	0.8	2.84	2665	9
K.12.75_939	0.0957	91	0.00232	17	1.46716	1.88667	8	0.282405	26	0.282379	-1	0.9	1.29	603	9
K.12.75_940	0.0215	18	0.00069	4	1.46717	1.88653	9	0.282652	21	0.282644	9	0.8	0.77	610	9
K.12.75_941	0.0302	25	0.00085	5	1.46710	1.88710	11	0.280971	32	0.280927	-4	1.1	3.18	2727	12
K.12.75_942	0.0293	42	0.00095	13	1.46720	1.88696	9	0.281319	24	0.281274	3	0.9	2.63	2465	10
K.12.75_943	0.0302	27	0.00083	6	1.46711	1.88660	9	0.282629	30	0.28262	7	1.1	0.84	569	9
K.12.75_944	0.0248	21	0.00074	5	1.46719	1.88666	10	0.281951	22	0.281938	-10	0.8	2.03	897	14
K.12.75_945	0.0287	24	0.00080	5	1.46713	1.88588	8	0.281498	28	0.281469	-4	1.0	2.51	1897	17
K.12.75_946	0.0379	30	0.00100	6	1.46706	1.88696	7	0.28197	21	0.281951	-8	0.7	1.98	961	15
K.12.75_947	0.0223	20	0.00057	4	1.46717	1.88655	12	0.28229	20	0.282283	-3	0.7	1.45	665	10
K.12.75_948	0.0864	185	0.00167	31	1.46717	1.88623	11	0.282373	48	0.282353	0	1.7	1.32	666	10
K.12.75_949	0.0261	21	0.00069	4	1.46712	1.88664	10	0.282327	24	0.282317	1	0.9	1.33	802	14
K.12.75_950	0.0643	54	0.00179	12	1.46715	1.88638	11	0.282378	21	0.282363	-5	0.7	1.38	459	7
K.12.75_951	0.0229	21	0.00060	5	1.46720	1.88669	8	0.282742	29	0.282739	5	1.0	0.72	289	5
K.12.75_952	0.0270	22	0.00073	5	1.46718	1.88668	9	0.280986	32	0.280948	-3	1.1	3.14	2724	12
K.12.75_953	0.0331	33	0.00092	6	1.46703	1.88682	10	0.281436	49	0.281401	-4	1.8	2.59	2007	16
K.12.75_954	0.0134	11	0.00038	2	1.46715	1.88663	6	0.282082	31	0.282076	-7	1.1	1.80	800	12
K.12.75_955	0.0297	27	0.00078	6	1.46715	1.88714	10	0.28262	26	0.28261	8	0.9	0.82	645	10
K.12.75_956	0.0491	40	0.00143	9	1.46715	1.88644	8	0.282226	26	0.282203	-1	0.9	1.53	865	13
K.12.75_957	0.0231	19	0.00067	4	1.46720	1.88678	12	0.28252	19	0.282512	5	0.7	1.01	667	10
K.12.75_958	0.0156	13	0.00049	3	1.46715	1.88674	10	0.281838	20	0.281828	-11	0.7	2.19	1031	21
K.12.75_959	0.0098	15	0.00026	4	1.46717	1.88625	8	0.281136	24	0.281124	-3	0.9	2.92	2473	9
K.12.75_960	0.0478	54	0.00135	13	1.46720	1.88579	7	0.282436	28	0.282425	-3	1.0	1.26	458	7
K.12.75_961	0.0423	39	0.00119	9	1.46721	1.88721	10	0.282402	19	0.282384	4	0.7	1.20	811	20
K.12.75_962	0.0301	26	0.00088	6	1.46721	1.88660	9	0.281299	44	0.281254	7	1.6	2.57	2668	9
K.12.75_963	0.0464	37	0.00126	8	1.46716	1.88663	9	0.282467	21	0.282447	7	0.7	1.05	858	13
K.12.75_964	0.0339	28	0.00090	6	1.46717	1.88672	8	0.281053	23	0.281009	-5	0.8	3.12	2528	15
K.12.75_965	0.0144	12	0.00036	2	1.46711	1.88677	13	0.282536	17	0.282532	5	0.6	0.98	633	10
K.12.75_966	0.0317	32	0.00097	8	1.46718	1.88670	8	0.281242	25	0.281193	4	0.9	2.69	2665	10
K.12.75_967	0.0323	26	0.00091	5	1.46711	1.88679	8	0.282391	26	0.282382	-3	0.9	1.33	504	8
K.12.75_968	0.0215	17	0.00060	4	1.46717	1.88674	10	0.282207	19	0.282199	-7	0.7	1.63	631	9
K.12.75_969	0.0212	23	0.00060	5	1.46720	1.88677	8	0.282309	24	0.282303	-5	0.9	1.47	540	8
K.12.75_970	0.0100	9	0.00028	2	1.46718	1.88652	10	0.280747	19	0.280732	-12	0.7	3.59	2673	9
K.12.75_971	0.0201	16	0.00056	3	1.46714	1.88660	9	0.282292	20	0.282281	5	0.7	1.31	1014	36
K.12.75_972	0.0625	52	0.00173	11	1.46714	1.88673	10	0.282491	21	0.28248	-3	0.7	1.20	337	5
K.12.75_973	0.0179	15	0.00050	3	1.46714	1.88697	9	0.282638	21	0.282632	9	0.8	0.78	642	10
K.12.75_974	0.0102	8	0.00029	2	1.46721	1.88689	10	0.281246	21	0.281232	4	0.8	2.66	2576	16
K.12.75_975	0.0304	25	0.00092	6	1.46713	1.88680	12	0.282352	20	0.282343	-4	0.7	1.40	505	9
K.12.75_976	0.0262	21	0.00074	5	1.46714	1.88692	10	0.282224	17	0.282217	-8	0.6	1.64	528	8
K.12.75_977	0.0426	40	0.00118	9	1.46707	1.88625	11	0.281907	62	0.281896	-21	2.2	2.28	478	7
K.12.75_978	0.0842	69	0.00231	15	1.46714	1.88625	12	0.282408	19	0.282389	-4	0.7	1.34	432	7
K.12.75_980	0.0325	26	0.00095	6	1.46717	1.88691	9	0.282605	21	0.282592	9	0.7	0.82	727	13
K.12.75_981	0.0331	64	0.00095	17	1.46716	1.88611	10	0.282613	32	0.282607	2	1.1	0.95	353	6
K.12.75_982	0.0381	32	0.00110	7	1.46713	1.88716	10	0.282438	21	0.282433	-6	0.8	1.32	274	4
K.12.75_988	0.0477	38	0.00137	8	1.46721	1.88625	6	0.282351	26	0.282327	5	0.9	1.25	938	14

K.12.75_989	0.0717	58	0.00193	12	1.46719	1.88636	7	0.282291	30	0.282264	-2	1.1	1.45	758	11
K.12.75_990	0.0166	15	0.00050	3	1.46713	1.88618	9	0.282599	23	0.282591	11	0.8	0.78	816	12
K.12.75_991	0.0505	48	0.00129	11	1.46711	1.88663	8	0.282773	28	0.282766	6	1.0	0.67	283	5
K.12.75_992	0.0568	45	0.00150	9	1.46718	1.88669	11	0.282365	21	0.282336	7	0.7	1.19	1040	21
K.12.75_993	0.0251	22	0.00070	5	1.46715	1.88664	8	0.281045	27	0.281011	-6	0.9	3.12	2508	11
K.12.75_994	0.0549	44	0.00148	9	1.46714	1.88637	9	0.282249	21	0.28222	3	0.8	1.42	1031	28
K.12.75_995	0.0263	22	0.00074	5	1.46714	1.88620	10	0.281868	30	0.281854	-10	1.1	2.14	1019	30
K.12.75_996	0.0285	26	0.00084	6	1.46719	1.88678	11	0.282357	14	0.282348	-2	0.5	1.35	601	9
K.12.75_997	0.0375	31	0.00109	7	1.46711	1.88655	11	0.28242	21	0.282414	-6	0.7	1.34	324	5
K.12.75_998	0.0250	21	0.00086	5	1.46719	1.88682	9	0.281085	22	0.281041	-1	0.8	2.99	2674	10
K.12.75_999	0.0488	40	0.00143	9	1.46714	1.88683	11	0.282362	26	0.282349	-5	0.9	1.41	465	7
K.12.75_1000	0.0426	36	0.00116	7	1.46714	1.88668	10	0.281421	23	0.281377	-5	0.8	2.66	1970	13
K.12.75_1001	0.0551	45	0.00157	10	1.46719	1.88665	12	0.282436	16	0.282422	-3	0.6	1.27	462	7
K.12.75_1002	0.0882	86	0.00249	19	1.46714	1.88704	9	0.282435	22	0.282385	9	0.8	1.09	1053	17
K.12.75_1003	0.0349	28	0.00095	6	1.46718	1.88673	11	0.282448	18	0.282442	-5	0.6	1.28	334	5
K.12.75_1004	0.0607	51	0.00159	11	1.46702	1.88607	9	0.282448	33	0.282439	-6	1.2	1.31	281	5
K.12.75_1005	0.0364	30	0.00104	7	1.46720	1.88664	12	0.281404	16	0.281364	-5	0.6	2.67	1988	15
K.12.75_1006	0.1183	98	0.00284	18	1.46713	1.88657	9	0.282647	23	0.282616	7	0.8	0.83	593	9
K.12.75_1007	0.0284	23	0.00076	5	1.46717	1.88644	7	0.282547	40	0.282537	7	1.4	0.94	700	11
K.12.75_1008	0.0411	35	0.00099	6	1.46722	1.88634	8	0.282535	43	0.282523	5	1.5	1.00	637	9
K.12.75_1009	0.0311	26	0.00089	6	1.46715	1.88673	11	0.282344	21	0.282336	-6	0.7	1.44	437	7
K.12.75_1010	0.0310	28	0.00085	6	1.46718	1.88699	9	0.282267	26	0.282257	-5	0.9	1.52	622	11
K.12.75_1011	0.0363	45	0.00099	8	1.46721	1.88644	9	0.282353	34	0.282342	-2	1.2	1.37	595	9
K.12.75_1012	0.0490	44	0.00127	9	1.46710	1.88708	9	0.281043	37	0.280979	-4	1.3	3.13	2623	9
K.12.75_1013	0.0133	11	0.00040	2	1.46715	1.88655	8	0.282628	23	0.282623	8	0.8	0.80	636	10
K.12.75_1014	0.0242	25	0.00060	4	1.46718	1.88629	8	0.281787	28	0.281765	7	1.0	1.92	1909	37
K.12.75_1015	0.0446	42	0.00128	9	1.46702	1.88614	8	0.28163	36	0.281584	0	1.3	2.29	1876	13
K.12.75_1016	0.0347	37	0.00097	9	1.46715	1.88622	11	0.282482	27	0.282471	2	1.0	1.11	601	9
K.12.75_1017	0.0245	45	0.00072	11	1.46714	1.88606	10	0.282575	28	0.282564	11	1.0	0.83	842	12
K.12.75_1018	0.0829	68	0.00240	15	1.46713	1.88630	7	0.282035	24	0.282006	-13	0.8	2.00	642	9
K.12.75_1019	0.0252	21	0.00078	5	1.46720	1.88649	8	0.282346	25	0.282331	6	0.9	1.22	989	16
K.12.75_1021	0.0211	18	0.00061	4	1.46713	1.88627	11	0.282578	28	0.282571	6	1.0	0.92	592	9
K.12.75_1022	0.0244	22	0.00064	5	1.46713	1.88647	10	0.281948	19	0.28194	-16	0.7	2.14	607	9
K.12.75_1023	0.0268	22	0.00072	5	1.46721	1.88636	9	0.282065	19	0.282052	-4	0.7	1.77	993	15
K.12.75_1024	0.0439	42	0.00124	10	1.46717	1.88612	5	0.282815	77	0.282807	9	2.7	0.55	363	6
K.12.75_1025	0.0339	28	0.00092	6	1.46716	1.88606	11	0.282427	25	0.282421	-6	0.9	1.33	320	5
K.12.75_1026	0.0792	64	0.00229	14	1.46716	1.88678	13	0.282374	17	0.282355	-5	0.6	1.40	459	7
K.12.75_1027	0.0621	59	0.00179	13	1.46718	1.88680	9	0.282406	28	0.282376	5	1.0	1.18	880	13
K.12.75_1028	0.0672	54	0.00162	10	1.46720	1.88667	9	0.28204	19	0.282016	-10	0.7	1.93	779	11
K.12.75_1029	0.0117	10	0.00031	2	1.46715	1.88681	10	0.281743	23	0.28174	-23	0.8	2.51	647	10
K.12.75_1030	0.0651	57	0.00174	12	1.46707	1.88623	10	0.281954	23	0.281937	-18	0.8	2.17	548	8
K.12.75_1031	0.0191	17	0.00038	3	1.46716	1.88642	9	0.28193	30	0.281925	-16	1.1	2.16	632	10
K.12.75_1032	0.0748	64	0.00208	13	1.46713	1.88661	10	0.282484	32	0.282452	6	1.1	1.06	814	12
K.12.75_1033	0.0297	24	0.00085	5	1.46716	1.88675	13	0.282217	19	0.282203	0	0.7	1.50	925	13
K.12.75_1034	0.0298	24	0.00085	5	1.46704	1.88702	11	0.282342	23	0.282325	8	0.8	1.20	1077	18
K.12.75_1035	0.0281	23	0.00080	5	1.46711	1.88661	9	0.281218	16	0.281188	-12	0.6	3.02	1990	15

LA-MC-ICPMS Lu-Hf isotope data of zircon from sample K.12.78 (Kasimlar Formation)

K.12.78_seq1_292	0.0156	14	0.00045	3	1.46721	1.88654	9	0.281798	18	0.281794	-22.8	0.6	2.44	551	16
K.12.78_seq1_293	0.0248	26	0.00077	8	1.46727	1.88625	10	0.282318	25	0.282307	-0.5	0.9	1.38	736	12
K.12.78_seq1_294	0.0198	18	0.00058	4	1.46733	1.88662	4	0.282311	33	0.282304	-3.4	1.2	1.44	611	11
K.12.78_seq1_296	0.0104	9	0.00029	2	1.46727	1.88670	7	0.281071	27	0.281056	-3.7	1.0	3.02	2530	12
K.12.78_seq1_297	0.0796	86	0.00217	20	1.46718	1.88600	7	0.282701	39	0.282675	10.5	1.4	0.69	644	11
K.12.78_seq1_298	0.0142	12	0.00039	2	1.46724	1.88684	8	0.282534	26	0.282529	5.2	0.9	0.98	638	17
K.12.78_seq1_299	0.0457	44	0.00124	10	1.46724	1.88632	8	0.282570	24	0.282553	7.7	0.9	0.91	710	17
K.12.78_seq1_300	0.0216	23	0.00057	5	1.46720	1.88653	8	0.282486	23	0.282477	7.9	0.8	1.00	839	14
K.12.78_seq1_301	0.0610	50	0.00179	12	1.46728	1.88616	10	0.282641	27	0.282619	8.7	0.9	0.80	651	10
K.12.78_seq1_302	0.0335	39	0.00083	8	1.46720	1.88678	13	0.282617	16	0.282613	-0.3	0.6	0.98	259	11
K.12.78_seq1_303	0.0186	16	0.00047	3	1.46725	1.88642	9	0.282247	22	0.282242	-5.8	0.8	1.56	601	18
K.12.78_seq1_304	0.0493	43	0.00151	10	1.46716	1.88654	7	0.281060	24	0.280977	0.9	0.8	3.03	2844	10
K.12.78_seq1_305	0.0266	21	0.00072	4	1.46724	1.88644	8	0.280926	21	0.280888	-4.7	0.7	3.25	2742	17
K.12.78_seq1_306	0.0336	27	0.00096	6	1.46725	1.88681	10	0.282364	21	0.282356	-5.5	0.8	1.41	435	11
K.12.78_seq1_307	0.0154	13	0.00041	3	1.46721	1.88603	9	0.282305	24	0.282300	-3.6	0.9	1.45	606	11
K.12.78_seq1_308	0.0265	24	0.00073	5	1.46725	1.88671	8	0.282523	20	0.282515	3.1	0.7	1.04	569	14
K.12.78_seq1_309	0.0234	21	0.00060	4	1.46721	1.88673	9	0.282122	20	0.282113	-5.4	0.7	1.72	821	12
K.12.78_seq1_310	0.0164	13	0.00045	3	1.46723	1.88654	11	0.282452	20	0.282447	1.0	0.7	1.17	582	11
K.12.78_seq1_311	0.0191	16	0.00051	3	1.46725	1.88646	9	0.282066	29	0.282056	-3.9	1.0	1.77	976	20
K.12.78_seq1_312	0.0222	22	0.00057	5	1.46726	1.88660	8	0.282574	25	0.282568	5.3	0.9	0.93	581	19
K.12.78_seq1_313	0.0156	13	0.00042	3	1.46727	1.88620	7	0.281916	25	0.281910	-12.9	0.9	2.12	809	33
K.12.78_seq1_314	0.1439	148	0.00368	30	1.46733	1.88645	10	0.281865	29	0.281839	-25.2	1.0	2.42	373	24
K.12.78_seq1_316	0.0078	6	0.00022	1	1.46730	1.88621	9	0.282378	21	0.282376	-3.3	0.8	1.34	501	12
K.12.78_seq1_317	0.0442	37	0.00121	8	1.46719	1.88643	7	0.281852	22	0.281829	-11.4	0.8	2.20	1000	23
K.12.78_seq1_319	0.0407	33	0.00120	7	1.46725	1.88632	9	0.282453	22	0.282432	8.2	0.8	1.05	923	19
K.12.78_seq1_320	0.0173	15	0.00046	3	1.46727	1.88673	8	0.280834	25	0.280810	-8.3	0.9	3.42	2705	15
K.12.78_seq1_321	0.0317	26	0.00091	6	1.46722	1.88672	9	0.282569	23	0.282560	3.9	0.8	0.97	533	10
K.12.78_seq1_322	0.0144	12	0.00036	2	1.46723	1.88657	9	0.281326	25	0.281309	4.4	0.9	2.55	2490	13
K.12.78_seq1_323	0.0367	30	0.00099	6	1.46724	1.88638	10	0.282115	22	0.282102	-8.9	0.8	1.80	684	15
K.12.78_seq1_324	0.0265	23	0.00077	5	1.46714	1.88621	7	0.281690	22	0.281684	-28.6	0.8	2.68	464	12
K.12.78_seq1_325	0.0381	31	0.00098	6	1.46725	1.88658	11	0.282050	21	0.282038	-12.0	0.8	1.94	646	11
K.12.78_seq1_326	0.0400	33	0.00119	7	1.46719	1.88635	10	0.281600	30	0.281577	-19.5	1.1	2.67	1039	46
K.12.78_seq1_327	0.0383	31	0.00104	6	1.46719	1.88648	8	0.282322	23	0.282306	1.5	0.8	1.34	823	14
K.12.78_seq1_334	0.0111	9	0.00029	2	1.46723	1.88607	9	0.282546	27	0.282542	6.7	1.0	0.94	687	12
K.12.78_seq1_335	0.0649	119	0.00184	31	1.46723	1.88717	9	0.282524	24	0.282500	5.6	0.9	1.01	701	21
K.12.78_seq1_336	0.0147	12	0.00040	2	1.46722	1.88636	8	0.282491	24	0.282485	6.2	0.8	1.02	754	11
K.12.78_seq1_337	0.0262	27	0.00070	6	1.46726	1.88650	9	0.282304	23	0.282294	-1.9	0.8	1.42	693	15
K.12.78_seq1_339	0.0354	30	0.00107	7	1.46716	1.88623	7	0.281240	28	0.281190	-0.9	1.0	2.80	2446	18
K.12.78_seq1_340	0.0359	30	0.00103	6	1.46718	1.88657	9	0.282427	15	0.282421	-5.7	0.5	1.32	323	11
K.12.78_seq1_341	0.0321	26	0.00085	5	1.46716	1.88716	9	0.282292	25	0.282282	-3.9	0.9	1.47	620	17
K.12.78_seq1_342	0.0098	9	0.00030	2	1.46723	1.88654	10	0.280899	24	0.280885	-10.2	0.9	3.37	2513	14
K.12.78_seq1_343	0.0418	38	0.00118	8	1.46729	1.88669	8	0.281525	27	0.281483	-3.4	1.0	2.49	1888	17
K.12.78_seq1_344	0.0643	58	0.00166	12	1.46727	1.88617	7	0.282484	66	0.282460	5.8	2.3	1.06	771	15

K.12.78_seq1_345	0.0315	26	0.00086	5	1.46726	1.88653	8	0.282103	24	0.282093	-10.8	0.9	1.84	614	15
K.12.78_seq1_346	0.0227	23	0.00066	5	1.46729	1.88698	9	0.281619	28	0.281596	0.3	1.0	2.27	1878	33
K.12.78_seq1_347	0.0245	21	0.00089	6	1.46721	1.88665	9	0.282914	16	0.282908	12.4	0.6	0.35	364	10
K.12.78_seq1_348	0.0351	29	0.00118	7	1.46722	1.88618	11	0.282597	17	0.282579	10.8	0.6	0.81	810	15
K.12.78_seq1_349	0.0178	15	0.00044	3	1.46719	1.88598	10	0.281296	50	0.281281	-10.5	1.8	2.88	1891	23
K.12.78_seq1_351	0.0450	39	0.00127	8	1.46721	1.88640	10	0.282518	19	0.282496	10.2	0.7	0.93	910	10
K.12.78_seq1_352	0.0389	36	0.00111	10	1.46725	1.88603	8	0.282536	34	0.282517	10.8	1.2	0.89	904	20
K.12.78_seq1_353	0.0341	38	0.00096	10	1.46717	1.88662	12	0.282435	18	0.282425	-0.6	0.6	1.23	545	12
K.12.78_seq1_354	0.0414	33	0.00116	7	1.46718	1.88643	10	0.282104	23	0.282083	-3.5	0.8	1.72	951	12
K.12.78_seq1_355	0.0351	40	0.00103	10	1.46718	1.88648	9	0.281801	20	0.281782	-12.9	0.7	2.28	1010	14
K.12.78_seq1_356	0.0358	35	0.00098	9	1.46719	1.88682	12	0.282417	20	0.282407	-0.6	0.7	1.25	573	10
K.12.78_seq1_357	0.0277	28	0.00077	6	1.46718	1.88676	7	0.280879	28	0.280836	-3.2	1.0	3.29	2884	9
K.12.78_seq1_359	0.0404	33	0.00111	7	1.46727	1.88632	10	0.282607	36	0.282594	6.7	1.3	0.87	601	18
K.12.78_seq1_360	0.0258	21	0.00078	5	1.46728	1.88626	8	0.282176	29	0.282161	0.6	1.0	1.54	1013	38
K.12.78_seq1_361	0.0198	16	0.00056	3	1.46721	1.88691	9	0.282630	24	0.282625	4.4	0.8	0.87	452	9
K.12.78_seq1_362	0.0151	12	0.00040	3	1.46728	1.88633	9	0.281266	33	0.281251	-8.9	1.2	2.89	2008	37
K.12.78_seq1_366	0.0455	40	0.00127	10	1.46718	1.88655	11	0.282691	21	0.282685	1.9	0.8	0.84	243	8
K.12.78_seq1_367	0.0431	40	0.00115	8	1.46728	1.88605	8	0.282040	31	0.282020	-6.7	1.1	1.86	911	18
K.12.78_seq1_369	0.0231	19	0.00063	4	1.46724	1.88640	10	0.281917	26	0.281911	-19.5	0.9	2.23	513	11
K.12.78_seq1_370	0.0341	31	0.00089	6	1.46721	1.88656	9	0.282405	21	0.282394	1.5	0.7	1.23	689	19
K.12.78_seq1_371	0.0184	17	0.00056	4	1.46722	1.88632	9	0.282257	24	0.282247	2.1	0.8	1.41	945	13
K.12.78_seq1_372	0.0170	16	0.00046	4	1.46719	1.88600	9	0.282059	20	0.282054	-13.7	0.7	1.95	544	40
K.12.78_seq1_373	0.0259	23	0.00074	5	1.46718	1.88640	9	0.281911	24	0.281897	-9.4	0.9	2.07	983	20
K.12.78_seq1_374	0.0340	27	0.00087	5	1.46717	1.88667	8	0.281069	25	0.281028	-6.8	0.9	3.12	2441	15
K.12.78_seq1_376	0.0491	42	0.00161	10	1.46720	1.88631	10	0.282570	25	0.282552	5.7	0.9	0.95	624	13
K.12.78_seq1_377	0.0358	36	0.00091	8	1.46722	1.88706	9	0.282445	25	0.282432	5.1	0.9	1.11	786	10
K.12.78_seq1_378	0.0557	45	0.00153	10	1.46727	1.88596	7	0.282493	35	0.282464	11.5	1.2	0.95	1020	34
K.12.78_seq1_379	0.0835	71	0.00203	14	1.46726	1.88714	12	0.281517	19	0.281444	-4.7	0.7	2.56	1893	21
K.12.78_seq1_380	0.0451	80	0.00131	26	1.46728	1.88626	10	0.281925	26	0.281887	2.6	0.9	1.86	1524	21
K.12.78_seq1_381	0.0318	26	0.00090	6	1.46721	1.88623	7	0.282305	26	0.282295	-3.5	0.9	1.45	622	13
K.12.78_seq1_382	0.0403	32	0.00108	7	1.46721	1.88601	9	0.282054	24	0.282035	-5.6	0.8	1.82	938	11
K.12.78_seq1_388	0.0569	62	0.00149	13	1.46727	1.88681	9	0.282084	27	0.282057	-4.2	1.0	1.77	964	10
K.12.78_seq1_389	0.0212	25	0.00065	6	1.46730	1.88614	9	0.281478	25	0.281456	-6.5	0.9	2.58	1798	44
K.12.78_seq1_392+	0.0240	20	0.00072	5	1.46722	1.88662	11	0.281715	19	0.281702	-16.7	0.7	2.45	967	15
K.12.78_seq1_394	0.0273	22	0.00083	5	1.46721	1.88603	11	0.281422	23	0.281411	-32.6	0.8	3.11	720	12
K.12.78_seq1_395	0.0235	19	0.00069	4	1.46715	1.88658	8	0.281388	21	0.281361	-5.2	0.7	2.67	1997	15
K.12.78_seq1_397	0.0138	37	0.00035	10	1.46720	1.88595	12	0.281981	15	0.281977	-14.3	0.5	2.06	643	10
K.12.78_seq1_398	0.0241	19	0.00066	4	1.46729	1.88698	9	0.282564	24	0.282558	4.0	0.8	0.97	540	18
K.12.78_seq1_399	0.0388	32	0.00102	6	1.46718	1.88632	8	0.281861	25	0.281835	-2.9	0.9	2.03	1369	27
K.12.78_seq1_400	0.0194	16	0.00042	3	1.46726	1.88680	10	0.281226	21	0.281206	0.7	0.7	2.75	2489	10
K.12.78_seq1_402	0.0257	21	0.00069	4	1.46726	1.88661	9	0.281906	19	0.281893	-9.0	0.7	2.07	1005	18
K.12.78_seq1_404	0.0235	28	0.00062	6	1.46718	1.88649	9	0.281920	27	0.281907	-6.5	1.0	2.01	1098	41
K.12.78_seq1_405	0.0395	32	0.00121	7	1.46724	1.88639	12	0.282631	21	0.282617	8.0	0.7	0.82	623	10
K.12.78_seq1_406	0.0341	29	0.00098	6	1.46718	1.88617	6	0.281646	28	0.281610	2.1	1.0	2.22	1933	24
K.12.78_seq1_407	0.0556	49	0.00154	10	1.46727	1.88672	7	0.282515	23	0.282492	7.8	0.8	0.98	813	23
K.12.78_seq1_408	0.0337	27	0.00098	6	1.46732	1.88637	6	0.281089	38	0.281039	-1.2	1.4	3.00	2660	39
K.12.78_seq1_409	0.0600	60	0.00152	12	1.46718	1.88640	12	0.281825	28	0.281794	-10.7	1.0	2.23	1086	34
K.12.78_seq1_410	0.0161	19	0.00045	4	1.46721	1.88636	10	0.282342	23	0.282334	6.2	0.8	1.22	989	15
K.12.78_seq1_411	0.0195	16	0.00060	4	1.46722	1.88617	9	0.281245	20	0.281222	-11.2	0.7	2.97	1952	13
K.12.78_seq1_412	0.0561	48	0.00152	9	1.46728	1.88610	10	0.282724	23	0.282717	2.9	0.8	0.78	237	7

LA-MC-ICPMS Lu-Hf isotope data of zircon from sample K.13.104 (Guvercinlik Formation)

K13.104_1179	0.0009	1	0.00002	0	1.46718	1.88668	8	0.281205	25	0.281203	1	0.9	2.75	2502	12
K13.104_1180	0.0178	16	0.00054	4	1.46716	1.88681	8	0.282459	23	0.282454	-1	0.8	1.19	494	14
K13.104_1181	0.0238	20	0.00075	5	1.46717	1.88651	7	0.282433	26	0.282428	-6	0.9	1.32	305	12
K13.104_1182	0.0515	69	0.00138	15	1.46719	1.88653	7	0.282439	23	0.282431	-6	0.8	1.31	310	7
K13.104_1183	0.0395	38	0.00115	9	1.46714	1.88634	7	0.28246	26	0.282453	-5	0.9	1.27	304	6
K13.104_1184	0.0270	22	0.00086	5	1.46718	1.88657	6	0.281558	24	0.281523	3	0.9	2.31	2094	11
K13.104_1185	0.0268	22	0.00085	5	1.46719	1.88658	8	0.282394	26	0.282389	-7	0.9	1.39	302	8
K13.104_1186	0.0214	18	0.00071	5	1.46722	1.88654	7	0.282429	22	0.282422	-2	0.8	1.26	465	12
K13.104_1187	0.0192	17	0.00080	6	1.46726	1.88643	7	0.282561	25	0.282551	6	0.9	0.94	647	9
K13.104_1188	0.0348	36	0.00113	9	1.46717	1.88659	7	0.282661	24	0.282653	4	0.9	0.85	375	9
K13.104_1189	0.0284	24	0.00095	6	1.46719	1.88621	8	0.282229	23	0.282218	-7	0.8	1.61	585	11
K13.104_1191	0.0494	40	0.00175	11	1.46728	1.88645	5	0.282398	24	0.282379	-1	0.9	1.30	599	11
K13.104_1192	0.0171	20	0.00058	6	1.46715	1.88653	7	0.281304	21	0.281283	-8	0.7	2.83	2000	15
K13.104_1193	0.0094	14	0.00023	3	1.46717	1.88666	9	0.281617	23	0.281608	5	0.8	2.16	2063	14
K13.104_1194	0.0138	12	0.00040	3	1.46725	1.88657	8	0.282206	26	0.282201	-7	0.9	1.63	620	10
K13.104_1195	0.0347	29	0.00113	7	1.46721	1.88577	5	0.282525	23	0.282517	-1	0.8	1.12	378	6
K13.104_1206	0.0054	4	0.00014	1	1.46714	1.88671	9	0.281229	23	0.281224	-10	0.8	2.95	1989	11
K13.104_1210	0.0236	24	0.00069	6	1.46722	1.88670	8	0.28135	26	0.281323	-5	0.9	2.71	2072	14
K13.104_1211	0.0254	21	0.00074	5	1.46718	1.88652	9	0.282012	22	0.281999	-7	0.8	1.90	910	11
K13.104_1213	0.0265	22	0.00137	9	1.46714	1.88637	13	0.281725	23	0.28169	-8	0.8	2.31	1361	30
K13.104_1214	0.0246	29	0.00074	7	1.46716	1.88684	9	0.282448	22	0.282443	-5	0.8	1.28	318	8
K13.104_1215	0.0122	11	0.00043	3	1.46712	1.88725	6	0.282605	25	0.282602	2	0.9	0.96	359	13
K13.104_1216	0.0154	13	0.00046	3	1.46719	1.88666	7	0.281442	21	0.281426	-7	0.8	2.63	1816	27
K13.104_1218	0.0099	8	0.00031	2	1.46720	1.88661	10	0.280809	22	0.280793	-11	0.8	3.50	2607	9
K13.104_1219	0.0122	10	0.00042	3	1.46718	1.88663	10	0.282612	18	0.28261	1	0.6	0.95	332	6
K13.104_1221	0.0137	11	0.00041	3	1.46715	1.88658	8	0.281175	19	0.28116	-14	0.7	3.09	1943	31
K13.104_1222	0.0218	18	0.00074	4	1.46715	1.88643	9	0.282219	20	0.282205	3	0.7	1.44	1051	19
K13.104_1223	0.0290	23	0.00091	5	1.46725	1.88653	8	0.282489	23	0.282479	2	0.8	1.10	590	9
K13.104_1224	0.0257	21	0.00076	5	1.46720	1.88663	10	0.281432	19	0.281402	-4	0.7	2.59	1998	11
K13.104_1225	0.0382	40	0.00102	9	1.46706	1.88613	7	0.282251	24	0.282236	-2	0.8	1.51	763	11
K13.104_1229	0.0287	25	0.00090	6	1.46719	1.88671	8	0.282434	22	0.282429	-6	0.8	1.31	315	9
K13.104_1238	0.0177	16	0.00052	4	1.46715	1.88661	8	0.282347	21	0.282341	-2	0.7	1.37	592	9
K13.104_1239	0.0234	19	0.00069	4	1.46721	1.88657	8	0.282217	26	0.282209	-7	0.9	1.63	594	10
K13.104_1241	0.0290	23	0.00083	5	1.46719	1.88641	11	0.281033	22	0.280991	-4	0.8	3.12	2595	10
K13.104_1242	0.0203	16	0.00059	4	1.46716	1.88665	8	0.281219	25	0.281198	-15	0.9	3.06	1841	13
K13.104_1243	0.0080	11	0.00022	3	1.46722	1.88613	8	0.281234	21	0.281225	-10	0.8	2.94	2006	10
K13.104_1244	0.0353	30	0.00100	6	1.46726	1.88652	7	0.282259	27	0.282246	-3	0.9	1.50	736	10
K13.104_1247	0.0221	18	0.00068	4	1.46720	1.88658	9	0.282365	23	0.28236	-6	0.8	1.41	419	6
K13.104_1249	0.0194	17	0.00059	4	1.46719	1.88597	6	0.282478	25	0.282474	-3	0.9	1.20	368	15

K13.104_1250	0.0223	18	0.00071	4	1.46718	1.88651	9	0.281318	24	0.281292	-9	0.8	2.83	1960	12
K13.104_1252	0.0521	48	0.00161	12	1.46720	1.88662	8	0.282298	20	0.282267	4	0.7	1.34	1004	70
K13.104_1253	0.0174	14	0.00054	3	1.46716	1.88644	9	0.282206	20	0.282199	-7	0.7	1.64	609	9
K13.104_1254	0.0370	30	0.00105	7	1.46709	1.88649	9	0.282439	25	0.282431	-3	0.9	1.27	409	12
K13.104_1255	0.0520	42	0.00162	10	1.46722	1.88649	8	0.282432	22	0.282413	1	0.8	1.22	616	9
K13.104_1257	0.0302	24	0.00099	6	1.46713	1.88645	8	0.282596	20	0.282582	10	0.7	0.83	751	13
K13.104_1258	0.0159	13	0.00048	3	1.46723	1.88635	8	0.282238	22	0.282232	-6	0.8	1.58	599	11
K13.104_1259	0.0233	24	0.00068	6	1.46723	1.88684	7	0.281089	26	0.281055	-1	0.9	2.97	2651	16
K13.104_1262	0.0416	36	0.00149	10	1.46718	1.88679	6	0.282882	26	0.282872	11	0.9	0.43	354	8
K13.104_1263	0.0171	14	0.00053	3	1.46716	1.88622	8	0.282051	24	0.282041	-4	0.9	1.78	1018	22
K13.104_1264	0.0348	33	0.00109	8	1.46718	1.88667	8	0.282762	23	0.282751	11	0.8	0.58	558	11
K13.104_1266	0.0283	23	0.00084	5	1.46722	1.88662	8	0.282413	24	0.282408	-6	0.8	1.35	331	6
K13.104_1272	0.0234	27	0.00068	7	1.46718	1.88658	10	0.281485	21	0.28146	-2	0.8	2.49	1974	13
K13.104_1273	0.0186	15	0.00060	4	1.46714	1.88642	8	0.281615	26	0.281591	7	0.9	2.15	2155	19
K13.104_1274	0.0384	32	0.00117	7	1.46720	1.88601	8	0.282392	25	0.282381	-3	0.9	1.34	491	7
K13.104_1276	0.0330	28	0.00102	7	1.46716	1.88655	9	0.282378	22	0.282371	-7	0.8	1.41	346	5
K13.104_1277	0.0221	18	0.00067	4	1.46717	1.88662	8	0.282409	22	0.282405	-6	0.8	1.36	314	7
K13.104_1278	0.0184	15	0.00055	4	1.46719	1.88682	7	0.282581	23	0.282574	7	0.8	0.90	631	17
K13.104_1280	0.0306	28	0.00086	6	1.46716	1.88670	8	0.282217	21	0.282206	-6	0.7	1.61	660	16
K13.104_1281	0.0321	26	0.00093	6	1.46714	1.88620	8	0.282574	25	0.282564	6	0.9	0.93	613	11
K13.104_1282	0.0419	36	0.00121	8	1.46717	1.88602	11	0.282457	25	0.28245	-5	0.9	1.27	308	6
K13.104_1284	0.0238	24	0.00078	7	1.46721	1.88663	8	0.281006	23	0.280965	-2	0.8	3.10	2752	11
K13.104_1285	0.0130	11	0.00040	3	1.46723	1.88658	8	0.280744	26	0.280722	-8	0.9	3.53	2840	10
K13.104_1286	0.0219	18	0.00068	4	1.46719	1.88671	9	0.282344	25	0.28234	-9	0.9	1.48	316	9
K13.104_1287	0.0284	24	0.00090	6	1.46717	1.88636	7	0.281324	23	0.28129	-8	0.8	2.82	1977	31
K13.104_1288	0.0332	27	0.00100	6	1.46716	1.88642	9	0.282414	22	0.282408	-6	0.8	1.35	325	6
K13.104_1289	0.0682	55	0.00202	12	1.46719	1.88652	10	0.282211	21	0.282176	-1	0.8	1.55	923	12
K13.104_1290	0.0485	43	0.00167	12	1.46723	1.88676	7	0.281726	26	0.281697	-18	0.9	2.48	919	19
K13.104_1291	0.0296	26	0.00090	6	1.46715	1.88645	10	0.282137	24	0.282127	-10	0.9	1.78	602	9
K13.104_1292	0.0050	5	0.00018	1	1.46720	1.88629	9	0.281689	21	0.281685	-16	0.7	2.47	1016	21
K13.104_1293	0.0249	20	0.00077	5	1.46723	1.88658	8	0.282373	22	0.282367	-6	0.8	1.40	393	6
K13.104_1294	0.0344	31	0.00090	6	1.46709	1.88651	6	0.282243	24	0.28223	-2	0.8	1.51	769	13
K13.104_1296	0.0159	13	0.00045	3	1.46720	1.88682	8	0.281967	23	0.281962	-15	0.8	2.09	626	11
K13.104_1297	0.0395	32	0.00128	8	1.46720	1.88670	8	0.281518	26	0.281468	-1	0.9	2.45	2022	11
K13.104_1298	0.0339	28	0.00106	6	1.46717	1.88673	7	0.282315	24	0.282309	-10	0.9	1.55	306	7
K13.104_1300	0.0396	32	0.00113	7	1.46720	1.88658	9	0.281756	22	0.281733	-13	0.8	2.36	1062	18
K13.104_1301	0.0145	12	0.00051	3	1.46719	1.88662	7	0.282561	22	0.282553	11	0.8	0.85	839	13
K13.104_1307	0.0234	19	0.00069	4	1.46715	1.88647	7	0.282146	25	0.28214	-12	0.9	1.81	470	19
K13.104_1308	0.0473	38	0.00149	9	1.46722	1.88666	10	0.281468	20	0.281412	-5	0.7	2.60	1950	14
K13.104_1309	0.0106	11	0.00033	3	1.46718	1.88650	8	0.281141	23	0.281129	-14	0.8	3.14	1975	11
K13.104_1310	0.0082	7	0.00025	1	1.46723	1.88656	8	0.281173	23	0.281163	-12	0.8	3.05	2015	36
Temora (n=26)	0.0379	352	0.00110	104	1.46719	1.88666	10	0.282691	31	0.282682	6	1.0	0.78	417	4
Plesovice (n=19)	0.0065	74	0.00013	18	1.46718	1.88673	13	0.282470	26	0.282470	-4	0.9	1.22	338	3
GJ-1 (n=57)	0.0086	11	0.00025	1	1.46720	1.88669	10	0.282013	23	0.282011	-14	0.8	2.01	606	6
JMC 475 (n=6)					1.46719	1.88669	11	0.282149	8						

Quoted uncertainties (absolute) relate to the last quoted figure. The effect of the inter-element fractionation on the Lu/Hf was estimated to be about 6 % or less based on analyses of the GJ-1 and Plesoviče zircon. Accuracy and reproducibilty was checked by repeated analyses (n = 19 to 57) of reference zircon Temora, GJ-1 and Plesoviče (data given as mean with 2 standard deviation uncertainties)

(a) $^{176}Yb/^{177}Hf = (^{176}Yb/^{173}Yb)_{true} \times (^{173}Yb/^{177}Hf)_{meas} \times (M_{173(Yb)}/M_{177(Hf)})^{\beta(Hf)}$, $\beta(Hf) = \ln(^{179}Hf/^{177}Hf_{true} / {}^{179}Hf/^{177}Hf_{measured}) / \ln (M_{179(Hf)}/M_{177(Hf)})$, M=mass of respective isotope. The $^{176}Lu/^{177}Hf$ were calculated in a similar way by using the $^{175}Lu/^{177}Hf$.
(b) Mean Hf signal in volt.
(c) Uncertainties are quadratic additions of the within-run precision and the daily reproducibility of the 40ppb-JMC475 solution. Uncertainties for the JMC475 quoted at 2SD (2 standard deviation).
(d) Initial $^{176}Hf/^{177}Hf$ and εHf calculated using the apparent Pb-Pb age determined by LA-ICP-MS dating (see column f), and the CHUR parameters: $^{176}Lu/^{177}Hf = 0.0336$, and $^{176}Hf/^{177}Hf = 0.282785$ (Bouvier *et al*., 2008).
(e) two stage model age in billion years using the measured $^{176}Lu/^{177}Hf$ of each spot (first stage = age of zircon), a value of 0.0113 for the average continental crust (second stage), and a depleted mantle (DM) $^{176}Lu/^{177}Hf$ and $^{176}Hf/^{177}Hf$ of 0.0384 and 0.283165, respectively.
(f) apparent Pb-Pb age determined by LA-ICP-MS

LA-MC-ICPMS Lu-Hf isotope data of zircon from meta-granites

A141 TM.17.33	0.0340	30	0.00103	7	1.46736	1.88634	9	0.282366	34	0.282359	-7.7	1.2	1.59	329	5
A142	0.0317	26	0.00097	6	1.46732	1.88571	13	0.282402	21	0.282396	-6.8	0.8	1.52	311	4
A143	0.0406	36	0.00119	8	1.46729	1.88663	12	0.282452	22	0.282444	-4.9	0.8	1.43	321	4
A144	0.0278	24	0.00083	5	1.46734	1.88650	13	0.282398	20	0.282393	-6.7	0.7	1.53	321	4
A145	0.0334	27	0.00101	6	1.46726	1.88652	13	0.282418	21	0.282412	-6.4	0.7	1.49	307	4
A151	0.0466	39	0.00139	9	1.46728	1.88651	14	0.282384	17	0.282376	-7.5	0.6	1.56	311	4
A152	0.0394	33	0.00117	7	1.46731	1.88652	12	0.282399	19	0.282392	-6.8	0.7	1.53	321	4
A153	0.0500	45	0.00142	10	1.46731	1.88662	13	0.282424	26	0.282416	-6.3	0.9	1.49	304	7
A154	0.0266	22	0.00080	5	1.46723	1.88636	12	0.282425	19	0.282421	-6.1	0.7	1.48	306	4
A155	0.0238	21	0.00072	5	1.46729	1.88648	13	0.282427	16	0.282423	-5.7	0.6	1.47	319	4
A156	0.0097	13	0.00029	3	1.46722	1.88568	14	0.282095	25	0.282093	-17.6	0.9	2.11	308	6
A157	0.0444	36	0.00133	8	1.46725	1.88629	11	0.282412	21	0.282404	-6.5	0.7	1.51	313	4
A158	0.0182	27	0.00050	7	1.46726	1.88645	13	0.282393	21	0.282391	-7.0	0.7	1.53	313	4
A159	0.0401	36	0.00119	8	1.46727	1.88651	13	0.282405	19	0.282398	-6.7	0.7	1.52	315	4
A160	0.0501	54	0.00148	13	1.46720	1.88661	11	0.282387	18	0.282378	-7.2	0.6	1.55	322	4
A161	0.0467	45	0.00140	11	1.46725	1.88658	14	0.282416	23	0.282408	-5.9	0.8	1.49	336	4
A162	0.0300	25	0.00091	6	1.46724	1.88651	13	0.282423	21	0.282417	-6.2	0.7	1.48	307	4
A163	0.0290	31	0.00087	7	1.46729	1.88567	12	0.282206	26	0.282201	-13.7	0.9	1.90	315	4
A164	0.0306	25	0.00096	6	1.46731	1.88649	11	0.282390	19	0.282384	-7.2	0.7	1.55	313	4
A165	0.0524	58	0.00154	15	1.46729	1.88648	13	0.282384	19	0.282375	-7.3	0.7	1.56	326	4
A166	0.0352	32	0.00102	8	1.46730	1.88642	12	0.282409	19	0.282403	-6.6	0.7	1.51	311	4
A167	0.0233	22	0.00070	5	1.46730	1.88654	12	0.282423	25	0.282419	-6.0	0.9	1.48	312	4
A168	0.0286	25	0.00086	6	1.46726	1.88649	13	0.282399	19	0.282393	-6.8	0.7	1.53	319	4
A169	0.0457	38	0.00137	9	1.46725	1.88647	10	0.282399	23	0.282391	-7.1	0.8	1.53	309	4
A170	0.0384	37	0.00113	9	1.46731	1.88639	13	0.282386	20	0.282379	-7.7	0.7	1.56	301	4

A171	0.0314	26	0.00101	7	1.46722	1.88569	12	0.282444	22	0.282438	-5.3	0.8	1.44	313	4
A172	0.0321	26	0.00102	6	1.46725	1.88650	14	0.282425	19	0.282419	-6.0	0.7	1.48	313	4
A173	0.0641	58	0.00185	13	1.46730	1.88574	13	0.282412	22	0.282401	-6.1	0.8	1.50	338	7
A174	0.0410	34	0.00126	8	1.46731	1.88661	13	0.282365	21	0.282357	-8.2	0.8	1.60	313	4
A175	0.0682	55	0.00206	13	1.46750	1.88600	13	0.282347	20	0.282335	-9.2	0.7	1.65	300	4
A176	0.0396	37	0.00114	9	1.46728	1.88642	15	0.282414	18	0.282406	-4.5	0.6	1.47	400	5
A177	0.0450	38	0.00131	8	1.46731	1.88659	14	0.282398	23	0.282391	-7.0	0.8	1.53	314	4
A178	0.0316	29	0.00092	6	1.46728	1.88633	11	0.282421	24	0.282416	-6.4	0.9	1.49	300	4
A179	0.0328	27	0.00096	6	1.46730	1.88645	12	0.282389	18	0.282383	-7.1	0.6	1.54	318	4
A180	0.0348	83	0.00102	23	1.46741	1.88660	15	0.282284	67	0.282278	-10.8	2.4	1.75	320	8
A181	0.0367	30	0.00110	7	1.46731	1.88651	14	0.282422	20	0.282415	-6.1	0.7	1.49	314	4
A182	0.0542	44	0.00161	10	1.46730	1.88640	13	0.282430	21	0.282420	-6.0	0.7	1.48	313	5
A183	0.0296	24	0.00087	5	1.46729	1.88645	14	0.282421	22	0.282416	-6.1	0.8	1.48	314	4
A184	0.0397	32	0.00115	7	1.46732	1.88646	17	0.282415	18	0.282408	-6.2	0.6	1.50	324	4
A185	0.0300	24	0.00087	5	1.46724	1.88648	12	0.282418	19	0.282413	-6.3	0.7	1.49	308	4
A186	0.0250	20	0.00075	5	1.46724	1.88662	12	0.282440	23	0.282435	-5.4	0.8	1.45	312	4
A548 TM.17.34	0.0248	26	0.00074	6	1.46730	1.88643	10	0.282401	22	0.282396	-6.7	0.8	1.52	318	3
A554	0.0588	48	0.00175	11	1.46733	1.88650	14	0.282413	18	0.282403	-6.9	0.6	1.52	296	3
A555	0.0514	49	0.00157	12	1.46730	1.88643	14	0.282411	21	0.282402	-6.1	0.7	1.50	334	3
A556	0.0452	39	0.00134	9	1.46737	1.88640	14	0.282403	22	0.282395	-6.7	0.8	1.52	321	2
A557	0.0282	27	0.00086	7	1.46746	1.88609	9	0.282325	28	0.282320	-9.4	1.0	1.67	316	2
A558	0.0578	54	0.00165	13	1.46728	1.88647	11	0.282402	24	0.282392	-6.8	0.8	1.53	319	2
A559	0.0346	28	0.00100	6	1.46733	1.88624	12	0.282399	21	0.282393	-7.0	0.8	1.53	308	3
A560	0.0441	37	0.00135	9	1.46725	1.88660	12	0.282394	20	0.282386	-7.0	0.7	1.54	320	3
A561	0.0347	30	0.00103	7	1.46734	1.88625	10	0.282394	24	0.282388	-7.2	0.9	1.54	306	2
A562	0.0329	29	0.00105	8	1.46732	1.88643	10	0.282367	26	0.282360	-8.1	0.9	1.59	313	3
A563	0.0450	40	0.00134	10	1.46736	1.88639	14	0.282452	20	0.282444	-5.1	0.7	1.43	314	2
A564	0.0747	106	0.00222	28	1.46736	1.88630	13	0.282408	23	0.282394	-6.6	0.8	1.52	323	4
A565	0.0349	34	0.00102	8	1.46724	1.88652	13	0.282371	33	0.282365	-7.7	1.2	1.58	320	3
A566	0.0352	39	0.00105	9	1.46751	1.88615	13	0.282349	26	0.282343	-8.4	0.9	1.62	327	3
A567	0.0436	40	0.00127	9	1.46730	1.88661	12	0.282398	19	0.282390	-7.0	0.7	1.53	312	2
A568	0.0334	30	0.00098	7	1.46742	1.88649	12	0.282369	28	0.282363	-8.0	1.0	1.59	313	3
A569	0.0447	37	0.00130	8	1.46733	1.88646	12	0.282371	22	0.282363	-8.0	0.8	1.59	310	3
A570	0.0343	29	0.00099	7	1.46727	1.88649	13	0.282501	20	0.282495	-3.2	0.7	1.33	317	3
A571	0.0513	62	0.00148	15	1.46732	1.88620	13	0.282439	21	0.282430	-5.5	0.8	1.46	315	3
A572	0.0560	59	0.00166	15	1.46734	1.88641	14	0.282392	21	0.282382	-7.1	0.7	1.55	323	3
A573	0.0355	30	0.00108	7	1.46733	1.88637	13	0.282369	22	0.282362	-7.7	0.8	1.58	327	2
A574	0.0504	70	0.00154	18	1.46730	1.88652	13	0.282403	20	0.282393	-6.6	0.7	1.52	325	7
A575	0.0356	30	0.00104	7	1.46736	1.88613	11	0.282341	26	0.282335	-9.0	0.9	1.64	312	3
A576	0.0511	50	0.00150	13	1.46731	1.88634	10	0.282398	23	0.282389	-6.9	0.8	1.53	320	3
A577	0.0243	27	0.00072	7	1.46729	1.88654	10	0.282344	24	0.282340	-8.7	0.9	1.63	316	3
A578	0.0370	30	0.00119	8	1.46735	1.88613	11	0.282448	23	0.282441	-4.7	0.8	1.43	335	5
A579	0.0422	42	0.00128	11	1.46737	1.88624	13	0.282365	19	0.282357	-8.3	0.7	1.60	308	2
A580	0.0441	37	0.00130	8	1.46731	1.88633	15	0.282406	21	0.282398	-6.9	0.7	1.52	307	3
A581	0.0297	25	0.00088	6	1.46730	1.88626	13	0.282413	19	0.282408	-6.2	0.7	1.50	321	2
A582	0.0369	30	0.00113	7	1.46732	1.88621	12	0.282414	23	0.282407	-6.3	0.8	1.50	316	2
A583	0.0200	16	0.00063	4	1.46727	1.88649	13	0.282393	21	0.282393	-13.9	0.7	1.65	0	0
A584	0.0226	20	0.00072	5	1.46727	1.88659	13	0.282324	18	0.282314	0.4	0.6	1.50	763	7
A585	0.0342	40	0.00101	10	1.46722	1.88597	13	0.282428	26	0.282422	-6.0	0.9	1.47	308	3
A586	0.0210	17	0.00063	4	1.46730	1.88638	13	0.282404	25	0.282400	-6.4	0.9	1.51	322	2
A587	0.0607	53	0.00176	12	1.46725	1.88629	11	0.282454	24	0.282443	-5.1	0.9	1.43	315	3
A588	0.0358	35	0.00107	9	1.46729	1.88628	13	0.282413	21	0.282406	-6.3	0.7	1.50	317	2
A589	0.0310	25	0.00092	6	1.46729	1.88629	15	0.282403	18	0.282397	-6.5	0.6	1.52	323	2
A590	0.0221	23	0.00067	6	1.46732	1.88628	14	0.282503	19	0.282499	-3.3	0.7	1.33	305	3
A591	0.0396	37	0.00117	9	1.46728	1.88651	15	0.282430	20	0.282424	-6.0	0.7	1.47	307	3
A592	0.0355	38	0.00102	10	1.46728	1.88658	13	0.282355	19	0.282349	-8.2	0.7	1.61	325	4
A593	0.0396	41	0.00117	11	1.46733	1.88640	14	0.282402	21	0.282395	-6.7	0.7	1.52	317	3
A594	0.0290	24	0.00088	6	1.46737	1.88626	13	0.282363	21	0.282358	-8.1	0.7	1.60	315	2
A157 TM.17.35	0.0317	35	0.00093	8	1.46720	1.88686	12	0.282274	22	0.282262	-3.6	0.8	1.64	666	6
A158	0.0258	21	0.00081	5	1.46724	1.88675	14	0.282325	21	0.282320	-9.3	0.8	1.67	323	4
A159	0.0573	47	0.00153	10	1.46710	1.88684	15	0.282396	18	0.282387	-6.9	0.7	1.54	323	3
A160	0.0268	27	0.00090	7	1.46719	1.88691	12	0.282229	24	0.282221	-9.8	0.9	1.80	456	5
A161	0.0207	19	0.00057	4	1.46715	1.88684	15	0.282428	21	0.282424	-5.8	0.7	1.47	313	3
A162	0.0136	12	0.00040	3	1.46715	1.88686	11	0.282299	20	0.282295	-3.8	0.7	1.60	607	6
A163	0.0476	42	0.00137	10	1.46718	1.88704	18	0.282451	20	0.282441	-3.8	0.7	1.41	377	3
A164	0.0103	9	0.00030	2	1.46718	1.88706	13	0.281272	27	0.281258	0.8	1.0	2.83	2414	27
A165	0.0416	33	0.00130	8	1.46721	1.88696	12	0.282439	23	0.282432	-5.5	0.8	1.45	315	4
A166	0.0437	35	0.00129	8	1.46710	1.88687	10	0.282443	22	0.282430	-0.6	0.8	1.37	534	8
A167	0.0342	29	0.00111	7	1.46723	1.88654	15	0.282436	19	0.282429	-5.3	0.7	1.45	327	3
A168	0.0332	27	0.00098	6	1.46717	1.88672	19	0.282399	17	0.282392	-5.9	0.6	1.51	361	3
A169	0.0388	31	0.00123	8	1.46719	1.88684	14	0.282367	17	0.282360	-8.0	0.6	1.59	317	3
A170	0.0265	21	0.00081	5	1.46707	1.88709	10	0.282351	27	0.282342	-2.3	0.9	1.51	600	6
A171	0.0327	27	0.00099	6	1.46727	1.88660	18	0.282360	19	0.282354	-7.6	0.7	1.59	344	3
A172	0.0420	37	0.00120	8	1.46720	1.88698	14	0.282316	20	0.282302	-3.5	0.7	1.59	607	7
A173	0.0581	47	0.00169	10	1.46719	1.88679	14	0.282363	17	0.282348	-5.3	0.6	1.56	458	4
A174	0.0420	40	0.00114	8	1.46724	1.88655	18	0.282242	25	0.282232	-8.3	0.9	1.76	507	5
A175	0.0280	23	0.00088	6	1.46716	1.88671	13	0.281002	27	0.280950	5.8	1.0	3.11	3095	9
A176	0.0124	10	0.00036	2	1.46720	1.88682	14	0.281195	29	0.281178	0.7	1.0	2.93	2533	11
A177	0.0265	22	0.00077	5	1.46715	1.88674	14	0.282426	24	0.282421	-5.9	0.8	1.47	315	3
A178	0.0261	26	0.00085	8	1.46715	1.88689	16	0.282422	24	0.282417	-5.6	0.8	1.47	333	3
A179	0.0263	36	0.00080	9	1.46718	1.88674	12	0.282493	22	0.282487	-2.7	0.8	1.33	350	4
A180	0.0633	67	0.00186	16	1.46716	1.88694	14	0.282409	20	0.282395	-5.1	0.7	1.49	391	4
A181	0.0316	51	0.00091	14	1.46713	1.88702	11	0.282300	24	0.282290	-3.8	0.9	1.61	613	8
A182	0.0273	22	0.00079	5	1.46711	1.88691	15	0.282429	19	0.282424	-5.3	0.7	1.46	333	4
A183	0.0281	27	0.00087	7	1.46713	1.88666	14	0.282192	19	0.282180	-4.8	0.7	1.77	742	8
A184	0.0266	22	0.00098	6	1.46712	1.88670	11	0.282668	20	0.282657	8.9	0.7	0.90	603	5
A185	0.0120	12	0.00030	2	1.46717	1.88678	12	0.282393	24	0.282391	-6.7	0.9	1.53	324	3

A186	0.0374	34	0.00109	8	1.46721	1.88674	14	0.282398	19	0.282391	-5.7	0.7	1.51	373	3
A187	0.0458	42	0.00133	10	1.46716	1.88675	13	0.282528	21	0.282518	-0.7	0.8	1.26	391	4
A188	0.0141	12	0.00040	3	1.46710	1.88676	14	0.282558	21	0.282553	5.7	0.8	1.09	624	5
A189	0.0369	67	0.00105	18	1.46725	1.88656	16	0.282118	30	0.282107	-11.3	1.0	1.98	569	8
A190	0.0326	31	0.00097	8	1.46728	1.88652	14	0.282380	19	0.282374	-6.9	0.7	1.55	343	6
A191	0.0419	39	0.00126	9	1.46716	1.88679	19	0.282417	21	0.282403	-0.5	0.7	1.40	584	12
A192	0.0214	18	0.00067	4	1.46716	1.88652	13	0.282101	18	0.282093	-10.5	0.6	1.98	628	5
A193	0.0437	37	0.00129	9	1.46720	1.88693	11	0.282452	29	0.282437	2.0	1.0	1.31	642	7
A199	0.0552	45	0.00163	10	1.46716	1.88672	19	0.282263	17	0.282252	-11.4	0.6	1.79	336	3
A200	0.0168	14	0.00052	3	1.46716	1.88687	13	0.282223	24	0.282220	-12.6	0.9	1.85	333	4
A201	0.0528	46	0.00157	11	1.46717	1.88691	10	0.282380	23	0.282370	-7.6	0.8	1.57	319	4
A202	0.0174	17	0.00055	4	1.46730	1.88650	14	0.282384	23	0.282379	-2.1	0.8	1.46	550	5
Temora (n=21)	0.0312	213	0.00097	60	1.46740	1.88622	12	0.282657	34	0.282649	4.5	1.2	0.99	338	3
GJ-1 (n=22)	0.0078	1	0.00025	0	1.46732	1.88646	9	0.282017	24	0.282014	-13.8	0.8	2.14	606	6
JMC 475 (n=6)					1.46718	1.88669	11	0.282135	8						

Quoted uncertainties (absolute) relate to the last quoted figure. The effect of the inter-element fractionation on the Lu/Hf was estimated to be about 6 % or less based on analyses of the GJ-1 and Plesoviče zircon. Accuracy and reproducibilty was checked by repeated analyses (n = 30 and 20, respectively) of reference zircon GJ-1 and Plesoviče (data given as mean with 2 standard deviation uncertainties)

(a) $^{176}Yb/^{177}Hf = (^{176}Yb/^{173}Yb)_{true} \times (^{173}Yb/^{177}Hf)_{meas} \times (M_{173(Yb)}/M_{177(Hf)})^{\beta(Hf)}$, $\beta(Hf) = \ln(^{179}Hf/^{177}Hf_{true} / {}^{179}Hf/^{177}Hf_{measured}) / \ln(M_{179(Hf)}/M_{177(Hf)})$, M=mass of respective isotope. The $^{176}Lu/^{177}Hf$ were calculated in a similar way by using the $^{175}Lu/^{177}Hf$ and $\beta(Yb)$.

(b) Mean Hf signal in volt.

(c) Uncertainties are quadratic additions of the within-run precision and the daily reproducibility of the 40ppb-JMC475 solution. Uncertainties for the JMC475 quoted at 2SD (2 standard deviation).

(d) Initial $^{176}Hf/^{177}Hf$ and εHf calculated using the apparent Pb-Pb age determined by LA-ICP-MS dating (see column f), and the CHUR parameters: $^{176}Lu/^{177}Hf = 0.0336$, and $^{176}Hf/^{177}Hf = 0.282785$ (Bouvier *et al*., 2008).

(e) two stage model age in billion years using the measured $^{176}Lu/^{177}Lu$ of each spot (first stage = age of zircon), a value of 0.0113 for the average continental crust (second stage), and a juvenile crust (NC) $^{176}Lu/^{177}Lu$ and $^{176}Hf/^{177}Hf$ of 0.0384 and 0.28314, respectively.

(f) apparent Pb-Pb age determined by LA-ICP-MS